Characterization of Mouse Two-Pore Channels (TPCs) in NAADP-mediated Ca^{2+} Signalling

Kai-Ting Chuang

New College

Supervisor: Prof. Antony Galione

Department of Pharmacology

University of Oxford

A thesis submitted for the degree of

Doctor of Philosophy

Trinity Term, 2011

Characterization of Mouse Two-Pore Channels (TPCs) in NAADP-mediated Ca^{2+} Signalling

Kai-Ting Chuang, New College

A thesis submitted for the degree of Doctor of Philosophy, Trinity Term 2011

Abstract

Recent studies have identified Two-Pore Channels (TPCs) as the channels activated by NAADP. To date, most studies that characterized these channels have employed heterologous expression or overexpression systems. The research reported here has focused principally on endogenous TPC activity by using single and dual gene knockout (KO) in a mouse system and has yielded insights into TPC expression levels, subcellular localisation, NAADP binding, and channel function.

Mouse models that had been generated by both the "gene-trapping" and the "gene-targeting" techniques were obtained and validated. These included a knock-down strain ("hypomorph"). Surprisingly, all TPC mutant mice showed no gross phenotypes.

In addition to the two known isoforms in mouse, TPC1 and TPC2, the expression of a shorter variant of TPC1 was discovered; this has an alternative (truncated) N-terminus, and has been termed ΔN-TPC1. All TPC variants/isoforms were widely expressed in all mouse tissue types tested. Overexpression of mouse TPCs in mouse embryonic fibroblasts showed that ΔN-TPC1 and TPC2 were expressed primarily in late endosomes/lysosomes while TPC1 was expressed in both endosomes and lysosomes. Dileucine sorting motifs target TPCs to late endosomes/lysosomes; it was shown that truncation or mutation of dileucine motifs significantly reduced localization in late endosomes/lysosomes.

Furthermore, TPCs were shown not to be the direct binding target of NAADP, as the high affinity NAADP binding was retained in hepatic membranes from TPC double KO (DKO) mice. It is concluded that NAADP binds to an (as yet, unidentified) accessory protein.

The functional role of TPCs was studied in depth using mouse pancreatic acinar cells. NAADP is known to release Ca^{2+} from the acidic stores in response to the stimulation by the hormone cholecystokinin (CCK). In all TPC mutant mice, CCK was still able to evoke Ca^{2+} oscillations, but with slower and attenuated oscillations in the TPC1 hypomorph, and with slower oscillations in TPC DKO. In all TPC KOs, oscillations were disrupted by known inhibitors of the NAADP-signalling pathway (Ned-19, GPN and bafilomycin A1), indistinguishable from the responses with wild-type cells. This suggests that TPCs are not involved in CCK signalling, although it is possible that functional compensation masked the phenotype arising from the impaired signalling.

Publications

P. J. Calcraft, M. Ruas, Z. Pan, X. Cheng, A. Arredouani, X. Hao, J. Tang, K. Rietdorf, L. Teboul, **K.-T. Chuang**, P. Lin, R. Xiao, C. Wang, Y. Zhu, Y. Lin, C. N. Wyatt, J. Parrington, J. Ma, A. M. Evans, A. Galione, and M. X. Zhu. Naadp mobilizes calcium from acidic organelles through two-pore channels. Nature, 459(7246):596–600, May 2009.

N. T. Durlu-Kandilci, M. Ruas, **K.-T. Chuang**, A. Brading, J. Parrington, and A. Galione. Tpc2 proteins mediate nicotinic acid adenine dinucleotide phosphate (naadp)- and agonist-evoked contractions of smooth muscle. The Journal of biological chemistry, 285(32):24925–32, Aug 2010.

Poster presentations

Gordon Research Conference – Calcium signalling, Lucca, Italy. June 2009

K.-T. Chuang, A. Arredouani, M. Ruas, J. Parrington, A. Galione. Two-Pore Channel 2 (TPC2) in NAADP signalling in Pancreatic Acinar and β-Cells.

Awards

Christopher Welch Scholarship	2007–2011	University of Oxford
Full Clarendon Fund Award	2007–2011	University of Oxford

Acknowledgement

I would like to thank my supervisor, **Prof. Antony Galione**, for his support and guidance throughout my time as his student and for his ideas and research insights.

I am very grateful to all lab members for such a fantastic time I had over the past four years, their useful discussion and critiques in completing my thesis, and in particular:

- **Dr. Magarida Ruas** for teaching molecular biology and binding techniques
- **Dr. Abdelilah Arredouani, Dr. Anthony Morgan, and Dr. Katja Rietdorf** for teaching Ca^{2+} imaging technique
- **Dr. Lianne Davis** for her constant cheering spirit
- **Dr. Timothy Funnell** for being such an awesome labmate and a lifetime friend
- **Clive Garnham** for his secret stashes of miscellaneous laboratory goods, and his kind willingnessto help
- **Keiko Watanabe and Paula Heister** for their support in the lab

I must also thank members of **Dr. John Parrington's** and **Dr. Grant Churchill's group** for their advice, suggestions, fun and support. I am grateful to Christopher Welch Scholarship and Clarendon Fund for the funding.

This thesis would not have been possible without **Robbie Shade**; for his "PeakFinder" software that has spared the time-assuming analysis, and him and his family for unwavering support and encouragement, and my good friends: **Cristina, Candy, Scott, Nienke, Anu, Ed, and Dave** for keeping me sane. Lastly, I owe my deepest gratitude to my parents for everything that they have taught me in life.

Contents

Abbreviations

β-geo	Fusion of the *lacZ* gene, which encodes the marker β-galactosidase, and the *neo* gene, which encodes neomycin phosphotransferase that confers resistance to neomycin
$\boldsymbol{P_{Ca2+}/P_{K+}}$	Relative permeability to Ca^{2+} and K^{+}
$\mathbf{K_d}$	Equilibrium dissociation constant
ACh	Acetylcholine
ADP	Adenosine diphosphate
ADPR	ADP-ribose
$\mathbf{ADPR_2}$	dimeric ADPR
AM	Acetoxymethyl ester
AP	Clathrin adaptor
Ap2a	adenosine 5'-pyrophosphate-5'-adenosine
AR42J	Rat pancreatic acinar cell line
ARC	ADP-ribosyl cyclase
At	*Arabidopsis thaliana* - Thale cress
ATP	Adenosine triphosphate
BCA	Bicinchoninic acid
bp	Base pairs
BSA	Bovine serum albumin
CaBP	Ca^{2+} binding protein
cADPR	Cyclic ADP ribose
CAGE	Cap-analysis gene expression
CaM	Calmodulin
CAMKII	Ca^{2+}/calmodulin-dependent protein kinase II
CatSper	Cation channel of Sperm
CCK	Cholecystokinin
cDNA	Complementary DNA
CHO	Chinese hamster ovary cell line
CICR	Calcium-induced calcium release
COS-7	Monkey kidney cell line
DAG	Diacylglycerol
DBTSS	Database of transcriptional start sites
DEPC	Diethylpyrocarbonate
DKO	Double knockout
DMEM	DulbeccoÕs modified Eagle medium
DMSO	Dimethyl sulfoxide
DNA	Deoxyribonucleic acid
dNTP	Deoxyribonucleotide triphosphate
DTT	Dithiothreitol
$\mathbf{E_2}$	Oestradiol
$\mathbf{EC_{50}}$	Half maximal effective concentration
ECL	Enhanced chemiluminescence
EDTA	Ethylene diamine-tetraacetic acid
EEA1	Early endosome antigen 1
EGTA	Ethylene glycol-bis (2-amino-ethylether)-N,N,N',N'-tetraaceticacid
ER	Endoplasmic reticulum
ES	Embryonic stem
ExPASY	Expert protein analysis system
FBS	Foetal bovine serum
FKBP	FK506 binding protein
FL	Full-length
GFP	Green fluorescent protein
Gg	*Gallus gallus -chicken*
GLP-1	Glucagon-like peptide-1
Glu-IM	Intracellular-like medium containing gluconate
GLUT4	Glucose transporter type 4
GPCR	G protein-coupled receptor
GPN	Glycylphenylalanine 2-naphthylamide
H	Hypomorph
HEK	Human embryonic kidney cell line
HPLC	High performance liquid chromatography
HRP	Horseradish peroxidase
Hs	*Homo sapiens* - Human
IgG	Immunoglobulin G

IL-1R	Interleukin-1 receptor
IMAGE	Integrated molecular analysis of genomes and their expression
IP_3	Inositol 1,4,5-trisphosphate
IP_3R	IP_3 Receptor
ISP	Interspike period
k_{ob}	Observed rate constant
k_{off}	Dissociation rate constant
k_{on}	Association rate constant
KAR	Kainate receptor
kDa	Kilo Daltons
KDEL	lys-asp-glu-leu - ER marker
KO	Knockout
LAK	Lymphokine-activated killer cell
LAMP	Lysosomal-associated membrane protein
LB	Luria broth
LIMP	Lysosome membrane protein
LSD	Lysosomal storage disorder
M6PRs	Mannose 6-phosphate receptors
MAPK	Mitogen-activated protein kinase
MCU	Mitochondrial Ca^{2+} uniporter
MEF	Mouse embryonic fibroblast
MIN6	Mouse insulinoma cell line
Mm	*Mus musculus* - mouse
mRNA	Messenger RNA
NAAD	Nicotinic acid adenine dinucleotide
NAADP	Nicotinic acid adenine dinucleotide phosphate
NAD	Nicotinamide adenine dinucleotide
NADP	Nicotinamide adenine dinucleotide phosphate
NCKX	Na^+/Ca^{2+}-K^+ exchangers
NCX	Na^+/Ca^{2+} exchanger
NMDAR	*N*-Methyl-D-aspartate receptor
NPC1	Niemann-Pick disease, type C1
ORegAnno	Open regulatory annotation
P_o	Channel open probability
pA	Polydneylation signal
PAGE	Polyacrylamide gel electrophoresis
PBS	Phosphate-buffered saline
PBST	PBS, 0.5 % (v/v) Tween-20
PCR	Polymerase chain reaction
PFA	Paraformaldehyde
PIP_2	Phosphatidylinositol 4,5-bisphosphate
PKA	Protein kinase A
PKC	Protein kinase C
PLC	Phospholipase C
PMCA	Plasma membrane Ca^{2+} ATPase
PNGaseF	Peptide N-glycosidase F
PrP	Prion protein
PVDF	Polyvinylidene fluoride
RNA	Ribonucleic acid
RT-PCR	Reverse transcription PCR
RT-qPCR	RT quantitative PCR
RyR	Ryanodine Receptor
S.E.M.	Standard error of the mean
S1P	Sphingosine-1-phosphate
SA	Splicing acceptor
SDM	Site-directed mutagenesis
SDS	Sodium dodecyl sulphate
SERCA	Sarcoendoplasmic reticular Ca^{2+} ATPase
siRNA	Small interfering RNA
SKBR3	Human breast cancer cell line
Sp	*Strongylocentrotus purpuratus* - sea urchin
SPCA	Secretory pathway Ca^{2+} ATPase
SR	Sarcoplasmic reticulum
ssRNA	Single stranded RNA
STIM	Stromal interaction molecule
TAE	Tris-acetate, EDTA buffer
TEMED	Tetramethylethylenediamine
TfR	Transferrin receptor
TGN	*trans*-Golgi network
TKR	Receptor tyrosine kinases
TMD	Transmembrane domains
TPC	Two-pore channel
TRP	Transient receptor potential
TRPM2	Transient receptor potential melastatin 2
TRPML1	Transient receptor potential mucolipin 1
TRPV1	Transient receptor potential vanilloid receptor
V-H^+-ATPase	Vacuolar H^+-ATPase
WT	Wild-type
ZG	Zymogen granules

Chapter 1

General Introduction

"In the furnaces of the stars the elements evolved from hydrogen. When oxygen and neon captured successive α particles, the element calcium was born. Roughly 10 billion years later, cell membranes began to parse the world by charge, temporarily and locally defying relentless entropy. To adapt to changing environments, cells must signal, and signaling requires messengers whose concentration varies with time. Filling this role, calcium ions (Ca^{2+}) and phosphate ions have come to rule cell signaling." (Clapham, 2007)

1.1 Calcium (Ca^{2+}): a pivotal cell regulator

Ca^{2+} governs an abundance of cellular processes throughout the life of an organism from fertilization to cell differentiation, cell proliferation, transcription, contraction, secretion/exocytosis, and eventually death (apoptosis). That Ca^{2+} possesses such an incredible power lies in the versatility of its signalling mechanisms. The diverse duration and amplitude of Ca^{2+} signalling is dependent on (1) the comprehensive Ca^{2+}-signalling toolkit [28, 29] including hundreds of effector proteins that are endowed with affinities for Ca^{2+} from nano- to millimolar [72], and (2) the highly diverse spatial and temporal patterns [28, 29].

1.1.1 Spatial and temporal organization of Ca^{2+} signals

"Spatial organization" refers to the localization of the Ca^{2+} signals, which can be detected at various levels from the highly localized elementary to the global level (described in details in Sections 1.3.2 and 1.4.3). Transient local Ca^{2+} spikes can be amplified globally by Ca^{2+}-induced Ca^{2+} release (CICR). However, to sustain global Ca^{2+} signals in response to prolonged stimulation, transient Ca^{2+} signals repeat themselves to form oscillations

(organized in space as waves) [28, 29].

Ca^{2+} signals that occur at a highly localized domain or globally can govern different cellular processes. For example, local Ca^{2+} release from N- or P/Q-type voltage-gated Ca^{2+} channels at the synaptic terminal triggers exocytosis of vesicles. Additionally, local Ca^{2+} release can also trigger the Ca^{2+}-sensitive K^+ channels to control cell excitability [29]. In pancreatic acinar cells, local Ca^{2+} release was shown to trigger only fluid secretion whereas global Ca^{2+} signals was to trigger both fluid and enzyme secretion [171].

"Temporal organization" refers to the duration and frequency of Ca^{2+} signals. Short-lasting Ca^{2+} signals (micro to milliseconds) can activate cellular processes such as exocytosis of synaptic vesicles and contraction of skeletal and cardiac muscles. The longer Ca^{2+} signals (seconds to minutes) can initiate metabolism and transcription. Sustained signals generated by Ca^{2+} oscillations can activate specific cellular responses depending on the frequency decoded by the Ca^{2+}-binding proteins such as Ca^{2+}/calmodulin-dependent protein kinase II (CAMKII) and protein kinase C (PKC) [28, 29].

Tight regulation in all aspects of the Ca^{2+} signalling pathway is thus required to enable Ca^{2+} to perform precisely with versatility and universality [29].

1.2 Ca^{2+} homeostasis

At rest, cytosolic Ca^{2+} concentration is maintained at a relatively low level (∼100 nM) to avoid activation of effectors. Prolonged high concentrations of Ca^{2+} are toxic, as this leads to continuous activation of proteases which eventually leads to cell death [61]. Furthermore, Ca^{2+} can easily form less soluble complexes with another important signalling molecule, phosphate. For successful signalling via phosphorylation, cytosolic free Ca^{2+} must be maintained at a low concentration to reduce phosphate being precipitated out of the solution [61, 72]. Ca^{2+} is a simple ion; it cannot be chemically broken down like the more complex molecules to reduce the concentration. Cells therefore employ other mechanisms to regulate free Ca^{2+} concentrations: compartmentalization, extrusion, or chelation [72].

1.2.1 Ca^{2+}-sequestering stores

Most of the Ca^{2+} is compartmentalized in organelles. The best known Ca^{2+}-sequestering organelle is the sarcoplasmic/endoplasmic reticulum (SR/ER) which basally contains 100–

800 μM free Ca^{2+} [48] (Figure 1.1). Less well understood are the acidic Ca^{2+} stores, the lumina of which have a pH of ∼4–6.5 and luminal Ca^{2+} concentrations in the micromolar range [166]. Acidic Ca^{2+} stores comprise not only the members of the endo-lysosomal system but also secretory vesicles, the Golgi apparatus, and other lysosome-related organelles such as secretory lysosomes, melanosomes, platelet dense granules, and yolk platelets [70, 82, 216]. It is important to note that Ca^{2+} can be stored in these organelles because of the low Ca^{2+} permeability of the ER and acidic store membranes. Thus, passive diffusion is minimized. Interestingly, Ca^{2+} leak from these stores may be important as it could offset the Ca^{2+} influx generated by the pumps to reach a Ca^{2+} steady state in the lumen [53].

For a long time, the endo-lysosomal system has been known for its digestive function in endocytic or autophagic protein degradation; only recently has research started to reveal its role as a Ca^{2+}-releasing store. It was found that upon endocytosis, extracellular fluid (containing ∼1 mM Ca^{2+}) is effectively accumulated in the invaginated membrane-bound vesicles. Proteins to be degraded are then transported down in the vesicles to the early endosomes [166]. More interestingly, "endosomal acidification" by the vacuolar H^+-ATPase (V-H^+-ATPase) releases a large amount of Ca^{2+} back into the cytosol - a process that can be blocked by bafilomycin (an inhibitor of the V-H^+-ATPase). It was also noted that this acidification was not observed when the concentration of extracellular Ca^{2+} decreased [111, 166].

The early endosome is mildly acidic (pH of ∼6) and has a Ca^{2+} concentration of 4–40 μM [166, 251] (Figure 1.1). Mildly acidic conditions promote uncoupling of the ligand-receptor complexes that were invaginated in the vesicles, and dissociated proteins are then recycled back to the plasma membrane by recycling endosomes or to the *trans*-Golgi network (TGN). Early endosomes that contain the rest of the cargo proteins are sorted by cycles of vesicle fusion and fission, and mature into late endosomes and then into lysosomes where their cargo protein are finally degraded [166, 277]. Accumulation of Ca^{2+} in late endosomes and lysosomes is dependent on the proton gradient across the membranes [67]; late endosomes have a pH of ∼5 although their Ca^{2+} concentration is yet to be determined while lysosomes have been shown to have a pH of ∼4–4.5 and a Ca^{2+} concentration of ∼500 μM (Figure 1.1) [166, 277].

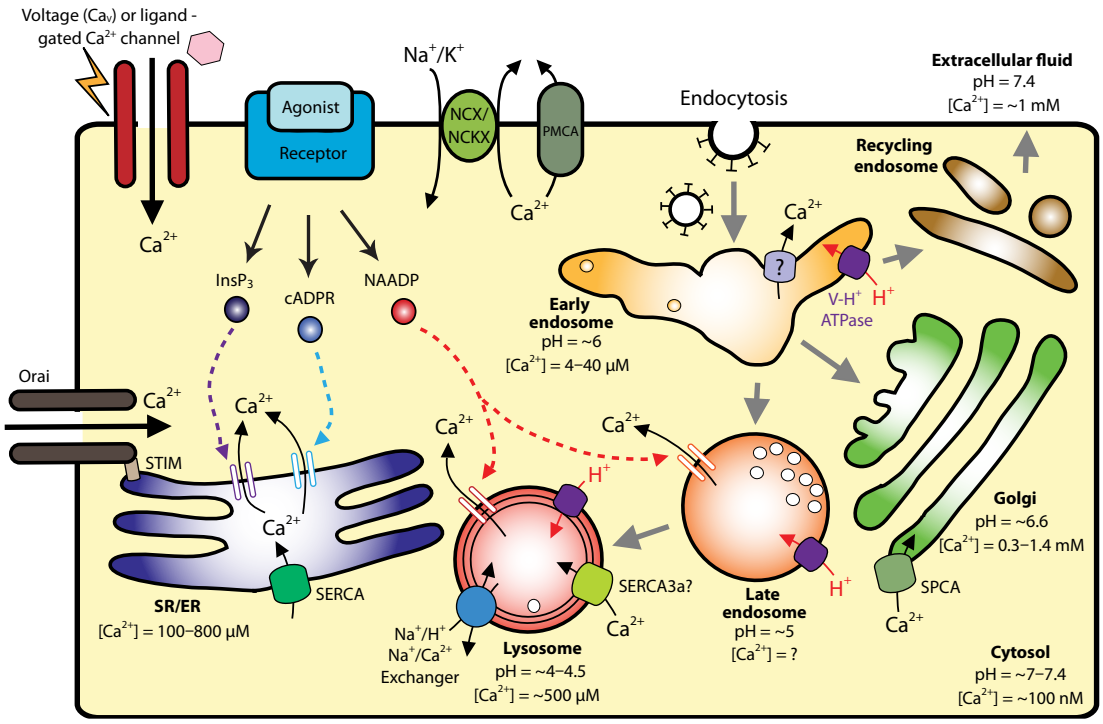

Figure 1.1: Schematic representation of intracellular Ca^{2+} signalling regulations. Ca^{2+} can enter the cytosol from the extracellular fluid via plasma membrane ion channels, or from intracellular Ca^{2+}-sequestering stores such as the ER or the acidic Ca^{2+} stores in response to second messengers: $InsP_3$, cADPR and NAADP. Ca^{2+} released to the cytosol is then exchanged, or actively transported back to the Ca^{2+} stores or the extracellular fluid to restore a relatively low cytosolic concentration of Ca^{2+}.

Mitochondria can also sequester Ca^{2+} but in a different manner to that of the ER or the acid stores. Ca^{2+} uptake across the inner mitochondrial membrane has been reported to be via the mitochondrial Ca^{2+} uniporter (MCU) [21, 258]. MCU has a high selectivity for Ca^{2+} [140] and that Ca^{2+} uptake occurs when the Ca^{2+} concentration is >200 nM [123]. Under physiological conditions, such concentrations are observed at the local Ca^{2+} releasing sites such as the ER or at the Ca^{2+} influx site at the plasma membrane [258, 266]. However, mitochondrial Ca^{2+} sequestration does not result in a long term Ca^{2+} storage. Rapid accumulation of Ca^{2+} through the MCU is balanced by being slowly transported out into cytosol via a Na^+/Ca^{2+} exchanger, recently identified as NCLX [123, 208, 233, 266].

1.2.2 Regulation of intracellular Ca^{2+} concentration

1.2.2.1 Activation of Ca^{2+} signalling

Ca^{2+} signalling can be initiated by one of two mechanisms: Ca^{2+} influx from the extracellular fluid, or Ca^{2+} release from intracellular Ca^{2+}-sequestering stores. Ca^{2+} can enter directly from the extracellular fluid down the electrochemical gradient via opening of the voltage- or ligand-gated channels (such as the P2X receptor), or by Ca^{2+}-release-activated Ca^{2+} channels (CRAC channels, which are identified as Orai channels [234]) on the plasma membrane [29].

Ca^{2+} release can be triggered by multiple messengers, such as inositol-1,4,5-trisphosphate ($InsP_3$) and cyclic adenosine diphosphoribose (cADPR) from the ER [28, 29], and by nicotinic acid adenine dinucleotide phosphate (NAADP) from the acidic stores [70, 293] (Figure 1.1). Sphingosine-1-phosphate (S1P) has also been reported to trigger Ca^{2+} release from the ER [29]. Depending on the agonist, specific secondary messenger(s) are recruited to elicit Ca^{2+} release: for instance, NAADP operates in an agonist-specific manner in various cell types to release Ca^{2+} from the acidic stores: for example, cholecystokinin (CCK) and not acetylcholine (ACh) in pancreatic acinar cells [293], glucose and not ACh in pancreatic beta cells [293], and thrombin and not ADP nor vasopressin in human platelets [169].

In skeletal muscle cells, Ca^{2+} is released from the SR by membrane depolarization, as the ryanodine receptor (RyR1) is mechanically coupled to voltage-gated Ca^{2+} channels ($Ca_V1.1$) [149]. Most strikingly, Ca^{2+} can regulate the Ca^{2+} release itself via the Ca^{2+}-sensitive Ca^{2+} channels such as $InsP_3$ receptors ($InsP_3Rs$) and ryanodine receptors (RyRs) on the ER [29].

Sustainable Ca^{2+} signals can lead to specific physiological responses, such as gene expression. The finite capacity of the Ca^{2+} stores imposes a limit on the amount of Ca^{2+} that can be released. To refill the Ca^{2+} stores, and thus generate sustainable Ca^{2+} signals, there must be coordination between local intracellular Ca^{2+} release and the extracellular Ca^{2+} entry. Indeed, a reduction of Ca^{2+} concentration in the ER leads to store-operated Ca^{2+} entry. Two crucial players are involved in store-operated Ca^{2+} entry: stromal interaction molecules (STIM1 and STIM2), and members of the Orai

family (Orai1, Orai2, and Orai3). When STIM, the ER Ca^{2+} sensor, detects a drop in the ER [Ca^{2+}], it aggregates and rearranges its position juxtaposed to the plasma membrane to activate Orais [160, 253].

1.2.2.2 Termination of Ca^{2+} signalling

In order to maintain homeostasis, once a Ca^{2+} signal has been activated, it must also be terminated. There are two main Ca^{2+} extrusion mechanisms that maintain basal cytosolic Ca^{2+} concentration: pumps and exchangers (Figure 1.1). Pumps, which actively transport Ca^{2+}, and their destinations include the plasma membrane Ca^{2+} ATPase (PMCA) to the extracellular fluid, sarcoendoplasmic reticular Ca^{2+} ATPase (SERCA) into the SR/ER, secretory pathway Ca^{2+}-ATPase (SPCA) into the Golgi apparatus and specific secretory vesicles, mitochondrial Ca^{2+} uniporter into mitochondria, and perhaps SERCA3a into lysosomes [123, 166, 216]. Exchangers effectively replace Ca^{2+} ions with other ions. For example, at the plasma membrane, Na^+/Ca^{2+} exchangers (NCX; SLC8A1–3) exchange one Ca^{2+} ion for three Na^+ ions, and the Na^+/Ca^{2+}-K^+ exchangers (NCKX; SLC24A1–5) exchange one Ca^{2+} for four Na^+ ions while cotransporting one K^+ ion. In the acidic Ca^{2+} stores, it is believed that Ca^{2+} ions are exchanged for Na^+ ions by Na^+/Ca^{2+} exchanger in cooperation with a Na^+/H^+ exchanger [72, 166, 216]. H^+/Ca^{2+} exchangers are unlikely to play a role in mammals as their genes are absent from the genomes [166, 216].

1.3 $InsP_3$-gated Ca^{2+} signalling

$InsP_3$ was the first Ca^{2+} mobilizing messenger to be identified (in 1983), and is established as the archetypal Ca^{2+} mobilizing messenger [259]. It therefore serves as a model for this family, which now includes cADPR and NAADP. $InsP_3$ is generated by activation of different isoforms of membrane-bound phospholipase C (PLC) by a variety of different mechanisms (Table 1.1) [28]. Activated PLC cleaves phosphatidylinositol 4,5-bisphosphate (PIP_2) into water-soluble $InsP_3$ and membrane-bound diacylglycerol (DAG). Binding of $InsP_3$ to the $InsP_3$ receptor ($InsP_3R$) releases Ca^{2+}, mainly from the ER where the highest concentration of $InsP_3Rs$ is found [49, 265]. However, other studies have also reported release from the Golgi apparatus, the nuclear envelope and secretory vesicles (although that latter is debated) [265, 267]. Surprisingly, in addition to the Ca^{2+} release from the intracellular stores, $InsP_3$ has also been implicated in Ca^{2+} entry across the cell membrane, possibly directly through plasma membrane $InsP_3Rs$ [83, 84] or indirectly via mechanical coupling of the $InsP_3Rs$ with the plasma membrane hTrp3 Ca^{2+} channels [141].

PLC isoform	PLC activation mechanism
PLCβ	G protein-coupled receptors (GPCR; $G_{q/11}$) activation
PLCγ	Receptor tyrosine kinases (TKR) activation
PLCδ	An increased Ca^{2+} concentration
PLCε	Ras activation
PLCζ	in sperm before injected into the egg to activate egg fertilization

Table 1.1: $InsP_3$ is generated by activation of various PLC isoforms via different mechanisms.

1.3.1 $InsP_3$ receptors ($InsP_3Rs$)

There are three subtypes of $InsP_3R$ in mammals: $InsP_3R1$, $InsP_3R2$ and $InsP_3R3$, and these share 60–80% amino acid similarity [265]. Of these, at least two are co-expressed at significant levels in almost all tissues and cell lines tested: $InsP_3R1$ is predominantly expressed in the cerebellum [180, 201, 265], $InsP_3R2$ in the brain, skeletal muscle, heart, and kidney, and $InsP_3R3$ in pancreatic β-cells, gastrointestinal tract, testis, and thymus [266]. The three subtypes were suggested to have distinct functions as they exhibit different affinities for $InsP_3$: $InsP_3R2$ being the highest (K_d = 14 nM), then $InsP_3R1$ (K_d = 50 nM), and finally $InsP_3R3$ (K_d = 160 nM) [130, 267].

1.3.1.1 Targeting of $InsP_3Rs$

$InsP_3Rs$ are directed to the ER by cotranslational protein targeting, in which $InsP_3Rs$ are initially synthesized on cytosolic ribosomes, then the $InsP_3Rs$-ribosome complexes is translocated to the ER where protein synthesis, folding, and modification is completed. The first two transmembrane domains (TMD 1 and 2) of $InsP_3R1$ have hydrophobic residues that are critical for targeting $InsP_3Rs$ to the ER [209]. Unlike other ER proteins that normally contain cytosolic diarginine motifs (XXRR; X stands for any amino acid residue) or C-terminal dilysine motifs (KKXX or KXKXX), the majority of the $InsP_3R1s$ are targeted to the ER through the action of TMD pairs. In contrast, all TMD pairs (TMD 1–2, 3–4, and 5–6) are important for retaining $InsP_3R1$ in the ER or retrieve them from the Golgi apparatus. It remains unclear as to how some $InsP_3Rs$ escape the retention and retrieval mechanisms to assemble on the other organelles (mentioned above) where $InsP_3$-induced Ca^{2+} release was observed [266].

1.3.1.2 Regulations of $InsP_3Rs$

Interestingly, $InsP_3R$-gating not only requires $InsP_3$ but also cytosolic Ca^{2+}. All three subtypes are regulated by cytosolic Ca^{2+} concentration [267]. This regulation is biphasic and follows a bell-shaped curve: an increase in Ca^{2+} concentration (to 100–300 nM) amplifies the $InsP_3$-evoked responses (probability of an open channel) to a point where the high Ca^{2+} cytosol concentration (>300 nM) becomes inhibitory [28, 267]. This sensitivity of $InsP_3Rs$ to $[Ca^{2+}]$ is central to the role of $InsP_3R$ in amplifying local Ca^{2+} signals to global Ca^{2+} waves by CICR (described later in Section 1.3.2).

Two Ca^{2+} binding sites, one stimulatory and one inhibitory, have been proposed to account for the $InsP_3R$ regulations. Binding of $InsP_3$ to its receptor modulates its Ca^{2+} sensitivity as the inhibitory site becomes masked, and this allows Ca^{2+} to bind at the stimulatory site, which results in channel opening (Figure 1.2) [29, 267]. The identity of the Ca^{2+} binding sites, however, is still unclear [96]. The stimulatory site has been suggested to reside within $InsP_3R$, whereas an accessory protein might be involved for the inhibitory site [267].

Physiologically, functional $InsP_3Rs$ assemble as large tetramers (∼1200 kDa) as determined by single-particle analysis in electron microscopy [77]. $InsP_3Rs$ may form

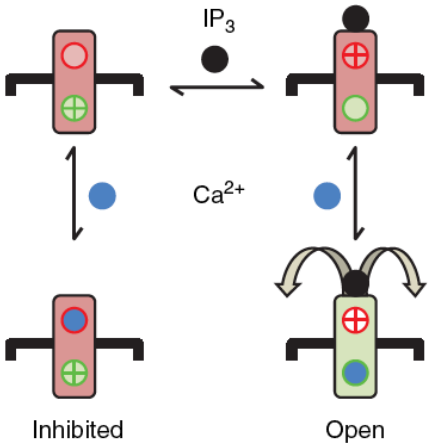

Figure 1.2: Regulation of InsP$_3$R by cytosolic Ca^{2+}. There are two Ca^{2+}-binding sites on the InsP$_3$R, one stimulatory (green) and one inhibitory (red). Binding of InsP$_3$ (black circle) to InsP$_3$R masks the inhibitory site and allows Ca^{2+} (blue circle) to bind to the stimulatory site. Binding of Ca^{2+} to the stimulatory site activates channel opening. The diagram is taken from [267].

homo- or heterotetrametic channels from identical or different InsP$_3$ subtypes or their splice variants [267]. The current consensus is that at least two InsP$_3$ binding sites (but not all four sites) need to be occupied for channel opening [267]. Furthermore, InsP$_3$ and Ca^{2+} are not the sole factors that regulate InsP$_3$Rs. G-protein subunits ($\beta\gamma$) and a Ca^{2+} binding protein (CaBP1) have also been reported to play a role in InsP$_3$R activation, while another Ca^{2+} binding protein calmodulin (CaM), causes in InsP$_3$R inhibition [267]. Additionally, post-translational modifications such as phosphorylation/dephosphorylation [279] and *O*-linked glycosylation of InsP$_3$Rs [34, 238] can further regulate the Ca^{2+} release activity of InsP$_3$Rs.

1.3.2 InsP$_3$-gated Ca^{2+} release from local to global

A crucial factor in expanding the versatility of Ca^{2+} signals is the spatial organization of local Ca^{2+} release; and this depends essentially on the subcellular distribution of the receptors. As mentioned, a handful of InsP$_3$Rs that successfully evaded the ER retention and assembled on the plasma membrane; these profoundly contribute to agonist-mediated Ca^{2+} entry [266]. However, the majority of InsP$_3$Rs are localized on the ER [49, 265] where a hierarchy of elementary events is initiated.

An initial low-level stimulus opens a single InsP$_3$R channel on the SR/ER; this results

in "blips": the release of localised short (<130 ms) and small (<40 nM) Ca^{2+} release. However, it is important to note that $InsP_3Rs$ are not homogeneously distributed in the ER, but aggregate in clusters [265]. At a higher elementary level, the opening of $InsP_3R$ clusters leads to "puffs": a higher (50–600 nM) and slightly longer (∼1 s) local Ca^{2+} release [29, 266]. Puffs normally extend for only a few micrometres. As the intensity of stimulus (and hence $InsP_3$ concentration) increases, puffs occur more frequently; and because $InsP_3Rs$ are sensitive to Ca^{2+}, puffs recruit neighbouring $InsP_3Rs$ to release more Ca^{2+}. This results in a regenerative process of global intracellular Ca^{2+} waves (i.e. CICR). The intracellular waves expand into intercellular communication when the waves diffuse further through the gap junctions and amplify connected cells (Figure 1.3) [29].

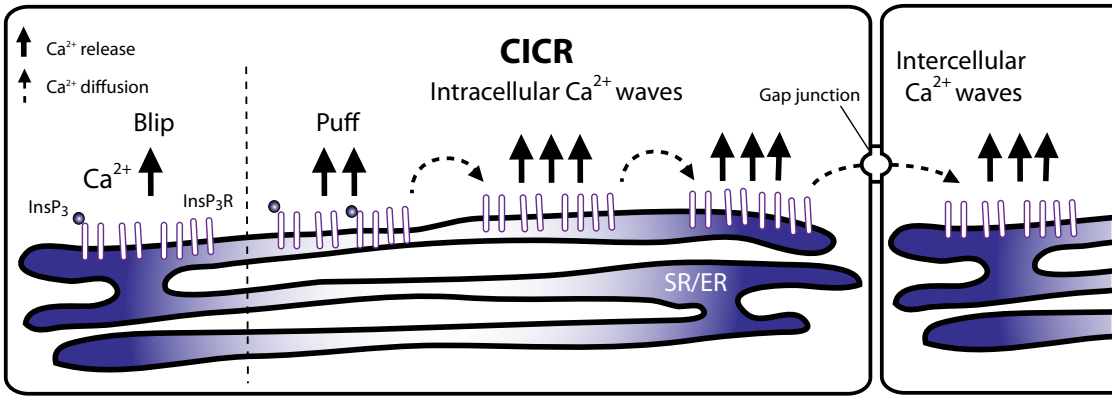

Figure 1.3: Schematic representation of the hierarchical recruitment of elementary Ca^{2+} release mediated by $InsP_3$.

In pancreatic acinar cells, $InsP_3Rs$ are clustered in the apical regions [225]. This probably explains why the Ca^{2+} signal is initiated in the apical pole where exocytosis occurs [225] even though hormone and neurotransmitter receptors are located in the basolateral pole. The close proximity of $InsP_3R$ on the ER to other organelles, such as mitochondria [239] and the nucleus [163], causes neighbouring organelles to be exposed to a local high Ca^{2+} concentration. This exposure results in a large amount of Ca^{2+} being taken up into mitochondria. This can immediately adjust the mitochondrial energy metabolism (increasing ATP production) to meet the requirement of the cell [29, 239]. Mitochondria also act as Ca^{2+} 'buffers' to regulate and shape the local signalling by transiently uptake of high levels of Ca^{2+} which otherwise might trigger amplification [266]. As Ca^{2+} is dissipated slowly from the mitochondria, this thereby provides a localized

Ca^{2+} source to recharge the SR/ER Ca^{2+} stores [206]. For the nucleus, puffs have been reported to increase the nucleoplasmic Ca^{2+} concentration, which is known to regulate functions such as transcription [163]. Thus, the nucleoplasmic Ca^{2+} concentration may be increased without global changes in cytosolic Ca^{2+} concentration, further mitigating side-effects such as protease activation or apoptosis that are activated by higher Ca^{2+} concentrations [163].

In addition to spatial organization of $InsP_3Rs$, other crucial factors such as expression level, post-translational modifications (e.g. glycosylation) and the accessory proteins can also tune the signals to generate specific cellular processes and further expand the versatility of Ca^{2+} signalling network initiated by $InsP_3$ [267].

1.3.3 $InsP_3R$ knockout (KO) mice

To investigate the physiological roles of individual endogenous $InsP_3R$, and to identify the causal relationships between $InsP_3R$ and human diseases, individual single $InsP_3Rs$ genes were deleted in mice by gene targeting via homologous recombination [99, 181]. The $InsP_3R1$ knockout (KO) proved to be either lethal *in utero*, suggesting a role of $InsP_3R1$ in embryonic development, or the newborns suffered from severe neurological disorders such as ataxia and epilepsy [181], which is consistent with a high $InsP_3R1$ cerebellar expression (Section 1.3.1).

Interestingly, $InsP_3R2$ and $InsP_3R3$ single KOs were viable, and did not appear to exhibit any significant abnormal phenotypes [99]. However, severe phenotypic abnormalities were observed when both $InsP_3R2$ and $InsP_3R3$ were abolished: individuals with $InsP_3R2$/$InsP_3R3$ double knockout (DKO) suffered from exocrine dysfunctions [99]. Additionally, the amount of saliva produced in salivary gland acinar cells was significantly reduced and the level of digestive enzymes (amylase, lipase, and trypsinogen) was completely abolished in pancreatic acinar cells. Similarly, the level of secretagogue-induced Ca^{2+} release was significantly reduced in salivary gland acinar cells (via carbacol) and completely abolished in pancreatic acinar cells (via ACh and CCK) [99]. This suggests that functional $InsP_3R2$ and $InsP_3R3$ are crucial for secretagogue-induced Ca^{2+} release that leads to the subsequent digestive enzyme secretion in exocrine cells.

1.4 cADPR-mediated Ca^{2+} signalling

Approximately 10 years after the discovery of $InsP_3$, another Ca^{2+} mobilizing messenger was identified: cADPR, an enzymatic metabolite of the pyridine nucleotide, nicotinamide adenine dinucleotide (NAD^+) [73, 154]. In sea urchin egg homogenate, $InsP_3$, cADPR, and NAADP (discussion in Section 1.5) can independently induce homologous desensitization to inhibit further Ca^{2+} release evoked by itself but not by other messengers (Figure 1.4) [73, 80, 106, 153, 154]. This phenomena was observed independent of the order in which the messengers was added [153], suggesting that they act on different receptors.

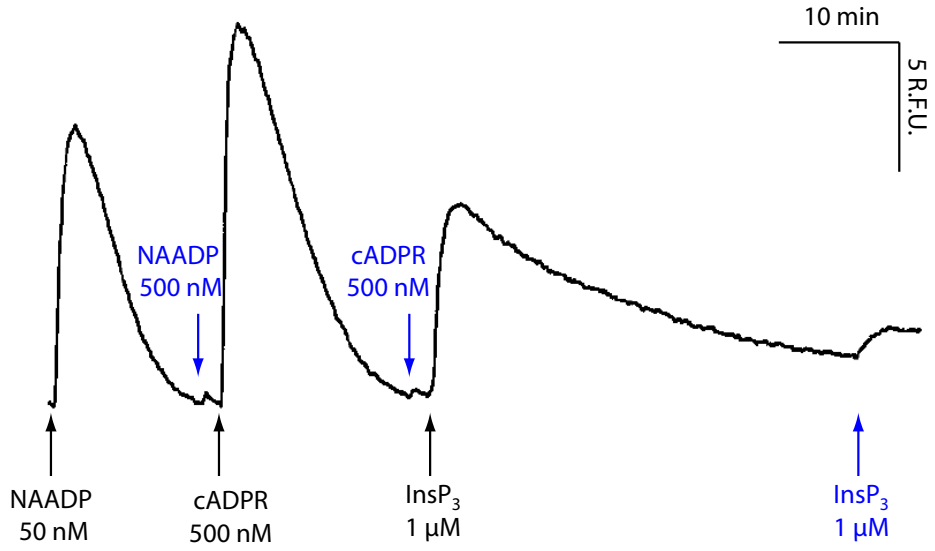

Figure 1.4: Homologous desensitization of Ca^{2+} release induced by NAADP, cADPR, or $InsP_3$ in sea urchin egg homogenate. The subsequent addition of the same agonist (blue arrows) failed to release further Ca^{2+}, however, the release by the other Ca^{2+} mobilising messengers was not affected. This suggests that NAADP, cADPR and $InsP_3$ act on different receptors. The trace is adapted from [106].

Since its discovery, cADPR has been shown to induce Ca^{2+} release from the SR/ER in many cells types of various species from plants to mammals [150]. cADPR-mediated Ca^{2+} release via activation of the ryanodine receptor (RyR) was first reported in sea urchin egg homogenates [102]. Since then, the concept that cADPR as an endogenous regulator of RyRs has been widely accepted, although the molecular mechanisms by which cADPR activates the channel remain disputed.

1.4.1 cADPR synthesis

cADPR is synthesized by cyclization of NAD^+ by ADP-ribosyl cyclases (ARCs) (Figure 1.5) [152]. ARCs was first purified from *Aplysia californica* ovotestis [118]. Two mammalian homologues of ARCs have subsequently been found, based on sequence homology: CD38 [256] and CD157 [129].

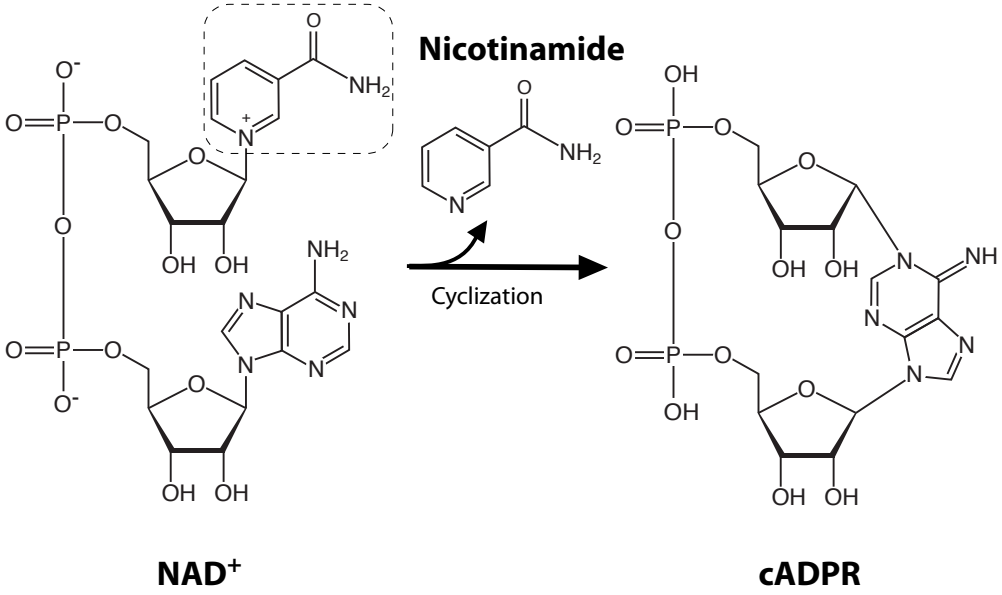

Figure 1.5: Synthesis of cADPR by cyclization of NAD^+.

Interestingly, while it was known that *Aplysia* ARC is cytosolic, CD38 and CD157 were first discovered at the plasma membrane, with an extracellular-facing enzymatic site. The paradoxical location of the synthesis site of cADPR (outside the cell) raised questions as to how cADPR releases Ca^{2+} from intracellular stores [94]. Later studies revealed that in addition to the plasma membrane, CD38 is also present on intracellular organelles such as mitochondria, SR/ER, nuclei [3], and early endosomes [74].

Inspired by its homology to *Aplysia* ARC (∼24% sequence identity), soluble CD38 was purified and subsequently shown to be able to synthesize cADPR enzymatically from NAD^+ [124]. This was the first evidence that CD38 is a cADPR synthase. Later studies using CD38 KO mice further confirmed this finding: in CD38 KO mice, there was no cADPR in various tissue types including uterus, heart, liver, kidney, and spleen. Tissue from these CD38 KO mice failed to perform *in vitro* the cyclization reaction [255]. Furthermore, CCK-induced cADPR production in pancreatic acinar cells was undetectable

in CD38 KO cells [74]. These studies provided persuasive evidence that clearly demonstrate an essential role of CD38 in cADPR synthesis.

In line with the expression profile of mammalian ARCs, a recent study showed that endogenous sea urchin ARCs (α, β, and γ) are localized both ectocellularly and intracellularly in sea urchin eggs. However, the localization was isoform-specific; ARCα is localized ectocellularly whereas both ARCβ and ARCγ are localized intracellularly, specifically in the lumen of acidic organelle (cortical granules) [81]. The intracellular localization is supported by another study using heterologous expression of sea urchin ARC1 (the homologue of ARCβ) in HEK cells and *Xenopus laevis* eggs, however, in a different organelle (ER) [68]. The apparently conflicting result might be attributable to the expression system. Highly expressed proteins are known to be possibly retained in the ER (a cortical granule residing protein, SFE9, has been shown to be retained in the ER when heterologously expressed) [81].

Sea urchin ARCs - either recombinant, endogenous [81], or heterologously expressed [68] - showed compartmentalized enzymatic activity at pH 7. The enzymatic activity was determined either by measuring the levels of cADPR and ADPR [81], or by assaying the cyclization activity [68]. A further study demonstrated that sea urchin ARC has greater activity at pH 5, which corresponds to the luminal pH of the cortical granules [81]. In light of this finding, a recent study revealed that upon agonist (CCK) stimulation, CD38 is endocytosed from the plasma membrane into the cells, possibly in the more acidic vesicles. The acidic environment may thus provide CD38 the optimal conditions to synthesis cADPR [74].

Complex autocrine and paracrine models have been proposed for cADPR-induced Ca^{2+} signalling through the actions of connexin 43 hemichannels, which transport NAD^{+}, and through nucleotide transporters for cADPR [94]. Together with the new evidence from sea urchin ARCs, it was speculated that the intracellular mammalian ARCs are perhaps more significant than ectocellular ARCs in generating cADPR. The current hypothetical scheme is that in response to stimuli, cADPR is synthesized in the acidic stores, and then transported out into the cytosol via nucleotide transporters where it subsequently releases Ca^{2+} from the intracellular stores (Figure 1.6) [81, 94].

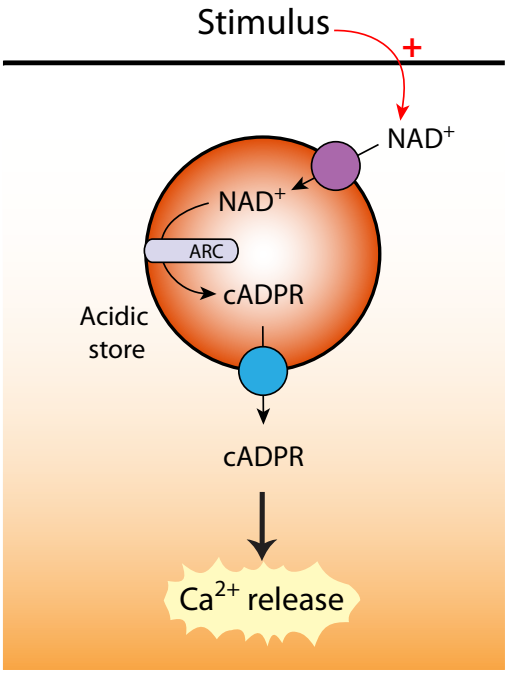

Figure 1.6: Hypothetical scheme of cADPR synthesis. Upon stimulation, NAD^+ is transported into the acidic store possibly via connexin 43 hemichannels (purple circle). NAD^+ is enzymatically converted by luminal ARCs into cADPR, which is then transported out into cytosol by nucleotide transporters (blue circle). Consequently, cADPR elicits Ca^{2+} release via activation of RyRs. The scheme is adapted from [81, 94].

1.4.2 Ryanodine receptors (RyRs)

RyRs are named after ryanodine, a plant alkaloid that exhibits high affinity for RyRs. Ryanodine activates RyRs in the nM range, locking them in an open subconductance state, and inhibits them at >100 μM [149]. The three of mammalian RyR isoforms (RyR1, RyR2 and RyR3) share ~70% amino acid sequence identity. RyRs are widely expressed in different tissue types with RyR1 predominantly in skeletal, and RyR2 in cardiac muscle [93]. RyR3 was previously termed the "brain isoform" as it was initially found in the brain. However, since then, RyR3 has been found in many other tissues including skeletal muscles, lung, kidney, ileum, spleen, stomach, and urinary bladder [149].

1.4.2.1 Targeting of RyRs

Like $InsP_3Rs$, RyRs have been demonstrated to primarily localize in the SR/ER. Additionally, localization has also been observed in the Golgi apparatus, lysosomes, secretory vesicles, perinuclear, and the plasma membrane [125, 139, 158, 183, 189, 246]. Furthermore, although RyR1 does not have cytosolic C-terminal dilysine motifs and its N-terminal

diarginine motifs are possibly ineffective, its TMDs are responsible for mediating ER retaining and retrieving. RyR1 has six TMDs and, specifically, the first and the last pairs of TMD (TMD 1–2 and 5–6) are required to effectively retain it in the ER. Additionally, only the first TMD is required to target RyR1 effectively to the ER [187].

1.4.2.2 Regulations of RyRs

To function, RyRs form homotetrameric channels (>2 MDa) - the largest known ion channels, even larger than $InsP_3R$ tetramers [149]. In addition to cADPR, RyRs are regulated by a large number of proteins such as voltage-gated Ca^{2+} channels ($Ca_V1.1$, $Ca_V1.2$), CaM, calsequestrin (Ca^{2+} buffer in the SR), FK506-Binding Proteins 12 and 12.6 (FKBP12 and FKBP12.6 also known as calstabin1 and 2, respectively), as well as ions (Ca^{2+}, Mg^{2+}, and ATP), phosphorylation by protein kinases (PKA, and CAMKII), and by reactive oxygen and nitrogen species [149]. Similarly to $InsP_3Rs$, RyRs are regulated by Ca^{2+} in a bell-shaped manner, although over a different range of concentrations. RyRs are activated when cytosolic Ca^{2+} concentration increases to the $\sim\mu$M range and inhibited when the concentration reaches the ~mM range [29, 184, 149]. Regulation by Ca^{2+} qualifies RyRs as a crucial component in CICR just like $InsP_3$ (see Section 1.4.3).

Since RyRs release Ca^{2+} from intracellular stores and are predominantly expressed in myocytes, it is unsurprising to discover that RyR1 and RyR2 are the key players in excitation-contraction (E-C) coupling. In skeletal muscle, action potentials lead to Ca^{2+} release from the SR via RyR1 as a result of mechanical coupling of RyR1 and $Ca_V1.1$ in transverse tubules (t-tubules). In contrast, in cardiac muscle, the SR Ca^{2+} release is via CICR of RyR2 attributed to the Ca^{2+} influx through $Ca_V1.2$ channel in response to membrane depolarization. An increase in cytosolic Ca^{2+} results in muscle contraction [30, 146].

It is well established that cADPR activates the RyRs by sensitising RyRs to cytosolic Ca^{2+}: RyRs are therefore more likely to be activated in response to events such as CICR [101]. The molecular mechanism of cADPR-induced Ca^{2+} sensitization is controversial, and two models have been proposed: either indirect binding of cADPR to a protein (e.g. FKBP12.6) [202, 304] that is either tightly bound to RyRs or translocates to interact with RyRs after binding to cADPR; or an increase in Ca^{2+} concentration in the

SR/ER (a mechanism known to sensitise the RyRs to cytosolic Ca^{2+}) by cADPR, possibly by promoting Ca^{2+} uptake by SERCA directly, or indirectly through an intermediate protein [295]. These conflicting models suggest that regulation of RyRs by cADPR is perhaps by more than one mechanism, and that regulation is likely to vary depending on the RyR isoform (due to association with different proteins) and cell type [284].

1.4.3 Ca^{2+} release via RyRs from local to global

Like $InsP_3Rs$ (see Section 1.3.2), the elementary Ca^{2+}-release event had been studied for RyRs. At the fundamental level, low level stimulus opens single RyRs on the SR/ER and releases "quarks": local small (∼37 nM) and short Ca^{2+} release [162]. At higher levels, opening of RyR clusters leads to "sparks": larger (∼300 nM) and slightly longer local Ca^{2+} releases [65]. Sparks, like puffs, are limited to ∼2 μm [64]. Since RyRs are sensitive to Ca^{2+}, elementary release recruits neighbouring RyRs by CICR in a saltatoric manner to initiate a regenerative process of global Ca^{2+} wave propagation [28, 64]. As mentioned (Section 1.3.2), the intracellular Ca^{2+} waves can spread intercellularly to connected cells via the gap junctions (Figure 1.7) [29].

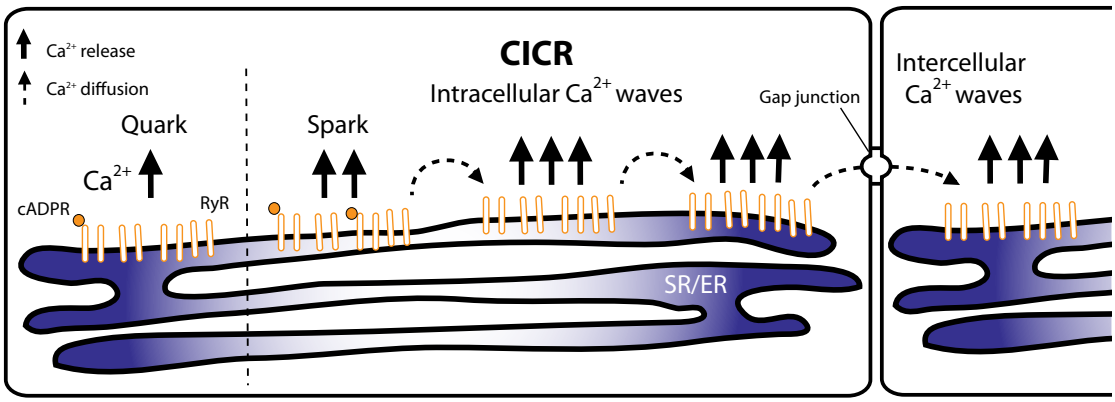

Figure 1.7: Schematic representation of the hierarchical recruitment of elementary Ca^{2+} release via RyRs.

Sparks, like puffs, provide local Ca^{2+} to regulate many important Ca^{2+}-dependent processes. Sparks allow Ca^{2+} to be taken up by the neighbouring mitochondria to elicit "Ca^{2+} marks": small Ca^{2+} signals in the mitochondrial matrix. Marks may thereby activate mitochondrial Ca^{2+}-sensitive proteins to mediate mitochondrial functions such

as energy metabolism and apoptosis [29, 206]. Furthermore, sparks have been reported to activate the large-conductance Ca^{2+}-sensitive K^+ channels (BK channels) in smooth muscle cells. The opening of BK channels hyperpolarizes the membrane and leads to relaxation [45].

1.4.4 RyR mutants and human diseases

KO mice have been used to investigate the physiological roles of RyRs. Mice with abrogation of the RyR1 (RyR1 KO) died perinatally with abnormalities in skeletal muscle [261]. In the skeletal muscle, electrical stimulation-evoked contraction was abolished, and caffeine-induced contraction was diminished. This suggests that RyR1 is essential for E-C coupling in skeletal muscle.

Mice with RyR2 abrogation (RyR2 KO) died in embryonic day 10 with abnormalities in the heart [263]. In RyR2 mutant cardiac myocytes, caffeine-evoked Ca^{2+} release via RyRs was completely abolished [263], however, the spontaneous rhythmic contractions were not affected. This suggests that RyR2 is not essential for E-C coupling in early embryonic cardiac myocytes, RyR2 might be more important as a Ca^{2+} leak channel to maintain Ca^{2+} homeostasis in the developing SR [263].

In contrast, RyR3 KO mice were both viable and fertile, and showed no gross abnormalities [31, 262]. Various studies have reported abnormalities in RyR3 KO that are related to functions of the hippocampus and striatum, such as long-term potentiation and depression. Additionally, altered behavioural phenotypes were observed, specifically in locomotion and social behaviour [182, 262].

Consistent with its predominant expression and the data from the single KO studies, RyR mutations are well unambiguously linked with a number of debilitating human myopathies. RyR1 mutations are associated with malignant hyperthermia (MH), neuromuscular disease with uniform type 1 fibres, centre core disease (CCD), multiminicore disease (MmD), and atypical periodic paralyses. Additionally, RyR2 mutations are associated with catecholaminergic polymorphic ventricular tachycardia (CPVT) and arhythmogenic right ventricular dysplasia type 2 (ARVD2) [149, 175].

The proposed mechanism for the etiology of these diseases is that RyR mutants are hypersensitive due to a reduced threshold for store overload-induced Ca^{2+} release, the

mechanism by which luminal Ca^{2+} triggers rapid Ca^{2+} release from the Ca^{2+} store when the store reaches a certain Ca^{2+} uptake threshold [175]. At rest, cells function normally when there is little or no Ca^{2+} spillover. However, even modest increases in store Ca^{2+} can trigger the release mechanism and this is responsible for severe clinical outcomes such as cardiac arrhythmia (RyR2 mutation) or muscle contracture (RyR1 mutation) [175]. The situation is exacerbated by certain drugs, such as halothane or caffeine that further lower the threshold, or catecholamine (via phosphorylated phospholamban) that increases free SR luminal Ca^{2+} level; in each case, the threshold is reached more readily [175].

1.5 NAADP-gated Ca^{2+} signalling

In the same landmark paper that described cADPR for the first time, an impurity of nicotinamide adenine dinucleotide phosphate ($NADP^+$) was also reported to release Ca^{2+} [73]. Ca^{2+} mobilization properties of this impurity were distinct in that it was able to release Ca^{2+} from $InsP_3$- and cADPR-densitized microsomes (Figure 1.4), suggesting that it acts on a different receptor from $InsP_3$ and cADPR. Moreover, it released Ca^{2+} from a store, separated by Percoll density gradients, different from those associated with $InsP_3$ and cADPR [73]. This impurity was subsequently identified as NAADP [153], and it has been shown to release Ca^{2+}, primarily from acidic stores, in many cell types and tissues of different species [103]. Interestingly, in some studies NAADP was shown to release Ca^{2+} also from the ER [110, 257], and from the nuclear envelope [108]. Concomitant with the Ca^{2+} release, NAADP was also found to alkalinize the acid stores [192, 193].

1.5.1 Characteristic of Ca^{2+} responses evoked by NAADP

Calcium signalling evoked by NAADP displays different properties from that by $InsP_3$ or cADPR in some important respects: (1) NAADP is the most effective messenger in that it elicits Ca^{2+} in the nM rather than the μM range (as for $InsP_3$ and cADPR) [57]; (2) NAADP predominantly mobilizes Ca^{2+} from acidic stores, unlike $InsP_3$ and cADPR that release from the SR/ER [40, 44, 70, 138, 189, 293]; (3) NAADP-evoked Ca^{2+} release is not regulated by cytosolic Ca^{2+} unlike $InsP_3$ or cADPR [15, 17]; and (4) pharmacologically, unlike $InsP_3$ or cADPR, NAADP-mediated Ca^{2+} release is completely abolished by NAADP self-inactivation [57, 153], drugs affecting acidic stores [138, 293], and Ned-19 (a specific antagonist for NAADP) [200]. Additionally, unlike $InsP_3$ or cADPR, NAADP-mediated Ca^{2+} response is significantly reduced by L-type Ca^{2+}-channel blockers or K^+-channel antagonists [107].

Two well known drugs that affect acidic stores, and thereby NAADP-evoked Ca^{2+} responses, are bafilomycin A1 and glycyl-L-phenylalanine-2-naphthylamide (GPN). Bafilomycin A1 collapses the proton gradient by inhibiting the proton uptake via the vacuolar (V)-type H^+-ATPase. Alkalization of acidic stores by bafilomycin A1 concomitantly inhibits Ca^{2+} uptake into the stores. GPN causes the rupture of lysosome-related organelles that contain cathepsin C. Cathepsin C hydrolyses the membrane-permeant GPN into

membrane-impermeant products (glycyl-phenylalanine and 2-naphthalamide), leading to increasing organelle osmotic pressure, and resulting in osmotically lysis [101].

NAADP activates and self-inactivates by two distinct mechanisms depending on species. In plants [199], sea urchin egg [106], rat brain [17], and rat liver [177], the NAADP concentration-response curve is sigmoidal (Figure 1.8A). Pretreatment of sub-threshold (non-Ca^{2+}-releasing; ~1 nM) concentrations of NAADP completely inhibit further NAADP-induced Ca^{2+} release. In contrast, in many other mammalian cells such as mouse pancreatic cells (acinar [57] and β [131, 178]), myoblast [5], human T-lymphocytes [24], cardiac myocyte [174], and tissues from bladder [90] or uterus [6], the NAADP concentration-response curve is bell-shaped where activation occurs in the nM range and inactivation in the μM range (Figure 1.8B) [194].

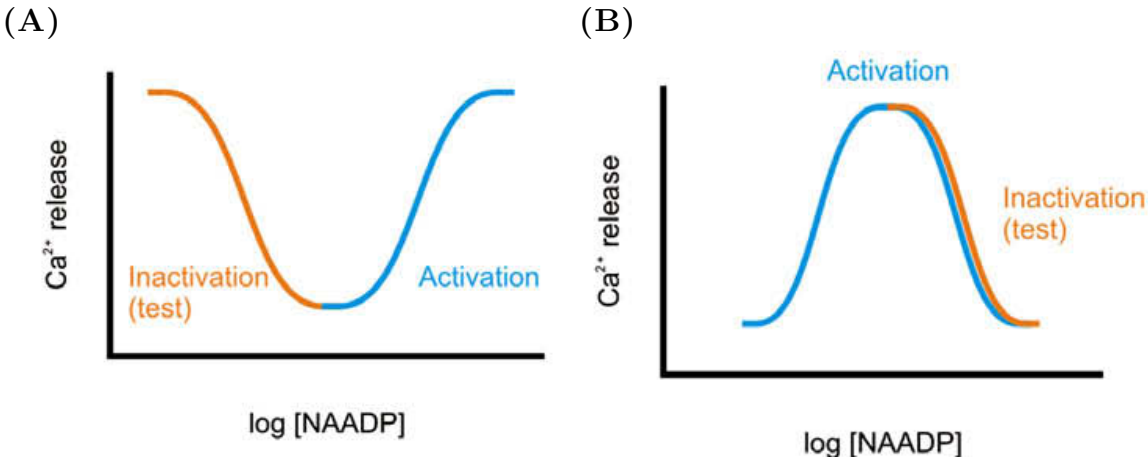

Figure 1.8: Schematics of NAADP activation and inactivation. (A) NAADP activation has a sigmoidal concentration-response curve (blue). In this scenario, pretreatment of subthreshold concentrations of NAADP inhibit Ca^{2+} response elicited by a maximal NAADP (test) concentration (orange). (B) NAADP activation has a bell-shaped concentration-response curve (blue). Here, pretreatment of supra-maximal NAADP concentrations inhibit Ca^{2+} response evoked by an optimal NAADP (test) concentration (orange). Schemes were taken from [194].

1.5.1.1 NAADP-gated Ca^{2+} release from local to global

Local NAADP-induced Ca^{2+} release from the acidic stores is likely to be important for effective lysosome biogenesis, in particular, vesicle fusion, and vesicle trafficking [165, 243]. The local Ca^{2+} release evoked by NAADP is thought to promote fusion of endosomes and lysosomes that are tethered in a trans-Soluble NSF Attachment Protein REceptor (SNARE) formation into hybrid endosome-lysosomes (Figure 1.9) [230, 243].

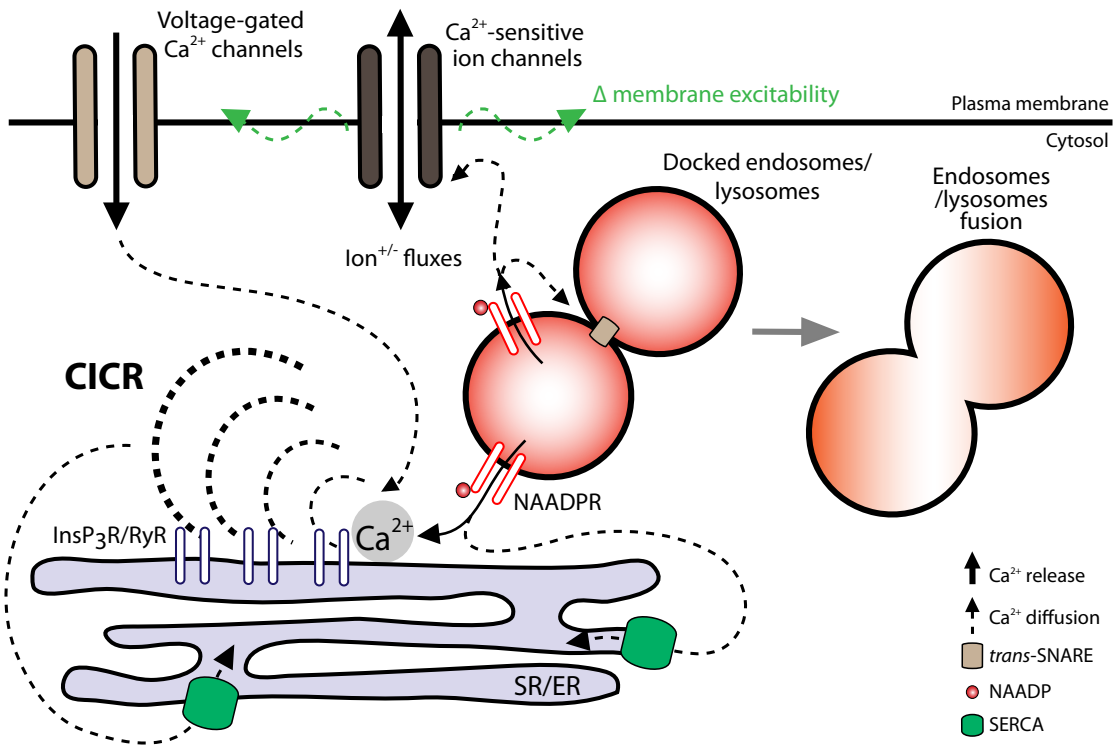

Figure 1.9: Local to global Ca^{2+} responses mediated by NAADP. Locally, the Ca^{2+} release from acidic stores is likely to be vital for normal functions of the endo-lysosomal system such as vesicle fusion in lysosomal biogenesis. Like the Ca^{2+} release from RyRs or $InsP_3Rs$, NAADP-mediated Ca^{2+} release near the plasma membrane might also contribute to modulation of the cellular excitability (excitable cells), or ion fluxes (non-excitable cells). Changes in the membrane potential could further activate, for example, voltage-gated Ca^{2+} channels, to allow Ca^{2+} influx and initiate a global response via CICR. Furthermore, local release evoked by NAADP could act as a trigger to directly initiate CICR from the SR/ER and generate global signals. Modified from [29, 103].

Furthermore, it is speculated that close proximity of the NAADP-gated channels to the plasma membrane Ca^{2+}-sensitive ion channels (Cl^-, Ca^{2+}, K^+, or other monovalent cations), because of the highly mobility of endo-lysosomal vesicles or endo-lysosomal vesicles residing near the plasma membrane, can fine-tune the ionic fluxes across the plasma membrane in non-excitable cells or modulate membrane excitability in excitable cells [103]. Indeed, local Ca^{2+} signals elicited by NAADP have been shown to cause depolarization by activation of the plasma membrane non-selective cation channels in neurons of rat medulla oblongata [43]. Changes in the membrane potential may further activate, for example, voltage-gated Ca^{2+} channels, to allow Ca^{2+} influx and initiate a global response via CICR amplification (Figure 1.9) [101, 103].

As mentioned, NAADP-evoked Ca^{2+} response is not regulated by cytosolic Ca^{2+} so, unlike $InsP_3$ and cADPR, the response cannot initiate CICR autocatalytically. NAADP is

hypothesized to generate global Ca^{2+} signals by CICR of the local Ca^{2+} release from the acidic stores. The local Ca^{2+} release evoked by NAADP acts a trigger to release further Ca^{2+} from the closely adjacent SR/ER by activating the neighbouring Ca^{2+}-sensitive $InsP_3Rs$ or RyRs, or by priming SR/ER stores (Figure 1.9) [36, 42, 52, 57, 69, 70, 138, 243, 293].

This 'trigger' hypothesis (Figure 1.9) helps to explain why in some systems NAADP-evoked Ca^{2+} response is attenuated by well-established inhibitors of $InsP_3R$, RyR, or ER SERCA [36, 40, 57, 69, 138]. In sea urchin eggs, NAADP evoked an initial transient response followed by Ca^{2+} oscillations. The initial transient is thought to prime CICR stores resulting in Ca^{2+} oscillations. The NAADP-evoked Ca^{2+} transient was attenuated but not completely abolished by thapsigargin, indicating that a part of Ca^{2+} release came from a thapsigargin-resistant store. However, NAADP-induced Ca^{2+} oscillations were completely abolished by a combination of $InsP_3R$ (heparin) and RyR (8-NH_2-cADPR) inhibitors, or by thapsigargin [69], suggesting that the oscillations were entirely dependent on the CICR Ca^{2+} stores. Furthermore, the amount of Ca^{2+} in the CICR Ca^{2+} stores increased after NAADP-evoked Ca^{2+} transient, suggesting that the Ca^{2+} released by NAADP had been taken up into the CICR Ca^{2+} stores. Uptake of Ca^{2+} might lead to store overload, thereby resulting in spontaneous Ca^{2+} release. This Ca^{2+} release can then be further taken up and released via $InsP_3Rs$ and RyRs [69].

In pulmonary arterial smooth muscle cells, NAADP evoked a distinct biphasic response, in which localized Ca^{2+} release was followed by global Ca^{2+} waves. Inhibitors of SERCA (thapsigargin) and RyRs (ryanodine; 20 μM), but not of $InsP_3Rs$ (xestospongin) were able to abolish the global Ca^{2+} waves but not the localized Ca^{2+} release [36]. On the other hand, bafilomycin A1 abolished responses in both phases [138]. This further supports the theory of a trigger mechanism mediated by NAADP.

1.5.2 NAADP synthesis

Currently, how NAADP is synthesized is not clearly understood. Several candidates have been proposed for this process, of which ARCs are perhaps the most convincing. ARCs are not limited to the cyclization reaction for synthesizing cADPR (described in Section 1.4.1), but they are multifunctional enzymes that can also synthesize NAADP, ADP ribose

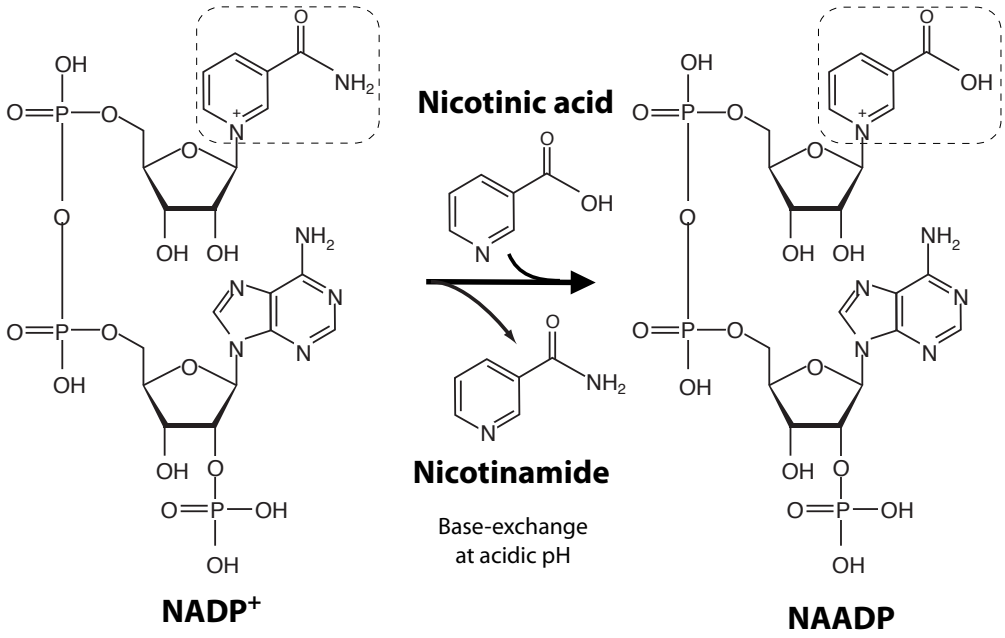

Figure 1.10: Synthesis of NAADP by the base-exchange reaction, which involves substituting the nicotinamide of $NADP^+$ with nicotinic acid at acidic pH.

(ADPR), dimeric ADP ribose ($ADPR_2$), nicotinic acid adenine dinucleotide (NAAD), and adenosine 5'-pyrophosphate-5'-adenosine (Ap2a) and its N1-isoadenosine and N3 isoadenosine derivatives [207]. To synthesize NAADP, ARCs catalyse the base-exchange reaction at acidic pH [2, 68] and substitute the nicotinamide of $NADP^+$ with nicotinic acid (Figure 1.10) [2].

To date, two mammalian ARCs have been found; CD38 and CD157 [151]. CD157 was shown to possess cyclase activity in the synthesis of cADPR [120]; however, no study has yet demonstrated its ability to synthesize NAADP. Although CD38 has been more extensively studied, whether it is an endogenous NAADP synthase remains controversial [207]. The most compelling evidence supporting the theory that CD38 is not the endogenous NAADP synthase came from a study by Soar *et al.* using CD38 KO mice [255]. The study showed that in myometrial cells, the basal and the histamine-induced NAADP levels were independent of CD38 and the base-exchange reaction [255]. On the other hand, in pancreatic acinar cells of CD38 KO mice, CD38 was shown to be the endogenous NAADP synthase. In pancreatic acinar cells, CCK-induced endogenous NAADP production was likely via the base-exchange reaction, and this production was completely absent in acinar cells of CD38 KO [74]. Thus, it appears that the involvement of CD38 as an NAADP

synthase may be tissue-specific.

Interestingly in both studies, there was still a basal level of endogenous NAADP in the unstimulated tissues or cells of CD38 KO [74, 255]. This suggests that there are other mammalian NAADP synthases that, unlike CD38, synthesize NAADP via another pathway independently of the base-exchange reaction [74, 255]. An NAADP synthase was found in sea urchin sperm: unlike sea urchin ARCs, it possesses enzymatic activity for the base-exchange but not for the cyclization reaction [282]. The presence of this NAADP synthase in additional to ARCs in sea urchin may support the idea that there are families of mammalian NAADP synthase besides CD38.

In the unstimulated rat AR42J pancreatic acinar cell line, CD38 is localized at the plasma membrane and intracellularly in the early endosomes. Upon CCK stimulation, CD38 in the plasma membrane is endocytosed inside the cell, likely into a more acidic environment (Section 1.4.1). Since the base-exchange reaction occurs at acidic pH, the endosomal localization thereby provides an optimal condition for synthesizing NAADP. It is possible that NAADP synthesis is similar to cADPR synthesis, and substrates such as nicotinic acid and $NADP^+$ are transported via nucleotide or other transporters into the ARC-residing (acidic) lumen. NAADP synthesized in the lumen is then transported out via transporters, consequently, it is able to activate neighbouring NAADP receptors [68, 81]. Thus, the interaction between the vesicles in the endo-lysosomal system may allow NAADP to be released near its target receptor [74].

1.5.3 NAADP binding

Studies of NAADP binding allow further insights and characterization of the NAADP receptor. NAADP binding was first characterized in sea urchin egg homogenates by radioligand binding. In sea urchin egg homogenates, NAADP binds with an equilibrium dissociation constant (K_d) of ~200 pM. The binding was unaffected by the presence of derivatives of NAADP (such as NADPH, NADP, NAD, and NAAD), other Ca^{2+} mobilizing messengers ($InsP_3$ and cADPR), or pH [1, 33, 213]. However, the binding was inhibited by high concentrations of NaCl [213]. Furthermore, the reversibility (dissociation) of the binding is dependent on the concentration of K^+: binding of NAADP to the receptor becomes irreversible at high K^+ concentrations [87].

NAADP binding to its receptor was reported to occur at multiple binding sites. Two sites have been proposed in sea urchin egg homogenates: a high-affinity inhibitory allosteric site at subthreshold NAADP concentrations (inactivation), and a low-affinity orthosteric site for the Ca^{2+} release (Figure 1.11) [87, 241]. The irreversibility of NAADP binding is likely related to the self-inactivation mechanism in this system where pretreatment of subthreshold concentrations of NAADP bind to the inhibitory site and inactivate further NAADP-elicited Ca^{2+} release.

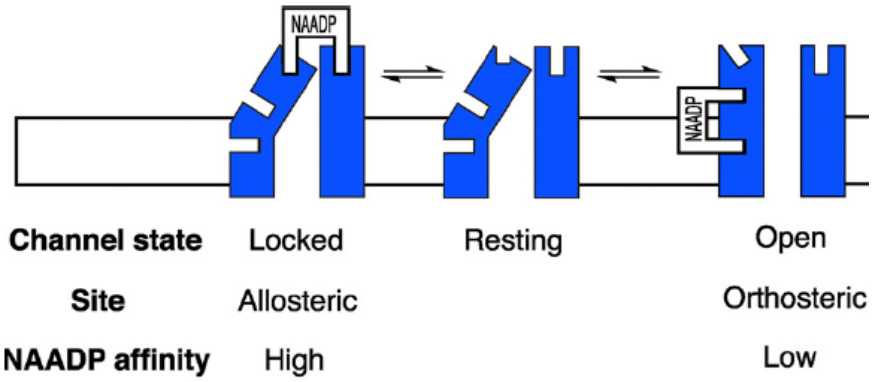

Figure 1.11: Schematic representation of NAADP binding to the high-affinity allosteric site or the low-affinity orthosteric site at the receptor in the sea urchin egg to mediate its function. The figure is taken from [241].

Like the case for sea urchin, NAADP binds to multiple sites in mammals [215]. Two-site binding, in which NAADP binds biphasically with nM and μM affinities, is the most convincing model [52, 178], although three-site binding in cardiac microsomes has also been reported [16]. Furthermore, consistent with the sea urchin studies, mammalian NAADP binding is unaffected by NAADP derivatives or other Ca^{2+}-mobilizing messengers. In contrast to sea urchin, mammalian NAADP binding is reversible in a physiological buffer [16, 215].

Many mammalian cells exhibit a bell-shaped NAADP-induced concentration-response relationship, and NAADP binding has been hypothesized to follow a two-site model that is the reverse of the sea urchin model; in this, the high-affinity is the active site for NAADP, and the low-affinity the inhibitory site [241]. Multiple conformations of NAADP binding to its receptors have been proposed based on the observed positive and negative cooperativity of NAADP binding to its receptor [16]. The cooperativity was suggested to be positive, as low concentrations of unlabelled NAADP increased binding of [^{32}P]NAADP.

Negative cooperativity was suggested as the binding was shown to occur at three affinities, which might arise if binding of a ligand at one site promoted binding of the ligand to the other binding site at a lower affinity [16].

Thus, compelling evidence from the radioligand binding assays in the sea urchin and mammalian systems strongly supports the hypothesis that NAADP acts on a unique receptor that is different from those activated by other Ca^{2+} mobilizing messengers, as NAADP did not compete with $InsP_3$ or cADPR. This receptor is also specific to NAADP as NAADP derivatives were not able to displace NAADP. Furthermore, the binding affinity of NAADP for the receptor can be low (nM), which is consistent with the low concentrations needed for NAADP to release Ca^{2+}.

1.5.4 NAADP receptors

Several ion channels have been reported to be sensitive to NAADP, such as two-pore channels (TPCs) [5, 39, 41, 42, 52, 90, 231, 243, 248, 307], transient receptor potential mucolipin 1 (TRPML1) [300, 303], transient receptor potential melastatin 2 (TRPM2) [22], ryanodine receptors (RyRs) [78, 79, 121, 148] and the $P2Y_{11}$ purinoceptor [191].

To be the *bona fide* receptor of NAADP, in addition to being activated by NAADP, other important properties are required including: (1) acidic organelle localization (as NAADP mobilizes Ca^{2+} from the acidic stores [70], this strongly suggests that the NAADP receptor resides on those stores); (2) the correct sensitivity to NAADP (the EC_{50} in the nM range); (3) Ca^{2+}-permeability; and (4) unique pharmacology (insensitive to $InsP_3R$ or RyR antagonists and SERCA inhibitors, but sensitive to some Ca^{2+} and Na^+-channel blockers, or drugs affecting the acidic stores such as bafilomycin A1 and GPN).

The following sections compare the characteristics of candidates which have been discussed in the literature.

1.5.4.1 Transient receptor potential mucolipin 1 (TRPML1)

TRPML1 is a nonselective cation channel that is localized predominantly in late endosomes/lysosomes. Identities of the permeating cations are still disputable but the following have been reported: Ca^{2+}, Fe^{2+}, Na^+, H^+, and K^+. Mutations in this protein lead to mucolipidosis type IV (MLIV), a neurodegenerative lysosomal storage disease [166, 236].

The localization of TRPML1, its Ca^{2+}-permeating properties, and some overlapping pharmacological profiles of NAADP-mediated Ca^{2+} release also propose TRPML1 as a credible candidate for the NAADP receptor.

Evidence supporting TRPML1 as the NAADP-gated channels primarily came from single-channel studies of the purified lysosomes that had been reconstituted in lipid bilayers [300, 301]. NAADP was shown to activate the channel, opening it in the nM range with a bell-shaped concentration-response relationship. This response refers to the "channel open probability" (NP_o). The NAADP-evoked NP_o was significantly reduced by known Ca^{2+} and Na^+-channel blockers such as nifedipine, diltiazem, verapamil and amiloride, but not by $InsP_3R$ or RyR inhibitors. Additionally, the NAADP-induced NP_o response was significantly reduced in preparations in which TRPML1 was either blocked (via an antibody against TRPML1) or depleted (by TRPML1 siRNA or immunoprecipitation using an antibody against TRPML1) [300, 301]. Furthermore, endothelin-1, which has been shown to employ NAADP to evoke Ca^{2+} release in coronary arterial myocytes failed to do so after TRPML1 siRNA treatment [300, 303]. All of the above evidence supports TRPML1 as the NAADP-gated channel.

However, many studies have disputed the idea that TRPML1 is the NAADP-gated channel. Microinjection of NAADP (10 nM) or treatment with NAADP-AM (a membrane permeant ester that is broken down by cytosolic esterases to release NAADP) failed to elicit a significant Ca^{2+} response in SKBR3 cells (human breast cancer cell line) overexpressing TRPML1 [292]. Additionally, NAADP-elicited Ca^{2+} responses was not altered when TRPML1 expression was silenced in fibroblast cells [166] or when TRPML1 expression was knocked out in pancreatic acinar cells [292]. Lastly, NAADP binding did not increase in the membranes overexpressing TRPML1 [235].

The studies that supported TRPML1 mainly came from purified lysosomes that were reconstituted in lipid bilayers. Since the other credible candidate, TPC, was reported to form complexes with TRPML1 [292], it is possible that the effect observed with TRPML1 blocking or depletion was due to an indirect effect on TPCs in the complex rather than a direct effect on TRPML1. Furthermore, the antibody used to block TRPML1 has been shown to be unspecific for TRPML1 (unpublished observations). Although whether TRPML1 is the NAADP-gated channel remains controversial, it is likely that TRPML1

plays an intricate part in NAADP signalling but is not the direct target for NAADP.

1.5.4.2 Transient receptor potential melastatin 2 (TRPM2)

TRPM2 is a nonselective cation channel that localizes in the plasma membrane and lysosomes. TRPM2 is regulated by many factors, including ADP-ribose (ADPR), hydrogen peroxide, Ca^{2+}, cADPR, and NAADP [217]. NAADP can activate the plasma membrane TRPM2, but only at high concentrations ($\sim$1 mM), and full activation can only be reached by the synergetic effect of NAADP with ADPR [22]. A similar activation profile was also observed for cADPR. Furthermore, NAADP-induced activation was inhibited by the cADPR antagonist (8-Br-cADPR) or a TRPM2 antagonist (adenosine monophosphate; AMP), thus suggesting that both cADPR and NAADP compete for the same site on TRPM2 [22].

Although TRPM2 was activated by NAADP, an extremely high concentration was required. Given that NAADP acts in the nM range, it seems very unlikely that TRPM2 is the NAADP receptor.

1.5.4.3 RyRs

Interestingly, RyRs, an established player in CICR and cADPR-mediated Ca^{2+} signalling, have also been suggested as the NAADP receptor. However, this hypothesis remains controversial.

In Jurkat T-lymphocytes, Ca^{2+} release evoked by NAADP (100 nM) was inhibited by an antagonist of RyRs, or by knocking down RyRs by antisense mRNA [148]. However, this may be explained by the trigger hypothesis, in which NAADP releases Ca^{2+} via another receptor and this small release of Ca^{2+} is sufficient to trigger CICR via RyRs. A subsequent study addressed this question and revealed that the RyR antagonist totally abolished the NAADP-mediated triggering (pre-CICR) response, suggesting that RyRs are the molecular target of NAADP [78]. The data from the latter study is still not entirely convincing as it may be argued that the unobserved trigger response is due to limitations of the microscopes to resolve tight coupling between the genuine NAADP receptor and RyRs.

More convincingly, NAADP in the nM range was shown to increase the open probability

(P_o) of the purified RyR1 (from rabbit white skeletal muscle) reconstituted in the lipid bilayer [121]. This result was supported by another study that used the high affinity of [^{3}H]Ryanodine binding to RyR1 to determine P_o [79]. NAADP (300 nM) was found to accelerate the [^{3}H]Ryanodine binding, and this corresponded with an increase in channel opening [79]. Additionally, NAADP-stimulated [^{3}H]Ryanodine binding to RyR1 was inhibited by BZ194 (an NAADP antagonist that has been shown to specifically inhibit NAADP-, but not $InsP_3$ or cADPR-induced Ca^{2+} release in T cells) [79]. However, it should be noted that the RyR1 sample was purified by sucrose density centrifugation, and the presence of RyRs was confirmed only using a specific antibody [121]. It is likely that the sample contains other SR proteins that may be the true NAADP-gated Ca^{2+} channel.

Perhaps the most compelling data supporting RyRs as the target of NAADP was from the study of pancreatic acinar cells [109]. NAADP (200 nM) was reported to release Ca^{2+} from the nuclear envelope via RyRs, as RyR antagonists such as ryanodine and ruthenium red inhibited the release. However, NAADP-mediated Ca^{2+} release was insensitive to drugs that interfere with acidic stores, such as bafilomycin A1, brefeldin A, and nigericin.

On the other hand, a plethora of functional studies have disputed that RyR is the NAADP-gated channel. In sea urchin egg homogenate, Ca^{2+} release evoked by NAADP (nM) was not inhibited by antagonists of RyR-mediated Ca^{2+} release such as procaine, ruthenium red [66] or 8-NH_2-cADPR [153]. Similarly, in cardiac [16] and vascular smooth muscle cell microsomes [298], cADPR-induced (but not NAADP-induced) Ca^{2+} release was affected by antagonist of RyR-mediated Ca^{2+} release, such as an inhibitory concentration of ryanodine (100 μM), ruthenium red, and 8-NH_2-cADPR. Furthermore, in MIN6 cells, Ca^{2+} release elicited by NAADP (100 nM) from secretory vesicles (where RyR1 is the predominant isoform) was insensitive to an inhibitory concentration of ryanodine (10 μM) or to a selective RyR1 and RyR3 inhibitor, dantrolene [189]. Lastly, in undifferentiated C2C12 cells which express RyR3 but not RyR1 or RyR2, stimulating concentrations of ryanodine failed to evoke any Ca^{2+} response. This suggests that the RyR3 gene was transcribed but may not have been translated into protein, as there was no response to ryanodine. NAADP in the nM range, however, was still able elicit Ca^{2+} responses in undifferentiated C2C12 cells, suggesting that RyR is not the target for NAADP [5].

Further evidence from bilayer studies showed that NAADP (100 nM) failed to signifi-

cantly increase the P_o of purified RyR1 or RyR2 [231], or the P_o of RyR in SR-enriched microsomes from coronary arteries reconstituted in lipid bilayers [303].

In conclusion, it appears that the evidence against RyRs as the NAADP-gated Ca^{2+} channel is much more convincing than that supporting it, although we cannot completely disregard the fact that there may be a splice variant RyR isoform in specific organelles and/or cell types that gates Ca^{2+} release mediated by NAADP.

1.5.4.4 Two-Pore Channels (TPCs)

TPC and its topology. The first member of TPC family to be cloned was in 2000, from the rat by Ishibashi *et al.* [127]. It was proposed that an intermediate channel must exist between voltage-gated Ca^{2+} and Na^+ channels, and K^+ channels [127]. Voltage-gated Ca^{2+} and Na^+ channels have four homologous transmembrane domains and belong to a family of four-pore domain channels. They are functional as monomers. Each transmembrane domain comprises six transmembrane α-helices (segments) and a pore loop. Primordial K^+ channels have one transmembrane domain with one-pore domain and are functional as tetramers. Other members of the one-pore domain family include the transient receptor potential (TRP) and cation channels of sperm (CatSper) channels (Figure 1.12).

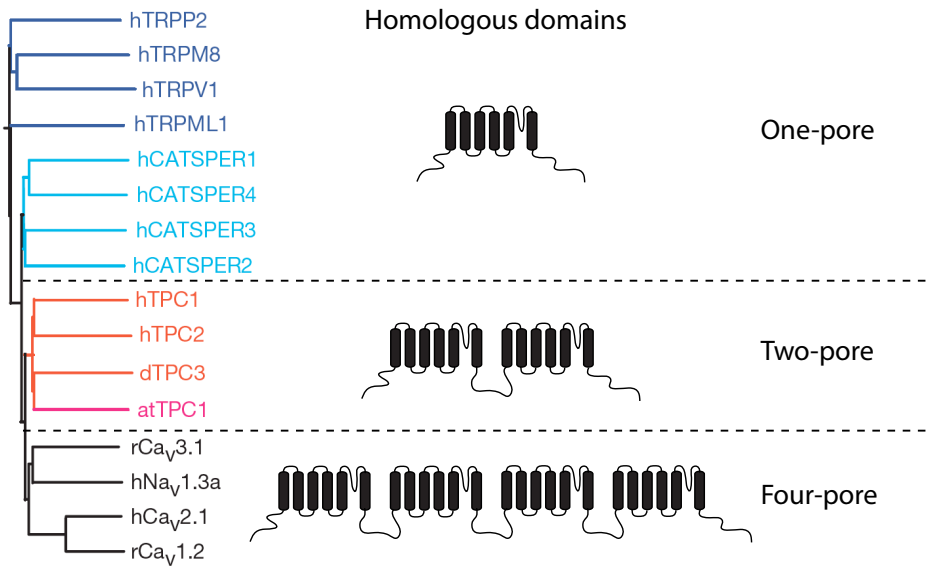

Figure 1.12: Phylogenetic tree of TPCs and their evolutionary relationship with channels that have one and four homologous transmembrane domains containing six transmembrane segments and a pore loop each. at, *Arabidopsis thaliana*; Ca_V, voltage-gated Ca^{2+} channel; d, dog; h, human; Na_V, voltage-gated Na^+; r, rat. channel. Modified from [52].

Structural analysis of TPC1 by hydropathy plot (Figure 1.13), phosphorylation and glycosylation site predictions, and sequence homology with voltage-gated Ca^{2+} and Na^{+} channels suggest that TPC1 is an evolutionary intermediate channel; it has two homologous transmembrane domains, and may be functional as dimers (Figure 1.12) [127]. Ishibashi *et al.* found that TPC1 has the highest homology with a putative Ca^{2+} channel of *Arabidopsis thaliana*, AtTPC1. Subsequent cloning and characterization revealed that AtTPC1 is a Ca^{2+}-activated Ca^{2+} release channel which is localized in the vacuole (an acidic Ca^{2+} store in plant). Furthermore, the channel possesses two Ca^{2+}-binding EF hands on the cytosolic linker region which probably account for its dependency on Ca^{2+} [98, 219]. Searches in the plant genome failed to find homologues of intracellular Ca^{2+} release channels such as $InsP_3Rs$ or RyRs [198]. This suggests that perhaps TPC1 is more important in simpler organisms such as plants, which do not require such complex signal transduction systems.

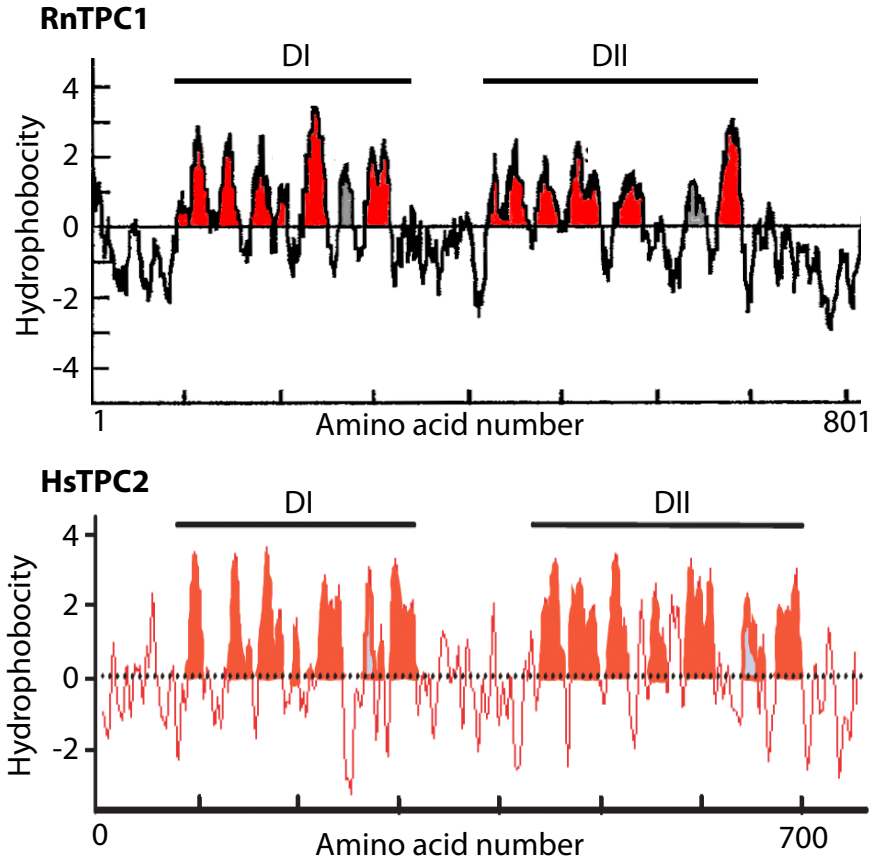

Figure 1.13: Hydropathy plots of rat (Rn) TPC1 (window setting = 12 amino acids) and human (Hs) TPC2 (window setting = 9 amino acids). Red fillings indicate regions of transmembrane segments and grey indicates regions of pore loops. D, domain. Modified from [52, 127].

Despite the gain in knowledge of the plant TPC1 since its discovery, information on animal TPCs remains scarce. The acidic store localization and the Ca^{2+}-permeating properties of the plant TPC, together with the structural homology of the plant and rat TPCs with the voltage-gated Ca^{2+} channels support the hypothesis that TPCs are the NAADP receptors. Extensive studies over the following years in mouse and human TPCs have accelerated our understandings and persuasively demonstrated its role as the receptor in NAADP-mediated Ca^{2+} signalling.

Interestingly, whilst Michael Zhu was hunting for novel TRP channels, he cloned the second animal TPC isoform, human TPC2 (pers. comm.). Similar to rat TPC1, hydropathy of TPC2 also showed two homologous transmembrane domains, each comprises of six transmembrane segments and a pore loop (Figure 1.13) [52]. Furthermore, a recent study using fluorescence protease protection assays and immunocytochemistry confirmed that human TPC1 and TPC2 have two homologous transmembrane domains with cytosolic N- and C-termini [122].

Searches of sequence databases revealed three TPC isoforms (TPC1, TPC2 and TPC3) that are present in many species including sea urchins and most vertebrates (Figure 1.14A) [52]. The TPC3 gene is interesting in that it is corrupted in some members of the *Euarchontoglires* lineage such as primates including human, chimpanzee and rhesus money, as well as in rodents such as mouse and rat (Figure 1.14B) [51]. The degeneration process is likely to involve many inactivating mutations resulting in a TPC3 pseudogene [51]. The three sea urchin TPCs and the two human and mouse TPCs share <30% sequence homology within the species [52, 243, 307].

TPC expression at tissue and subcellular levels. TPCs are widely expressed in rat and mouse tissue types with high TPC1 expression detected in kidney, liver, thymus and spleen [127, 307], and TPC2 expression in mouse and human kidney and liver [52, 307] (Figure 1.15). The expression of mammalian TPC3 has not yet been studied.

RT-qPCR analysis of mRNA expression showed that TPC1 was higher than TPC2 in human SKBR3 cells, rat PC12 cells, and sea urchin eggs [39]. In mouse tissue types, TPC1 mRNA expression was also reported to be higher than TPC2 by northern blotting, although two separate probes were used for TPC1 and TPC2, and the levels were not

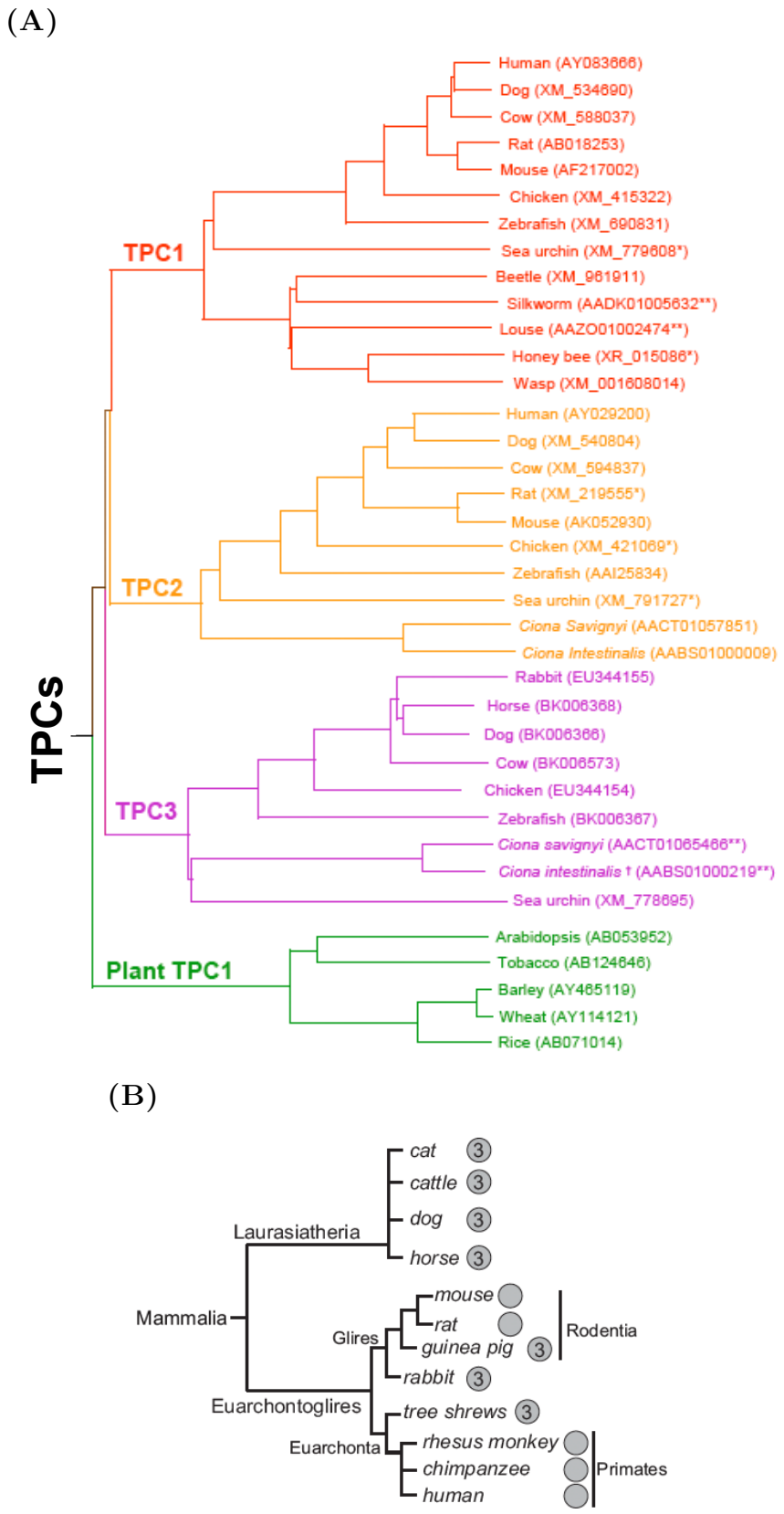

Figure 1.14: (A) A phylogenetic tree of TPCs indicating the evolutionary relationships between various species of TPCs. The diagram is taken from [52]. (B) Degeneration of the TPC3 gene in the *Euarchontoglires* lineage. The number 3 in the gray circle indicates that the species has the TPC3 gene. The empty circles indicate that TPC3 is absent or degenerated. The diagram is taken from [51].

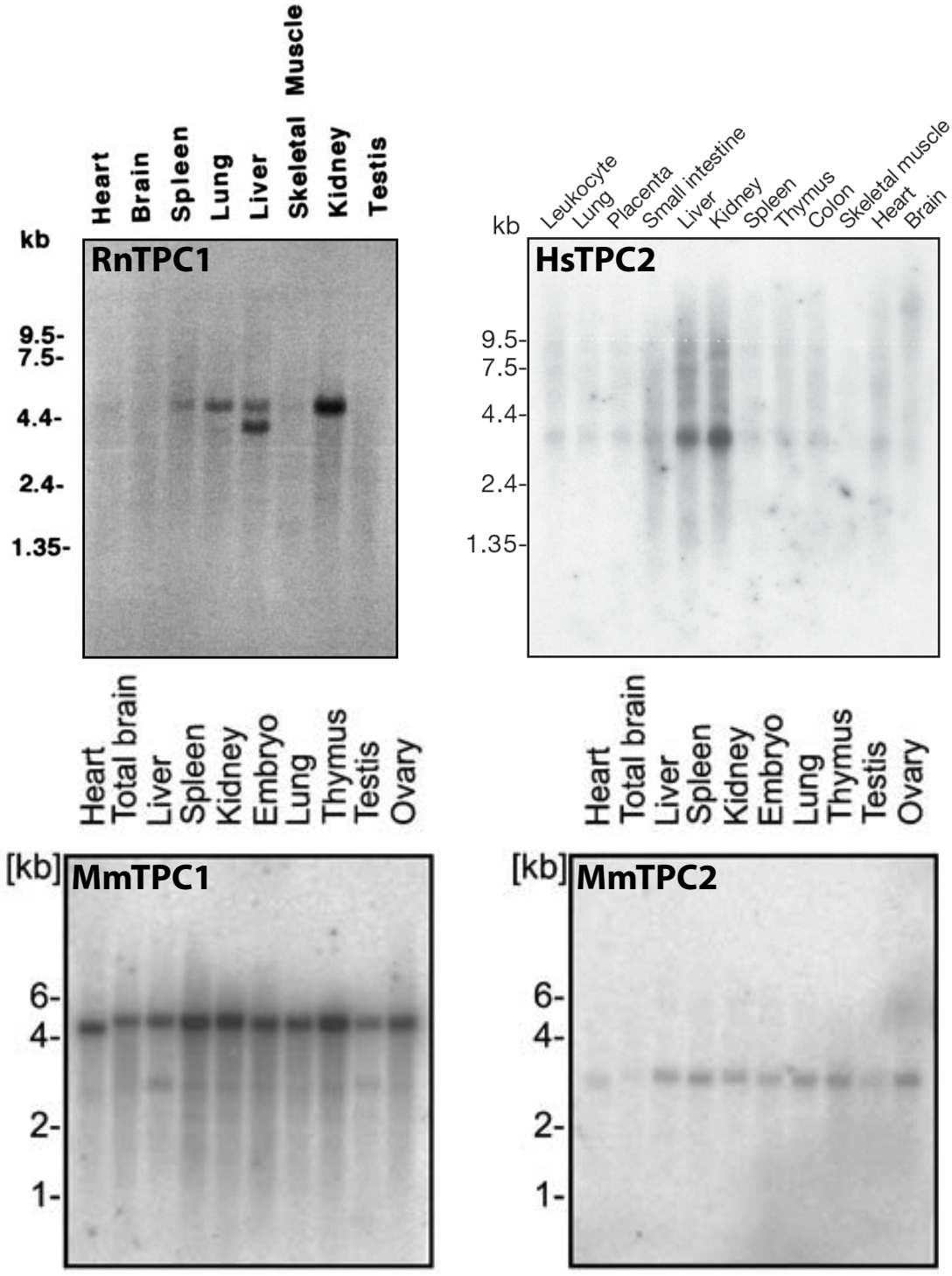

Figure 1.15: Northern blots demonstrating mRNA expression of TPC1 in rat (Rn) [127] and mouse (Mm) [307], and TPC2 in human (Hs) [52] and mouse (Mm) tissues [307].

normalized to a housekeeping gene. The detected expression level may be biased depending on the affinities of the probes (bottom panel in Figure 1.15) [307].

Consistent with the findings for AtTPC1, subcellular studies have revealed that endogenous and heterologously expressed TPCs of various species are localized intracellularly in acidic organelles [39, 41, 42, 52, 217, 219, 243, 307]. In animals, TPCs are localized in the endo-lysosomal system. Subcellular distribution of human TPC2 is more restricted to late endosomes/lysosomes [52], whereas the distribution of human TPC1 and chicken TPC3 are broader (endosomes, lysosomes and other undefined compartments) [39, 52]. Interestingly, mouse TPC2 was demonstrated to localize not only in late endosomes/lysosomes but also in the ER, though subsequent functional analysis demonstrated that the ER-localized TPC2 was non-functional [307]. Additionally, the ER-localized TPC2 might be a result of heterologous expression artefact.

NAADP binding to TPCs. The localization of TPCs to endo-lysosomes, and the homology of TPCs to known Ca^{2+} channels such as TRP and voltage-gated Ca^{2+} channels raise the question as to whether NAADP binds to TPCs to release Ca^{2+} from the acidic stores.

Indeed, NAADP binding was enhanced in membranes overexpressing human TPC2 and the binding was abolished by depleting human TPC2 from the membranes by immunoprecipitation [52]. Mirroring the binding in native mammalian systems, NAADP bound to membranes overexpressing human TPC2 biphasically, with affinities in the nM and μM range [52].

The importance of TPC complexes for NAADP binding was further confirmed by studying NAADP-binding in immunopurified endogenous sea urchin TPCs [243]. In these immunoprecipitates, NAADP binding was increased compared to controls (non- or pre-immune serum). In addition, it showed the distinctive properties of NAADP binding to the native NAADP receptors, such as the nM affinity, and the K^+ concentration-dependent reversible binding [243]. This strongly suggests that endogenous TPCs are important components of NAADP-binding complexes. However, it is also possible that NAADP binds to accessory proteins that are tightly associated with TPC complexes.

Functional evidence of TPCs as the NAADP-gated Ca^{2+} channel. The ability of NAADP to bind to TPC complexes raises two further questions: do animal TPCs indeed conduct Ca^{2+} release in response to NAADP, and does the release via TPCs satisfy all the criteria for NAADP-induced Ca^{2+} release?

NAADP-mediated Ca^{2+} release via TPCs. In cells overexpressing human TPC1 and TPC2, Ca^{2+} release evoked by nanomolar concentrations of NAADP was significantly enhanced [39, 52]. Additionally, the release was in line with the classic NAADP bell-shaped concentration-response relationship [52]. Furthermore, NAADP-mediated Ca^{2+} release was abolished when the pH gradient of the acidic stores was collapsed by bafilomycin A1, or when TPC expression was inhibited by short hairpin RNA [39, 52].

Consistent with the hypothesis that Ca^{2+} release evoked by NAADP acts as a trigger to amplify CICR, NAADP-mediated Ca^{2+} release in HEK cells overexpressing human TPC2 was biphasic, comprising an initial accumulating ramp followed by a much larger Ca^{2+} transient [52]. Combined pharmacological inhibition of $InsP_3Rs$ (heparin), RyRs (ryanodine; 10 μM), and the SERCA (thapsigargin) - or just heparin alone - abolished only the large transient but not the initial ramp, while bafilomycin A1 abolished both phases. This clearly suggests that the initial ramp corresponds to the Ca^{2+} release from acidic stores evoked by NAADP with the larger transient attributable to CICR via $InsP_3Rs$ triggered by the initial NAADP-mediated Ca^{2+} release.

In SKBR3 cells overexpressing human TPC1 or TPC2, NAADP-mediated Ca^{2+} release was sensitive to 10 μM ryanodine. The authors suggested that the Ca^{2+} release evoked by NAADP was coupled to CICR via RyRs [39, 42]. This hypothesis was later confirmed by uncoupling human TPC2 from RyRs by altering the endo-lysosomal targeting signals on human TPC2 such that TPC2 was redirected to the plasma membrane. Uncoupled human TPC2 on the plasma membrane was still able to conduct Ca^{2+} release in response to NAADP; however, the response was no longer sensitive to ryanodine [42].

What about TPCs from other species? Similar to human TPC2, NAADP evoked an increase in Ca^{2+} release with a bell-shaped concentration-dependent relationship in HEK293 cells overexpressing mouse TPC2. Additionally, the response evoked by NAADP

was also abolished by bafilomycin A1. In contrast to human TPC2, the response was not altered by thapsigargin [307], suggesting that CICR amplification was not involved. Furthermore, unlike cells overexpressing human TPC1, NAADP was not able to evoke Ca^{2+} release from HEK293 cells overexpressing mouse TPC1 [307]. This might reflect a species-specific difference, but is likely to be an artefact of the heterologous expression system. Although compatible for mouse TPC2, mouse TPC1 function might have been compromised by the overexpression environment.

In HEK293 or SKBR3 cells overexpressing sea urchin TPC1 or TPC2, NAADP also evoked Ca^{2+} release as described for the native system. Nanomolar concentrations of NAADP elicited Ca^{2+} release in cells overexpressing sea urchin TPCs which can be inhibited by pre-treatment with bafilomycin A1 [41, 243], NAADP-AM (1 nM) [243] or Ned-19 [243]. Like HEK293 cells overexpressing human TPCs, NAADP-mediated Ca^{2+} release also triggered CICR via $InsP_3Rs$ in HEK293 cells overexpressing sea urchin TPC1 and TPC2; heparin only inhibited the second (large) Ca^{2+} transient in the biphasic response. Furthermore, in the HEK293 overexpression system, the coupling to CICR appeared tighter in sea urchin TPC2 than TPC1 as the lag time to the CICR amplification was shorter [243].

The functional role of sea urchin TPC3 is currently unclear. In one study, overexpression of sea urchin TPC3 in HEK293 cells inhibited NAADP-evoked Ca^{2+} release from the sea urchin TPC2-overexpressing cells and the endogenous HEK TPCs [243]. However, another study showed that NAADP was able to elicit Ca^{2+} release in SKBR3 cells overexpressing sea urchin TPC3, although the response was smaller than that with sea urchin TPC1 and TPC2 [41]. In these studies, two sequence variants of sea urchin TPC3 were expressed in separate expression systems; in HEK293 cells CICR amplification is coupled to $InsP_3Rs$ whereas in SKBR3 cells, CICR amplification is coupled to RyRs. Both the differences in sequence and the expression system are likely to account for the conflicting data.

In summary, overexpression studies of TPCs from various species have provided compelling evidence that Ca^{2+} release via TPCs satisfies all the criteria required for NAADP-induced Ca^{2+} release. Firstly, when TPCs are overexpressed, NAADP-elicited Ca^{2+} release was enhanced, while when TPC expression was silenced NAADP-elicited Ca^{2+}

release was abolished. This demonstrates that the response was indeed from the presence of TPCs. Secondly, NAADP evoked Ca^{2+} release via TPCs at the expected nanomolar NAADP concentrations, and mammalian TPCs exhibited the classic bell-shaped NAADP concentration-response curve, while the response of sea urchin TPCs was sensitive to NAADP self-inactivation. Thirdly, Ca^{2+} released via TPCs originated from the acidic stores as the response was inhibited by bafilomycin A1. Fourthly, NAADP-evoked Ca^{2+} release via human and sea urchin TPCs acts as a trigger to initiate the amplified response by CICR. Taken together, these results provide compelling evidence that TPC is indeed the NAADP-gated Ca^{2+} channel.

Biophysical properties of TPCs. Although TPCs had been demonstrated to mediate Ca^{2+} release in response to NAADP, the above reports did not identify whether TPCs are the NAADP-activated ion channels responsible for conducting Ca^{2+}, or whether Ca^{2+} is released by another ion channel in complex with TPCs. To address this question, the biophysical properties of TPCs were examined.

The first study to examine the biophysical properties of TPCs used patching of isolated whole-lysosomes (from HEK293 cells) containing overexpressed mouse TPC2 [248]. This study showed that cation currents were activated by cytosolic NAADP at a nanomolar concentration, but not by NADP or NAADP at a high concentration. In control lysosomes (TPC2 not overexpressed), nanomolar NAADP was not able to elicit current. Using bi-ionic conditions, the relative permeability of mouse TPC2 to Ca^{2+} and K^+ (P_{Ca2+}/P_{K+}) was >1000, this suggests that the NAADP-evoked currents via mouse TPC2 are highly selective for Ca^{2+} over K^+. Mutation of a conserved asparagine residue in pore loop I of TPC2 abolished the NAADP-evoked current. Additionally, mutation of a conserved acidic residue in pore loop I significantly reduced selectivity for Ca^{2+} [248]. This study provided the first direct evidence that mouse TPC2 is the pore-forming subunit of the NAADP-gated Ca^{2+} channel and can indeed conduct Ca^{2+} ions in response to NAADP.

This finding is supported by two further studies. The first measures single channel activities from the immunopurified recombinant human TPC2 complexes in an artificial lipid bilayer [231]. The study demonstrated that, similar to whole-lysosome patching, cytosolic application of NAADP increased the P_o of human TPC2 channels. Additionally,

channels were closed by a high (inactivating) concentration of NAADP or Ned-19. Interestingly, in contrast to whole-lysosome patching, the relative permeability of human TPC2 channels to Ca^{2+} and K^+ (P_{Ca2+}/P_{K+}) was ~2.6, suggesting that it has no preference for either Ca^{2+} or K^+ and was permeable to both ions [231].

The second study also examined single channel activity by inside-out patching of cells overexpressing mutant human TPC2 [42]. Human TPC2 is normally localized intracellularly in late endosomes/lysosomes, and is thus inaccessible to patch-clamp techniques. To overcome this limitation, the N-terminal dileucine motif of TPC2, which is responsible for endo-lysosomal targeting, was truncated (TPC2ΔN) or mutated ($TPC2^{AA}$; two leucine residues mutated to alanine) in order to redirect human TPC2 to the plasma membrane. In line with the reported biophysical properties of TPC2, nanomolar NAADP significantly the increased NP_o of cells expressing TPC2ΔN or $TPC2^{AA}$ and enabled fluxes of cations such as Ca^{2+} and Cs^+. As expected, this opening was inhibited by Ned-19. Mutation of a conserved leucine residue in pore loop I of TPC2 significantly reduced the NAADP-evoked Cs^+ conductivity by at least 10-fold, but did not affect the NP_o.

Overall, the combined evidence from whole-lysosomal patching and single channel studies strongly suggest that TPC2 is indeed the Ca^{2+}-conducting channel that gates NAADP-evoked Ca^{2+} release.

Regulations of TPCs. While TPCs are currently accepted to be NAADP-gated Ca^{2+} channels, the search for roles for proteins or ions involved in regulating TPCs is still in infancy. Over the last year, two studies have demonstrated that NAADP-evoked responses via TPCs are regulated by luminal environment (Ca^{2+} and pH) [231, 248].

The whole-lysosome patching study showed that reducing the luminal Ca^{2+} concentration from 2 mM to 100 nM reduced the amplitude of NAADP-evoked current via mouse TPC2 [248]. This was supported by a single-channel study in which the immunopurified human TPC2 had been reconstituted into lipid bilayers [231]; it showed that a decrease in luminal Ca^{2+} concentration from 1 mM to 100 μM reduced the P_o of human TPC2 from approximately 0.45 to nearly 0. Furthermore, the sensitivity of the P_o of human TPC2 to NAADP increased in correlation with an increase in the lysosomal luminal

Ca^{2+} concentration (EC_{50} = 5 nM at 200 μM, and EC_{50} = 500 nM at 10 μM luminal Ca^{2+} concentration) [231]. Mouse and human TPC2 is expressed predominantly in late endosomes/lysosomes, where the physiological concentration of luminal Ca^{2+} at rest is ~500 μM. It is perhaps not surprising that the sensitivity of TPC2 to NAADP was higher and the NAADP-evoked response larger, at the physiological range of luminal Ca^{2+}.

Luminal pH was shown to regulate TPC-mediated responses, although the mechanism remains unclear. The whole-lysosome patching study showed that increasing the luminal pH from pH 4.8 to 7.2 completely abolished the NAADP-activated cation currents [248]. In contrast, two single-channel studies showed that NAADP still activated human TPC2 channel opening at pH 7.2 [42, 231]. These disparate results may be partly explained by differences in species, and importantly, by differences in membrane composition and environment of channels. Only the whole-lysosome patching study showed perhaps the endogenous 'normal' environment [248], the two single-channel studies would have the ER membrane [231] or the plasma membrane [42] composition.

Although NAADP was able to activate human TPC2 channel opening at pH 7.2 in both studies, one study showed that the activation was irreversible [231], whereas the other found that it was reversible [42]. As the reversible channel activation came from the study using mutant human TPC2, it is possible that mutation has side effects on pH regulation. The irreversible activation of human TPC2 suggests that pH modulates the P_o level by altering the dissociation rate of NAADP. This irreversibility is likely to account for the reshaping of the concentration-P_o response curve from the classic bell-shaped at pH 4.8 to sigmoidal at 7.2 [231]. NAADP has been shown to alkalinize acidic stores [192, 193], so the increase in luminal pH upon Ca^{2+} release by NAADP may provide a mechanism to retune TPC2 channel gating.

Physiological roles of TPCs. The majority of the links between NAADP and TPCs were established by using heterologous expression systems. Insights concerning the endogenous role of TPC-mediated Ca^{2+} release are scarce. One approach to improve this has used TPC KO mice. In view of this, techniques for the generation and characterization of TPC KO mice are described later (Chapter 3). Using the TPC KO mice, a crucial role for endogenous TPCs has been shown in glucose-evoked signalling in pancreatic

β-cells (Arredouani *et al.* unpublished data), and in ACh-induced bladder smooth muscle contraction [90]. Most recently, NAADP was reported to act via TPCs on the acidic stores to promote differentiation in skeletal muscle [5].

Role of TPCs in endo-lysosomal physiology. Local NAADP-induced Ca^{2+} release from the acidic stores could be important in the endo-lysosomal system to mediate effective vesicle fusion and condensation of the post-fusion luminal content [172]. Successful vesicle fusion is crucial in transporting the luminal contents and membrane proteins along the degradation or ubiquintination pathways [172, 230]. Indeed, in Niemann-Pick disease type C1 (NPC1), the lysosomal storage of sphingosine reduces the lysosomal Ca^{2+} content and thereby reduces NAADP-mediated Ca^{2+} release. This results in impediment to vesicle fusion and trafficking, and the subsequent storage of cholesterol and glycosphingolipids [165].

Disruption to NAADP-mediated Ca^{2+} release from late endosomes/lysosomes has been shown to cause a block in vesicular fusion and trafficking, and subsequent storage of lipids [165]. Consistent with the notion that TPC is the NAADP-gated receptor, abnormal lysosomal size, distribution and storage, and also endocytic trafficking faults were observed in cells overexpressing TPCs; administration of Ned-19 was able to alleviate these abnormalities. This indicates an important role of NAADP signalling via TPCs in normal endo-lysosomal physiology such as vesicular trafficking and lysosomal biogenesis. Dysfunction in regulations of the NAADP-TPC signalling pathway may therefore underlie some of the lysosomal storage disorders [243].

1.6 Mouse pancreatic acinar cells as a model to study Ca^{2+} signalling

Pancreatic acinar cells are non-excitable, i.e. they are not endowed with voltage-gated Ca^{2+} channels and do not propagate action potentials. Furthermore, the morphology and the signalling pathways have been well-characterized in pancreatic acinar cells, thus they represent an ideal model system for the study of Ca^{2+} release from the intracellular stores [228]. Indeed, the first member of the intracellular Ca^{2+}-mobilizing messenger group, $InsP_3$, was discovered in the pancreatic acinar cells [259]. Furthermore, it was also the first mammalian cell to show a response to NAADP [57]. The first part of this section will describe the physiology of pancreatic acinar cells and the second part will describe Ca^{2+} signalling in this cell type.

1.6.1 Physiology of pancreatic acinar cells

The major physiological function of pancreatic acinar cells is to synthesize, store and secrete the zymogens/digestive enzymes for carbohydrates, proteins, and lipids. Approximately 20–200 acinar cells are organized into an acinus adjacent to the small ducts that convey secreted proteins [113].

1.6.1.1 Morphology of pancreatic acinar cells

Each acinar cell has a polarized structure, optimised for secretion. It is comprised of an apical pole packed with secretory (or zymogen) granules (ZG) and an extensive dense ER network that surrounds the nucleus on the basolateral pole [225]. The ER is not confined to the basolateral pole: some of the terminals extend deep into the apical pole [110]. Interestingly, mitochondria are localized to three specific subcellular regions: a perigranular belt surrounding the ZG, a perinuclear belt surrounding the nucleus, and a peripheral belt along the basolateral plasma membrane. The Golgi apparatus is localized between the perinuclear belt and the perigranular belt (Figure 1.16) [113, 225, 227].

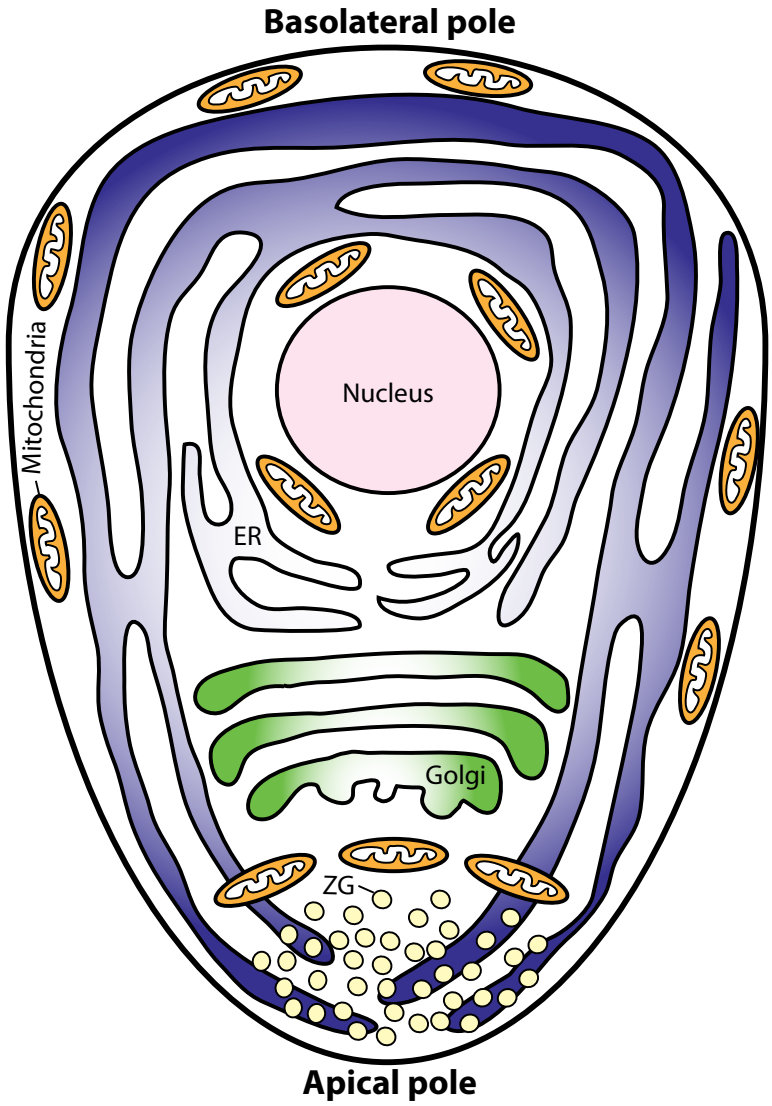

Figure 1.16: Schematic representation of the subcellular organelle localizations of a pancreatic acinar cell. Modified from [113, 225, 227].

1.6.2 Stimulus-secretion coupling in pancreatic acinar cells

"Stimulus-secretion coupling" describes the events in which stimulations of the plasma membrane receptors by extracellular physiological agonists such as circulating hormones (CCK) or neurotransmitters (ACh) result in an increase in intracellular Ca^{2+}. Depending on the agonist, different combinations of Ca^{2+} mobilizing messengers and Ca^{2+} stores are recruited to form specific Ca^{2+} signals [293]. The details of Ca^{2+} signalling evoked by specific agonists are described in the following sections. The Ca^{2+} increase activates secretion of enzymes by exocytosis of zymogen granules or fluid by activation of Ca^{2+}-dependent Cl^- channels in the apical membrane [224, 228, 289]. Cl^- extrusion into

the lumen initiates paracellular Na^+ influx and thereby osmotic water ingress into the pancreatic duct lumen [171] (Figure 1.17). The initial phase of secretion is governed by the intracellular Ca^{2+} release and is entirely independent of the extracellular Ca^{2+}. During the sustained phase (sustained stimulation, Ca^{2+} elevation, and secretion), Ca^{2+} entry is required to replenish the ER [224, 228].

1.6.2.1 CCK-evoked Ca^{2+} signalling

CCK is secreted into the blood by the enteroendocrine cells in the small intestine after food ingestion [56, 161]. There are two CCK receptors: CCK type 1 (CCK1) is the predominant type in rodent pancreatic acinar cells and binds specifically to sulphated CCK, while CCK type 2 (CCK2) is not expressed in rat or mouse pancreatic acinar cells [56].

CCK1 has a high and a low affinity site; physiological concentrations of CCK (1–50 pM) activate the high-affinity CCK1 receptors on the basolateral membrane of the pancreatic acinar cells [228, 289]. Activation of the low-affinity site on the CCK1 receptor by non-physiological concentrations of CCK leads to activation of PLC and production of $InsP_3$ [249]. The following section will focus on the signalling via the physiological concentrations of CCK.

In the whole-cell patching, characteristic of Ca^{2+} spikes evoked by physiological concentrations of CCK comprises both apically localized short repetitive spikes (lasting 1–2 s) at a frequency of one spike/min and longer-lasting global transients (0.2–1 min). The apical repetitive spikes were thought to be the signal responsible for the secretion of enzymes and fluid, while the global Ca^{2+} transients were for CCK-stimulated pancreatic cell growth [59]. Recent advances in technology (two-photon microscopy) have given a new insight into the stimulus-secretion coupling. The study demonstrated that the local spikes actually only activate the fluid secretion, whereas the global spikes activate secretion of both fluid and enzymes [170, 171].

Upon stimulation by physiological concentrations of CCK in the pancreatic acinar AR42J cell line, plasma membrane CD38 was recruited intracellularly, possibly via endocytosis into non-lysosomal acidic stores. This newly recruited CD38 together with the constitutive CD38 in early endosomes are likely to be responsible for synthesizing NAADP

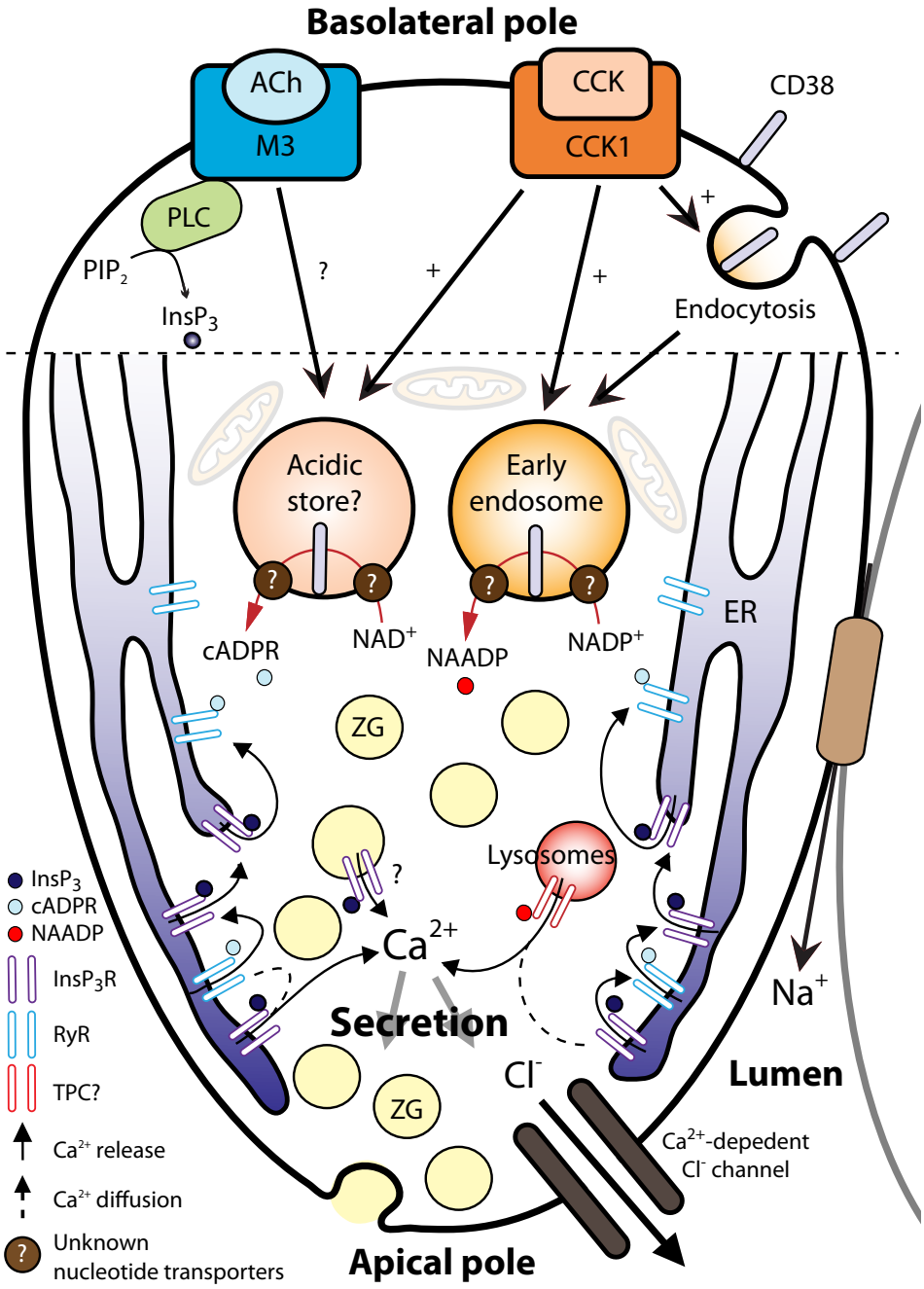

Figure 1.17: Schematic representation of the Ca^{2+} signalling in stimulus (CCK and ACh)-secretion coupling. Agonist-stimulated synthesis of specific Ca^{2+} mobilizing messengers ($InsP_3$, cADPR, and NAADP) by PLC or the constitutive/endocytosed CD38 initiates Ca^{2+} release from the apical pole. $InsP_3$ releases Ca^{2+} via $InsP_3$Rs primarily from the ER and possibly from the non-lysosomal acidic stores (perhaps zymogen granules (ZG)?), NAADP primarily releases Ca^{2+} possibly via TPCs? from the lysosomal acidic stores, and cADPR releases Ca^{2+} via RyRs from the ER. Local Ca^{2+} release is then amplified by CICR by concerted activity of RyRs and $InsP_3$Rs. A rise in intracellular Ca^{2+} triggers secretion of enzymes via exocytosis of zymogens, and of fluid via Ca^{2+}-dependent Cl^- channels into the lumen.

and cADPR in response to CCK, as CCK-evoked synthesis for both messengers had been eliminated in CD38 KO pancreatic acinar cells [74, 294]. The synthesis of cADPR and NAADP is likely to be intravesicular as suggested for sea urchin ARCs [68, 81].

In response to CCK stimulation, NAADP is synthesized rapidly and peaks within the first 30 seconds, whereas cADPR is synthesized later and peaks only after 2 min. The time frame of the messenger synthesis events supports the trigger hypothesis in which local Ca^{2+} release evoked by NAADP triggers a much larger response via CICR. Interestingly, CCK at physiological concentrations was unable to stimulate $InsP_3$ synthesis, as the level after stimulation remained similarly to the basal level [179].

In pancreatic acinar cells, one study has shown that NAADP releases Ca^{2+} from the nuclear thapsigargin-sensitive ER via RyRs [109]. However, in the process of nuclei isolation, homogenization of pancreatic acinar cells may have caused some membranes containing NAADP-gated channels (from acidic vesicles) to break and reform with membranes from nuclei. Alternatively, it might be that few NAADP-gated channels are expressed in these organelles. Since NAADP is a potent Ca^{2+}-mobilizing messenger, just a few channels may be sufficient to elicit detectable responses. In both cases, Ca^{2+} would be released from the nuclear ER, explaining why the response is insensitive to drugs that interfere with acidic stores. On the other hand, many other studies have demonstrated convincingly that NAADP releases Ca^{2+} from the acidic stores like cathepsin-C containing lysosomes [74, 185, 293]. Since TPCs are the most credible candidates for NAADP-gated Ca^{2+} channels (Section 1.5.4.4), it is likely that TPCs also gate NAADP-mediated Ca^{2+} release in pancreatic acinar cells.

Amplification of the NAADP-mediated Ca^{2+} trigger is dependent on both RyRs and $InsP_3Rs$, as inhibitors of RyRs (ryanodine or 8-NH_2-cADPR), and of $InsP_3Rs$ (heparin or high concentrations of caffeine (20 mM)) all abolished NAADP-elicited Ca^{2+} spikes [57, 59]. This is in line with the pharmacological profile of CCK-evoked spikes [57, 59, 60]. Thus, CCK-elicited Ca^{2+} signalling is dependent on the action of three receptors: the trigger NAADPRs (likely TPCs), and the amplifiers $InsP_3Rs$ and RyRs (Figure 1.17).

Spatio-temporal pattern of CCK-evoked Ca^{2+} signals. Spatio-temporal patterning of CCK-evoked Ca^{2+} signals comprises an initial Ca^{2+} increase from the apical pole followed by a wave to the basolateral pole [56, 57, 59, 272]. Consistent with the initiation of Ca^{2+} responses at the apical site, the Ca^{2+} trigger evoked by NAADP is restricted to the apical and not the basal pole [293]. Additionally, treatment of the lysotracker-stained acidic stores with GPN also demonstrated the apical localization of lysosome-related stores [185, 293]. Furthermore, the predominant types of $InsP_3Rs$ in pancreatic acinar cells, type 2 ($InsP_3R2$) and type 3 ($InsP_3R3$), are also localized to the apical pole [126, 156]. $InsP_3Rs$ at the apical pole are likely to be involved in amplifying the NAADP-evoked Ca^{2+} response.

The exact spatial pattern of cADPR-induced Ca^{2+} signalling is currently unresolved. Consistent with the apical releasing site, cADPR (or low activating concentrations of ryanodine) was shown to initiate Ca^{2+} release from the apical pole [12, 271]. However, cADPR has also been reported to release Ca^{2+} more sensitively in the basolateral side where RyRs are concentrated [145, 155, 156]. Perhaps because the localization RyRs are more broadly distributed, initiation was observed at both poles. The diffused localization of RyRs also suggests that RyRs are not limited to amplifying, but also propagate a Ca^{2+} signal initiated in the apical pole [289].

In summary, physiological concentrations of CCK evoke Ca^{2+} spikes which initiate from the apical pole. This is likely as a result of Ca^{2+} release from acidic stores evoked by NAADP. The local Ca^{2+} pulse is then amplified by concerted activity of apically localized $InsP_3Rs$ and RyRs and spreads as a wave to the basolateral pole via RyRs. Furthermore, stimulation by non-physiological concentrations of CCK activates $InsP_3$ production and switches to $InsP_3$-mediated signalling pathway.

1.6.2.2 ACh-evoked Ca^{2+} signalling

ACh released from the parasympathetic nerve endings activates muscarinic receptors on the basolateral membrane of the pancreatic acinar cells [228, 272]. Unlike CCK, the characteristic of Ca^{2+} spikes evoked by ACh in whole-cell patching experiments comprises only the apically localized short repetitive spikes and not global Ca^{2+} transients [59]. This may partly explain why CCK is involved in both secretion of enzymes and fluid and

pancreatic cell growth, whereas ACh only stimulates the secretion of enzymes and fluid.

There are three muscarinic receptors, of which M_3 is the predominant isoform in the rodent and human pancreata. The M_3 receptor is a G_q-protein coupled receptor and upon activation by physiological concentrations of ACh (50–300 nM), $InsP_3$ is produced from hydrolysis of PIP_2 by PLCβ [289]. $InsP_3$ generated near the basolateral pole diffuses rapidly over 15 μm to activate $InsP_3$Rs concentrated on the apical pole and cause subsequent Ca^{2+} release from the ER [11, 272, 289]. Interestingly, ACh has also been reported to recruit different acidic Ca^{2+} stores to elicit the Ca^{2+} response, perhaps lysosomes via Ca^{2+} and non-lysosomal acidic stores such as zymogen granules via $InsP_3$ [185].

Interestingly, although cADPR production was shown to increase in response to ACh [294], 8-NH_2-cADPR failed to significantly alter ACh-elicited Ca^{2+} spikes [59]. Furthermore, it has been shown that ACh does not synthesize [294] or utilize NAADP in its signalling pathway, as high self-inactivation concentrations of NAADP (100 μM) inhibited Ca^{2+} spikes evoked by CCK but not those by ACh [59]. This clearly demonstrates that, in contrast to CCK-evoked Ca^{2+} signalling, cADPR and NAADP are not involved in the ACh-evoked Ca^{2+} response.

ACh, like CCK, initiates Ca^{2+} release at the apical pole and the signal spreads towards the basal pole. This Ca^{2+} trigger is likely to be initiated by $InsP_3$ as NAADP and cADPR are not involved. Indeed, $InsP_3$ was also shown to initiate Ca^{2+} release at the apical pole [155, 272]. The amplification via CICR is dependent on $InsP_3$Rs and RyRs, as heparin and ryanodine were all able to abolish ACh-evoked Ca^{2+} spikes [11, 59, 228, 287].

Thus, in pancreatic acinar cells, CCK and ACh recruit different combinations of messengers to elicit agonist-specific Ca^{2+} signals. For CCK, the Ca^{2+} spiking is dependent on NAADP and cADPR, whereas for ACh, Ca^{2+} spiking is dependent on $InsP_3$. (But note that this action of cADPR in ACh-evoked spiking is still controversial.) Lastly, for both agonist-specific Ca^{2+} signals, activation of RyRs and $InsP_3$Rs are required for the CICR process.

1.7 The aims of this research

Overwhelming evidence from the heterologous expression studies has demonstrated that TPCs are the NAADP-gated channels. However, our understanding of the endogenous role of TPCs is minimal. To address this, our lab has generated TPC mutant mice. The first part of this thesis describes the characterization and validation of the TPC mutant mice, ensuring that the mRNA expression of the target TPC isoform(s) is abolished. The generated TPC single or double KO mice were viable and exhibited no gross phenotype abnormalities. Thus, the compensation exerted by the remaining TPCs in single KOs, or at a global level by other proteins will also be examined.

Since mice will be used as the model system, the expression of mouse TPCs will also be studied at the mRNA, protein and subcellular levels, in order to further understand the roles of mouse TPCs. An interesting question arises: how are TPCs targeted to their subcellular destinations? This is addressed by investigating the sorting (targeting) signals involved in directing TPCs to subcellular compartments.

The generation of TPC mutant mice provides a valuable tool to investigate the endogenous role of TPCs in NAADP-mediated Ca^{2+} signalling in a native system. An outstanding question in the TPC field is whether TPC is the endogenous binding protein for NAADP. The question is answered by assaying radioligand binding of NAADP in membranes from TPC KO mice. Furthermore, CCK-evoked Ca^{2+} responses in pancreatic acinar cells have been extensively studied, and it is known to be dependent on NAADP. In CCK signalling, the important missing link is whether TPC is the channel that gates NAADP-evoked Ca^{2+} release. The role of TPCs in CCK signalling is investigated by using isolated pancreatic acinar cells from TPC single and double KO mice.

In summary, using molecular, biochemical, radioligand binding and Ca^{2+} imaging methods, this research attempts to characterize expression and localization of mouse TPCs and gain insights into the endogenous role of TPCs in NAADP signalling.

Chapter 2

Materials and Methods

2.1 Materials

All reagents were purchased from Sigma-Aldrich, and all cell culture reagents were purchased from Invitrogen unless otherwise specified. Drugs were stored at -20 °C until further use.

2.1.1 Animals

Mice obtained from MRC Harwell[1] and Deltagen[2] were housed in individual ventilated cages (coloured perspex units which have their own air supply). The mice were housed in clean air at constant optimal temperature and humidity with 12 h of light per day in the Biomedical Science Building (Oxford). Mice were fed with standard dry pellets, and water *ad libitum*. Five strains of mice with differences in genetic background or mutations were used: Two wild-type (WT) mice of different genetic background; WT1 and WT2, and TPC mutant mice; TPC1 XG716, TPC1 D159, and TPC2 YHD437. Genetic backgrounds of the WTs and TPC mutant mice are detailed in Chapter 3.

[1] `http://www.har.mrc.ac.uk/`
[2] `http://www.deltagen.com/`

2.1.2 TPC I.M.A.G.E. clones

Mouse TPC1 and TPC2 cDNA I.M.A.G.E. (Integrated Molecular Analysis of Genomes and their Expression consortium) clones were obtained from Source BioScience LifeSciences (Table 2.1).

Gene	IMAGE clone ID	GenBank accession number	Vector
Mouse TPC1	6821376	BC058951	pYX-Asc
Mouse TPC2	9055807	BC141195	pCR4-TOPO

Table 2.1: Details of mouse TPC1 and TPC2 IMAGE clone constructs.

2.2 Genotyping

2.2.1 Ear clip digestion

To prepare mouse DNA for genotyping, DNA from mouse ear clips was extracted by digestion overnight at 55 °C in lysis buffer (50 mM Tris.HCl, 50 mM EDTA, 0.1% SDS and 1 mg/ml proteinase K; pH 8.0). The digestion was heated at 95 °C for 15 min to inactivate proteinase K and frozen at -20 °C until use. Before addition to the polymerase chain reaction (PCR) reaction, the undigested material was centrifuged at $10,000 \times g$ for 5 min.

2.2.2 3-primer PCR

3-primer PCR was used to genotype the mice via assessing the presence of the WT or mutant alleles. Two sense primers (1 μM), each specific for WT or mutant allele, and an antisense primer (1 μM, Table 2.2) were added in a reaction containing DreamTaq Green mix (Fermentas), and ear clip DNA (1 μl). The following parameters were used for PCR: 94 °C (5 min), 30 cycles of 94 °C (15 s), 56 °C (30 s) and 72 °C (1 min), followed by a final extension at 72 °C (6 min).

Alleles	Sense primer (5'-3')	Antisense primer (5'-3')	Amplicon size/bp
WT	AACTTGTTAGGATCTCCCCGC	GGCAGATCTTTGAAGGCAAG	496
TPC1 XG716	TGACGGTGAAAACCTCTGACAC		383
WT	CTGGCATCTTGAGGTTTGGT	GGGCTACACTCCCAAGCATA	376
TPC1 D159	CCAGCTCATTCCTCCCACTC		459
WT	CTTCGGAGCCTTCTTTCCTT	CTGTCCCTGACGAGTGGTTT	493
TPC2 YHD437	GTCGGGGCTGGCTTAACTATsG		336

Table 2.2: Primers used in PCR reactions to genotype the mice. The size of the amplicon was used to determine the wild-type (WT) or mutant alleles carried in the mice.

2.3 Cell culture

Mouse Embryonic Fibroblasts (MEFs) previously prepared and immortalized by serial passages in the lab, or Human Embryonic Kidney Cell-line 293T (HEK293T) were cultured in Dulbecco's Modified Eagle's Medium (DMEM) containing 4.5 g/L D-glucose and phenol red and supplemented with 10% (v/v) foetal calf serum, 2 mM L-Glutamine, 0.1 mg/ml streptomycin, and 100 U/ml penicillin in a humidified 37 °C cell culture incubator containing 5% CO_2.

2.3.1 Oestradiol treatment

To prepare MEFs for the oestradiol treatment, cells were washed once in PBS. Washed MEFs were cultured in DMEM containing 4.5 g/L D-glucose, without phenol red, and supplemented with 10% (v/v) HyClone Charcoal/Dextran Treated Fetal Bovine Serum (Thermo Fisher Scientific) for reduced levels of hormones and growth factors, 2 mM L-Glutamine, 0.1 mg/ml streptomycin, and 100 U/ml penicillin in a 37 °C cell culture incubator containing 5% CO_2 for approximately 24 h before oestradiol treatment.

2.4 Molecular cloning techniques

2.4.1 ΔN-TPC1 cloning using TOPO TA-cloning

The shorter variant of TPC1 (ΔN-TPC1) cDNA (2408 bp) was cloned using TOPO XL PCR Cloning Kit (Invitrogen) following the manufacturer's instructions. Briefly, purified cDNA fragments produced by reverse transcription-PCR (RT-PCR) (Section 2.5.4) were

mixed with linearized pCR-XL-TOPO plasmid vectors for 5 min at room temperature. The reaction was terminated by adding the TOPO Cloning Stop Solution. *Taq* polymerase was used in RT-PCR to amplify the products; because of its nontemplate-dependent terminal transferase activity, it adds a single deoxyadenosine (A) to the 3' ends of the PCR products (amplicons). The A on the 3' ends should ligate efficiently with the overhanging 3' deoxythymidine (T) on the linearized pCR-XL-TOPO plasmid vector.

2.4.2 Subcloning of TPC cDNAs into mCherry-tagged expression vectors

2.4.2.1 PCR truncation and incorporation of restriction enzyme sites in TPC cDNA sequences

PCR was performed using either High Fidelity PCR Master (Roche) or Expand Long Range (Roche) kits following the manufacturer's instructions. For PCR using the High Fidelity PCR Master kit, briefly, plasmid DNA (0.04 ng/μl), and gene-specific primers (0.3 μM) were added in a reaction containing High Fidelity PCR Master mix. For PCR using the Expand Long Range, PCR Nucleotide Mix dNTPmix (0.5 mM), plasmid DNA (0.02 ng/μl), DNA polymerase enzyme mix (0.07 U/μl), and gene-specific primers (0.4 μM) were added in a reaction containing Expand Long Range buffer with $MgCl_2$ in 3% DMSO.

Gene-specific primers were designed to clone out or truncate the open reading frame of the full-length (FL) TPC cDNAs with restriction sites of Afl II (TPC1) or Kpn I (TPC2) incorporated on the N-terminus, and Not I on the C-terminus omitting the stop codon (Table 2.3). The following parameters were used for PCR: 92 °C (3 min), and 10 cycles of: 92 °C (10 s), annealing temperature (indicated in Table 2.3, 15 s) and 68 °C (8 min), and 20 cycles of the above condition but with 20 s cycle elongation for each successive cycle, followed by a final extension at 68 °C (7 min). PCR products were analysed by agarose gel electrophoresis, extracted from the gel and purified (Section 2.4.2.4).

2.4.2.2 Restriction enzyme digestion

Plasmid expression vector (pcDNA5/TO.mCherry.SpTPC1, made previously in the lab) or purified PCR products were digested by the desired restriction enzymes depending on the sites that were incorporated in the PCR products (Table 2.3), following the manufacturer's

cDNA	FL or truncations (Δ) in terminal	Sense primer (5'-3') Antisense primer (5'-3')	Annealing temperature/°C	Amplicon size/bp
TPC1	FL	GATC**CTTAAG**CAGTTTAAAGCCCTGGCC GATC**GCGGCCGC**GGTGACAGTCTGGGAGCG	56	2525
	ΔN	GATC**CTTAAG**CCACCACGGCTTCTGAGT GATC**GCGGCCGC**GGTGACAGTCTGGGAGCG	56	2450
	ΔC	GATC**CTTAAG**CAGTTTAAAGCCCTGGCC GATC**GCGGCCGC**GCCTCGCTCCTCACGATA	57	2263
	ΔNC	GATC**CTTAAG**CCACCACGGCTTCTGAGT GATC**GCGGCCGC**GCCTCGCTCCTCACGATA	56	2126
TPC2	FL	GATC**GGTACC**ATGGCGGCAGAAGAGCAGCCC GATC**GCGGCCGC**CCTGCACAGATGCAAGTGTGG	60	2193
	ΔN	GATC**GGTACC**ATGGAGCTCTGCATAGACCAGGCT GATC**GCGGCCGC**CCTGCACAGATGCAAGTGTGG	60	2196
	ΔC	GATC**GGTACC**ATGGCGGCAGAAGAGCAGCCC GATC**GCGGCCGC**CTGCTTGGTCCCAACAAGGAG	60	2094

Table 2.3: PCR conditions used to incorporate restriction enzyme sites, and to generate full-length (FL) or truncated (ΔN) TPC cDNAs. PCR reaction was analysed by agarose gel electrophoresis and verified with the predicted size of amplicons. Blue and green coloured text indicate the restriction enzyme sites. Restriction sites of Afl II for TPC1 and Kpn I for TPC2 were incorporated in the sense primers (Green). Not I restriction site was incorporated in the antisense primers (Blue). Four extra nucleotides, GATC (orange), were added for efficient restriction enzyme digestion.

instructions. Briefly, plasmid DNAs or purified PCR products were digested by restriction enzymes (1 u enzyme/1 μg DNA, Fermentas) in a reaction containing restriction enzyme buffers provided by the manufacturer at 37 °C for 2 h or room temperature overnight. For digesting the plasmid expression vector, the reactions were analysed by agarose gel electrophoresis to confirm the digestion. The fragment of interest (pcDNA5/TO.mCherry) was extracted and gel purified (Section 2.4.2.4). If the PCR products were digested for ligation purposes, then the digested products were directly purified to remove the restriction enzyme and the reaction buffer (Section 2.4.2.5).

2.4.2.3 Agarose gel electrophoresis

DNA samples were mixed with DNA loading buffer (2% (v/v) glycerol, 0.1% (v/v) sodium dodecyl sulfate (SDS), 0.0005% (w/v) bromophenol blue, 10 mM EDTA; pH 8.0). The mix and the DNA markers of size 250–10,000 bp (GeneRuler DNA Ladder, Fermentas) were loaded in 1% (w/v) agarose gels in Tris-acetate-EDTA (TAE) buffer (40 mM Tris acetate and 1 mM EDTA; pH 7.6) containing ethidium bromide (0.5 μg/ml) and electrophoresed

between 100–130 V in TAE buffer. DNA was visualized by an UV transilluminator (SYNGENE, Model: GMV20).

2.4.2.4 DNA purification from agarose gel

Electrophoresed DNA was purified from agarose gel using QIAquick Gel Extraction Kit (QIAGEN) following the manufacturer's instructions. Briefly, the DNA band of interest was sliced from the agarose gel following electrophoresis. The gel was solubilized and applied to the anion-exchange QIAquick spin column. The DNA bound to the silica membrane in the column under the high-salt conditions, and was washed once by centrifugation at $17,900 \times g$. DNA on the silica membrane was eluted in distilled, deionised water, and stored at -20 °C until further use.

2.4.2.5 Purification of DNA fragments

PCR products were purified using the QIAquick PCR Purification Kit (QIAGEN) following the manufacturer's instructions. Briefly, DNA fragments were added to the binding buffer in a QIAquick column. The column was centrifuged to remove impurities while DNA bound to the silica-gel membrane. DNA was washed once, eluted in deionised, distilled water, and stored at -20 °C until further use.

2.4.2.6 Alkaline phosphatase treatment

To prevent digested plasmid DNA (pcDNA5/TO.mCherry) from self-ligation, the purified vector (40 ng/μl) was incubated with shrimp alkaline phosphatase (SAP, 0.06 U/μl) in Dephosporylation Buffer (Roche) at 37 °C for 10 min to dephosphorylate 5' phosphates from DNA, followed by incubation at 65 °C for 15 min to inactive SAP. The 5' dephosphorylated vector DNA was subsequently purified (Section 2.4.2.5) for ligation purposes.

2.4.2.7 Ligation of DNA

Purified digested cDNA fragment was ligated with 5' dephosphorylated digested expression vector by Rapid DNA Dephos & Ligation Kit (Roche) following the manufacturer's instructions. Briefly, a 1:3 molar ratio of vectors (50 ng) to inserts (cDNA fragment, 150 ng) was first diluted in DNA Dilution Buffer and then added in a reaction containing

T4 DNA Ligase (5 U) in T4 DNA Ligation Buffer. The reaction was incubated for 10 min at room temperature. Ligated plasmid (pcDNA5/TO.TPC.mCherry expression vectors) were either directly transformed into competent bacteria or store at -20 °C.

2.4.3 Site-directed mutagenesis (SDM)

Site-directed mutagenesis to mutate the [DE]XXXL[LI] motif to AXXXAA of mouse TPC1 or TPC2 was performed using QuikChange Site-Directed Mutagenesis Kit (Stratagene) following the manufacturer's instructions. Briefly, expression plasmid template (1 ng/μl), gene-specific primers (2.5 ng/μl) to introduce multiple-site mutations, PfuTurbo DNA polymerase (0.05 U/μl), and dNTP mix (proprietary concentration by Stratagene) were added in the reaction buffer provided by the manufacturer. Table 2.4 details the primer sequences to mutate specific [DE]XXXL[LI] sorting signals. Gene-specific primers to introduce mutations were designed by QuickChange Primer Design tool (Agilent Technologies). Cycling parameters were as follows: 95 °C (30 s), 16 cycles of: 95 °C (30 s), 55 °C (1 min), and 68 °C (9 min). During cycling, PfuTurbo DNA polymerase replicates the denatured plasmid strands with high fidelity and does not displace the primers containing specific mutations, allowing the target site to be mutated. The reaction was treated with *Dpn* I (10 U) at 37 °C for 1 h to remove the original (methylated and unmutated) template. The *Dpn* I-treated mutated DNA was directly transformed into XL10-Gold Ultracompetent Cells (Stratagene). The transformation was similar as detailed in Section 2.4.4 with an addition step of adding XL10-Gold β-Mercaptoethanol mix (4 %) in the cells before plasmid DNA.

2.4.4 Bacteria transformation by heat-shock

To transform the bacteria, $\leqslant$1:10 ratio of ligation mixture from TOPO TA-cloning or T4 DNA ligase reaction was added to 100 μl chemically-competent *Escherichia coli* bacteria (TOP10 (Invitrogen) or XL10-Gold (Stratagene) strains). The mixture was incubated for 30 min on ice, followed by heat-shock at 42 °C for 30 s. The mixture was immediately further incubated for 2 min on ice. Transformed bacteria were diluted with Luria Broth (LB: 10 g/L Tryptone, 5 g/L Yeast extract, 10 g/L NaCl). Depending on the antibiotic

Proteins	SDM terminal	Sense primer (5'-3') Antisense primer (5'-3')	Template
TPC1	N	GGCTGTAAGTTTAGATGCCGATGTGCCGGCCGCCCTGACCTTGGACGAG CTCGTCCAAGGTCAGGGCGGCCGGCACATCGGCATCTAAACTTACAGCC	pcDNA5/TO.FLTPC1.mCherry
	C	GCACCTCCTCTGCCGTGACCCGGGCGGCGGACACCCTCTC GAGAGGGTGTCCGCCGCCCGGGTCACGGCAGAGGAGGTGC	pcDNA5/TO.FLTPC1.mCherry
	NC	Same sense and antisense primers as SDMC	pcDNA5/TO.SDMNTPC1.mCherry
TPC2	N	CATGGCGGCAGCAGAGCAGCCCGCTGCGGGCCGGGGCC GGCCCCGGCCCGCAGCGGGCTGCTCTGCTGCCGCCATG	pcDNA5/TO.FLTPC2.mCherry

Table 2.4: Primer sequences designed to introduce site-directed mutagenesis (SDM; underline) on the N- or C- or both terminal [DE]XXXL[LI] motifs in the TPC-mCherry proteins to AXXXAA using pcDNA5/TO.TPC.mCherry plasmid expression vectors as the template.

resistance that the vector encodes, the diluted transformed bacteria were either pre-incubated at 37 °C for 1 h before plating on the LB-agar plates containing kanamycin (50 μg/ml) or immediately plated on the LB-agar plates containing ampicillin (50 μg/ml). The bacteria-containing plates were incubated at 37 °C overnight to form colonies.

2.4.5 Minipreparation of plasmid DNA

Colonies of bacteria were picked and cultured for 16 h at 37 °C in 5 ml LB containing the selective antibiotic (ampicillin: 100 μg/ml; kanamycin: 50 μg/ml). A ratio of 1 volume of the bacteria culture to 4 volume of the container was required to allow sufficient oxygen supply during the culture, thus typically a 25 ml vessel was used. The bacteria were then pelleted by centrifuging at $>8,000 \times g$ for 2 min. Plasmid DNA was purified using QIAprep miniprep system (QIAGEN) following the manufacturer's instructions. Briefly, pelleted bacteria were lysed under alkaline conditions and the lysate was neutralized. Protein precipitate was cleared by centrifugation, and the lysate was applied to the QIAprep spin column where DNA adsorbed to the silica-gel membrane, and impurities were filtered through and washed away. DNA was eluted in deionised, distilled water and stored at -20 °C until further use. Purified plasmid DNA were digested by restriction enzymes (Section 2.4.2.2) and analysed by DNA gel electrophoresis (Section 2.4.2.3) to confirm the insertion from ligation. If necessary, plasmids were sequenced to confirm its identity (Section 2.4.7).

2.4.6 Maxipreparation of plasmid DNA

Purified plasmid DNA of correct sequence was transformed into the competent bacteria and plated on the LB-agar plates to form colonies. Bacteria of single colonies were picked and cultured for 16 h at 37 °C in 200 ml LB containing the selective antibiotic (ampicillin: 100 μg/ml; kanamycin: 50 μg/ml) in a 1 litre container. The bacteria were then pelleted by centrifuging at $6,000 \times g$ for 15 min at 4 °C. Plasmid DNA was prepared using HiSpeed Plasmid Maxi Kit (QIAGEN) following the manufacturer's instructions. Briefly, pelleted bacteria were lysed under alkaline conditions and the lysate was neutralized. The lysate was cleared by the QIAfilter cartridge, and filtered through a HiSpeed Tip. Plasmid DNA in the lysate bound to the anion-exchange resin, and impurities were removed by gravity flow and washed away in a medium-salt buffer. Bound plasmid DNA was eluted in a high-salt buffer and then precipitated by isopropanol. Precipitated DNA was applied to the QIAprecipitator Module to enable trapping and further drying of precipitated DNA. Dried DNA was eluted in deionised, distilled water and stored at -20 °C until further use.

2.4.7 DNA sequencing

Plasmid DNA, PCR fragments and primers were diluted to required concentrations of 30–100 ng/μl, 10–50 ng/μl, and 10 pmol/μl, respectively in distilled, deionised water, and sent off to be sequenced by GATC Biotech.

2.5 mRNA expression analysis

2.5.1 Total RNA isolation

Total RNA was extracted from mouse tissues or cultured cells following RNeasy QiaRNA extraction procedure (QIAGEN).

For total RNA extraction from tissues, mice were killed by cervical dislocation. Harvested tissues were immediately frozen in liquid nitrogen and stored at -80 °C until use. Briefly, frozen mouse tissue (∼30 mg) was lysed and homogenized by a ULTRA-TURRAX homogenizer (IKA) until uniformly homogeneous in the presence of Buffer RLT, which contains guanidine thiocyanate and 1% β-Mercaptoethanol (β-ME) to denature RNase.

For total RNA extraction from the cultured cells, cells were washed twice with PBS

in the culture dish and lysed directly in the dish with Buffer RLT containing 1% β-ME. Lysate was collected by a scraper and homogenized by placing the lysate in a QIAshredder spin column and centrifuge at $13,000 \times g$ for 2 min. Homogenization occurred when the lysate passed through the spin column.

The homogenate from the mouse tissues or the cells was centrifuged at $13,000 \times g$ for 3 min and 1 volume of 70% ethanol was added to the supernatant. The ethanol/supernatant mix was filtered through a RNeasy mini spin column by centrifuging at $\leqslant 8,000 \times g$ and the total RNA in the sample was bound to the membrane in the spin column. Total RNA bound to the column was treated with DNase I ($\sim$0.5 Kunitz units/μg total RNA) for 15 min. The membrane was washed three times and total RNA was then eluted in 30–50 μl RNase-free water and stored at -80 °C.

2.5.2 RNA Quantification

RNA was quantified by either a NanoPhotometer (Implen GmbH) or Quant-iT RiboGreen RNA reagent (Invitrogen) following the manufacturer's instructions.

2.5.2.1 NanoPhotometer

To quantify the RNA using a NanoPhotometer, 1–5 μl of RNA was pipetted directly onto the centre of the submicroliter cell and was compressed by a dilution lid placed on top. The concentration of RNA was determined in NanoPhotometer by the Beer-Lambert equation where c = (A x ε)/b, where c is the concentration in ng/μl, A is the absorbance in absorbance units (AU), ε is the wavelength-dependent extinction coefficient in ng-cm/μl (For RNA, ε = 40 at 260 nm), and b is the path length in cm. The path lengths used were 1 and 0.2 mm.

2.5.2.2 Quant-iT RiboGreen RNA reagent

To quantify the RNA using Quant-iT RiboGreen RNA reagent (Invitrogen), Quant-iT RiboGreen reagent was diluted 1:1000 in TE buffer (10 mM Tris-HCl, 1 mM EDTA; pH 7.5 in DEPC treated water). One volume of the reagent was added to the RNA standards or samples in a 96-well microplate wells and incubated for 2 to 5 min at room temperature in the dark. Samples were excited at 488 nm and the fluorescence emission intensity was

measured at 520 nm using a Typhoon 9400 imager (GE healthcare). ImageQuant 5.2 software (Molecular Dynamics) was used to quantify the fluorescence emission intensity. Concentration of the unknown RNA sample was interpolated from its fluorescence emission intensity using a standard curve where the fluorescence emission intensity was plotted against known concentrations of RNA standards (0.01–1 ng/μl).

2.5.3 RNA integrity confirmation

Extracted total RNA was mixed with RNA loading dye (Fermentas) and together with RNA markers of size 200 to 6000 bases (RiboRuler High Range RNA Ladder, Fermentas) were loaded in 1% (w/v) agarose gels in TAE buffer containing ethidium bromide (0.5 μg/ml) and electrophoresed at 100 V in TAE buffer. RNA on the gel was visualized by an UV transilluminator (SYNGENE, Model: GMV20). Total RNA with good integrity should result in two sharp bands representing 28S (4.7 kb) and 18S (1.8 kb) rRNA.

2.5.4 Reverse transcription-PCR (RT-PCR)

RT-PCR was performed in a reaction containing extracted total RNA (1 ng to 1 μg), SuperScript III RT/ Platinum *Taq* High Fidelity Enzyme Mix (Invitrogen), and gene-specific sense and antisense primers (0.8 μM, Table 2.5) following the manufacturer's instructions. The following parameters were used for RT: 50 °C (30 min), 94 °C (2 min), and PCR: 30 cycles of 94 °C (15 s), annealing temperature is indicated in Table 2.5, 68 °C (1 min, except for the primer pairs indicated in bold (Table 2.5) where 3 min was used), followed by a final extension at 68 °C (10 min). The same parameters were used but for 45 cycles to amplify TPC2 exon 1 (E1) to gene trap (GT) fusion mRNA. The final reaction mixture was analysed by agarose gel electrophoresis (Section 2.4.2.3) to examine the amplicons produced. If necessary, amplified cDNAs were extracted from the gel for purification (Section 2.4.2.4). Purified amplicons (10–50 ng/μl) were then sequenced by GATC Biotech to confirm their identity (Section 2.4.7).

Gene	Sense primer (5'-3') Antisense primer (5'-3')	Location	Annealing temperature/°C	Amplicon size/bp
Tpcn1	AGTTTAGATGACGATGTGCCG	E2	58	819
	TTGACGATGCTGTTCTCCAG	E9		
	ACCTCTTCGTCCACAACCAC	E4	58	516
	TTGACGATGCTGTTCTCCAG	E9		
	ATTTTCCTGGTGGACTGTCG	E6	57	606
	CAGAGCAGCGACTTCGTAAA	E13		
	CCACCACGGCTTCTGAGTT	I2	57	497
	CACAATGGCCTCGATGAAC	E6		
	AGTTTAGATGACGATGTGCCG	E2	58	438
	GACAGTATCGGCCTCAGGAAGATCG	GT		
	CCACCACGGCTTCTGAGTT	**I2**	**58**	**2408**
	AGAAGAGGCTGGCTTGACG	**E27**		
Tpcn2	GGGCTTCATCATTTTCCTGA	E4	57	564
	TTGTTGGAAGTCGTCAGCAG	E8		
	TGTTACATTGGTGGGATGGC	E1	60	411
	GACAGTATCGGCCTCAGGAAGATCG	GT		
Actb	GATGACGATATCGCTGCGCTGGTCG	E2	58	447
	GCCTGTGGTACGACCAGAGGCATACAG	E4		

Table 2.5: Conditions used in RT-PCR to detect TPC mRNA expression, or to clone ΔN-TPC1 (in bold). RT-PCR reaction was analysed by agarose gel electrophoresis and verified with the predicted size of amplicons. E indicates exon, I indicates intron, and GT indicates gene trap.

2.5.5 Generation of TPC single stranded RNA (ssRNA) standards for quantitative PCR (qPCR)

qPCR standards were produced for the purpose of providing absolute copy numbers of TPC1 and TPC2 cDNA in the samples. To generate TPC ssRNA standards for qPCR, a template of the qPCR amplicon of the target gene with a T7 consensus promoter sequence on the 5' end must first be produced. This T7-template could then be transcribed *in vitro* to ssRNAs.

2.5.5.1 PCR incorporation of T7 consensus promoter sequence in qPCR standard DNA template for *in vitro* transcription

PCR was used to incorporate the T7 consensus promoter sequence, TAATACGACTCACTATAGGG, on the 5' end of mouse TPC1 and TPC2 qPCR amplicons for *in vitro* transcription. Gene-specific primers (0.8 μM), mouse TPC plasmid cDNA I.M.A.G.E. clones (Section 2.1.2, 50–100 pg/μl), dNTP mix (0.2 mM), and DreamTaq DNA polymerase

(0.025 u/μl, Fermentas) were added in the DreamTaq buffer (Fermentas). Gene-specific antisense primers have the same sequence as the antisense primers used in qPCR (Table 2.7). In contrast, sense primers were designed to add a T7 consensus promoter sequence to the 5' end of TPC1 and TPC2 cDNA sequences amplified in qPCR for *in vitro* transcription (Table 2.6). PCR parameters were set for 30 cycles of 94 °C (15 s), 58 °C (30 s) and 72 °C (30 min), followed by a final extension at 72 °C (10 min). PCR products were analysed by agarose gel electrophoresis, and the PCR products of expected size were extracted from the gel and further purified (Section 2.4.2.4).

Gene	Sense primer (5'-3') Antisense primer (5'-3')	Amplicon size/bp
Tpcn1	GGATCC**TAATACGACTCACTATAGGG**TCCAAGGCCTTCCAGTATTTC CTCCACCAGGATCCAGACAC	92
Tpcn2	GGATCC**TAATACGACTCACTATAGGG**CCCTGGCTGTATACCGATTG CCCTGGCTGTATACCGATTG	97

Table 2.6: Gene-specific primers used in PCR to add a T7 consensus promoter sequence (in bold) in mouse TPC1 and TPC2 qPCR amplicons on the 5' end. PCR reaction was analysed by agarose gel electrophoresis and verified with the predicted size of amplicons. This T7-PCR template can then be used for *in vitro* transcription.

2.5.5.2 *In vitro* transcription of qPCR standard DNA templates

Purified PCR products containing cDNA sequences of TPC1 or TPC2 with the T7 promoter sequence incorporated at the 5'-end (Section 2.5.5.1) were *in vitro* transcribed by MEGAscript T7 Kit (Ambion) to produce ssRNA standards following the manufacturer's instructions. Briefly, PCR templates (10 ng/μl) were added to a buffer containing four ribonucleotides (ATP, CTP, GTP, and UTP; 3 mM), and RNA Polymerase Enzyme Mix. The reaction was incubated at 37 °C for 6 h, followed by treating the sample with TURBO DNase (0.1 U/μl, Ambion) for 15 min at 37 °C to remove the template DNA. ssRNAs were analysed by agarose gel electrophoresis (Section 2.4.2.3), and then further purified to remove unincorporated nucleotides (Section 2.5.5.3). The concentration of ssRNA was quantified by Quant-iT RiboGreen RNA reagent (Section 2.5.2.2).

2.5.5.3 RNA purification

ssRNAs were purified by RNA Clean & Concentrator (Zymo Research) to remove impurities, such as unincorporated nucleotides, following the manufacturer's instructions. Briefly, the RNA sample was added to the binding buffer and applied to a Zymo-Spin IIC Column. The column was centrifuged in an empty collection tube at $13,000 \times g$ for 1 min to remove impurities while RNA bound to the column matrix. RNA was washed once by centrifuging at $13,000 \times g$ for 30 s, and eluted in DNase/RNase-free water by centrifuging at $10,000 \times g$ for 30 s. The eluted RNA was stored at -80 °C until further use.

2.5.5.4 Determination of ssRNA molecular weight and copy number

The molecular weight (M.W.) of the generated TPC1 and TPC2 ssRNAs were calculated by M.W. = (An x 329.2) + (Un x 306.2) + (Cn x 305.2) + (Gn x 345.2) + 159). An, Un, Cn, and Gn are the number of each nucleotide within the polynucleotide[3]. Each molecular weight of TPC1 and TPC2 standard ssRNA was determined to be 22438.8 and 24053.8 g/mole, respectively.

- **For TPC1 ssRNA**:

  gggtccaaggccttccagtatttcatgtacttggtggtggctgtcaacggtgtctggatcctggtggag

  A = 10, U = 21, C = 14, G = 24

  M.W. = (10 x 329.2) + (21 x 306.2) + (14 x 305.2) + (24 x 345.2) + 159 = 22438.8 g/mole

- **For TPC2 ssRNA**:

  gggccctggctgtataccgattgccgcactcaggatggaagccagagcagtatggcccactgtcgctctgggac

  A = 14, U = 14, C = 22, G = 24

  M.W. = (14 x 329.2) + (14 x 306.2) + (22 x 305.2) + (24 x 345.2) + 159 = 24053.8 g/mole

The mass of one copy (g) for ssRNA was calculated by dividing the molecular weight on ssRNA by Avogadro's constant (6.022×10^{23}). The copy number in the input ssRNA/cDNA template was then calculated by dividing the number of grams of input ssRNA/cDNA template by the mass of one copy (g).

[3] `http://www.ambion.com/techlib/append/na_mw_tables.html`

2.5.6 Reverse transcription-quantitative PCR (RT-qPCR)

2.5.6.1 Reverse transcription (RT)

cDNA was reversed transcribed using the High Capacity cDNA Reverse Transcription Kit (Applied Biosystems) following the manufacturer's instructions. Briefly, a reaction mixture containing control rodent RNA (25 ng/μl, TaqMan Rodent GAPDH Control Reagents, Applied Biosystems), or extracted total RNA (0.1 μg/μl), or mouse TPC single stranded RNA (ssRNA) standards made in-house (0.5 ng/μl), dNTP mix (4 mM), MultiScribe reverse transcriptase (2.5 U/μl), RNase inhibitor (0.05 U/ul), and reverse transcription random primers (1X) in reverse transcription buffer (1X) was incubated at 25 °C for 10 min, 37 °C for 120 min, followed by 85 °C to inactivate reverse transcriptase for 5 min. cDNA was stored at -80 °C until further use. cDNA for qPCR standards was serially diluted in 10 μg/ml Torulla yeast total RNA to increase stability during storage and freeze-thaw cycles (Applied Biosystems).

2.5.6.2 Quantitative PCR (qPCR)

All gene-specific sense and antisense primers and their matching Universal ProbeLibrary probe that detects sequence-specific amplicons were designed by Roche Universal ProbeLibrary Assay Design Centre[4]. Primer sequences and probes used are detailed in Table 2.7. The following cycling parameters were used: 50 °C (2 min), 95 °C (10 min), 40 cycles of 95 °C (15 s) and 60 °C (1 min), followed by cooling at 40 °C (30 s). Samples were analysed by Roche LightCycler 480 System (Roche).

Gene	Sense primer (5'-3')	Antisense primer (5'-3')	Universal ProbeLibrary probe number
Tpcn1	TCCAAGGCCTTCCAGTATTTC	CTCCACCAGGATCCAGACAC	77
Tpcn2	CCCTGGCTGTATACCGATTG	GTCCCAGAGCGACAGTGG	106
Accn5	TGAGTGTGCCTGAGTTACTTGC	AATTGTAATCAAACTAGCTCCACAGA	95
Klk1	GCTGCCCACTGCCATAAT	CAGAGGGTTCATCCTCCAAA	5
Cyc1	ACCTGGTGGGAGTGTGCTAC	CATCATCATTAGGGCCATCC	10
Gapdh	AGCTTGTCATCAACGGGAAG	TTTGATGTTAGTGGGGTCTCG	9
Actb	CTAAGGCCAACCGTGAAAAG	ACCAGAGGCATACAGGGACA	64
Eif4a2	CGATCTACCTACCAATCGTGAA	ACCTTTCCTCCCAAATCGAC	53
Ubc	GACCAGCAGAGGCTGATCTT	CCTCTGAGGCGAAGGACTAA	11

Table 2.7: Gene-specific primers and Universal ProbeLibrary probes used in qPCR.

[4] `http://www.roche-applied-science.com/sis/rtpcr/upl/index.jsp?id=UP030000`

2.5.6.3 Determination of the most stable reference genes

Five pairs of gene-specific sense and antisense primers (0.1 μM) were tested against three hepatic cDNA samples from five different mice strains (TPC1 XG716, TPC1 D159, TPC2 YHD437, WT1, and WT2) of each sex to obtain the most stable reference genes across all genotypes in mouse liver for future qPCR analysis. Briefly, cDNA samples (0.2 ng/μl), gene-specific sense and antisense primers (0.1 μM) for cytochrome c-1 (*Cyc1*), glyceraldehyde-3-phosphate dehydrogenase (*Gapdh*), beta-actin (*Actb*), eukaryotic translation initiation factor 4A2 (*Eif4a2*), and ubiquitin C (*Ubc*), and Universal ProbeLibrary probe (0.1 μM) were added in a reaction containing LightCycler 480 Probes Master (Roche). The cycling parameters used are detailed in Section 2.5.6.2. All crossing point (Cp) values obtained from RT-qPCR for five reference genes in three cDNA samples from five different genotypes of each sex were transformed into relative quantification data using the delta-Ct method (detailed in geNorm analysis[5] where the formula $2^{(\text{lowest Cp - Cp})}$ was applied per gene across all the samples. The transformed data were analysed by geNorm. geNorm determines the expression stability (M) of the tested reference genes across all cDNA samples. Tested reference gene were ranked according to their expression stability [280]. geNorm also determines the optimal number of reference genes required for normalization from calculating pairwise variation (V), where V is the variation levels in average expression stability of reference genes with the sequential addition of each reference gene to the equation for calculating the normalization factor. geNorm determined that using three reference genes were optimal for normalization, and of all five reference genes tested, *Gapdh*, *Cyc1*, and *Actb* were the most stably expressed in both male and female hepatic mRNA across the five different genotypes (Supplementary Figure 2.2).

2.5.6.4 Absolute and relative qPCR

cDNA samples or standards (0.05 ng/μl to 0.01 μg/μl), gene-specific sense and antisense primers (0.1 μM) for mouse *Tpcn1*, *Tpcn2*, *Accn5*, *Klk1*, *Gapdh*, *Cyc1*, or *Actb*, and their matching Universal ProbeLibrary probe (0.1 μM) were added in a reaction containing LightCycler 480 Probes Master (Roche, Table 2.7). The cycling parameters used are detailed in Section 2.5.6.2. For each sample, a Cp value at a fixed level of fluorescence

[5] `http://medgen.ugent.be/~jvdesomp/genorm/`

was generated.

For absolute quantification, log of known copy numbers of TPC cDNA standards and log of ng input cDNA reversed transcribed from control rodent RNA were plotted against Cp values of TPCs and reference genes to produce a standard curve. The copy numbers or ng of cDNA in the samples were extrapolated from their Cp values using the standard curve. Results are expressed as copies of the target gene per 1 ng input RNA normalized to geometric means of three reference genes: *Gapdh*, *Cyc1*, and *Actb* (see appendix Section 2.11.3 for detailed calculation). Geometric mean was used in preference to the arithmetic mean as it calculates the normalization factor more accurately by taken into account of the outlying values and variations in reference gene abundances [280].

Relative quantification was derived directly from Cp values of the samples using the delta-Cp method [280]. Briefly, the formula $2^{(\text{lowest Cp - Cp})}$ was applied per gene across all the samples. Relative expression of each target gene was calculated from the value derived from the formula $2^{(\text{lowest Cp - Cp})}$ for each sample of the target gene divided by a normalization factor. The normalization factor was calculated by the geometric mean of the values derived from the formula $2^{(\text{lowest Cp - Cp})}$ for each sample of the three reference genes (*Gapdh*, *Cyc1*, and *Actb*) (see appendix Section 2.11.4 for detailed calculation).

2.5.7 Microarray analysis

2.5.7.1 RNA isolation and cDNA synthesis

20 μg total RNA were isolated from six WT and TPC2 KO male mice of 8 weeks old (Section 2.5.1), and sent to the Microarray Facility in MRC Harwell[6] for microarray analysis. First, first single stranded cDNA was synthesized from total RNA using SMART PCR cDNA Synthesis kit (Clontech) following the manufacturer's instructions. Briefly, a reaction containing 0.2 μg/μl total RNA, 2 μM 3' SMART CDS Primer IIA, and 2 μM SMART IIA Oligonucleotide were incubated at 70 °C for 2 min, followed by cooling on ice for 2 min. 2 mM Dithiothreitol (DTT), 1 mM dNTP, and 10 U/μl PowerScript RT were gently mixed into the cooled reaction and incubated at 42 °C for 1 h, followed by incubation on ice to terminate the first strand cDNA synthesis. The reaction was stored at -20 °C until further use. The first-strand cDNA was then amplified and turned into

[6] `http://www.har.mrc.ac.uk/services/MPC/microarray/`

double strand using Advantage 2 PCR Kits (Clontech). Briefly, a reaction of a total 98 μl containing 0.2 mM dNTP, 0.2 μM 5' PCR Primer IIA, and Advantage 2 Polymerase Mix in Advantage 2 PCR buffer was added to 2 μl of the first stranded cDNA reaction. The mix was incubated at 95 °C (1 min), followed by 17 cycles of 95 °C (30 s), 65 °C (30 s), and 68 °C (6 min). Amplified cDNA was purified as detailed in Section 2.4.2.5, and stored at -20 °C until use.

2.5.7.2 cDNA labelling

Double-stranded cDNA was fluorescently labelled by a random-primed Klenow polymerase reaction using Bioprime kit (Invitrogen) following the manufacturer's instructions. Briefly, cDNA was mixed with random primer/reaction buffer mix and then boiled for 5 min, followed by cooling on ice. The reaction was then added with dNTP mix (60 μM of dCTP, and 120 μM of dATP, dGTP, and dTTP), Klenow, and fluorescently labelled Cy5-dCTP or Cy3-dCTP (50 μM) on ice and incubated at 37 °C between 1–18 h. The reaction was terminated by an addition of 50 mM EDTA (pH 8.0). The reaction containing fluorescently labelled cDNA was purified in a sephadex G50 spin column to remove unincorporated nucleotides (Amersham). Eluents from Cy3 and Cy5 tubes were combined and mixed with Cot-1 DNA (0.1 μg/μl) to block non-specific hybridization in microarray analysis. The reaction was dried using a speedVac and resuspended in 50 μl microarray hybridization solution (40% deionized formamide, 5x saline-sodium citrate (SSC) buffer (750 mM NaCl, and 75 mM trisodium citrate; pH 7.0), 1 mM sodium pyrophosphate, 50 mM Tris (pH 7.4), 5x Denhardt's solution, and 0.1% sodium dodecyl sulfate (SDS)).

2.5.7.3 Hybridization

The labelled mixture in microarray hybridization solution was incubated at 85 °C for 5 min, followed by 42 °C for 45 min prior to addition on the array. The array slide was placed into an hybridization chamber (Corning) and 15 μl water was added on each end of the chamber to ensure humidity. The chamber was sealed and place in an oven at 42 °C for 45 min. The labelled mixture was added onto the array slide and hybridized at 48 °C overnight. Array slides were washed once with 2x SSC (300 mM NaCl, and 30 mM trisodium citrate; pH 7.0), followed by five vigorous washes for 5 min in 0.1x

SSC (15 mM NaCl, and 1.5 mM trisodium citrate; pH 7.0), and 0.1% SDS. Lastly, array slides were vigorously washed twice in 0.1x SSC. Array slides were rapidly placed into a 50 ml Falcon tube with the labelled side on the bottom and centrifuged at 600 rpm for 5 min at room temperature to remove excess liquid and debris. Array slides were scanned by ProScanArray HT Microarray Scanner (PerkinElmer) and the data were analysed by ProScanArray Express software.

2.6 Bioinformatics

2.6.1 UCSC Genome Bioinformatics

ΔN-TPC1 of mouse and human mRNA/genomic alignments were obtained using UCSC Genome Bioinformatics[7]. Rat TPC1, mouse TPC1, and mouse TPC2 protein sequences (GenBank accession numbers: AAH62072 (*Rattus norvegicus* TPC1), AAH58951 (*Mus musculus* TPC1), and AAI41196 (*Mus musculus* TPC2)) were aligned using ClustalW2[8]. DBTSS (DataBase of Transcriptional Start Sites[9]) and histone 3 methylations analysis by Broad Institute ChIp-seq studies (UCSC Genome Bioinformatics) were used to investigate the alternative promoters for TPC1 in mouse and human.

2.6.2 CAP3 Sequence Assembly Program

DNA sequencing results were checked against the expected DNA sequence by the CAP3 Sequence Assembly Program[10], where it assembled and aligned the contiguous sequences in the sense and antisense direction. The assembled sequences were examined by eye for any unexpected differences compared to the predicted gene sequence.

2.6.3 NetPrimer

Primers were analysed for their melting temperatures using the nearest neighbor thermodynamic theory via NetPrimer (PREMIER Biosoft International[11]).

[7] http://genome.ucsc.edu/
[8] http://www.ebi.ac.uk/Tools/clustalw2/index.html
[9] http://dbtss.hgc.jp/
[10] http://pbil.univ-lyon1.fr/cap3.php
[11] http://www.premierbiosoft.com/netprimer/index.html

2.6.4 ExPASy Proteomics Server

2.6.4.1 Translate tool

cDNA sequences were translated to a protein sequence by Translate tool in ExPASy Proteomics Server (Swiss Institute of Bioinformatics[12]).

2.6.4.2 Compute pl/Mw tool

Protein isoelectric point and molecular weight were predicted by Compute pl/Mw tool in ExPASy Proteomics Server (Swiss Institute of Bioinformatics[13]).

2.6.4.3 ScanProsite

Protein dileucine- or tyrosine-sorting motifs were identified using the ScanProsite program on the ExPASy Proteomics Server (Swiss Institute of Bioinformatics[14]).

2.6.5 Mobyle

Protein sequence multiple-alignments were displayed in different colour letter and shades for similar, identical, conserved or different amino acid residues by BOXSHADE 3.31 in Mobyle@Pasteur (A portal for bioinformatics analyses[15]).

2.7 Protein expression analysis

2.7.1 Cell transfection

2.7.1.1 $CaPO_4$ transfection

HEK293T cells were seeded at approximately 10% confluency in a dish of 10 cm diameter and cultured overnight at 37 °C in a humidified cell culture incubator containing 5% CO_2. Cells were transfected using Calcium Phosphate Transfection Kit following the manufacturer's instructions. Briefly, pcDNA5/TO.TPC.mCherry was diluted to 20 μg/ml in 0.25 M $CaCl_2$ and added dropwise to an equal volume of 2x HEPES-Buffered Saline (50 mM HEPES, 280 mM NaCl, 1.5 mM Na_2HPO_4; pH 7.05) whilst vortexing. The mixture

[12] http://www.expasy.ch/tools/dna.html
[13] http://www.expasy.org/tools/pi_tool.html
[14] http://expasy.org/tools/scanprosite/
[15] http://mobyle.pasteur.fr/cgi-bin/portal.py#forms::boxshade

was incubated at room temperature for 20 min to allow $Ca_3(PO_4)_2$.DNA precipitate to form. The precipitate mixture was then subsequently distributed to the cells in the culture dish. Cells were incubated for 16 h to allow endocytosis to occur before changing the media to standard culture media. Cells were cultured for a further 30 h before harvesting.

2.7.1.2 jetPEI transfection

MEFs were seeded to 50–70% confluency on poly-D-lysine-coated (50 μg/ml) number 1 glass coverslips of 13 mm diameter (VWR) and cultured overnight at 37 °C in a humidified cell culture incubator containing 5% CO_2. Cells were transfected with 0.5 μg of full-length, truncated, or mutant TPC-mCherry expression vectors, together with an organelle marker plasmid of either: 0.5 μg of LAMP1-mGFP (kind gift from Esteban C. Dell'Angelica, UCLA), TfR-GFP (kind gift from Philip Woodman, Manchester University), EEA1-GFP (kind gift from Silvia Corvera, UMASS Medical School), or KDEL-GFP (kind gift from Sergio Grinstein, University of Toronto) constructs using jetPEI (Polyplus Transfection) following the manufacturer's instructions. jetPEI contains mainly linear polyethylenimine (PEI), which will compact DNA into positively-charged complexes that are subsequently endocytosed into the cells.

Briefly, 0.5 μg TPC-mCherry expression vectors, and 0.5 μg GFP-organelle marker vectors were each diluted to 10 ng/μl in the same volume of 150 mM NaCl. Thus, the total concentration of vectors in 150 mM NaCl would be 20 ng/μl. An equal volume of 4% jetPEI in 150 mM NaCl was then added to the solution containing two vectors. The mixture was vortexed and incubated at room temperature for 15–30 min. The jetPEI/DNA mix was added dropwise to the cells in culture medium. Cells were incubated in the culture containing the transfection reagent for ∼30 h before harvesting.

2.7.2 Cell fixation, filipin staining and mounting

After 30 h post-jetPEI transfection, cells on the coverslips were washed twice in cold PBS and immersed in 4% (w/v) paraformaldehyde in PBS (pH 7.3) for 15 min at room temperature for fixation. For cells requiring filipin staining, fixed cells were washed twice in PBS before and after staining with filipin in culture media (250 μg/ml) for 30 min at room temperature. Coverslips were then washed three times in PBS before mounting

with Prolong Gold or Prolong Gold with DAPI (if nuclei staining is required, Invitrogen).

2.7.3 Confocal microscopy

Images of cells overexpressing TPC-mCherry and GFP-organelle markers were acquired by a Zeiss LSM 510 META confocal laser scanning microscope with a 63x, 1.4 numerical aperture oil immersion objective. Images were taken using Multi Track mode and of single optical sections. Lasers, excitation, and emission wavelengths used for different fluorescent molecules are summarized in Table 2.8

Fluorescent molecule	Laser	Excitation wavelength/nm	Emission wavelength/nm
GFP	Argon	488	505–515
mCherry	HeNe	543	>560
Filipin	UV	351, 364	>385

Table 2.8: A summary of lasers, excitation, and emission wavelengths used for different fluorescent molecules.

2.7.4 Protein sample preparations

2.7.4.1 Cell membrane preparation

Transfected HEK239T cells were washed twice with ice-cold PBS. To prepare the membrane fraction, cells were scraped from dishes and collected by centrifugation at 1500 × g for 3 min at 4 °C. Pelleted cells were lysed in hypotonic buffer (20 mM Hepes, 1 mM EDTA, 1x protease inhibitor (Roche); pH 7.2) for 30 min on ice and homogenized by Dounce homogenizer. The homogenate was centrifuged at 1500 x g for 3 min at 4 °C to remove unbroken cells and the nuclei. Supernatant from the homogenate was centrifuged at 100,000 x g for 1 h at 4 °C. The pellet containing membranes was resuspended in hypotonic buffer and stored at -80 °C until use.

2.7.4.2 Tissue homogenate preparation

Mice (8–12 weeks old) were killed by cervical dislocation and livers were immediately frozen in liquid nitrogen and stored at -80 °C. Frozen livers were thawed and washed once with ice-cold PBS. Thawed livers were then homogenized at 4 °C using an ULTRA-TURRAX

homogenizer (IKA) in ice-cold hypotonic buffer. Homogenized solutions were centrifuged at 15,000 rpm for 30 min at 4 °C. Supernatant from the homogenate was immediately frozen in liquid nitrogen and stored at -80 °C until use.

2.7.4.3 Tissue membrane preparation

To prepare the membranes from the tissue homogenate (Section 2.7.4.2 for homogenate preparation), the homogenate was spun at 1,000 x *g* for 5 min at 4 °C and the supernatant was further centrifuged at 100,000 x *g* for 1 h at 4 °C. For [^{32}P]NAADP binding, the pellet was washed once and then centrifuged at 140,000 x *g* for 1 h at 4 °C to remove free NAADP. The membrane pellet was resuspended in the ice-cold hypotonic buffer, and stored at -80 °C until use.

2.7.5 Protein quantification

Proteins were quantified by Bicinchoninic Acid (BCA) protein assay. 10 μl protein bovine serum albumin (BSA) standards or samples diluted in 100 mM NaOH were added to each well of 96-well clear-bottomed microplate. 200 μl of BCA solution containing 3.2 mM $CuSO_4$, was added to each well and the reaction was incubated at 55 °C for 30 min. Absorbance of the samples was measured at 595 nm. Concentrations of the unknown protein samples were calculated from their absorbance values at 595 nm using a standard curve where the absorbance values at 595 nm were plotted against known concentrations of protein standards.

2.7.5.1 Protein electrophoresis via SDS-PAGE

SDS-PAGE, sodium dodecyl-sulphate polyacrylamide gel electrophoresis, separates denatured proteins according to their molecular weight. 7% resolving acrylamide gels were made by diluting 30% (v/v) 37.5:1 acrylamide:bis-acrylamide (National Diagnostics) to 7% in 375 mM Tris-HCl (pH 8.8), 0.1% (w/v) SDS, 0.1% (w/v) ammonium persulphate (APS), and 0.08% (v/v) Tetramethylethylenediamine (TEMED). The acrylamide gel mix was then loaded in an upright cast with saturated butanol covering the top of the gel mix. Cast resolving gels were left undisturbed to polymerize for at least 15 min. After polymerization, the butanol was removed, and the top of the resolving gel was washed

twice with deionised, distilled water and dried with tissue papers. 4% stacking gel was prepared by diluting 30% (v/v) 37.5:1 acrylamide:bis-acrylamide (National Diagnostics) to 4% in 125 mM Tris-HCl (pH 6.8), 0.1% (w/v) SDS, 0.1% (w/v) APS, and 0.1% (v/v) TEMED. The gel mix was poured on top of the resolving gel and a comb (1 mm thick) was inserted on top of the stacking gel to produce wells for protein loading.

For probing TPC, 25 μg of membranes overexpressing TPC or 50 μg mouse hepatic membranes were prepared in Laemmli buffer (62.5 mM Tris-HCl, 10% (v/v) glycerol, 2% (v/v) SDS, and 0.02% (w/v) bromophenol blue; pH 6.8) and 200 mM DTT. The samples were not heat treated so as to prevent heat-induced protein aggregation. For probing β-galactosidase, 50 μg mouse liver homogenate was heat-treated at 95 °C for 10 min in Laemmli buffer. Protein samples and standards (PAGEruler Plus, Fermentas) were loaded into the wells of the acrylamide gels. Proteins were electrophoresed at 100 V in running buffer (25 mM Tris-base, 192 mM glycine, and 0.1% (w/v) SDS; pH 8.3) for approximately 1 h depending on the molecular weight of the target protein. Protein electrophoresis was performed using a mini-PROTEAN 3 vertical electrophoresis system (Bio-Rad).

2.7.5.2 Western blotting

SDS-PAGE resolved proteins were transferred to PVDF membranes (Hybond-P PVDF, 0.45 μm pore size, GE Healthcare) in ice-cold TRIS-glycine buffer (25 mM Tris-base and 192 mM glycine; pH 8.3) at 300 mA for 1 h. Membranes containing regions for non-specific antibody interactions were either blocked by 5% (w/v) dried skimmed milk (Marvel) in PBS and 0.5% (v/v) Tween-20 (PBST) for probing mCherry or TPC or by 2% (w/v) ECL Advanced Blocking Agent (GE Healthcare) in PBST for probing β-galactosidase. Membranes were blocked for 1 h at room temperature or overnight at 4 °C. Blocked membranes were incubated in primary antibodies detailed in Table 2.9 for 1 h at room temperature or overnight at 4 °C. After the primary antibody incubation, membranes were washed four times, each of 10 min, with PBST. Membranes were then incubated with horseradish peroxidase (HRP) conjugated secondary antibodies detailed in Table 2.9 for 1 h at room temperature, and washed as above.

To probe mCherry or TPCs, immunoreactive bands were detected by chemiluminescence using Amersham ECL Plus Western-Blotting Detection Reagents (GE Healthcare)

following the manufacturer's instructions. To probe β-galactosidase, immunoreactive bands were detected by chemiluminescence using Amersham ECL Advance Western Blotting Detection Kit (GE Healthcare) following the manufacturer's instructions. Briefly, the side of the membrane containing protein was incubated with the chemiluminescent reagent for 1 min. Chemiluminescence was detected by exposing membranes to a blue-sensitive autoradiography film (Cole-Parmer), which was subsequently developed in Xograph film processor to reveal immunoreactive bands.

Protein to probe	**Primary antibodies (dilution)**	**Secondary antibodies (dilution)**	**Blocking & antibody dilution buffer**
mCherry	Rat monoclonal α-multi-red 5F8 (1:1000) [242]	HRP-conjugated goat α-rat IgG (1:10,000)	5% (w/v) milk in PBST
Mouse TPC1	Rabbit polyclonal α-MmTPC1 720 25F (1:500) Rabbit polyclonal α-MmTPC1 720 27F (1:500) Rabbit polyclonal α-HsTPC1 7047F (1:500) Rabbit polyclonal α-HsTPC1 7048F (1:500) Rabbit polyclonal α-HsTPC1 8253E (1:500) Rabbit polyclonal α-HsTPC1 8253F (1:500) Rabbit polyclonal α-HsTPC1 8254E (1:500) Rabbit polyclonal α-HsTPC1 8254F (1:500)	HRP-conjugated goat α-rabbit IgG (1:10,000)	
Mouse TPC2	Rabbit polyclonal α-MmTPC2 721 18F (1:500) Rabbit polyclonal α-MmTPC2 721 19F (1:500) Rabbit polyclonal α-HsTPC2 7049F (1:500) Rabbit polyclonal α-HsTPC2 7050F (1:500)		
β-galactosidase	Mouse monoclonal α-Ecβ-gal (1:1000)	HRP-conjugated rabbit α-mouse IgG (1:20,000)	2% (w/v) ECL Advanced Blocking Agent in PBST

Table 2.9: Primary and secondary antibodies, and blocking and antibody dilution buffer used in western blotting to probe different proteins. All α-TPC1 and α-TPC2 were in-house anti-sera collected from rabbits immunized with mouse or human TPC1 or TPC2 epitopes, which are detailed in Table 3.1 and 3.2. Mouse monoclonal α-Ecβ-gal clone 40–1a was developed by Joshua Sanes, and obtained from the Developmental Studies Hybridoma Bank (DSHB), University of Iowa. Abbreviations: α, anti; HRP, Horseradish peroxidase; Ec, *Escherichia coli*; Hs, *Homo sapiens* (Human); IgG, Immunoglobulin G; Mm, *Mus musculus* (Mouse); PBST, PBS and 0.5% (v/v) Tween-20 (PBST).

2.8 Radioligand Binding Analysis

2.8.1 [^{32}P]NAADP synthesis

2.8.1.1 [^{32}P]NAADP synthesis from [^{32}P]NAD

[^{32}P]NADP was enzymatically converted from [^{32}P]NAD by incubation of 6.25 μM of [^{32}P]NAD (29.6 TBq/mmol, Perkin Elmer) with 0.5 U/ml NAD kinase (Alexis Biochemicals), 5 mM MgATP, and 100 mM Hepes (pH 7.2) overnight. This reaction mixture was then incubated with 100 mM nicotinic acid and 1 μg/ml ADPR cyclase (a kind gift from H. C. Lee, University of Hong Kong) for 1 h to form [^{32}P]NAADP.

2.8.1.2 [^{32}P]NAADP synthesis from [^{32}P]ATP

[^{32}P]NADP was enzymatically converted by human NAD kinase by adding 7.1 μM [γ-^{32}P]ATP (111 TBq/mmol, Perkin Elmer) to a reaction containing 0.7 mM NAD, 0.6 mM $MnCl_2$, 70 mM Tris, 2.1 mM $MgCl_2$, and 0.5 U/ml human NAD kinase (Alexis Biochemicals). The phosphorylation reaction was incubated at 37 °C on a heating block for 2 h before an addition of 120 mM nicotinic acid and 2.4 μg/ml ADPR cyclase. The base exchange reaction was incubated at room temperature for 24 h to ensure a complete conversion of [^{32}P]NADP to [^{32}P]NAADP.

2.8.1.3 Purification of [^{32}P]NAADP

[^{32}P]NAADP synthesised from the reaction mixtures in Section 2.8.1.1 and 2.8.1.2 was separated by anion exchange resin (AG MP-1, Bio-Rad) in high-performance liquid chromatography (HPLC) using a non-linear concave upward gradient of trifluoroacetic acid (TFA) at a flow rate of 1 ml/min. The gradient is detailed in Table 2.10. [^{32}P]NAADP was collected at the elution peak at around 27 min (Supplementary Figure 2.1). The elution was neutralized by 20 mM Tris (pH 8) and stored at 4 °C until further use. The radioactivity was determined by Cerenkov scintillation counting.

Time/min	150 mM TFA/%	Water/%
0	0	100
6	2	98
11	4	96
16	8	92
21	16	84
26	32	68
26.1–30	100	0
30.1–40	0	100

Table 2.10: Non-linear concave upward gradient of TFA used in anion exchange HPLC to elute [^{32}P]NAADP.

2.8.1.4 Scintillation counting

1 μl of purified [^{32}P]NAADP was added to a GF/B glass fibre filter circle of 25 mm diameter (1 μm, Whatman) in a scintillation vial containing 10 ml water. The radioactivity of the sample was determined by Cerenkov scintillation counting.

2.8.1.5 Optimization of wash and binding buffers

Mouse hepatic membranes (5 mg/ml) were incubated with 66 pM [^{32}P]NAADP in one of the binding buffers listed in Table 2.11 for 1 h at room temperature in the presence and absence of unlabelled NAADP (1 mM). Unbound and bound [^{32}P]NAADP were separated by rapid vacuum filtration through GF/B glass fibre filter circles (1 μm, Whatman) using a manifold (Millipore) with a small amount of vacuum pressure. Filter circles were washed twice, each with 2–4 ml of ice-cold wash buffer listed in Table 2.11. pH of all buffers were adjusted to 7.2. Non-specific binding was determined by pre-incubating the membranes with 1 mM unlabelled NAADP for 10 min before the addition of [^{32}P]NAADP. The result from wash buffer indicated that binding signal to noise was best in wash buffer H, thus wash buffer H was used for optimization of binding buffer (Figure 5.1).

2.8.2 Dissociation binding

Mouse hepatic membranes (5 mg/ml) were incubated with 66 pM [^{32}P]NAADP in HK_{140} buffer at room temperature for 1 h to reach equilibrium before an addition of 1 mM unlabelled NAADP to terminate the reaction at various time points. Unbound and bound [^{32}P]NAADP were separated by rapid filtration.

Optimization of wash buffer

Binding buffer	Wash buffers
Glu-IM	Glu-IM
	H
	HK_{250}
	$HK_{250}M$
	HM

Optimization of binding buffer

Binding buffers	Wash buffer
Glu-IM	H
H	
HK_{250}	
$HK_{250}M$	
HM	

Table 2.11: Buffer compositions of Glu-IM: 250 mM potassium gluconate, 250 mM *N*-methyl D-glucamine, 20 mM Hepes, and 1 mM $MgCl_2$; of H: 20 mM Hepes; of HK_{250}: 20 mM Hepes and 250 mM potassium acetate; of $HK_{250}M$: 20 mM Hepes, 250 mM potassium acetate and 1 mM $MgCl_2$; and of HM: 20 mM Hepes and 1 mM $MgCl_2$.

2.8.3 Association binding

Mouse hepatic membranes (5 mg/ml) were added to 66 pM [^{32}P]NAADP in HK_{140} buffer for various length of time at room temperature. Non-specific binding was determined by an addition of 1 mM unlabelled NAADP to the reaction with [^{32}P]NAADP before the membrane addition. Unbound and bound [^{32}P]NAADP were separated by rapid filtration.

2.8.4 Saturation binding

Mouse hepatic membranes (5 mg/ml) were incubated with various concentrations of [^{32}P]NAADP in Glu-IM buffer at room temperature for 1 h to reach equilibrium. Non-specific binding was determined by pre-incubating the membranes with 1 mM unlabelled NAADP for 10 min before the addition of [^{32}P]NAADP. Unbound and bound [^{32}P]NAADP were separated by rapid filtration.

2.8.5 Competitive binding

Mouse hepatic membranes (5 mg/ml) were incubated with various concentrations of unlabelled compounds at room temperature for 10 min before an addition of 66 pM

[^{32}P]NAADP in HK_{140} buffer or 200 pM [^{32}P]NAADP in Glu-IM buffer. Non-specific binding was determined by the addition of 1 mM unlabelled NAADP to the reaction. The reaction was incubated for 1 h before rapid filtration.

2.8.6 Termination of binding reactions

Dissociation, association, saturation, and competitive binding reactions (Sections 2.8.2 to 2.8.5) were terminated by separating unbound from bound [^{32}P]NAADP by rapid vacuum filtration using a cell harvester (Brandel) through GF/B glass fibre filters (1 μm, Whatman). Filters were washed twice, each with 2–4 ml of ice-cold wash buffer. Glu-IM wash buffer was used if the binding was conducted in Glu-IM. Alternatively, H wash buffer was used if the binding buffer was HK_{140}.

2.8.7 Storage phosphor detection

Filter papers containing [^{32}P]NAADP were wrapped in cling film and exposed to a storage phosphor screen (GE Healthcare) overnight. The screen was scanned by a Typhoon 9400 Phosphor Imager (GE healthcare) using excitation at 633 nm and of a resolution of 100 μm. Emission at 390 nm was detected by the imager and the emission intensity is directly proportional to the amount of radioactivity in the sample. ImageQuant 5.2 software (Molecular Dynamics) was used to quantify the emission intensity. Specific binding of [^{32}P]NAADP to the membrane was calculated from subtracting non-specific binding from the total binding.

2.9 TPC function analysis

2.9.1 Isolation of Pancreatic Acinar Cells

Pancreata were excised from mice of 8–12 weeks old and immediately placed in ice-cold NaHepes buffer containing the following (in mM): 140 NaCl, 4.7 KCl, 1.13 $MgCl_2$, 1 $CaCl_2$, 10 Hepes, and 10 glucose (pH 7.2). Each individual pancreas was injected with 200 U collagenase CLSPA (Worthington Biochemical Coporation) until swollen and then incubated in the collagenase for 13–15 min in a 37 °C water bath. Digested pancreas was immediately placed and shaken in the ice-cold NaHepes buffer with addition of 0.15

mg/ml Trypsin inhibitor from *Glycine max* (soybean) to disperse small clusters or single pancreatic acinar cells. Cells were collected by centrifugation at 1,200 rpm for 3 min. Pelleted cells were washed twice and resuspended in ice-cold NaHepes buffer without trypsin inhibitor.

2.9.2 Ca^{2+} imaging using Fura-2 AM

Pancreatic acinar cells were seeded onto poly-D-lysine-coated number 1 glass coverslips of 25 mm diameter (ThermoFisher Scientific) for 15 min at room temperature. Cells were then loaded with 2–5 μM Fura-2 AM (Invitrogen) with 0.02% pluronic-127 (Invitrogen) in NaHepes buffer for 30–60 min at room temperature in the dark. Cells were washed twice in NaHepes buffer and the coverslip containing cells was mounted in a static chamber (Harvard apparatus). Ca^{2+} imaging was performed using microspectrofluriometry with Nikon DIAPHOT 200 Inverted Phase Microscope, with a 40x, 1.3 numerical aperture oil immersion objective.

Fluorescence in small clusters or single pancreatic acinar cells were excited alternatively with 340 and 380 nm light (emission measured at >510 nm) in NaHepes buffer, and ratio images were recorded every 3 s with a CCD camera (PTi Cool One). Images were analysed by PTi ImageMaster System. All experiments were performed at room temperature. Drugs were added to the cells in the chamber by mixing the drug first with the buffer previously withdrawn from the chamber, the buffer containing drug was then added back to the chamber at the indicated time. Final concentrations of the drugs in the chamber were: 2–50 pM for (Tyr[SO_3H]^{27}) Cholecystokinin fragment 26–33 Amide (CCK-8; CCK), 25–100 nM for acetylcholine (ACh), 50–200 μM for Gly-Phe β-naphthylamide (GPN), 3 μM for bafilomycin A1 (LC Laboratories), and 1 nM – 10 μM *trans*-Ned-19 (Enzo Life Sciences).

2.9.3 Imaging acidic organelles using LysoTracker Red DND-99

Acidic organelles in pancreatic acinar cells were detected by labelling the acinar cells with 200 nM LysoTracker Red DND-99 (Invitrogen) in NaHepes buffer for 10 min at room temperature in the dark. Cells were washed twice in NaHepes buffer and the coverslips containing cells were mounted in a static chamber (Harvard apparatus). Fluorescence in

cells was excited by 543 nm light from HeNe laser (emission measured at >590 nm) in NaHepes buffer. At the indicated time, GPN (50–200 μM) was added to the cells in the chamber by mixing first with the buffer previously withdrew from the chamber, the buffer containing GPN was then added back to the chamber. Images were recorded by Zeiss LSM 510 META confocal laser scanning microscope with a 63x, 1.4 numerical aperture oil immersion objective. Images were taken by Single Track mode from top to bottom of the cells with optimal slice interval of 0.41 μm. Cell images of all Z-sections were stacked by ImageJ software.

2.9.4 Analysis of Ca^{2+} oscillations induced by CCK

The interspike period (ISP; s) and peak height (Δ340/380 ratio) of CCK-induced Ca^{2+} oscillations were measured by PeakFinder software (kind gift designed by Robbie Shade[16], Supplementary Figure 2.6) before and after the drug addition. A peak was included if its height was greater than 0.05 Δ340/380 ratio (an amplitude lower than 0.05 discounts oscillations from the neighbouring cells). 'Responding cells' are defined as those that show at least two Ca^{2+} oscillatory spikes (to be able to determine the ISP).

2.10 Statistical Analysis

Pearson's coefficient of co-localization was calculated by Zeiss LSM 510 operating software. All data are expressed as means ± S.E.M. All statistical analyses were performed by Prism 5 software (GraphPad). The unpaired student's t-test was used between two data sets in most analysis except when comparing the expression level of TPCs in oestradiol-treated and untreated cells, and also the peak height and interspike period before and after drug treatment in pancreatic acinar cells where the paired student's t-test was used. One-way ANOVA with Dunnett's multiple comparison test was used for comparing three or more data sets with $P < 0.05$ being significant. $P < 0.05$, < 0.01 and < 0.001 are marked as *, ** and ***, respectively.

[16] `https://github.com/rjshade/PeakFinder`

2.11 Appendix

2.11.1 Purification of [^{32}P]NAADP

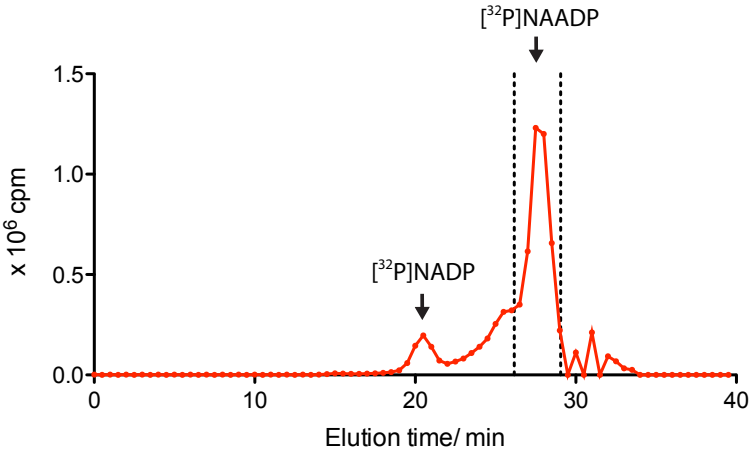

Figure 2.1: HPLC resolution of the final [^{32}P]NAADP synthesizing reaction mixture. [^{32}P]NAADP was collected at around 27 min between two dotted lines.

2.11.2 geNorm analysis to validate reference genes for qPCR

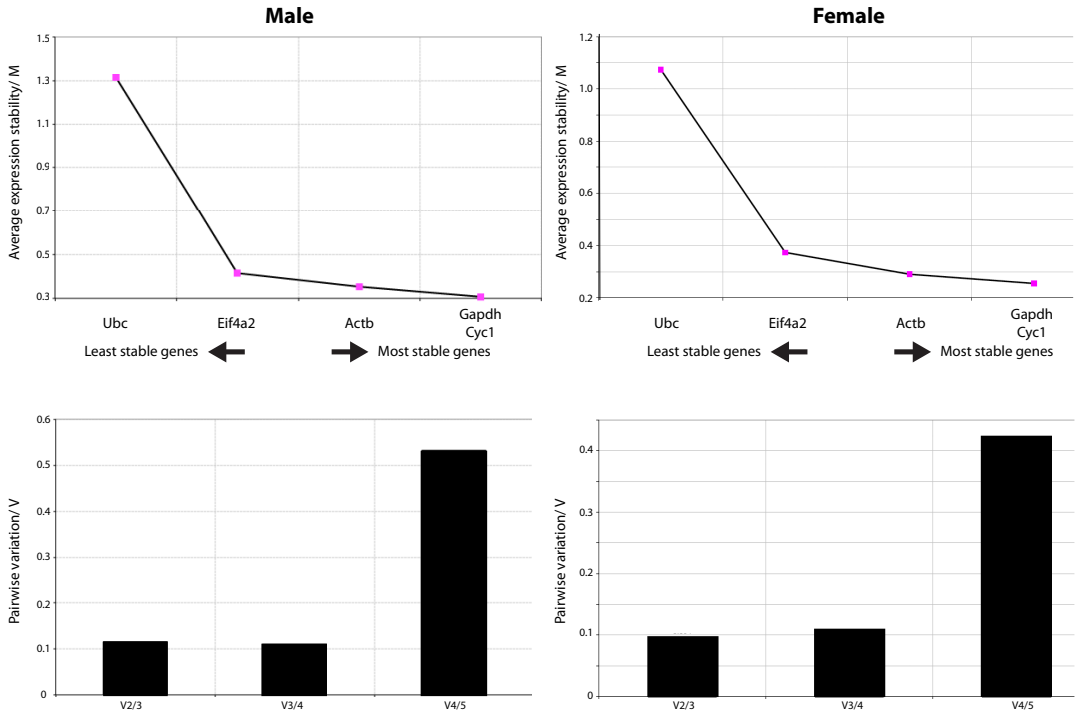

Figure 2.2: Validation of reference genes using geNorm analysis of five candidate reference genes (*Cyc1*, *Gapdh*, *Actb*, *Eif4a2*, and *Ubc*) in five different genotypes (TPC1 XG716, TPC1 D159, TPC2 YHD437, WT1, and WT2) of male and female mouse hepatic mRNAs. Top, Expression stability (M) of various reference genes. Lower M indicates a higher stability of the gene. Bottom, optimal number of reference genes required for normalization. This indicates the variation levels in average expression stability of reference genes with the sequential addition of each reference gene to the equation for calculating the normalization factor. The variation level of the two genes with the highest expression stability was indicated on the left followed by the inclusion of the third, fourth and fifth most stably expressed gene moving to the right. A V of < 0.15 would be ideal for the system.

2.11.3 Absolute quantification in qPCR

An example to calculate the number of TPC1 cDNA copies/ng normalized to three reference genes (*Gapdh*, *Cyc1*, *Actb*) in wild-type:

1. For TPC1: Log of known copies of TPC1 cDNA standards, and for three reference genes; log of known ng cDNA reverse transcribed from control rodent total RNA were plotted against respective Cp values obtained from RT-qPCR (Figure 2.3).

2. Log copies or ng of each gene in the samples were calculated from their Cp values using the the linear equation obtained from the standard graph (Figure 2.4).

    - Log TPC1 copies = (Cp value - 41.039)/-3.3811
    - Log Gapdh ng = (Cp value - 20.928)/-3.0879
    - Log Cyc1 ng = (Cp value - 25.276)/-3.2377
    - Log Actb ng = (Cp value - 21.041)/-3.2513

3. Copies or ng of each gene in the samples were calculated by anti-log of the log copies or ng values (Figure 2.4).

4. Any dilutions of the samples were taken into account in the calculation (Figure 2.4).

5. The number of TPC1 cDNA copies was normalized to the three reference genes by dividing the geometric mean of the reference gene ng to yield copies/ng RNA (Figure 2.4).

Standard

Gene	Dilution	Cp	Copies	Log Copies	Average Cp
Tpcn1	1:1E3	16.81	13419036.4	7.12772133	16.805
		16.8			
	1:5E3	19.44	2683807.29	6.42875133	19.38
		19.32			
	1:1E4	20.43	1341903.64	6.12772133	20.435
		20.44			
	1:5E4	22.7	268380.729	5.42875133	22.695
		22.69			
	1:1E5	23.74	134190.364	5.12772133	23.72
		23.7			
	1:5E5	25.98	26838.0729	4.42875133	25.965
		25.95			
	1:1E6	27.11	13419.0364	4.12772133	27.1
		27.09			

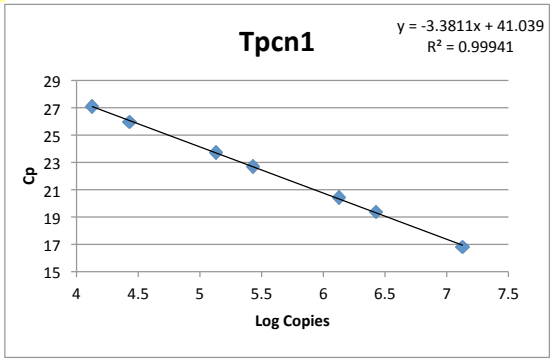

Gene	Dilution	Cp	ng	Log ng	Average Cp
Gapdh	1:10	19.99	2.5	0.39794001	19.965
		19.94			
	1:50	21.6	0.5	-0.30103	21.595
		21.59			
	1:100	22.61	0.25	-0.60206	22.6
		22.59			
	1:500	24.98	0.05	-1.30103	25.015
		25.05			
	1:1000	25.94	0.025	-1.60206	25.95
		25.96			
	1:5000	28.14	0.005	-2.30103	28.07
		28			

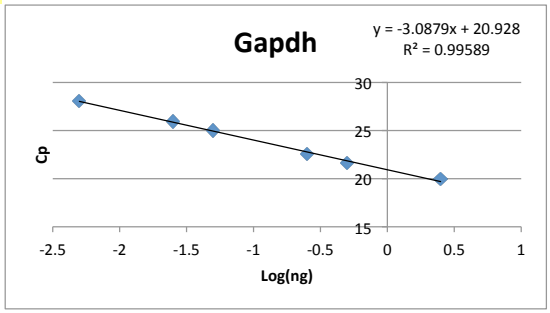

Gene	Dilution	Cp	ng	Log ng	Average Cp
Cyc1	1:10	24.47	2.5	0.39794001	24.465
		24.46			
	1:50	25.89	0.5	-0.30103	25.895
		25.9			
	1:100	26.95	0.25	-0.60206	26.975
		27			
	1:500	29.49	0.05	-1.30103	29.4
		29.31			
	1:1000	30.2	0.025	-1.60206	30.37
		30.54			
	1:5000	32.95	0.005	-2.30103	33.035
		33.12			

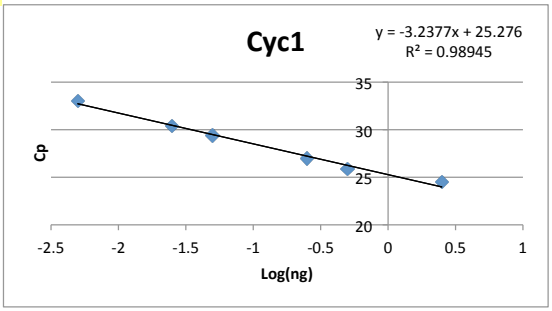

Gene	Dilution	Cp	ng	Log ng	Average Cp
Actb	1:10	20.26	2.5	0.39794001	20.165
		20.07			
	1:50	21.66	0.5	-0.30103	21.635
		21.61			
	1:100	22.78	0.25	-0.60206	22.82
		22.86			
	1:500	25.14	0.05	-1.30103	25.19
		25.24			
	1:1000	26.28	0.025	-1.60206	26.29
		26.3			
	1:5000	28.62	0.005	-2.30103	28.71
		28.8			

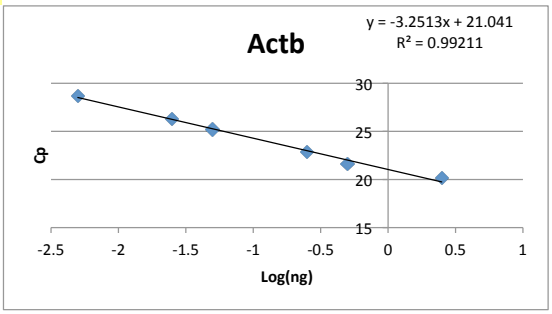

Figure 2.3: Calculation steps to create a standard curve of log known copies or ng of genes against respective Cp values obtained from RT-qPCR.

Strain	Gene	Dilution	Cp	Average Cp	Log (copies or ng)	Copies or ng	Non-diluted copies or ng	Reference gene geometric mean	Copies /ng RNA (Normalized to three reference genes)
Wild-type	Tpcn1	Neat	21.69	21.7	5.71973618	524488.754	524488.754		16401.96682
			21.71						
	Gapdh	1:200	22.51	22.51	-0.5123223	0.30738149	61.4762978	31.9771866	
			22.51						
	Cyc1	1:200	27	27	-0.5324768	0.29344265	58.6885308		
			27						
	Actb	1:200	25.51	25.41	-1.3437702	0.04531373	9.06274607		
			25.31						

Figure 2.4: Calculation steps to obtain number of TPC1 cDNA copies/ng normalized to three reference genes in a sample.

2.11.4 Relative quantification in qPCR

An example to calculate the relative level of Accn5 mRNA in four males of wild-type, and TPC2 KO.

1. For the Cp values obtained for each gene, the formula of $2^{(\text{lowest Cp- Cp})}$ was applied to calculate the relative level of each sample to the others.

    - For example, the lowest Cp value of Accn5 for WT and TPC2 KO was 22.525 in TPC2 KO.M4. Cp values for the gene were then converted by using the formula $2^{(22.525 - \text{Cp})}$.

2. The normalization factor was obtained by calculating the geometric mean of the relative levels of three reference genes.

3. The relative level of Accn5 was then normalized to three reference genes by dividing the relative level by the normalization factor. If necessary, the values can be rescaled so that the lowest value corresponds to 1.

Cp values

Strain	Accn5	Gapdh	Cyc1	Actb
WT.M1	22.825	22.44	26.02	24.9
WT.M2	23.16	22.84	26.5	25.575
WT.M3	23.06	21.92	25.935	24.71
WT.M4	23.52	21.955	25.79	24.96
TPC2 KO.M1	22.865	22.975	26.485	25.135
TPC2 KO.M2	23.425	23.535	27.18	25.88
TPC2 KO.M3	23.12	22.745	26.23	25.275
TPC2 KO.M4	22.525	22.84	26.26	25.275

2^(lowest Cp - Cp) for calculating relative levels

Strain	ACCN5	Gapdh	Cyc1	Actb	Normalization factor
WT.M1	0.8122524	0.69737183	0.85263489	0.87660572	0.804780172
WT.M2	0.64394081	0.52850902	0.61132014	0.54904641	0.561879758
WT.M3	0.69015868	1	0.90437938	1	0.967052867
WT.M4	0.50173587	0.97603176	1	0.84089642	0.936272247
TPC2 KO.M1	0.79004131	0.48129722	0.61770932	0.74483873	0.604997045
TPC2 KO.M2	0.53588673	0.32646495	0.3815648	0.44442134	0.381124256
TPC2 KO.M3	0.66204446	0.5644822	0.73713461	0.67595542	0.655196702
TPC2 KO.M4	1	0.52850902	0.7219646	0.67595542	0.636544524

	Normalized	Rescaled normalized
Strain	ACCN5	ACCN5
WT.M1	1.0092848	1.88339203
WT.M2	1.14604736	2.1386
WT.M3	0.71367213	1.33175928
WT.M4	0.53588673	1
TPC2 KO.M1	1.30585979	2.43682053
TPC2 KO.M2	1.40606829	2.62381621
TPC2 KO.M3	1.01045145	1.88556907
TPC2 KO.M4	1.57098202	2.9315561

Figure 2.5: Calculation steps to obtain relative levels of Accn5 normalized to three reference genes in four males of the WT and TPC2 KO.

2.11.5 PeakFinder software

(A)

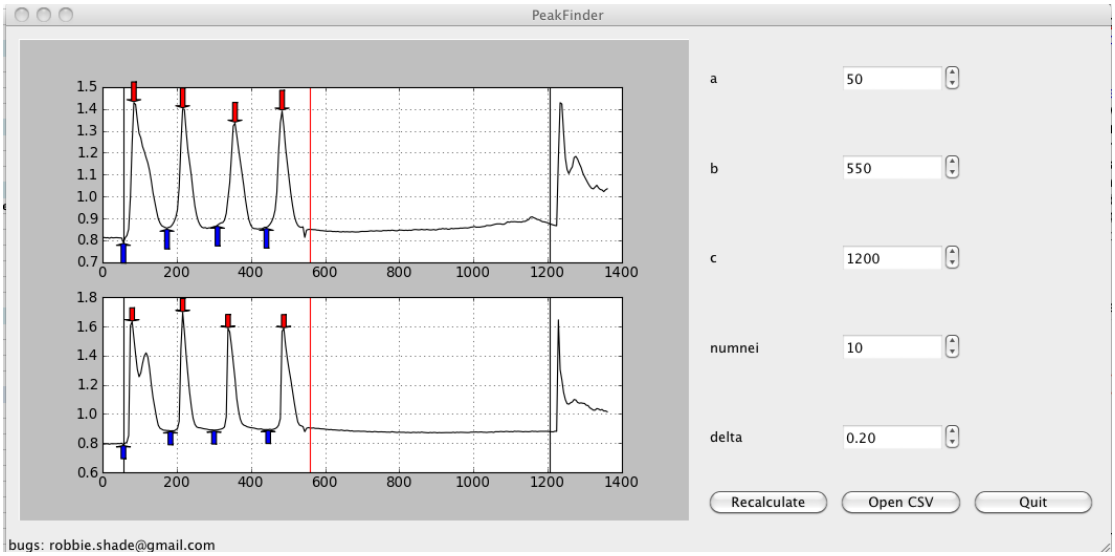

(B)

********** Data set 1 **********

	Start	End	Length	Peaks
--- A -> B ---	50	550	500	4
--- B -> C ---	550	1200	650	0

---------- A -> B ----------

Peak#	Time	Base	Peak	Delta	ISP
1	84.593	0.7909	1.42835	0.63745	
2	216.14	0.855377	1.40044	0.545063	131.547
3	357.187	0.869118	1.33465	0.465532	141.047
4	484.109	0.859372	1.38993	0.530558	126.922
Average				0.54465075	133.172

---------- B -> C ----------

Peak#	Time	Base	Peak	Delta	ISP

********** Data set 2 **********

	Start	End	Length	Peaks
--- A -> B ---	50	550	500	4
--- B -> C ---	550	1200	650	0

---------- A -> B ----------

Peak#	Time	Base	Peak	Delta	ISP
1	79.906	0.788746	1.63217	0.843424	
2	216.14	0.883963	1.69622	0.812257	136.234
3	338.343	0.889159	1.58691	0.697751	122.203
4	488.796	0.892695	1.58567	0.692975	150.453
Average				0.76160175	136.296667

---------- B -> C ----------

Peak#	Time	Base	Peak	Delta	ISP

Figure 2.6: PeakFinder software used to measure interspike period and peak height of CCK-induced Ca^{2+} oscillations. (A) Time of the drug addition is indicated on the right panel. Numnei indicates the number of neighbouring time points from either side of Ca^{2+} spike peak to search for the lowest 340/380 ratio as the base of the Ca^{2+} spike. Delta sets the threshold for Δ340/380 ratio to qualify as a peak. Red and blue arrows indicate the peak and the base of the Ca^{2+} spike respectively. Ca^{2+} spikes within three time points (A, B and C) containing two sections (A to B, and B to C) can be measured simultaneously. (B) PeakFinder also prints out the time of the Ca^{2+} spike peak (s), the base and the peak of the Ca^{2+} spike (Δ340/380 ratio), the amplitude (Delta, Δ340/380 ratio), and the interspike period (ISP; s).

Chapter 3

Characterization of TPC mutant mice

3.1 Introduction

Over the last few years, studies in heterologous systems have provided persuasive evidence that TPCs are the Ca^{2+} release channels gated by NAADP. NAADP-evoked Ca^{2+} responses were shown to increase in cells overexpressing TPCs of various species including human [39, 52], mouse [307], and sea urchin [41, 243], compared to endogenous (untransformed) TPC activity. Importantly, the heterologously expressed Ca^{2+} response was consistent with the classic behaviour of NAADP-induced Ca^{2+} release: specifically, the bell-shaped concentration response relationship, and its pharmacology (inhibition of the Ca^{2+} responses by acidic Ca^{2+} store-depletion (GPN and bafilomycin A1), and by the NAADP antagonist (Ned-19), but not by $InsP_3R$ or RyR inhibitors (heparin and ryanodine, respectively) or by ER Ca^{2+} store depletion (thapsigargin)). Furthermore, NAADP-elicited TPC channel Ca^{2+} responses were abolished by anti-TPC short hair-pin RNAs [52]. The most compelling evidence so far came from single channel studies in which it was shown that NAADP activated immunopurified human TPC2 channels in lipid bilayers [231], and also the mutant human TPC2 channels that had been redirected to the plasma membrane [42].

Despite the abundant evidence demonstrating that TPCs are NAADP-gated Ca^{2+} channels, little is known about the physiological role of TPCs. Three TPC isoforms have been identified: TPC1, TPC2, and TPC3. Most species express all three isoforms,

although some, including human and mice, only express TPC1 and TPC2 [52]. The lack of selective pharmacological inhibitors for specific TPC isoforms and the difficulties in abolishing gene expression in primary cell or tissue types prompted the need to generate TPC knockout (KO) mice. The mouse is an excellent model system because of the high homology of its genes to human (99%) [14], the ease of its genetic manipulation, and its short breeding cycle. Additionally, the mice can be inbred to minimise the effect of different backgrounds. Thus, it has become established as a powerful tool to study the endogenous physiological functions of individual proteins.

The first part of this chapter details the generation of TPC KO mice. In addition to TPC single KO mice—individuals in which the gene for one TPC isoform is deleted—TPC1 and TPC2 double KO (TPC DKO) mice were also generated. The former can be helpful in differentiating the endogenous role of individual isoforms in NAADP-mediated Ca^{2+} signalling. The latter can serve to overcome the phenomenon in which the remaining isoform can compensate for the missing gene. Furthermore, using TPC DKO mice, the endogenous role of the entire TPC family can be examined.

TPC KO mice generated will be used to test whether TPC is the *bona fide* NAADP-binding protein (Chapter 5), and, in addition, to investigate the endogenous role of TPCs in CCK-mediated signalling in pancreatic acinar cells (Chapter 6). By using TPC2 KO mice, my colleagues have demonstrated that in pancreatic β-cells, TPC2 is the key player in NAADP-elicited Ca^{2+} spikes in glucose signalling [52] [Arredouani et al., 2011, unpublished]. TPC2 KO mice were also used to show that TPC2 plays a crucial role in NAADP-mediated contraction in mouse bladder smooth muscle [90].

The second part of this chapter describes the characterization of mRNA and protein expression of mouse TPCs in wild-type (WT) and TPC KO mice. The expression patterns of TPCs could suggest tissue-specific roles for individual TPC isoforms. In knockout mice, compensation often occurs throughout embryo development to compensate for the loss of gene function [8, 176, 212]. Phenotypes arising from up- or down-regulation of the remaining TPCs in the TPC single KO mice, and of other genes in TPC single or double KOs may thereby disguise the phenotypes that might otherwise result from the ablation of a target TPC gene(s). Thus, the final part of this chapter discusses the extent of compensation by altered expression of the remaining TPC isoform, or of other genes.

3.2 Results

3.2.1 Generation and analysis of the TPC1 KO mouse

3.2.1.1 Identification of a TPC1 gene-trapped mutant ES cell line

In order to generate TPC1 KO mice, the embryonic stem (ES) cell line containing a TPC1 mutant was first obtained for injection into a blastocyst. Searches for TPC1 mutant ES cell lines were conducted in the gene trap consortiums. Since gene trapping is a high-throughput process; thousands of genes had already been randomly inactivated using this method, it is therefore likely to find a mutated TPC1 ES cell line that would result in a complete knockout. In gene trapping, mutation in the ES cell line is generated by a random insertion of a gene trap vector into an intron of genomic DNA. Searches revealed a TPC1 mutant mouse ES cell line, TPC1 XG716, from BayGenomics that was potentially suitable for generating TPC1 KO. This ES cell line was chosen because the gene trap vector insertion was near the 5' end of the *Tpcn1* gene (between exon 2 and 3, Figure 3.1B). This increases the chance of producing a non-functional protein (i.e. a knockout) as the protein would be very truncated with no transmembrane domains, thus it is unlikely to form a channel.

The gene trap vector used to generate the TPC XG716 ES cell line consisted of a splice acceptor sequence upstream of the promoterless selection/reporter gene, β-geo (a fusion of β-galactosidase and neomycin-resistance genes), followed by a polyadenylation signal (Figure 3.1B). During splicing, the endogenous splicing machinery recognizes the splice acceptor on the gene trap vector and splices *Tpcn1* exon 2, which is upstream of the insertion site, to β-geo (Figure 3.1B) instead of *Tpcn1* exon 3 (Figure 3.1A). Finally, the polyadenylation signal interrupts and terminates the transcription prematurely. The resulting mature mRNA comprises a fusion of truncated endogenous *Tpcn1* gene upstream of the gene trap insertion and β-geo. Translation of the TPC1-β-geo mRNA predicts a protein of only 37 N-terminal TPC1 amino acid residues fused to β-galactosidase (Figure 3.1B). In contrast, translation of the wild-type TPC1 predicts 817 amino acid residues.

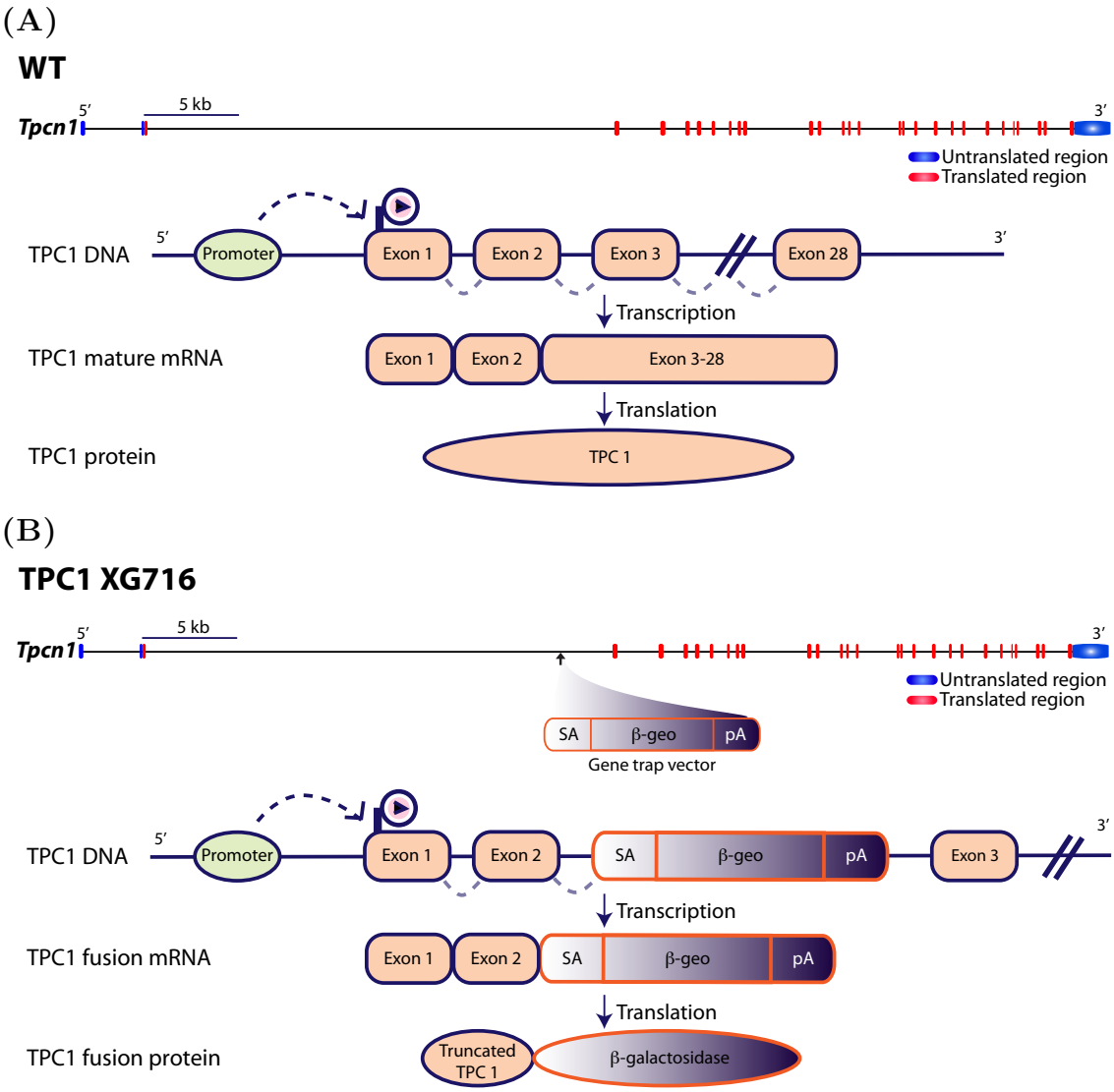

Figure 3.1: (A) Top, TPC1 mRNA/genomic DNA alignment. The blocks represent exons and the line indicates introns. Blue and red blocks indicate the untranslated and translated regions of mRNA, respectively. Bottom, in wild-type ES cell line, the endogenous promoter initiates transcription of *Tpcn1*, followed by normal splicing to form mature mRNA. Translation of this mRNA forms the native TPC1 protein. (B) Gene trapping in the TPC1 XG716 ES cell line. Top, the gene trap vector is randomly inserted in intron 2 of *Tpcn1* as indicated. The vector comprises a splice acceptor (SA) sequence, the *β-geo* gene, and a polyadenylation (pA) signal. Bottom, insertion of this vector interrupts the normal splicing and results in β-geo becoming spliced to endogenous TPC1 mRNA. This results in a truncated TPC1-*β*-geo fusion mRNA. When translated, the resulting peptide comprises 37 N-terminal amino acid residues of TPC1 protein fused to *β*-galactosidase.

3.2.1.2 Generation of TPC1 XG716 mutant mice

TPC1 mutant mice were generated in collaboration with MRC Harwell (Oxfordshire, UK; Figure 3.2). TPC1 XG716 ES cells that have a genetic background of 129P2/OlaHsd (white fur) were injected into a blastocyst from a mouse of C57BL/6 genetic background (black fur). The blastocyst (containing both TPC1 wild-type and TPC1 mutant ES cells) was then implanted into a pseudopregnant female mouse. Chimeric offspring contain both WT and mutant *Tpcn1* genes, and are identified by a mixture of patches of black and white fur respectively. These were then crossed with a WT C57BL/6 mouse (black), to confirm that the *Tpcn1* mutant allele has been incorporated into the germ cells. The resulting TPC1 XG716 heterozygous (+/–) mutant offspring (white) were crossed to obtain WT (+/+) and TPC1 XG716 homozygous (–/–) mutant mouse colonies.

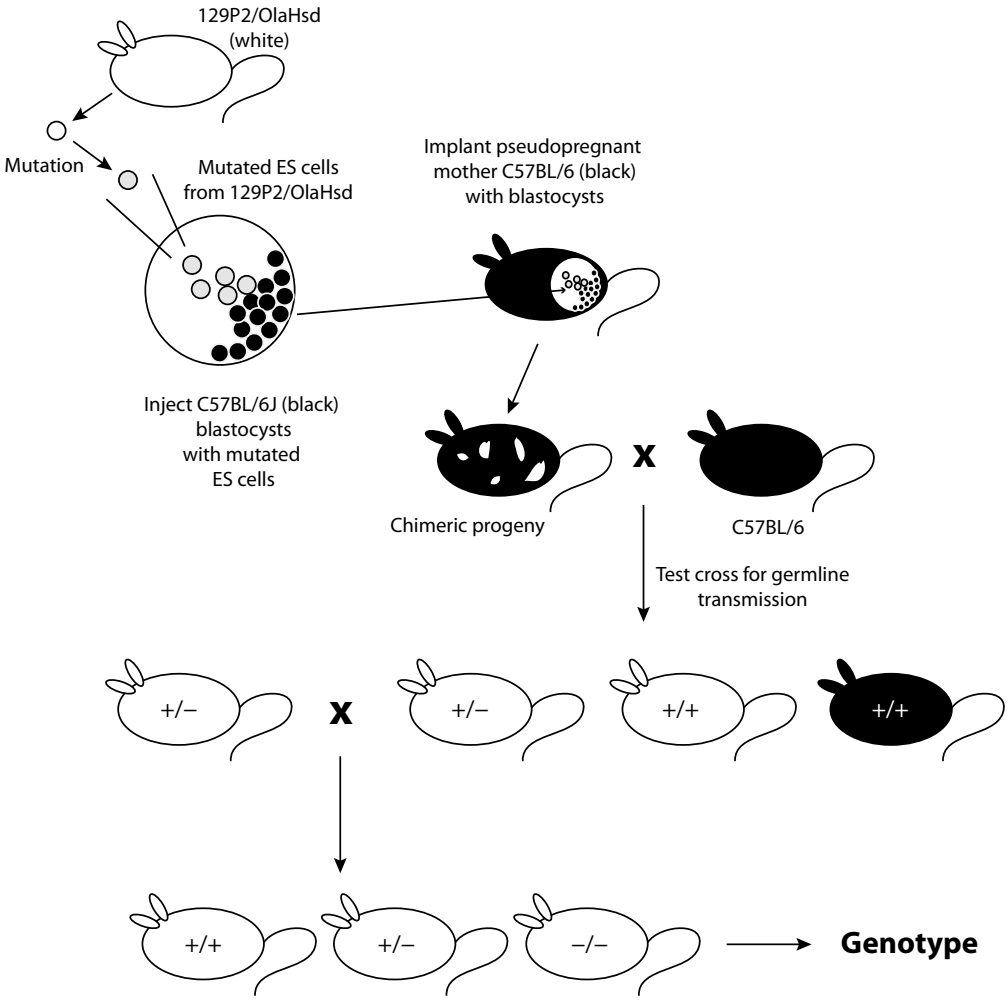

Figure 3.2: Generation of TPC mutant mice.

3.2.1.3 Genotypic analysis of TPC1 XG716 mutant mice

To confirm the generation of TPC1 XG716 homozygotes (–/–), the mice were genotyped by 3-primer PCR using genomic DNA isolated from ear clips. PCR primers were designed based on the gene trap insertion site previously identified. WT (+/+), TPC1 XG716 homozygous (–/–) and heterozygous (+/–) mutant mice were identified by the presence of WT TPC1 only, TPC1-β-geo mutant only, or both alleles respectively (Figure 3.3). WT and TPC1-β-geo mutant alleles were identified by the PCR products of 496 bp and 383 bp respectively on agarose gels. TPC1 XG716$^{-/-}$ mice were then bred further to continue germ-line transmission of TPC1 mutant alleles.

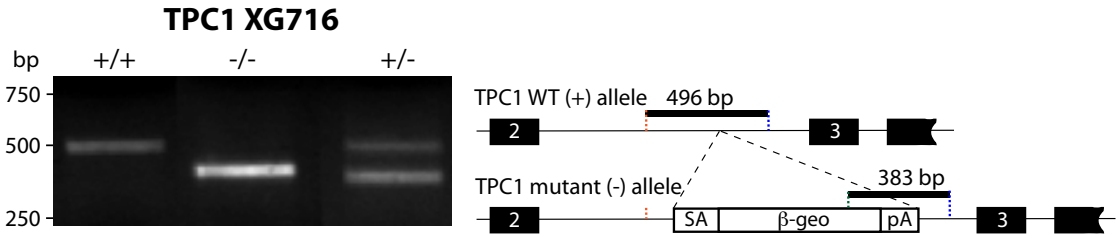

Figure 3.3: 3-primer PCR analysis of genomic DNA isolated from mouse ear clips. Left, wild-type (WT, +/+), TPC1 XG716 homozygous (–/–) and heterozygous (+/–) mutant mice were identified by PCR product size on an agarose gel: 496 bp (+/+), 383 bp (–/–), or both 496 and 383 bp (+/–), respectively. Right, amplified regions in the genomic DNA. Thick lines represent the amplified regions; black boxes with numbers indicate the exons and exon numbers, white box indicates the gene trap vector (splice acceptor (SA) sequence, *β-geo* gene, polyadenylation (pA) signal), thin lines represent the introns, and vertical lines show primer loci.

3.2.1.4 TPC1 XG716$^{-/-}$ as an incomplete TPC1 KO mouse

To ensure that the gene trap vector was effective in trapping TPC1 mRNA, RT-PCR was carried out to study the expression of TPC1 mRNA. Previously, TPC mRNA expression has been shown to have a broad distribution across mouse tissue types [307]. Liver was selected for the RT-PCR analysis because of its ease of RNA extraction and the integrity of liver RNA does not degrade rapidly over time compared to other tissues that contain a high abundance of ribonucleases such as the pancreas.

Although genotypic analysis showed that the gene trap vector had been successfully inserted in both alleles of TPC1 XG716$^{-/-}$ (Figure 3.3), RT-PCR probing for the region downstream of the gene trap insertion showed that TPC1 mRNA was still being expressed

in TPC1 XG716$^{-/-}$ (Exon 4–9; 516 bp, Figure 3.4A). This suggests that the insertion of the vector failed to trap the expression of TPC1.

An interesting question arises as to whether the vector failed to trap all the expression or whether the vector partially trapped some expression? To address this question, gene-specific primers were designed to probe the TPC1-β-geo mRNA (Exon 2–β-geo, 438 bp). RT-PCR showed that TPC1-β-geo mRNA was detected in TPC1 XG716$^{-/-}$, but not in WT (Figure 3.4B). This demonstrated that the vector inserted between exons 2 and 3 of the *Tpcn1* gene has been successful in trapping and preventing some TPC1 mRNA being expressed in TPC1 XG716$^{-/-}$.

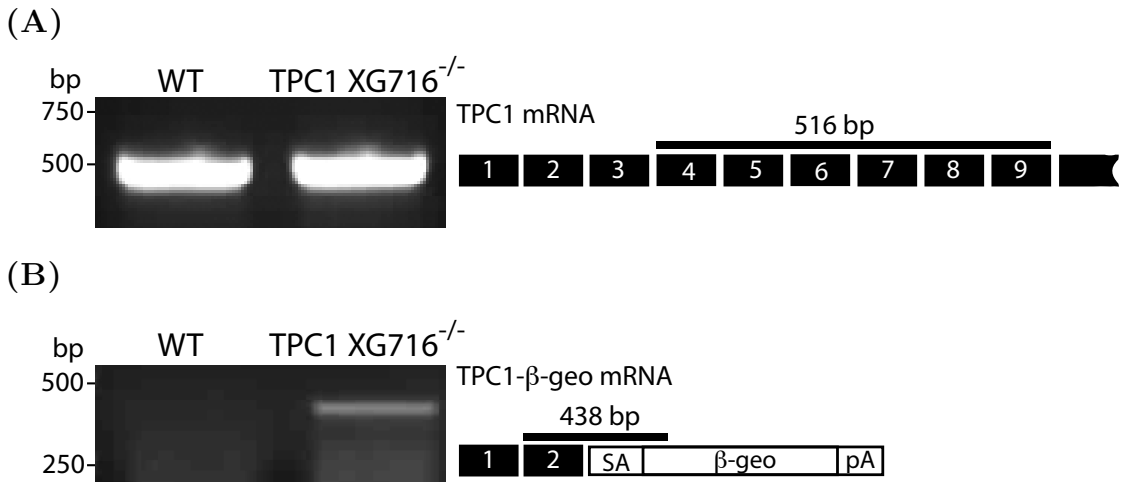

Figure 3.4: Validation of TPC1 XG716$^{-/-}$ mutant mice as an incomplete TPC1 KO. (A) Left, RT-PCR analysis of the mouse hepatic total RNA showed that TPC1 mRNA (Exon 4–9; 516 bp) was expressed in both WT and TPC1 XG716$^{-/-}$. (B) However, some TPC1 mRNA was still being trapped as indicated by the presence of TPC1-β-geo mRNA (Exon 2–β-geo, 438 bp). Right, amplified regions in mRNA. Thick lines represent the amplified regions, black boxes with numbers indicate the exons and exon numbers, and white box indicates the gene trap vector (splice acceptor (SA) sequence, β-*geo* gene, polyadenylation (pA) signal).

3.2.1.5 Possible explanations for the remaining TPC1 expression in TPC1 XG716$^{-/-}$ mice

There are two possible explanations to account for the unexpected TPC1 expression in TPC1 XG716$^{-/-}$. First, it is possible that the gene trap has been skipped. Second, there might be an alternative TPC1 mRNA that escaped the gene trap, yet shared the same exons (4–9).

Gene trap skipping. The gene trap skipping scenario is based on alternative splicing. Alternative splicing occurs when exons are re-connected (i.e. spliced) in multiple manners (Figure 3.5A). Often in alternative splicing, the alternatively skipped exons are often flanked by longer introns [137]. It is possible that in TPC1 XG716$^{-/-}$, gene trap skipping has occurred as the gene trap vector was inserted in a long (>30 kb) intron between exons 2 and 3 (Figure 3.1). The length of this intron may be responsible for the endogenous splicing apparatus being able to skip the splice acceptor sequence of the gene trap vector and execute normal splicing (Figure 3.5B).

To determine whether gene trap skipping could occur, gene-specific primers were designed in order to probe the TPC1 mRNA, up- (Exon 2) and down-stream (Exon 9) of the gene trap insertion (Intron 2). Successful amplification of TPC1 exon 2–9 would indicate that the gene trap has been skipped. Indeed, exon 2–9 of TPC1 mRNA was detected in TPC1 XG716$^{-/-}$ similar to the WT (819 bp; Figure 3.5C). This suggests that gene trap has been skipped.

Alternative TPC1 mRNA. The second possibility is that there is an alternative promoter of *Tpcn1* that escapes the gene trapping and initiates transcription of an alternative TPC1 mRNA that shares the same exons (4–9) as the other transcript when probed by RT-PCR. Studies using northern blotting to probe for the *Tpcn1* mRNA expression showed that in rat liver, there was both a longer (∼5 kb) and a shorter (∼4 kb) TPC1 mRNA [127]. Subsequently, a longer (∼5 kb) and a shorter (∼3 kb) mRNA has been identified in all mouse tissues tested [307]. The presence of the shorter transcript demonstrated that *Tpcn1* has more than one variant of mature mRNA. This further supports the idea that *Tpcn1* has alternative promoters.

Searches were conducted in the mouse mRNA (cDNA) GenBank library using UCSC Mouse Genome Browser Gateway[1]. 7 mRNAs of mouse TPC1 were found and 5 shared the same RT-PCR amplification region (Exons 4–9; Figure 3.6A). The longer TPC1 variant (accession number BC058951) represents the full-length mouse TPC1. Although 5 TPC1 mRNAs shared the same RT-PCR amplification region (exons 4–9), only one (accession number AK137626) seemed to have the potential to escape the gene trap. AK137626 mRNA only begins in intron 2 (52 bp before exon 3), therefore it is likely that the initiation

[1] `http://genome.ucsc.edu/cgi-bin/hgGateway`

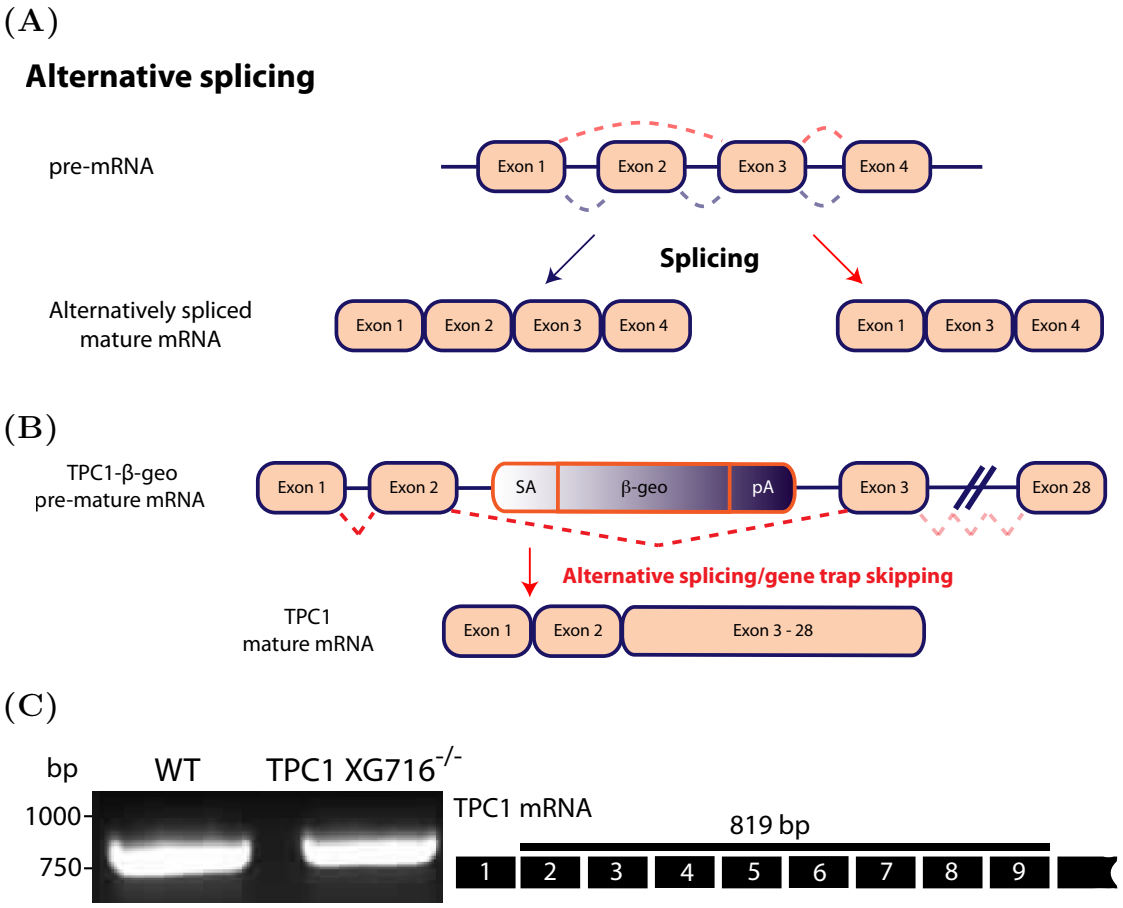

Figure 3.5: (A) Alternative splicing occurs when exons are re-connected in multiple manners. (B) Possible scenario of alternative splicing in TPC1 XG716$^{-/-}$ resulting in gene trap skipping. (C) Left, RT-PCR analysis of the mouse hepatic total RNA showed that TPC1 has escaped the entrapment (Exon 2–9; 819 bp). Right, amplified regions in mRNA. Thick lines represent the amplified regions and black boxes with numbers indicate the exons and exon numbers.

of AK137626 transcription occurred after the gene trap insertion in intron 2 (blue arrow in Figure 3.6A). On the other hand, the transcription of the other 4 TPC1 mRNAs occurred before exon 2 and was therefore more susceptible to trapping.

The long intron between exons 2 and 3 prompted a search for possible alternative promoter sites for the transcription of AK137626. Both Cap-analysis gene expression (CAGE) analysis by DataBase of Transcriptional Start Sites (DBTSS), and histone 3 methylation analysis by Broad Institute ChIp-seq studies (UCSC Genome Bioinformatics) revealed possible transcriptional start sites and alternative promoters in intron 2; these might be responsible for initiating the AK137626 transcription (green blocks in Figure 3.6A). The position of the alternative promoter is likely to be downstream of the gene trap insertion, thus allowing the transcription of AK137262 to escape the entrapment (Figure 3.6A).

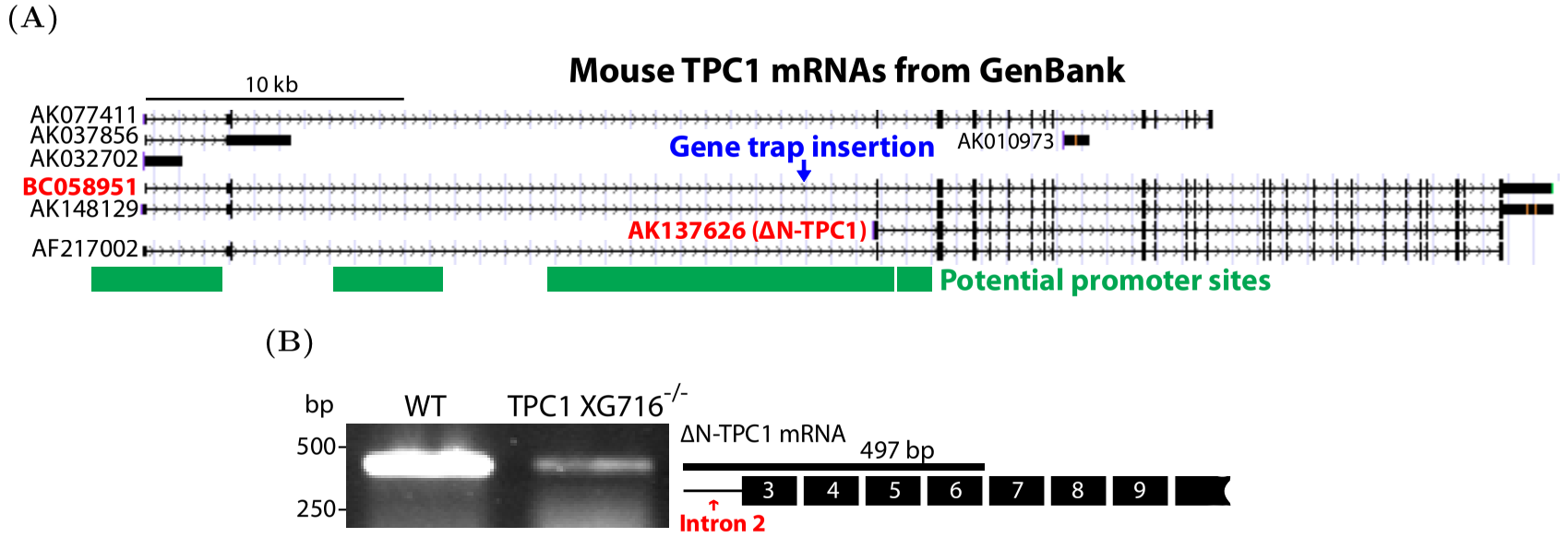

Figure 3.6: (A) mRNA/genomic DNA alignments of the mouse mRNAs in GenBank cDNA libraries. Potential promoter sites of mouse *Tpcn1* were found at the start of the gene and within the very long second intron (green blocks). The blue arrow indicates the gene trap insertion in TPC1 XG716$^{-/-}$. An alternative mRNA of mouse TPC1, accession number AK137626 (red), contributed to the observed TPC1 expression in TPC1 XG716$^{-/-}$. Transcription of AK137626 was initiated at the end of intron 2 and terminated at the end of exon 27. It is likely that AK137626 was initiated via an alternative promoter in intron 2, downstream of the gene trap insertion, thus escaping the entrapment. AK137626 is designated ΔN-TPC1 as the predicted translation of AK137626 has a truncated N-terminus. Thin lines indicate the introns and the black blocks indicate the exons. Arrows on the thin line indicate the direction of transcription. Accession numbers are given at the left of the mRNAs. (B) Left, RT-PCR analysis of the mouse hepatic total RNA demonstrated the presence of a shorter alternative TPC1 mRNA (ΔN-TPC1; intron 2 (I2)–exon 6; 497 bp). Right, the amplified regions in mRNA. The thick line represents the amplified region, black boxes with numbers indicate the exons and exon numbers, and the thin line represents the intron.

AK137626 shares the same coding regions as the longer TPC1 variant (BC058951) from exon 3–27. Translation of the AK137626 cDNA sequence predicted a smaller protein of 748 amino acid compared to the longer TPC1 variant (817 amino acid residues) as translation is initiated from an alternative start codon. AK137626 will hence forth be designated as ΔN-TPC1 indicating the 69 amino acid truncation at the N-terminus of the protein compared to the longer TPC1 variant.

The unique intron 2 region of ΔN-TPC1 was extremely useful because it could be used in RT-PCR to exclusively amplify the ΔN-TPC1 mRNA. Primers were designed to amplify intron 2–exon 6 of TPC1 in order to probe for ΔN-TPC1 mRNA. RT-PCR analysis showed that ΔN-TPC1 mRNA was expressed endogenously in the WT mouse. Additionally, it was not trapped by the gene trap vector as indicated by the RT-PCR amplification of intron 2–exon 6 in TPC1 XG716$^{-/-}$ (Figure 3.6B). This further suggests that ΔN-TPC1 has an alternative promoter that is likely to be situated downstream of the gene trap, thus escaping entrapment.

The important difference between ΔN-TPC1 and the longer mouse TPC1 mRNA is that the transcription of ΔN-TPC1 is initiated in intron 2 and therefore ΔN-TPC1 does not have exon 1–2 compared to the longer TPC1 variant. As mentioned, gene trap skipping in TPC1 XG716$^{-/-}$ was confirmed by the RT-PCR that probed TPC1 exon 2–9 (Figure 3.5C). As exon 1–2 is not present in ΔN-TPC1, it would not be detected in the RT-PCR that probed TPC1 exon 2–9, thus the expression detected in TPC1 XG716$^{-/-}$ was solely due to the longer TPC1 variant that has skipped the gene trap.

In summary, in TPC1 XG716$^{-/-}$ mutant mice, the insertion of the gene trap vector in *Tpcn1* alleles disrupts TPC1 expression (Figure 3.4B), however, the disruption is incomplete. The residual TPC1 expression is attributable to both gene trap skipping (Figure 3.5C) and the presence of the shorter TPC1 variant (ΔN-TPC1; Figure 3.6B). Although TPC1 XG716$^{-/-}$ is not a true knockout, it is still potentially useful to provide information regarding to TPC1 functions. Furthermore, TPC1 XG716$^{-/-}$ can yield insights into endogenous TPC1 expression, as the reporter gene in the gene trap vector of TPC1 XG716$^{-/-}$ allows the endogenous TPC1 expression to be assessed by monitoring expression of β-galactosidase [252]. For the subsequent characterization of TPC1 XG716$^{-/-}$, TPC1 XG716$^{-/-}$ will be referred to as TPC1 XG716.

3.2.1.6 Endogenous TPC1 mRNA expression in mouse tissue types

To investigate tissue-dependent expression of the two TPC1 variants, endogenous expression of TPC1 and ΔN-TPC1 mRNAs were examined in various WT mouse tissue types. RT-PCR that probed TPC1 exon 4 to 9 (516 bp) showed that TPC1 is widely expressed in all mouse tissues tested including brain, kidney, liver, spleen, heart, pancreas and trachea (Figure 3.7A). Similarly, ΔN-TPC1 was shown to be expressed in all the tissues tested including spleen, brain, kidney, liver, and trachea (amplified region: intron 2–exon 6; 497 bp, Figure 3.7B).

Tissue distribution of the endogenous TPC1 mRNA expression can also be studied indirectly, by using the reporter *β-geo* gene in TPC1 XG716. The *β-geo* gene in the gene trap vector is promoterless so its transcription depends on endogenous promoters. The expression of *β-geo* in TPC1 XG716 therefore gives an indication of where endogenous *Tpcn1* is expressed [205]. Similar to the results from direct probing (Figure 3.7A), RT-PCR that probed TPC1 exon 2 to β-geo (438 bp) showed that TPC1-*β-geo* is expressed in brain, kidney, liver, spleen, and heart of TPC1 XG716, confirming that TPC1 has a broad tissue expression. As expected, in WT, where the vector was not inserted, there was no expression of TPC1-*β-geo* (Figure 3.7C).

Overall, the ubiquitous expression of TPC1 and ΔN-TPC1 is consistent with the reported expression of TPC1 in mouse tissue types as examined by northern blotting [307], suggesting that they both may play fundamental roles in the organism.

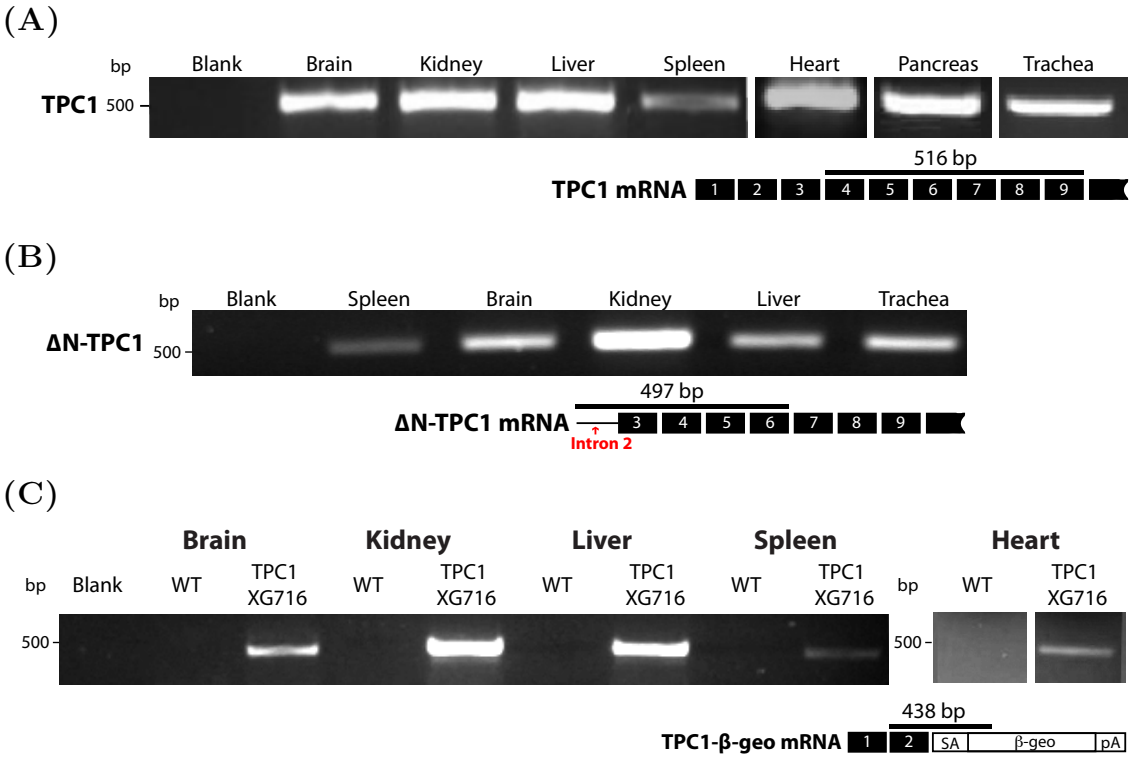

Figure 3.7: RT-PCR analysis demonstrating the mRNA expression of (A) TPC1 and (B) ΔN-TPC1 in a range of WT mouse tissue types, and of (C) TPC1-β-geo in a range of TPC1 XG716 mouse tissue types to report tissue-related TPC1 expression. The amplified mRNA regions are depicted below (TPC1 exon 4–9, 516 bp; TPC1 intron 2 (I2)–exon 6 (ΔN-TPC1), 497 bp, and TPC1 exon 2–β-geo, 438 bp). Thick lines represent the amplified regions, the thin line represents the intron, black boxes with numbers indicate the exons and exon numbers, and the white box indicates the gene trap vector (splice acceptor (SA) sequence, *β-geo* gene, and a polyadenylation (pA) signal).

3.2.1.7 Detection of endogenous TPC1 protein in TPC1 XG716 mice by western blotting using antibodies against β-galactosidase

As β-geo proved a valid reporter for TPC1 mRNA, it was next used as a reporter of tissue-dependent protein expression. For this, an anti-β-galactosidase antibody was applied in western blotting to probe for the TPC1-β-geo fusion protein in various tissue types of TPC1 XG716 mice.

Western blots in Figure 3.8 showed bands consistent with the predicted size of the TPC1-β-galactosidase fusion protein in liver, brain, kidney, and spleen homogenate of TPC1 XG716 and, as expected, not in WT. The detected bands were slightly higher than the predicted size of 153 kDa which may be a consequence of post-translational modifications such as glycosylation of TPC1-β-galactosidase.

In summary, β-galactosidase in TPC1 XG716 mice proved useful for reporting both mRNA and protein tissue-dependent expression profiles. These results can be taken to infer that in WT mice, the endogenous TPC1 protein would probably be expressed similarly in the tissues tested. This is consistent with the broad distribution pattern found for TPC1 mRNA expression (Figure 3.7).

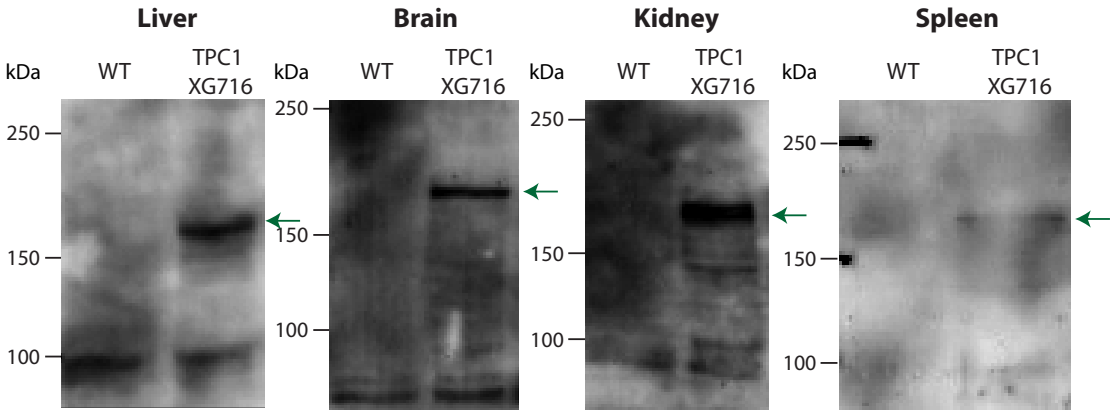

Figure 3.8: Western blots of 50 μg WT and TPC1 XG716 mouse tissue homogenates were probed with an anti-β-galactosidase antibody to detect TPC1-β-galactosidase protein (green arrows). The expression of TPC1-β-galactosidase protein in TPC1 XG716 is assumed to indicate the expression of endogenous TPC1 in the WT. Predicted size of TPC1-β-geo is 153 kDa.

3.2.1.8 Identification of a TPC1 gene-targeted mutant ES cell line

One of the shortcomings of generating knockout animals from gene trap mutagenesis is the potential for gene trap skipping during transcription, as described above. In this application, although *Tpcn1* gene was successfully mutated, the expression was not completely abolished due to a combination of gene trap skipping and the presence of ΔN-TPC1. In order to create true TPC1 KO mice, ES cell lines were searched in an attempt to find a TPC1 mutant that would not be compromised by gene trap skipping, and in which the expression of ΔN-TPC1 could also be eliminated.

As an alternative to gene trapping, mutant ES cell lines can also be generated by gene-targeted homologous recombination. Generation of mutant ES cell lines by homologous recombination on a large-scale is laborious and time-consuming, thus consortia for the homologous recombination of ES cell lines are less common, and the number of genes targeted are far fewer [116]. However, gene targeting is much more powerful and guarantees to knockout almost every targeted gene.

Fortunately, searches in the European Mouse Mutant Archive (EMMA[2]) revealed a mouse ES cell line, TPC1 D159, where *Tpcn1* had been mutated by homologous recombination. In homologous recombination, the mutation is introduced as a result of non-reciprocal exchange between the endogenous gene and the targeting vector. In TPC1 D159, the targeting vector had been designed to interrupt transcription of *Tpcn1* both by deleting a portion of exons 4 and 5, and also by introducing the *LacZ-neo* marker gene (Figure 3.9). This method avoids gene trap skipping and should ensure a complete abolition of both the longer and the shorter variant of TPC1 mRNAs. Thus, TPC1 D159 provides a TPC1 mutant ES cell line that yields a more robust knockout than that with TPC XG716.

[2] `http://www.emmanet.org/`

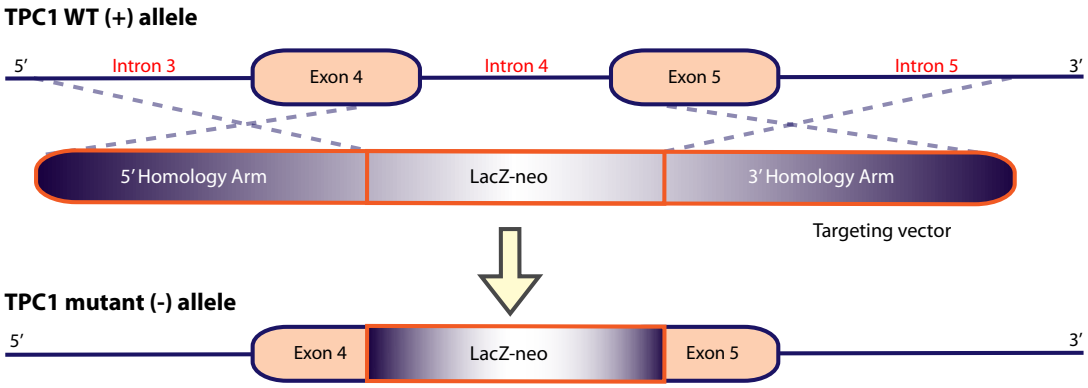

Figure 3.9: The gene targeting vector used to generate the TPC1 D159 mutant ES cell line. The vector comprises 5' and 3' arms that are homologous to regions in intron 3–exon 4 and exon 5–intron 5, respectively. Between the arms, there is a selection/reporter gene, *LacZ-neo*, which encodes β-galactosidase and neomycin phosphotransferase. During homologous recombination, the entire intron 4 and parts of the exon 4 and 5 were replaced with *LacZ-neo*.

3.2.1.9 Generation of TPC1 D159 mutant mice

TPC1 D159 heterozygous (+/–) mutant mice that had been generated from the TPC1 D159 mutant ES cell line were purchased from Deltagen[3]. TPC1 D159 heterozygous (+/–) mouse were crossed to obtain WT (+/+) and TPC1 D159 homozygous (–/–) mutant mouse colonies. Although similar to TPC1 XG176 where its genetic background involves 129P2/OlaHsd and C57BL/6, the ratio is different; this mouse strain has a higher C57BL/6 component.

3.2.1.10 Genotypic analysis of TPC1 D159 mutant mice

To genotype the mice, 3-primer PCR was designed based on the insertion site of the gene targeting vector provided by EMMA. WT (+/+), TPC1 D159 homozygous (–/–), and heterozygous (+/–) mice were identified by the presence of WT TPC1 only, homologous recombinant TPC1 mutant only, or both alleles respectively (Figure 3.10). WT and TPC1-*LacZ-neo* mutant alleles were identified by the PCR products of 376 bp and 459 bp, respectively on agarose gels. TPC1 D159$^{-/-}$ mice were then bred further to continue germ-line transmission of TPC1 mutant alleles.

[3] `http://www.deltagen.com/`

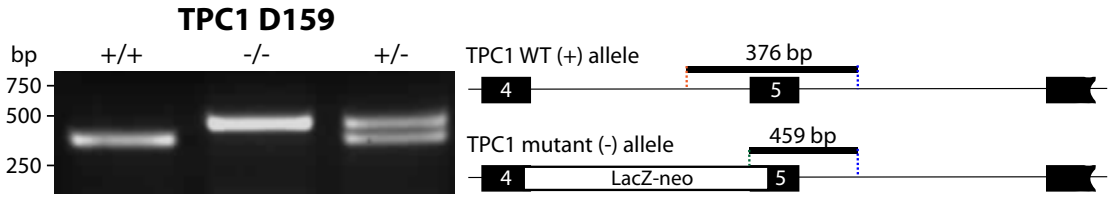

Figure 3.10: 3-primer PCR analysis of genomic DNA isolated from mouse ear clips in TPC1 D159 mice. Left, WT (+/+), TPC1 D159 homozygous (–/–) and heterozygous (+/–) mice were identified by PCR product sizes: WT allele (376 bp) and homologous recombinant TPC1 mutant allele (459 bp). Right, amplified regions in the genomic DNA. Thick lines represent the amplified regions, black boxes with numbers indicate the exons and exon numbers, the white box indicates *LacZ-neo* marker/selection gene from the targeting vector, and thin lines represent the intron.

3.2.1.11 TPC1 D159 as the TPC1 knockout (TPC1 KO) mouse

RT-PCR that probed TPC1 exon 6 to 13 (606 bp) was used to examine whether TPC1 mRNA expression had been successfully knocked out by gene targeting in TPC1 D159$^{-/-}$. Figure 3.11 demonstrated that the expression of TPC1 had indeed been abolished in TPC1 D159$^{-/-}$, and as expected, not in the WT. This verified that TPC1 D159$^{-/-}$ is a true TPC1 knockout, and will from now on be referred to as TPC1 KO.

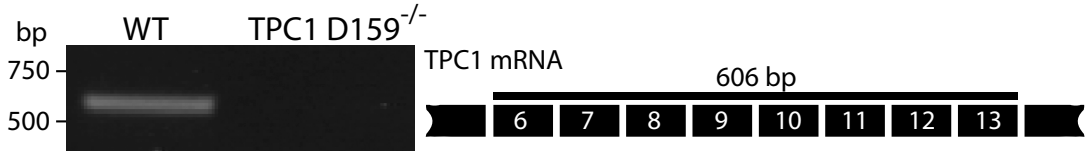

Figure 3.11: Validation of TPC1 D159$^{-/-}$ mutant mice as TPC1 KO by RT-PCR. Left, analysis of mouse hepatic total RNA showed that TPC1 mRNA expression (Exon 6–13; 606 bp) was abolished in TPC1 D159$^{-/-}$ but not in the WT. This confirms that TPC1 D159$^{-/-}$ mice are a true knockout. Right, the amplified region in TPC1 mRNA. The thick line represents the amplified region, and black boxes with numbers indicate the exons and exon numbers.

3.2.1.12 Detection of TPC1 protein by western blotting using in-house TPC1 antibodies

The reporter β-galactosidase in TPC1 XG716 suggested that TPC1 protein is endogenously expressed in a broad range of tissues (Figure 3.8). Although this data is consistent with the mRNA expression pattern, it is possible that during gene disruption, the vector might affect promoter activity of *Tpcn1*, thereby resulting in a non-physiological expression profile. In addition to doubts over the validity of the β-galactosidase-derived data, it is also necessary to establish whether TPC1 protein is absent in these tissues of TPC1 KO mice.

To address this, endogenous TPC1 protein was assessed by western blotting using antibodies against TPC1. Our lab had previously raised antibodies against mouse or human TPC1 by injecting rabbits with peptides of either mouse or human TPC1 (Table 3.1). For each set of immunogenic peptides, two rabbits were injected.

To examine whether anti-human TPC1 antibodies might cross-react with mouse TPC1 epitopes, the human TPC1 anti-genic peptide sequence was compared with the homologous section of mouse TPC1. The analysis showed an identity of $\geq$84% between the species (Table 3.1). This suggests that the anti-human TPC1 antibodies raised in-house might additionally be useful in detecting mouse TPC1 protein.

Species	TPC1 epitope		Epitope set	Identity to MmTPC1 (%)
Mus musculus	TPC1 N-tail	QEQLPSKNGGSHSI	A	100
	TPC1 C-tail	SRTKSDLSLKMYQE		100
Homo sapiens	TPC1 C-tail	IQEWYEEHAREQEQQR	B	93
	TPC1 C-tail	APAAQQPPGSRQRSQTVT		100
	TPC1 C-tail	FRMNYSRKNQDSEVDGGITLEKEISKEE LVAVLELYREARGASSDVTRLLETLSQME RYQQHSMVFLGRRSRTKSDLSLKMYQE EIQEWYEEHAREQEQQRQLSSSAAPAAQ QPPGSRQRSQTVT	C	85
	TPC1 N-tail	AAVSLDDDVPLILTLDEGGSAPLAPSNG LGQEELPSKNGGSYAIHDSQAPSLSSGG ESSPSSPAHNWEMNYQEAAIYLQEGENN DKFFTHPKDAKALAAYL	D	84

Table 3.1: Epitopes used to raise in-house anti-mouse (*Mus musculus*) or anti-human (*Homo sapiens*) TPC1 antibodies. The % identity of the anti-genic peptide to the homologous section in the mouse TPC1 protein is indicated on the right.

First, TPC1 anti-sera for the four epitope sets were examined for their specificity in detecting mouse TPC1 in western blotting. Screening the anti-sera against membranes of HEK293T cells overexpressing mouse TPC1-mCherry in western blotting showed that anti-sera against epitope set A or B were able to recognize a band at the expected size of mouse TPC1 (121 kDa) in the TPC1-mCherry-overexpressing compared to the mCherry-alone membranes (Figure 3.12). No specific TPC1-mCherry band was detected using the anti-sera against epitope sets C and D.

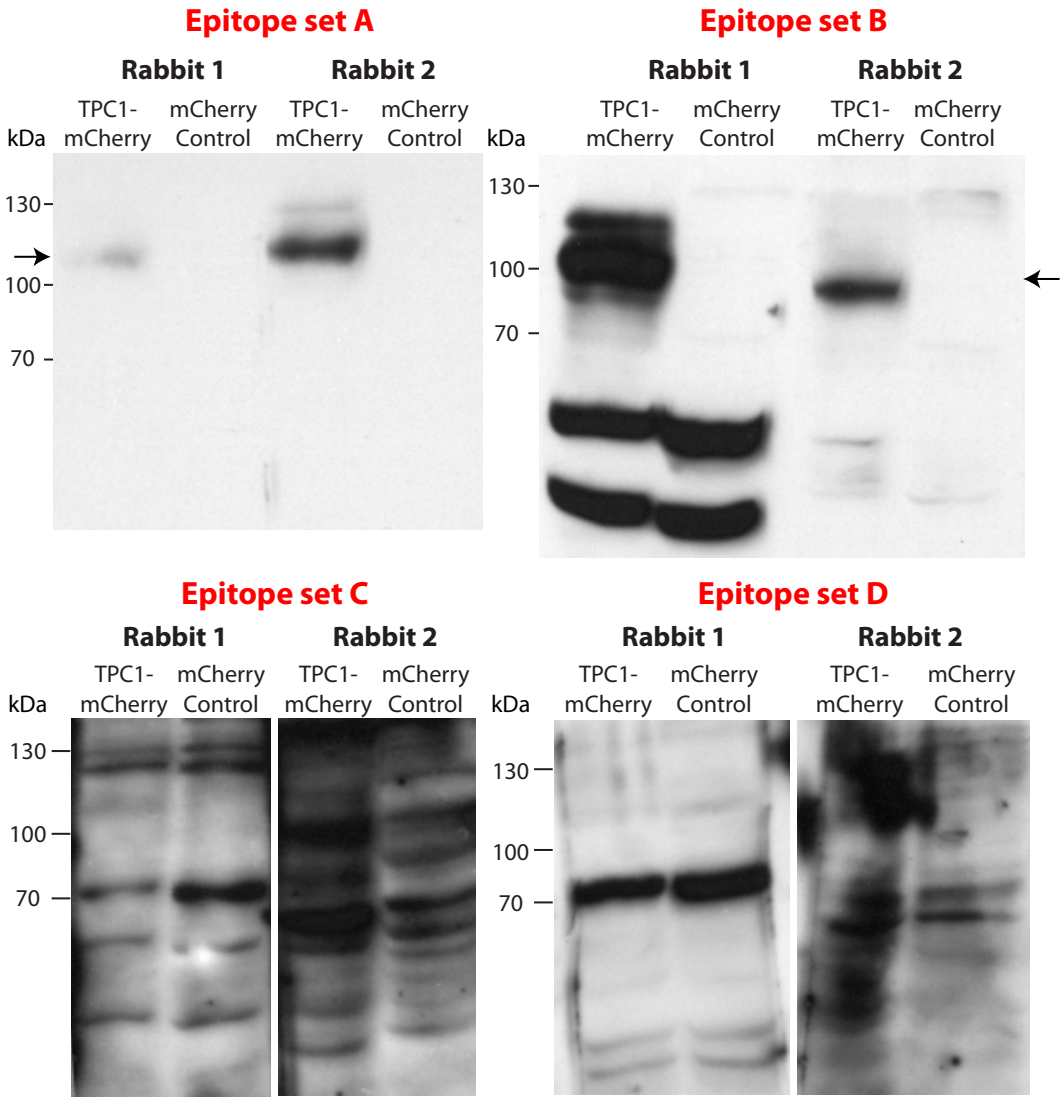

Figure 3.12: Examining the specificity of in-house anti-sera raised against mouse (epitope set A) or human (epitope set B-D) TPC1 in western blotting using 50 μg membranes from HEK293T cells overexpressing mouse TPC1-mCherry or mCherry (control). Anti-sera were collected from two rabbits immunized with each epitope set. The arrows indicate the mouse-TPC1-mCherry protein (predicted size of 121 kDa).

Next, to test whether TPC1 anti-sera were able to detect the endogenous mouse TPC1 protein, TPC1 anti-sera were tested against the WT and TPC1 KO mouse hepatic membranes in western blotting. As TPC1 KO showed no expression of TPC1 mRNA (Figure 3.11), it was assumed that there could be no expression of TPC1 protein and so this could be used as a negative control.

Western blots showed that none of the TPC1 anti-sera tested were able to detect a band of expected size (94 kDa) that distinguishes WT from the TPC1 KO (Figure 3.13). This was surprising since anti-sera against epitope set A or B were able to detect overexpression of mouse TPC1 protein in western blotting (Figure 3.12). It is likely that the endogenous level of TPC1 protein is too low to be detected by this western blotting method. If TPC1 anti-sera did bind endogenous TPC1, the signal was probably masked by the other non-specific signals.

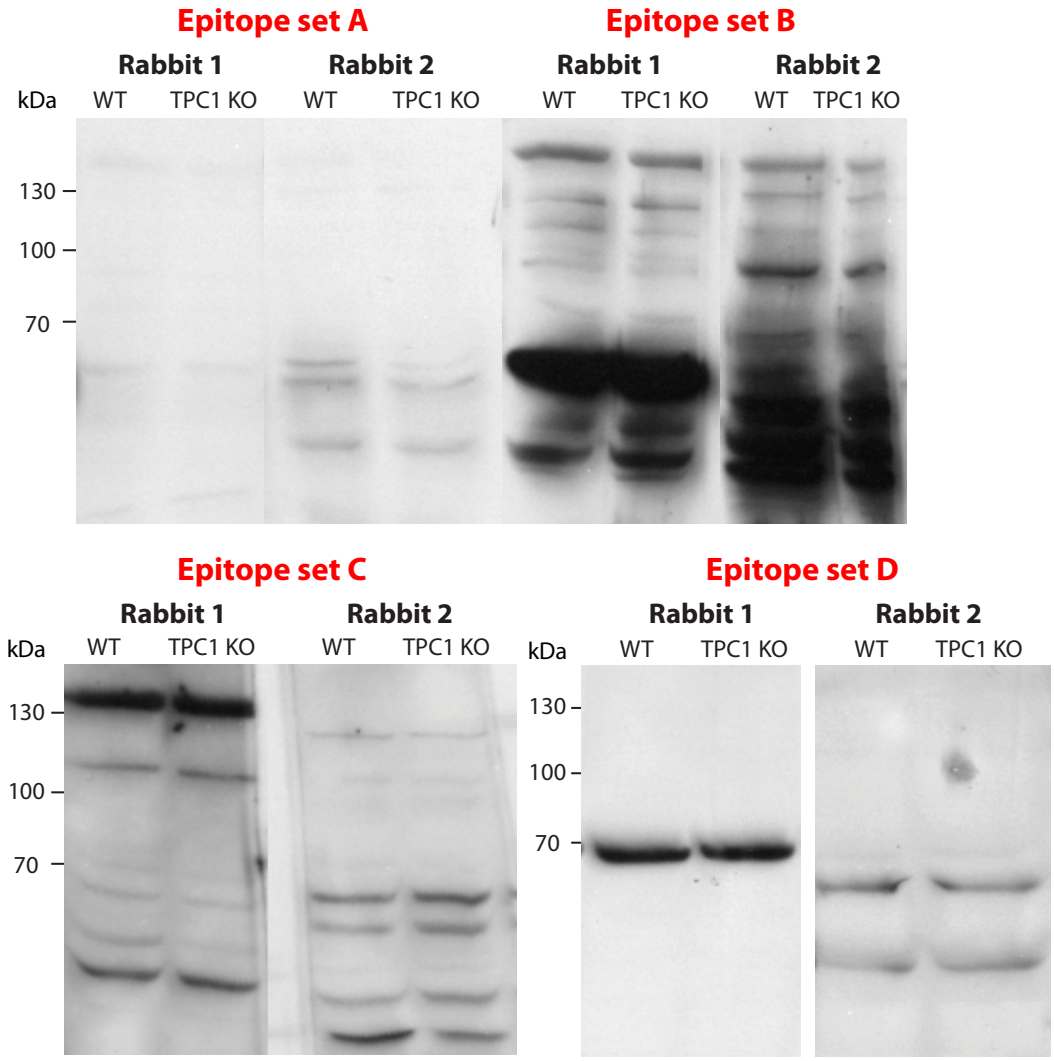

Figure 3.13: Western blots of 50 μg WT and TPC1 KO mouse hepatic membranes were probed with in-house anti-sera raised against mouse (epitope set A) or human (epitope sets B-D) TPC1 to detect endogenous TPC1 protein. TPC1 KO hepatic membranes were used as the negative control. The predicted size of TPC1 protein is 94 kDa.

3.2.2 Generation and analysis of TPC2 KO mouse

3.2.2.1 Identification of a TPC2 gene-trapped mutant ES cell line

Searches in the gene trap consortia also revealed a potential TPC2 mutant mouse ES cell line for generating TPC2 KO mice, TPC2 YHD437 (BayGenomics). Similar to the gene trap vector in TPC1 XG716 ES cell line, the gene trap vector of the YHD437 cell line comprised a splice acceptor sequence, *β-geo*, and a polyadenylation signal. Furthermore, the insertion site of this vector was also near the 5'-end of *Tpcn2* gene between exon 1 and 2 (Figure 3.14B). This suggests that TPC2-β-galactosidase protein, like TPC1-β-galactosidas, is also likely to be non-functional, as the protein would be very truncated with no transmembrane domains. Translation of the TPC2-β-geo mRNA predicts a protein of only 20 N-terminal TPC2 amino acid residues fused to β-galactosidase (Figure 3.14B).

Although the gene trap vector in TPC1 XG716 failed to generate a full TPC1 knockout mouse, it was probable that the same problems would not compromise a TPC2 gene-trapped knockout: a study that analysed all OmniBank gene trapped ES clones showed that >96% of non-embryonic lethal mouse lines led to a complete abolition of WT mRNA [299]. Thus, gene trap mutagenesis is very effective, and gene trap skipping occurs only in the rare cases like TPC1 where the insertion was in a very long intron (>30 kbp). Analysis of the vector insertion locus in TPC2 YHD437 showed that the intron was only ∼4 kbp, suggesting the skipping is less likely to occur. TPC2 YHD437 ES cell line was therefore purchased for the purpose of generating a TPC2 KO mouse.

3.2.2.2 Generation of TPC2 YHD437 mutant mice

In collaboration with MRC Harwell (Oxfordshire, UK), a similar procedure that was used to generate TPC1 XG716 mice was employed to generate TPC2 YHD437 mutant mice (Figure 3.2). TPC2 YHD437 ES cells that have a genetic background of 129P2/OlaHsd (white fur) were injected into a blastocyst from a mouse of C57BL/6 genetic background (black fur). The blastocyst containing both TPC2 wild-type (WT) and mutant ES cells was then implanted into a pseudopregnant female mouse. Chimeric offspring contained both WT and mutant *Tpcn2* genes, and are identified by a mixtures of patches of black and white fur respectively. These were then crossed with a WT C57BL/6 mouse (black),

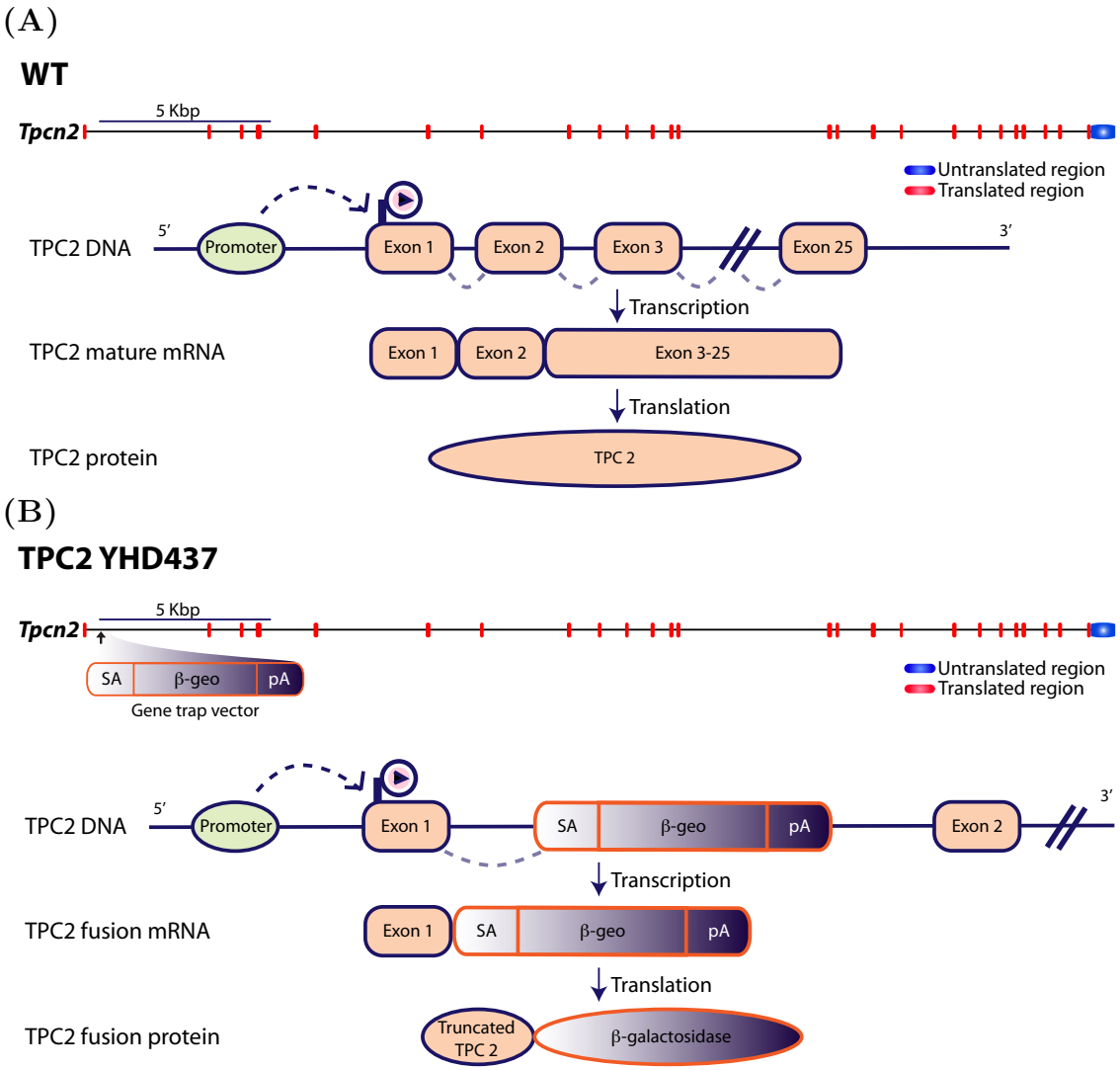

Figure 3.14: (A) Top: TPC2 mRNA/genomic DNA alignment. Blocks represent exons and the line indicates introns. Blue and red blocks indicate the untranslated and the translated regions of mRNA respectively. Middle: in wild-type ES cell line, the endogenous promoter initiates transcription of *Tpcn2*, followed by normal splicing to form mature mRNA. Translation of this mRNA forms the native TPC2 protein. (B) Gene trapping in TPC2 YHD437 ES cell line. Top: the gene trap vector is randomly inserted in intron 1 of *Tpcn2* (arrow). The vector comprises a splice acceptor (SA) sequence, the *β-geo* gene, and a polyadenylation (pA) signal. Bottom: insertion of this vector interrupts the normal splicing and causes β-geo to be spliced to endogenous TPC2 mRNA. This results in a truncated TPC2-β-geo fusion mRNA. When translated, the resulting peptide comprises 20 N-terminal amino acid residues of TPC2 protein fused to the β-galactosidase.

to ensure that the *Tpcn2* mutant allele has been incorporated into the germ cells. The resulting TPC2 YHD437 heterozygote (+/–) was then crossed to obtain WT (+/+) and TPC2 YHD437 homozygous (–/–) mutant mouse colonies. Since TPC2 YHD437 was generated in the same way as TPC1 XG716, they also share the same genetic background.

3.2.2.3 Genotypic analysis of TPC2 YHD437 mutant mice

To confirm the generation of TPC2 YHD437 homozygotes (–/–), the mice were genotyped by 3-primer PCR using genomic DNA isolated from ear clips. PCR primers were designed based on the gene trap insertion site previously identified. WT (+/+), TPC2 YHD437 homozygous (–/–) and heterozygous (+/–) mice were identified by the presence of WT TPC2 only, TPC2-β-geo mutant only, or both alleles respectively (Figure 3.15). WT and TPC2-β-geo mutant alleles were identified by the PCR products of 493 bp and 336 bp, respectively on agarose gels. TPC2 YHD437$^{-/-}$ mice were then bred further to continue germ-line transmission of TPC2 mutant alleles.

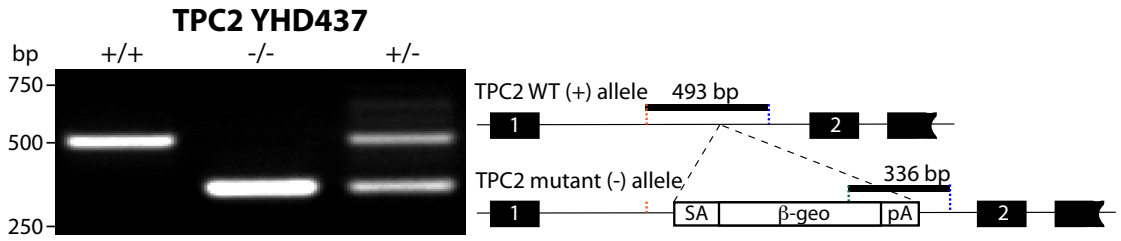

Figure 3.15: 3-primer PCR analysis of genomic DNA isolated from mouse ear clips. Left, WT (+/+), TPC2 YHD437 homozygous (–/–) and heterozygous (+/–) mice were identified by PCR product size: 493 bp (+/+), 336 bp (–/–), or both 493 and 336 bp (+/–). Right, amplified regions in the genomic DNA. Thick lines represent the amplified regions, black boxes with numbers indicate the exons and exon numbers, white box indicates the gene trap vector (splice acceptor (SA) sequence, β-*geo* gene, polyadenylation (pA) signal), thin lines represent the introns, and vertical lines show primer loci.

3.2.2.4 TPC2 YHD437 as the TPC2 knockout (TPC2 KO) mouse

RT-PCR that probed for TPC2 between exons 4 to 8 (564 bp) was used to examine whether TPC2 mRNA expression is abolished by the gene trapping and check that no skipping of the gene trap vector occurred in TPC2 YHD437$^{-/-}$. RT-PCR analysis demonstrated that the expression of TPC2 was completely abolished in TPC2 YHD437$^{-/-}$, and as expected, TPC2 was expressed in the WT (Figure 3.16). Additionally, RT-PCR successfully amplified TPC2 exon 1 fused with β-geo mRNA in TPC2 YHD437$^{-/-}$ (411 bp), confirming that TPC2 expression was trapped. As expected, TPC2-β-geo mRNA was not observed in the WT (Figure 3.16).

Results from this section verified that the transcription of *Tpcn2* in TPC2 YHD437$^{-/-}$ had been successfully interrupted by the insertion of the gene trap vector (Figure 3.15), resulting in a truncated TPC2-β-geo mRNA (Figure 3.16). Since TPC2 is no longer expressed in TPC2 YHD437$^{-/-}$, it will from now on be referred to as TPC2 KO.

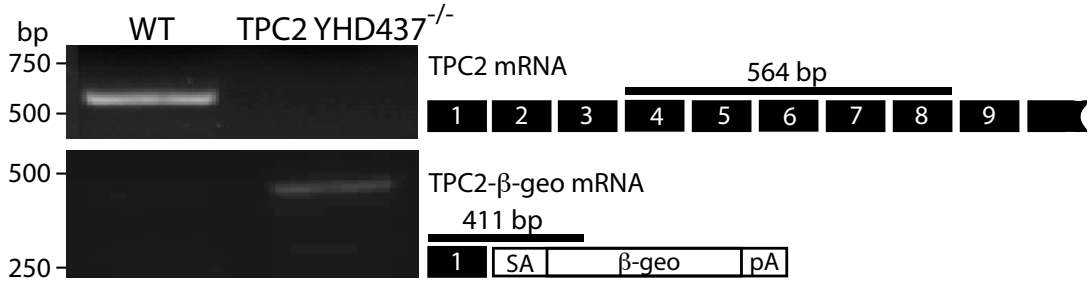

Figure 3.16: Validation of TPC2 YHD437$^{-/-}$ mutant mice by RT-PCR. Left, analysis of mouse hepatic total RNA showed that TPC2 mRNA (Exon 4–8; 564 bp) was abolished in TPC2 YHD437$^{-/-}$ but not in the WT. This confirms that TPC2 YHD437$^{-/-}$ mice are a true knockout. RT-PCR also amplified the TPC2-β-geo mRNA, confirming the abolition of TPC2 mRNA expression was due to successful gene trapping (Exon 1–β-geo; 411 bp). Right, amplified regions in the mRNA. Thick lines represent the amplified regions, black boxes with numbers indicate the exons and exon numbers, and white box indicates the gene trap vector (splice acceptor (SA) sequence, β-*geo* gene, polyadenylation (pA) signal).

3.2.2.5 Endogenous TPC2 mRNA expression in mouse tissues

The tissue distribution of TPC2 mRNA was analysed by RT-PCR, which directly probed for the TPC2 exon 4–8 (564 bp) in the WT mice, or indirectly probed for the promoterless reporter *β-geo* mRNA (from the gene trap vector) that has been spliced into TPC2 mRNA in TPC2 KO mice (TPC2 exon 1-*β*-geo; 411 bp). RT-PCR analysis demonstrated that TPC2 is expressed in all tissue types tested including brain, kidney, liver, spleen, heart, pancreas, and trachea (Figure 3.17A and 3.17B). This is consistent with the reported expression of TPC2 in mouse tissues as examined by northern blotting [307]. This ubiquitous expression of TPC2, like TPC1 (Figure 3.7), suggests that it may have a fundamental role in the organism. Furthermore, the expression of TPC2 was abolished in all TPC2 KO tissues tested (Figure 3.17A), confirming a complete disruption of *Tpcn2* gene.

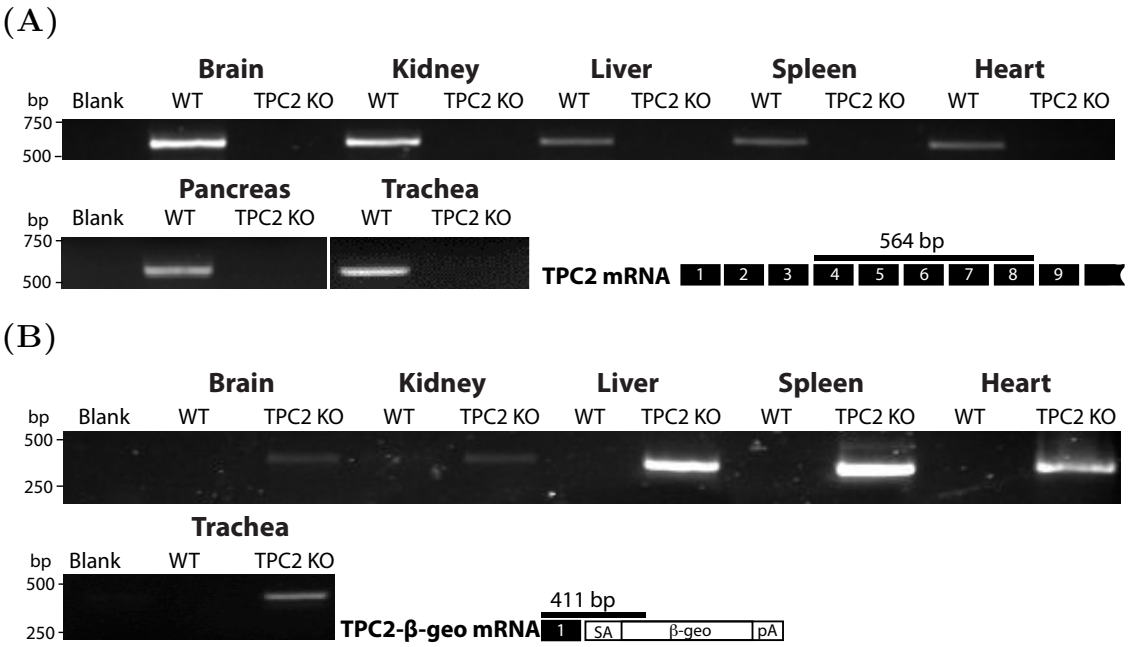

Figure 3.17: RT-PCR analysis demonstrating the mRNA expression of (A) TPC2 in a broad range of the WT but not TPC2 KO mouse tissue types, and of (B) TPC2-*β*-geo in a range of TPC2 KO mouse tissue types to report tissue-related TPC2 expression. The amplified mRNA regions are depicted below (TPC2 exon 4–8, 564 bp; TPC2 exon 1-*β*-geo, 411 bp). Black lines represent the amplified region, black boxes with numbers indicate the exons and exon numbers, and white box indicates the gene trap vector (splice acceptor (SA) sequence, *β-geo* gene, and a polyadenylation (pA) signal).

3.2.2.6 Detection of endogenous TPC2 protein in TPC2 YHD437 mice by western blotting using antibodies against β-galactosidase

In TPC1 XG716, the TPC1-β-galactosidase fusion protein proved useful for reporting tissue-dependent TPC1 expression profile (Figure 3.8). To have an indication of endogenous tissue-dependent TPC2 expression profile, TPC2-β-galactosidase protein in various TPC2 KO tissue homogenates was probed by an anti-β-galactosidase antibody in western blotting. Tissues homogenates from TPC1 XG716 were used as a positive control.

Figure 3.18 showed that western blotting failed to detect any band representing TPC2-β-galactosidase protein in the tested tissue types of TPC2 KO (predicted size of 152 kDa). It is speculated that the level of the endogenous TPC2 protein is lower than the endogenous TPC1 in the WT, thus, the level of TPC2-β-galactosidase protein might be too low to be detected by the conditions used for western blotting. Alternatively, the gene trap vector inserted in the *Tpcn2* gene might affect promoter activity of *Tpcn2*, which results in a non-physiological expression profile or inhibits the translation of TPC2-β-geo into TPC2-β-galactosidase.

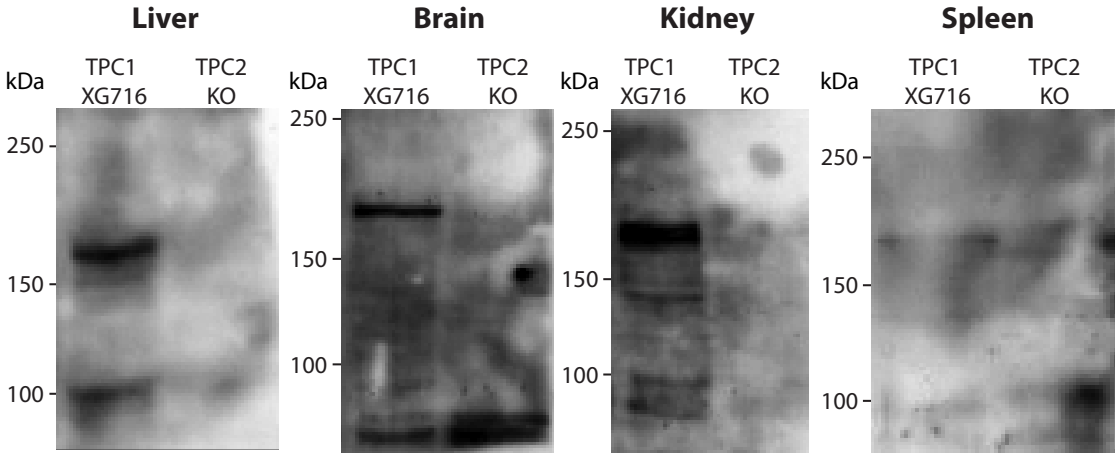

Figure 3.18: Western blots of 50 μg TPC1 XG716 and TPC2 KO mouse tissue homogenates were probed with an anti-β-galactosidase antibody to detect TPC-β-galactosidase protein. The expression of TPC2-β-galactosidase protein in TPC2 KO is assumed to indicate the expression of endogenous TPC2 in the WT. Predicted size of TPC2-β-galactosidase is 152 kDa. Tissues homogenates from TPC1 XG716 were used as the positive control for β-galactosidase detection.

3.2.2.7 Detection of TPC2 protein by western blotting using in-house TPC2 antibodies

To avoid the side-effect generated by gene trap insertion, endogenous TPC2 protein was assessed by western blotting using antibodies against TPC2. Similar to TPC1, our lab has raised antibodies against mouse or human TPC2 by injecting rabbits with two peptides of either mouse or human TPC2 (Table 3.2). For each set of immunogenic peptides, two rabbits were injected.

To examine whether anti-human TPC2 antibody might cross-react with mouse TPC2 epitopes, the human TPC2 anti-genic peptide sequence was compared with the homologous section of mouse TPC2. Analysis showed that there was only ∼50–60% identity between the species (Table 3.2). This suggests that the anti-human TPC2 antibodies raised in-house might be less advantageous in detecting mouse TPC2 protein.

Species	**TPC2 epitope**		**Epitope set**	**Identity to MmTPC2 (%)**
Mus musculus	TPC2 N-tail	FIEDAIKYRSIYHR	E	100
	TPC2 C-tail	NFLHRWDPQGHKQL		100
Homo sapiens	TPC2 internal	GGKQDDGQDRERLTY	F	53
	TPC2 internal	VKEHPPRPEYQSPFL		66

Table 3.2: Epitopes used to raise in-house anti-mouse (*Mus musculus*) or anti-human (*Homo sapiens*) TPC2 antibodies. The % identity of the anti-genic peptide to the homologous section in the mouse TPC2 protein is indicated on the right.

First, TPC2 anti-sera for the two epitope sets were tested against membranes of HEK293T cells overexpressing mouse TPC2-mCherry to examine their specificity in detecting mouse TPC2 protein in western blotting. Disappointingly, none of the in-house TPC2 antibodies were able to detect a specific band of mouse TPC2 (predicted size of 110 though normally observed at 90 kDa [307]) in the TPC2-mCherry-overexpressing compared to mCherry alone membranes in western blotting (Figure 3.19). This suggests that the TPC2 antibodies might not be useful in detecting mouse TPC2 protein.

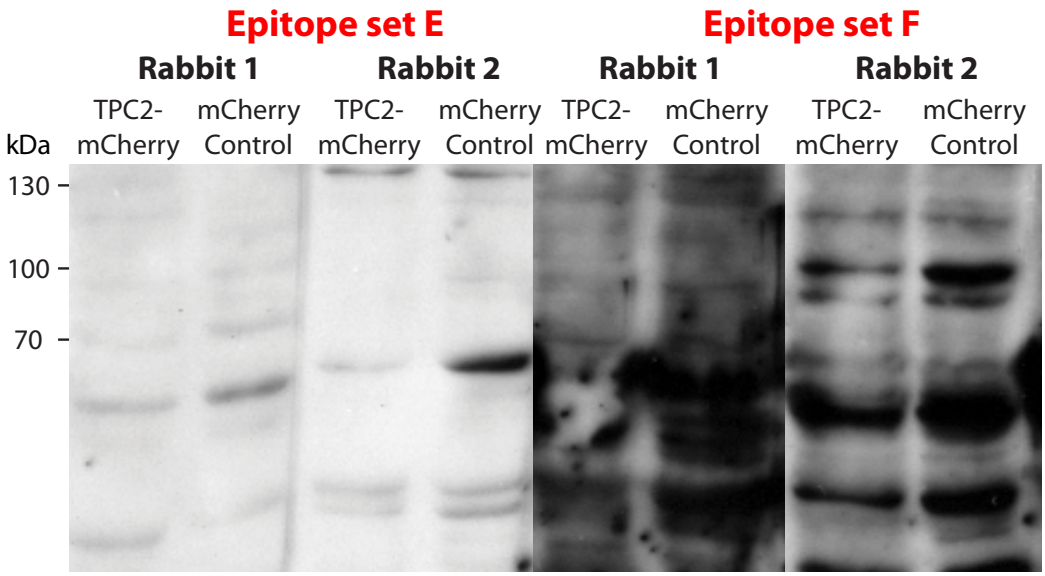

Figure 3.19: Western blotting of 50 μg membranes from HEK293T cells overexpressing TPC2-mCherry or mCherry (control) using in-house TPC2 anti-sera to examine whether the antibodies could detect mouse TPC2 protein. Anti-sera were collected from two rabbits immunized with each epitope set (Table 3.2). The predicted size of TPC2-mCherry protein is 110 kDa.

To ascertain whether TPC2 anti-sera could be used to detect endogenous TPC2 protein, TPC2 anti-sera were tested against the WT and TPC2 KO mouse hepatic membranes in western blotting. TPC2 KO was used as a negative control as it was assumed that there would be no expression of TPC2 protein. Figure 3.20 shows that none of the in-house TPC2 anti-sera were able to detect a band of the expected molecular weight of 86 kDa (though normally observed at ∼70 kDa [307]) that distinguishes WT from the TPC2 KO. This agrees with the previous results from overexpressing mouse TPC2 (Figure 3.19).

In summary, western blots suggest that the in-house TPC2 antibodies were unable to recognize their specific antigen in the western blotting technique. In order to detect endogenous expression of TPC2 protein to gain further insight into the tissues in which it plays a role, it is important to develop or search for more specific antibodies that would recognize mouse TPC2.

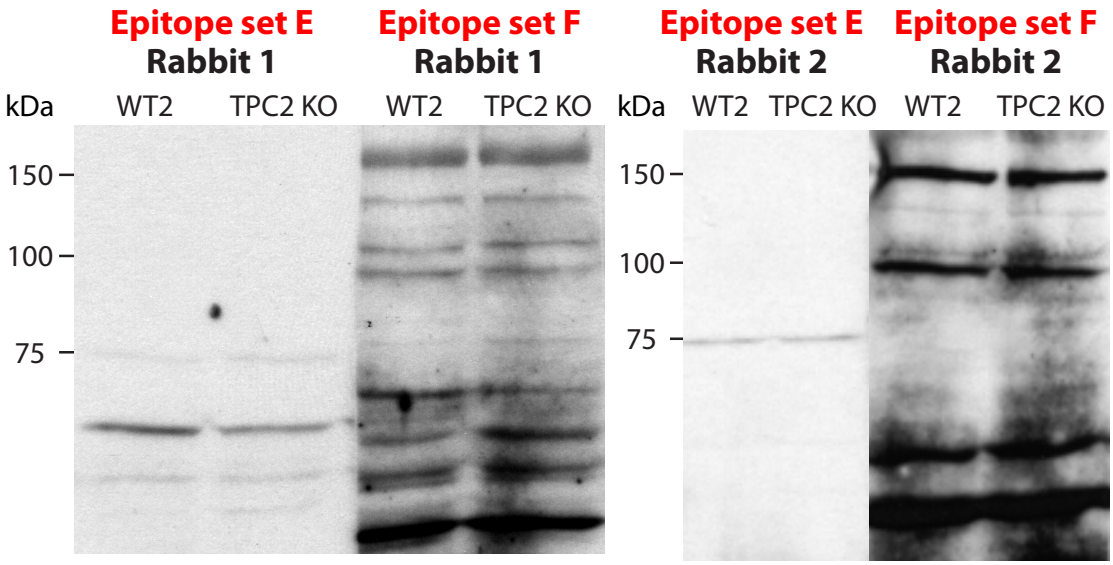

Figure 3.20: Western blotting of 50 μg WT or TPC2 KO mouse hepatic membranes using in-house TPC2 anti-sera to detect endogenous expression of TPC2 protein. Anti-sera were collected from two rabbits immunized against each epitope set (Table 3.2). TPC2 KO hepatic membranes were used as the negative control. The predicted size of TPC2 protein is 86 kDa.

3.2.3 Quantitative TPC mRNA expression in mouse liver

Thus far, the RT-PCR technique used to determine mRNA expression has been end-point RT-PCR. End-point RT-PCR only determines the presence or absence of TPC expression but gives no indication of the quantity. In order to measure the mRNA level of TPC1 and TPC2 quantitatively, RT-quantitative PCR (RT-qPCR) was employed. Any differences observed in the expression levels of TPCs might yield insights into their distinct physiological regulatory roles.

Furthermore, TPC single KOs exhibited no gross phenotypes; this might be due to redundancy and/or compensation by the remaining TPC. Thus, it is informative to investigate whether any up-regulation of the remaining isoform has occurred in single KOs to compensate for the eliminated TPC, and if so, the extent of the compensation.

Finally, residual expression of TPC1 in TPC1 XG716 suggested that TPC1 XG716 might be a hypomorph (partial knockdown of TPC1, Figure 3.4), so it would be interesting to quantify the reduction in TPC1 expression. If the expression is significantly reduced (compared to the WT), TPC1 XG716 would be useful in investigating TPC1 functions.

Liver was also used to measure the level of TPC mRNAs for the reasons described in Section 3.2.1.4. Additionally, the sex of the mice was also taken into account as many genes have shown tissue-specific sexual dimorphism [296]. It is also interesting to examine any effect the genetic background might have on TPC expression. The genetic backgrounds of TPC1 and TPC2 single KOs are different, each knockout strain therefore has its own distinct WT. To avoid confusion, the wild-types for TPC1 KO and TPC2 KO will be referred to as WT1 and WT2, respectively.

3.2.3.1 TPC1 and TPC2 mRNA expression levels in wild-type mice

To address the question of whether the level of TPC mRNA expression is different, TPC1 and TPC2 mRNA levels in WT liver were compared in two different background strains, and in both sexes. RT-qPCR revealed that the expression level of TPC1 mRNA was at least five-fold higher than TPC2, regardless of the sex or genetic background (Figure 3.21). Additionally, the expression level of TPC2 mRNA was significantly higher in females compared to males in both mouse strains (Figure 3.21). A similar sex-trend was also observed in TPC1 but the level was only significantly higher in the WT2 but not WT1

(Figure 3.21). Furthermore, the TPC2 mRNA level is significantly higher in females of WT2 than WT1 (Figure 3.21).

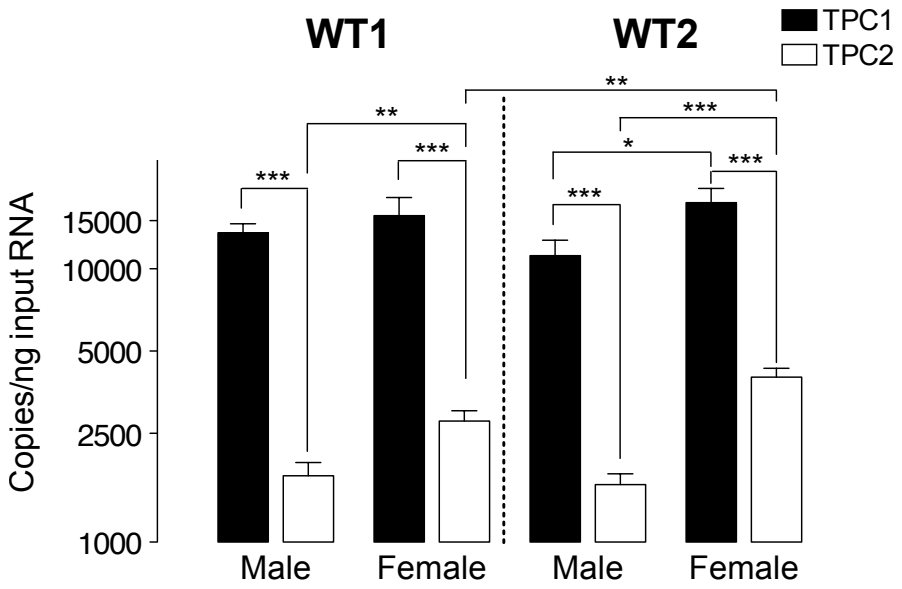

Figure 3.21: RT-qPCR reveals the expression levels of TPC1 and TPC2 WT liver mRNA in two different genetic background strains, and in each sex. The wild-types for TPC1 KO and TPC2 KO are referred to as WT1 and WT2 respectively. Results are expressed as mean ± S.E.M. in a log scale, n = 4-8, ***P $<$ 0.001, **P $<$ 0.01, and *P $<$ 0.05. The results were log transformed to enable a more symmetrical distribution, thereby allowing parametric statistical tests to be performed [23, 85].

The results from the RT-qPCR analysis suggest that TPC1 is the predominant isoform in both sexes. The relatively low expression of TPC2 mRNA may account for the inability to detect TPC2-β-galactosidase protein in TPC2 KO under the conditions used for western blotting (Figure 3.18). Additionally, sex and the genetic background were shown to have a significant effect on the expression of TPCs, highlighting the importance of using animals of the same genetic background and sex in future studies.

It is necessary to emphasize that the study was only conducted in liver; the ratio of TPC1 to TPC2 may vary between different tissue types. Furthermore, some tissues may be more susceptible to sex hormone regulation than the others. Future studies on the expression level of other mouse tissue types will be needed to validate the above conclusions.

3.2.3.2 Compensation exerted by the remaining TPC expression in TPC single KOs.

Given that numerous pieces of evidence indicate that TPCs are the NAADP-gated Ca^{2+} channels and that NAADP is known to play an important role in many tissue and cell systems including skeletal muscle differentiation [5, 103], it was surprising that single KO mice were viable and exhibited no gross phenotypes. One possible explanation is that TPCs are redundant. Additionally, it is likely that compensation has occurred, and the expression of the remaining TPC or other proteins linked in the signalling pathway has up or down-regulated in order to compensate for the eliminated TPC.

The possibility of compensation by the remaining TPC isoform in TPC single KOs was examined by RT-qPCR. Since sex had been shown to have an effect on TPC expression in WT mice, any compensation was also likely to vary depending on the sex of the KO mice. RT-qPCR analysis showed that when TPC1 was knocked out, there was no change in the expression level of TPC2 mRNA in the male (Figure 3.22A), in contrast, the expression level of TPC2 mRNA in the female mice was significantly increased by 15% (Figure 3.22B). On the other hand, when TPC2 was knocked out, the level of TPC1 mRNA increased significantly (by 41%) in the male (Figure 3.22C) but not in the female (Figure 3.22D). These results reveal that the expression of the remaining TPC is up-regulated to compensate for the eliminated TPC, and that interestingly, this compensation is sex-specific.

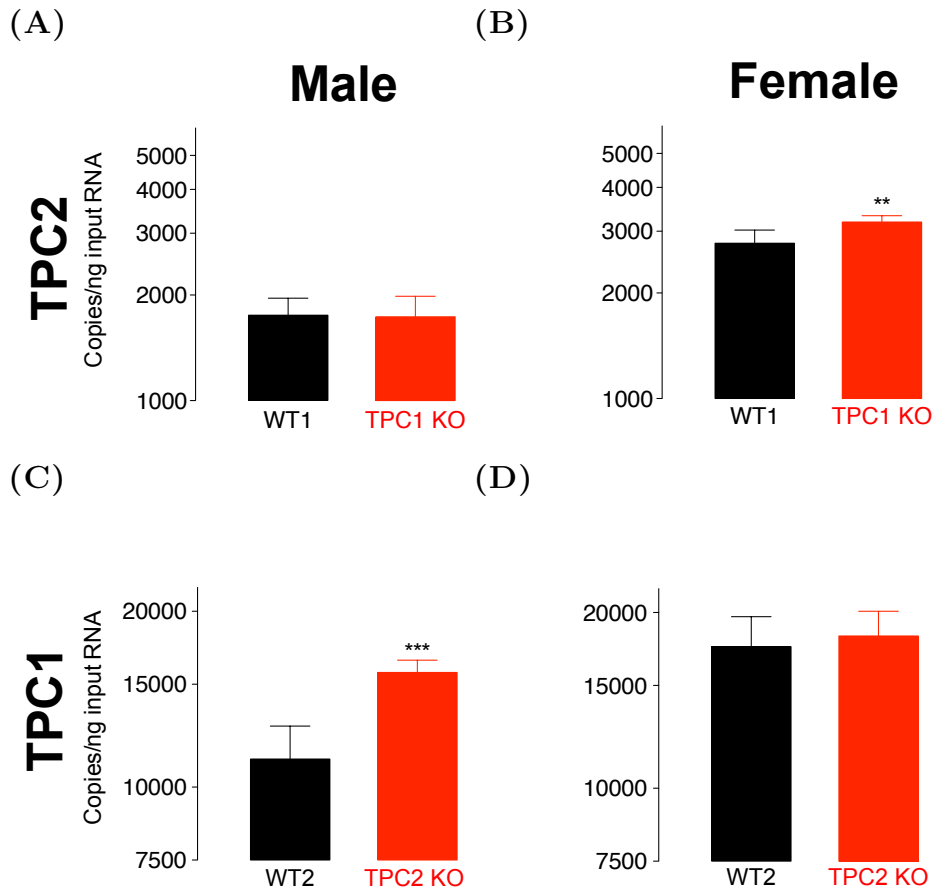

Figure 3.22: Hepatic mRNA levels of TPC1 and TPC2 in the WT and TPC single KO mice of each sex. Each TPC single KO was compared with the WT of the same genetic background. TPC1 KO shares the same background as WT1, and TPC2 KO shares the same genetic background as WT2. n = 4–8, ***P $<$ 0.001, and **P $<$ 0.01. The results were log transformed to enable a more symmetrical distribution, thereby allowing parametric statistical tests to be performed [23, 85].

3.2.4 Determining the level of TPC1 expression knocked down and the possible compensatory TPC2 expression in TPC1 XG716.

In Section 3.2.1.4, the potential TPC1 KO generated by gene trapping (referred to as TPC1 XG716) was suggested to be a TPC1 hypomorph, as some TPC1 expression has been disrupted (detected by the TPC1-β-geo mRNA) but not all (Figure 3.4).

Indeed, RT-qPCR showed that the level of TPC1 mRNA was significantly decreased (49%) in the female TPC1 XG716 compared to WT2 (Figure 3.23B), however, no difference was observed in the male (Figure 3.23A). These results demonstrated that the female TPC1 XG716 mouse is a TPC1 hypomorph, but not the male. Thus, the female TPC1 XG716 could be used as an appropriate model for studying the effects of partial TPC1 knock down in NAADP-mediated Ca^{2+} signalling. Furthermore, in TPC1 XG716, differences of the TPC1 expression between sexes support the idea that the expression of TPC mRNAs is sex-dependent. Sex-dependent regulation of TPC1 expression may have an impact on the gene disruption in TPC1 XG716, resulting in the observed sex differences.

Interestingly, although the level of TPC1 mRNA in TPC1 XG716 was decreased significantly in females, no difference was observed in the level of TPC2 compared to WT (Figure 3.23D). This may be explained by the redundancy effect. As TPC1 expression was not completely abolished in TPC1 XG716, the residual TPC1 together with the basal level of TPC2 may be sufficient to compensate for the loss of some TPC1 expression, therefore there is no need for TPC2 expression to be up-regulated. In contrast, although the level of TPC1 mRNA was not reduced in the male TPC1 XG716, the level of TPC2 mRNA still increased significantly (2.2-fold) compared to WT (Figure 3.23C). This is highly unexpected, so it is assumed that insertion of gene trap vector had non-specific effects on gene expression.

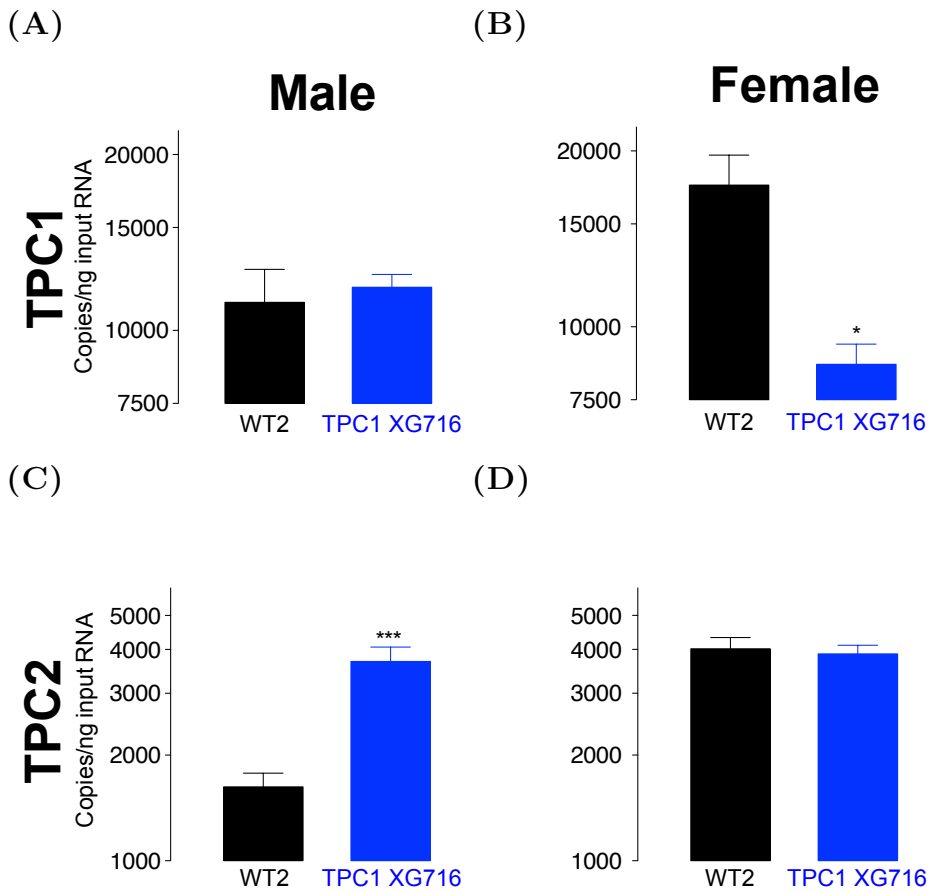

Figure 3.23: Hepatic mRNA levels of TPC1 and TPC2 in TPC1 XG716 and its respective wild-type (WT2). n = 4–8, ***P $<$ 0.001, and *P $<$ 0.05. The results were log transformed to enable a more symmetrical distribution, thereby allowing parametric statistical tests to be performed [23, 85].

3.2.5 Sex-dependent regulation of TPC mRNA expression

The observed sex-specific differences (Figure 3.21, 3.22 and 3.23) raise an interesting question as to whether there are any sex-specific regulatory elements in TPC genes. Searches in the ORegAnno (Open Regulatory Annotation) for reported regulatory regions and transcription factor binding sites revealed an estrogen receptor α (ERα)-binding site within the long intron of *Tpcn1* in mouse liver, upstream of the gene trap insertion (Figure 3.24A) [105]. The presence of this ERα-binding site provides a plausible explanation for the higher TPC1 mRNA level in the wild-type (WT2) female compared to their male counterparts (Figure 3.21). Furthermore, the close proximity between the ERα-binding site, the gene trap, and the promoter sites of *Tpcn1* suggests that the insertion of gene trap might affect the regulation of the alternative promoter by the estrogen receptor (Figure 3.24A). This may account for the reduced level of TPC1 mRNA in female and not male TPC1 XG716 (Figure 3.22).

Surprisingly, although the sex-specific difference in the TPC2 mRNA expression was more pronounced than that for TPC1 in both wild-types (Figure 3.21), no sex-specific regulatory element was found near/in the *Tpcn2* gene.

In an attempt to study the effect of the ERα-binding site on the regulation of TPC mRNA expression, TPC mRNA levels was measured in mouse embryonic fibroblasts (MEFs) after three-hour incubation in the presence and absence of the female hormone, oestradiol (E_2; 100 nM). RT-qPCR showed that the levels of both TPC1 and TPC2 mRNAs were significantly increased (13% and 14%, respectively) after E_2 incubation (Figure 3.24B). This provides preliminary evidence that a female sex hormone is involved in regulating expression of both TPC1 and TPC2.

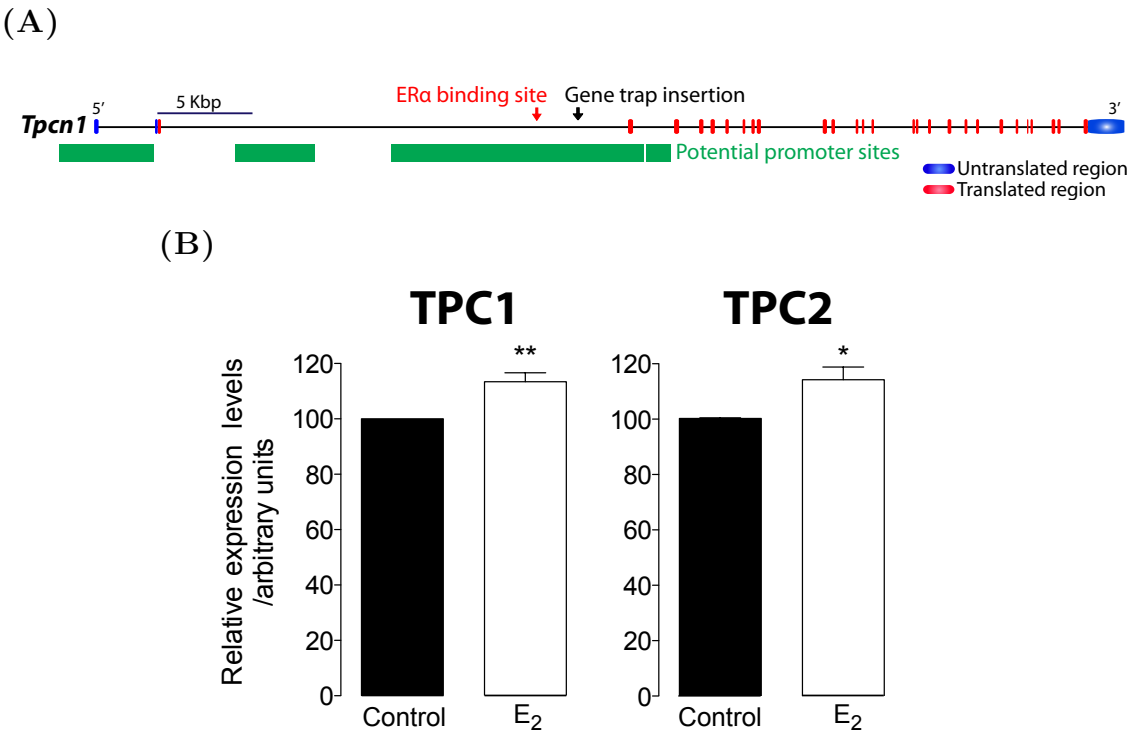

Figure 3.24: (A) TPC1 mRNA/genomic DNA alignment indicating sites for ERα-binding (red arrow), potential promoter sites (green boxes) and the gene trap insertion site (black arrow). Blue and red boxes indicate the untranslated and the translated exonic regions of mRNA, respectively. The line indicates introns. (B) The effect of 100 nM oestradiol (E_2) on the expression levels of TPC1 and TPC2 mRNA in MEFs. E_2 and control MEFs were incubated with 100 nM E_2 or the control culture media for three hours. Results were normalized to the control value, n = 7, **P $<$ 0.01, and *P $<$ 0.05.

3.2.6 Compensation exerted by the other proteins in TPC2 KO

Although in TPC single KOs, the redundancy and compensation of the remaining TPC might alleviate some phenotypic effects that would otherwise be caused by the eliminated TPC, it is likely that other proteins in the same signalling pathway also play a part in compensation. In collaboration with MRC Harwell (Oxfordshire, UK), microarray analysis was conducted with male TPC2 KO mice (and the respective WT) on the global scale in an attempt to identify proteins involved in the compensation. (Only male mice were analyzed due to cost limitations). Thus, the expression levels of thousands of genes were monitored simultaneously from the same RNA preparation.

Expression analysis from microarray showed that in total, 140 genes were up- or down-regulated upon deletion of TPC2. Specifically, there was at least two-fold increase in mRNA expression of 11 genes (Figure 3.25), and at least two-fold decrease in mRNA expression of 129 genes in TPC2 KO compared to the WT (Figure 3.26). Description of the genes is detailed in Appendix Tables 3.1 and 3.2. This supports the previous hypothesis and suggests that the compensation occurred on a global scale.

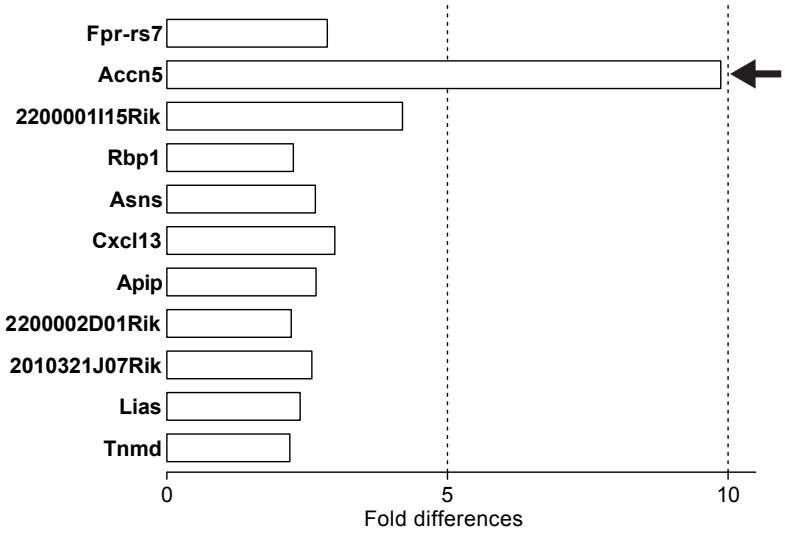

Figure 3.25: Genes for which expression was up-regulated by at least two-fold in the liver of male TPC2 KO mice in comparison to the WT as measured by microarray analysis (n = 6). The arrow indicates the gene further analysed by RT-qPCR. Description of the genes is detailed in Appendix Table 3.1.

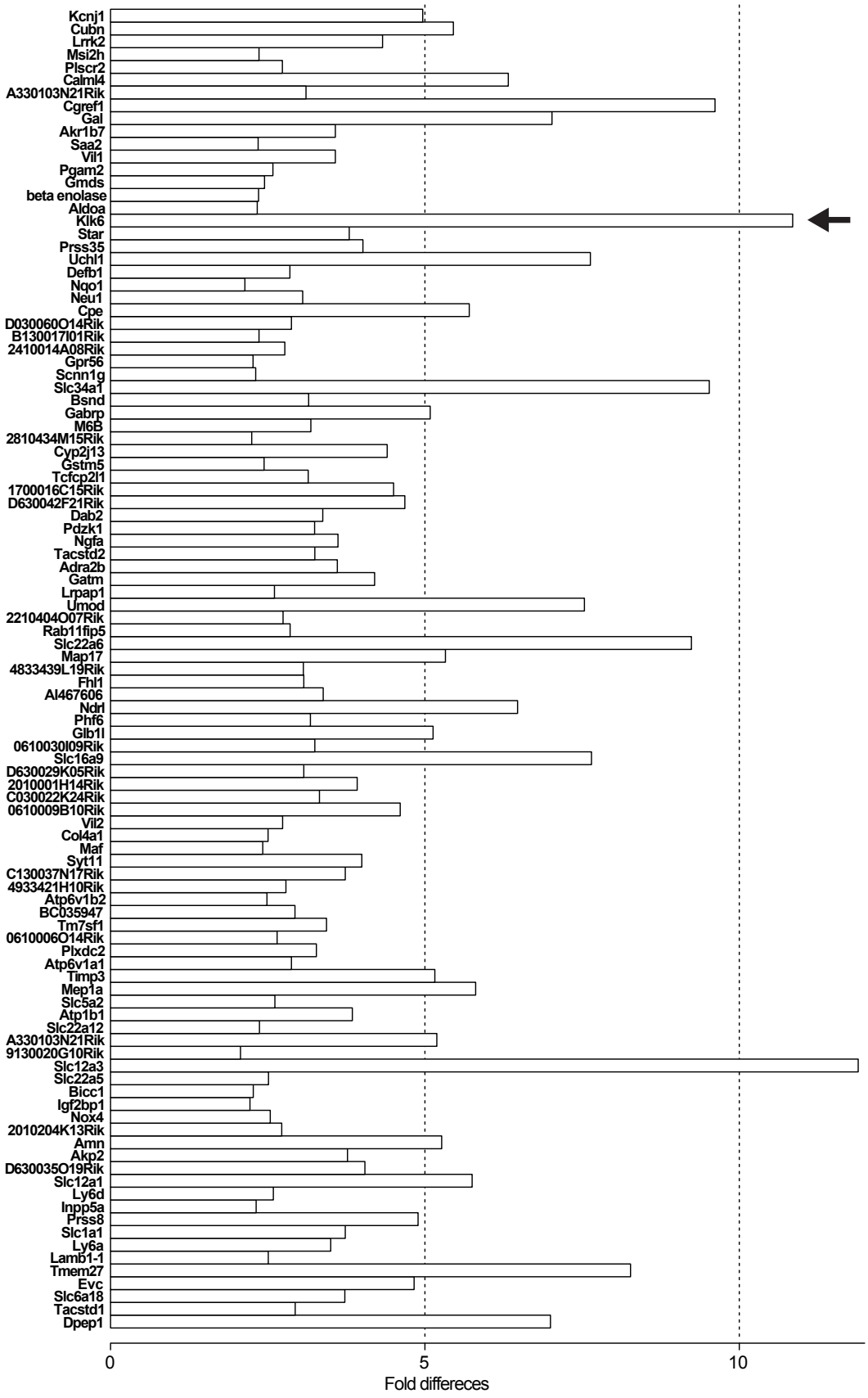

Figure 3.26: Genes for which expression was down-regulated at least two-fold in the liver of male TPC2 KO mice in comparison to the WT as determined by microarray analysis (n = 6). The arrow indicates the gene further analysed by RT-qPCR. Description of the genes is detailed in Appendix Table 3.2.

The ability to screen thousands of genes simultaneously makes microarray analysis a powerful tool to identify genes that are differentially expressed. However, the exact level of expression still requires a more sophisticated technique, such as RT-qPCR. To validate the microarray analysis by RT-qPCR, one gene that was up-regulated (*Accn5*) and another gene that was down-regulated (*Klk6*) were chosen to be further analysed by RT-qPCR. These genes were chosen as they exhibited the greatest differential expression values. *Accn5* is the gene for intestinal amiloride-sensitive cation channel 5; *Klk6* is abbreviation of kallikrein 6. *Slc12a3* was initially chosen as the down-regulated gene for further investigation, but under the experimental conditions a good signal could not be detected so *Klk6* was selected instead.

RT-qPCR analysis showed that the level of Accn5 mRNA was indeed up-regulated in TPC2 KO compared to the WT. In contrast to microarray analysis where nearly 10-fold up-regulation was observed, RT-qPCR showed that the expression was only increased roughly 1.6-fold in TPC2 KO compared to the WT (Figure 3.27). Surprisingly, although the expression of Klk6 mRNA was shown to be down-regulated in the microarray analysis, RT-qPCR showed that the expression was in fact up-regulated in TPC2 KO compared the WT (Figure 3.27). It is important to note that during the RT-qPCR analysis, there was a high degree of variations in the expression level of Klk6 in TPC2 KO. This suggests that the probe and primer pair chosen to detect Klk6 might benefit from further optimisation.

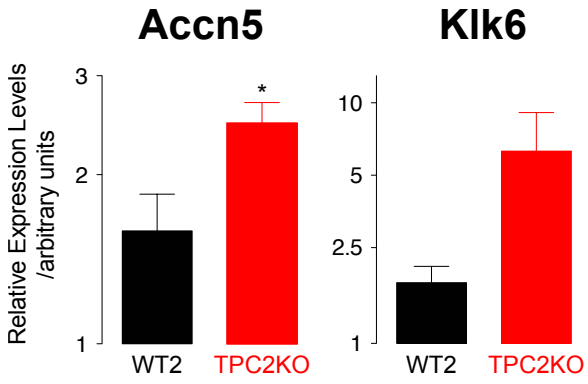

Figure 3.27: Expression analysis by RT-qPCR to confirm the results from microarray. The expression levels of Accn5 and Klk6 mRNA were measured in WT and TPC2 KO male liver. Accn5 and Klk6 were chosen based on their high degree of differential expression in microarray analysis. Results are normalized to the lowest value of the control, n = 4, *P $<$ 0.05.

Overall, analyses from microarray and RT-qPCR showed that the expression levels of many other proteins, in addition to the remaining isoform in TPC single KO (Figure 3.22), are up- or down-regulated to compensate for the eliminated protein. This further suggests that the lack of gross phenotypes observed in TPC DKO may be a result of multiple compensatory mechanisms that have been invoked to counterbalance the deletion of the proteins.

3.2.7 Generation and analysis of TPC double KO (DKO) mouse

Thus far, TPC1 and TPC2 single KOs were generated as valuable tools for investigating the physiological roles of each endogenous TPC. Interestingly, TPC single KOs exhibited no gross phenotypes. One possibility is that the function of TPCs is redundant and the eliminated TPC can be compensated for by the remaining TPC to resume normal functions. To avoid the redundancy issue, TPC1 KOs (TPC1 D159) were further bred with TPC2 KOs (TPC2 YHD437) to generate TPC double knockouts (DKO). Offspring from breeding of TPC1 KO and TPC2 KO should be heterozygote for TPC1 and TPC2 ($TPC1^{+/-}/TPC2^{+/-}$). $TPC1^{+/-}/TPC2^{+/-}$ mice were then crossed to obtain WT ($TPC1^{+/+}/TPC2^{+/+}$) and TPC1 and TPC2 homozygous mutant ($TPC1^{-/-}/TPC2^{-/-}$) mice.

3.2.7.1 Genotypic analysis of TPC1 D159/TPC2 YHD437 mutant mice

Offspring from crossing $TPC1^{+/-}/TPC2^{+/-}$ mice were genotyped using genomic DNA isolated from ear clips via the same 3-primer PCR strategy to identify the WT or TPC mutant alleles that they carry. For TPC1, WT (+/+), TPC1 D159 homozygous (–/–) and heterozygous (+/–) mice were defined by their WT TPC1 only (376 bp), homologous recombinant TPC1 mutant only (459 bp), or both alleles respectively. For TPC2, WT (+/+), TPC2 YHD437 homozygous (–/–) and heterozygous (+/–) mice were defined by the presence of WT TPC2 only (493 bp), TPC2-β-geo mutant only (336 bp), or both alleles respectively.

To increase the chance of breeding mice homozygous for the mutant alleles ($TPC1^{-/-}/TPC2^{-/-}$), mice that were homozygous mutants for one gene and heterozygous for another gene (such as $TPC1^{-/-}/TPC2^{+/-}$) were bred with each other. Double TPC mutants i.e. $TPC1^{-/-}/TPC2^{-/-}$ were further bred to continue germ-line transmission of TPC1 and TPC2 mutant alleles.

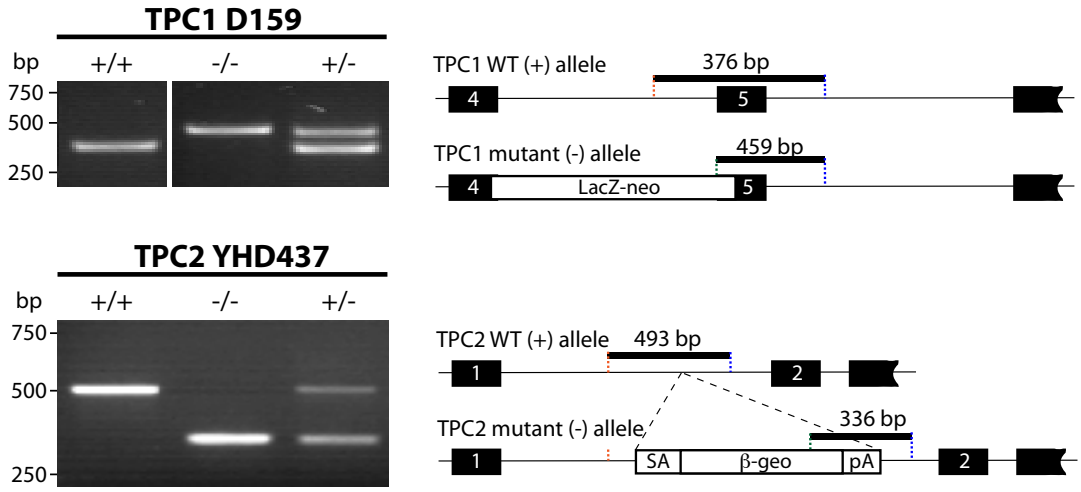

Figure 3.28: 3-primer PCR analysis of genomic DNA isolated from mouse ear clips. Left, for TPC1, WT (+/+), TPC1 D159 homozygous (−/−) and heterozygous (+/−) mice were defined by their WT TPC1 only (376 bp), homologous recombinant TPC1 mutant only (459 bp), or both alleles respectively. For TPC2, WT (+/+), TPC2 YHD437 homozygous (−/−) and heterozygous (+/−) mice were defined by their WT TPC2 only (493 bp), TPC2-β-geo mutant only (336 bp), or both alleles respectively. Right, amplified regions in the genomic DNA. Thick lines represent the amplified regions, black boxes with numbers indicate the exons and exon numbers, white boxes indicate the gene targeting vector containing *LacZ-neo* marker/selection gene, or the gene trap vector (splice acceptor (SA) sequence, β-*geo* gene, and polyadenylation (pA) signal), thin lines represent the introns, and vertical lines show primer loci.

3.2.7.2 TPC1 D159/TPC2 YHD437 as the TPC double knockout (TPC DKO) mouse

To confirm that the expression of both TPCs is abolished in TPC1$^{-/-}$/TPC2$^{-/-}$, RT-PCR that probed TPC1 (exon 6–13; 606 bp) and TPC2 (exon 4–8; 564 bp) mRNA expression was conducted. Analysis confirmed that expression of both TPCs were indeed abolished in TPC1$^{-/-}$/TPC2$^{-/-}$ in contrast to the WT, where both TPC1 and TPC2 were expressed.

To ensure that the lack of TPC1 and TPC2 expression in TPC1$^{-/-}$/TPC2$^{-/-}$ was not due to a batch of bad RNA extraction, a housekeeping gene, beta-Actin (*Actb*), was chosen as a positive control. As expected, analysis showed that *Actb* was expressed in the WT and TPC1$^{-/-}$/TPC2$^{-/-}$ (447 bp, Figure 3.29). The results verified that TPC1$^{-/-}$/TPC2$^{-/-}$ is a true TPC DKO where the expression of both TPCs was abolished.

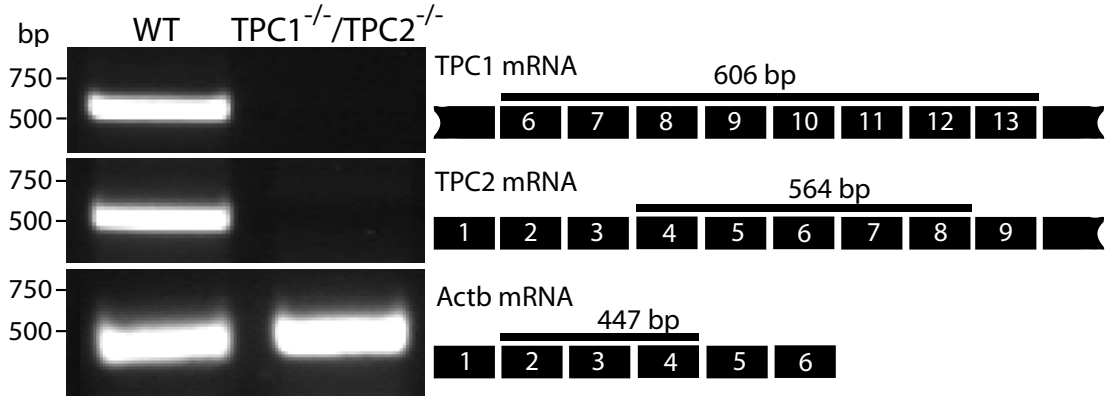

Figure 3.29: Left, RT-PCR analysis of the mouse hepatic total RNA showed that TPC1 (Exon 6–13, 606 bp) and TPC2 mRNA (Exon 4–8; 564 bp) were both expressed in the WT, but completely abolished in TPC1$^{-/-}$/TPC2$^{-/-}$. A housekeeping gene, beta-Actin (*Actb*), that acted as a positive control was shown to express in both WT and TPC1$^{-/-}$/TPC2$^{-/-}$ (Exon 2–4, 447 bp). Right, amplified regions in the mRNAs. Black lines represent the amplified regions, and black boxes with numbers indicate the exons and exon numbers.

3.3 Discussion

The lack of selective inhibitors and the difficulties in abolishing gene expression in primary cells prompted generation of TPC single KO mice in order to distinguish the physiological roles of each TPC isoform. Three TPC single mutant ES cell lines, TPC1 XG716, TPC1 D159, and TPC2 YHD437, were obtained from government funded knockout consortia. TPC mutant mice were then generated in collaboration with Harwell or obtained directly from EMMA; these mutant mice were first validated by 3-primer PCR to ensure they are homozygous carrying mutant alleles (–/–) introduced by either gene trapping or gene targeting (Figure 3.3, 3.10, and 3.15). Disruption of the gene expression resulting from the mutation was then examined by RT-PCR. RT-PCR established that single TPC mutants, TPC1 D159 and TPC2 YHD437 were the true TPC1 and TPC2 single KOs, respectively (Figure 3.11, and 3.16).

3.3.1 TPC1 mRNA expression in TPC1 XG716

Although the *Tpcn1* gene was mutated by the insertion of the gene trap vector, TPC1 mRNA was still expressed in TPC1 XG716 (Figure 3.4). The observed TPC1 mRNA expression in TPC1 XG716 comprised both the ΔN-TPC1 (the shorter TPC1 variant), and the longer TPC1 mRNA that escaped from the trap (Figure 3.30). Initiation of the ΔN-TPC1 transcription was possibly driven from an alternative promoter downstream of the gene trap vector insertion, thus avoiding the trap. Long introns have been associated with flanking alternatively skipped exons and this is likely to be the reason for the gene trap skipping [137]. Indeed, in TPC1 XG716, the gene trap vector was inserted in the long intron (intron 2) of *Tpcn1*, which is more likely to be involved in alternative splicing. It is possible that alternative splicing occurred around the long intron of *Tpcn1*, thereby escaping the entrapment.

Although the gene trap was skipped, this was not constitutive as some TPC1 mRNAs were being trapped. This suggests that the expression of TPC1 was partially knocked down in TPC1 XG716. Precise quantitation by RT-qPCR revealed that TPC1 XG716 was indeed a hypomorph (a partial knockdown of TPC1), the expression level of TPC1 mRNA being significantly reduced, but interestingly only in the female and not male liver (Figure 3.22). The expression level was reduced by roughly 50%, suggesting that TPC1

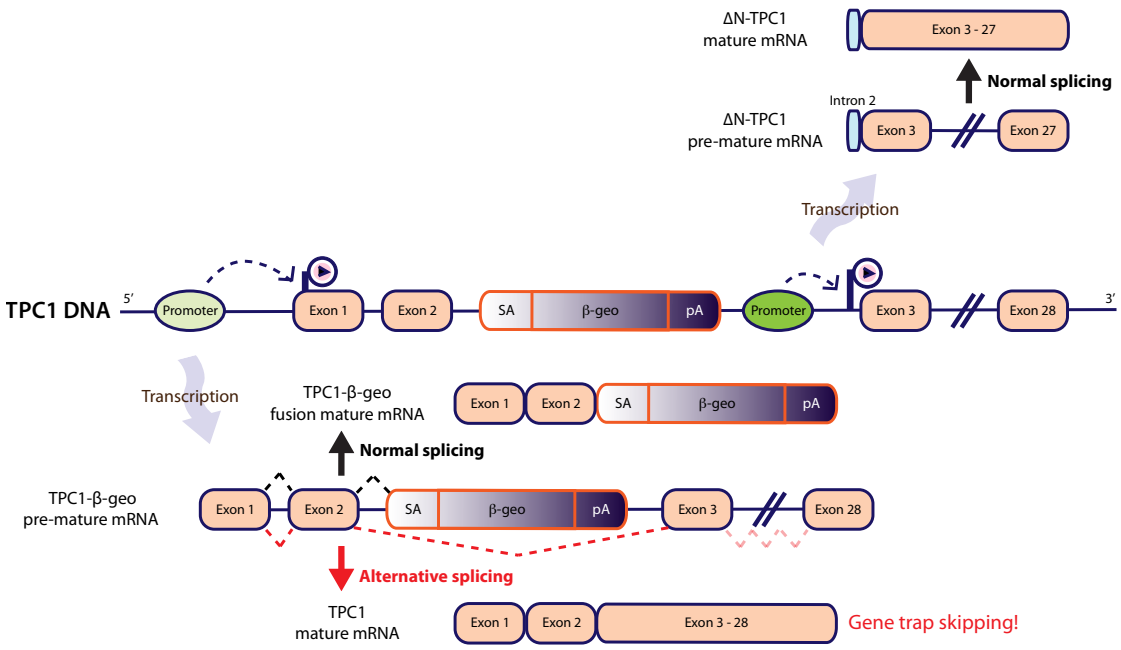

Figure 3.30: An explanation of the observed TPC1 mRNA expression in TPC1 XG716. The gene trap vector comprises a splice acceptor (SA) sequence, the *β-geo* gene, and a polyadenylation (pA) signal. During transcription, the SA sequence recruits the endogenous splicing machinery and interrupts normal splicing. The splicing process terminates at the pA signal and produced a TPC1-*β*-geo mRNA. Although the gene trap vector was inserted in the intron 2 of *Tpcn1*, the observed TPC1 mRNA expression may be attributed to a longer TPC1 mRNA that escaped the trapping as a result of alternative splicing, and the presence of the shorter ΔN-TPC1 mRNA. During normal splicing, TPC1 was fused to *β*-geo mRNA whereas during alternative splicing, the endogenous splicing machinery bypassed the SA sequence and spliced exons downstream of the vector, producing the longer mRNA. The promoter for transcribing ΔN-TPC1 was possibly downstream of the gene trap vector, therefore the expression of ΔN-TPC1 mRNA was unaffected.

XG716 could be used as an informative model to study TPC1 functions. The degree of compensation in TPC1 XG716 might be much milder than in the full KO, thus possibly allowing a truer phenotypic representation of the effect of reducing TPC1 expression.

In an attempt to explain the sex-specific TPC1 mRNA reduction in TPC1 XG716, a sex-specific regulatory element, ER*α*-binding site was found in the *Tpcn1* gene (Figure 3.24A). This regulatory element was located in intron 2 in close proximity to the gene trap insertion site, and also to the alternative promoters of ΔN-TPC1. It is possible that the insertion of the vector affects the regulation of the alternative promoter by estrogen receptor. Additionally, whether the reduced level was due to disruptions of the longer or the alternative TPC1 mRNA expression remains to be clarified, as RT-qPCR amplification was

performed between *Tpcn1* exon 15 to 16, which is included in both mRNAs. Furthermore, it is important to note that RT-qPCR was only conducted on liver tissue, and the level of reduction might vary between different tissue types due to different regulatory elements.

3.3.2 Expression of TPC1 and TPC2

TPC1 and TPC2 mRNAs were shown to co-express in a broad range of tissues (Figure 3.7 and 3.17A). This together with the reported versatility of NAADP signalling in various cell or tissue systems [103] suggests that TPCs have a fundamental role in organisms. However, the co-expression of TPCs makes it difficult to identify their individual roles. The TPC single KO mice generated here should help to differentiate the physiological roles of each TPC isoform. Additionally, to further dissect their roles, the subcellular localizations of TPCs will be investigated in Chapter 4.

RT-qPCR in mouse livers of two genetic background strains revealed that TPC1 is the predominant isoform over to TPC2 at the RNA level (Figure 3.21). This agrees with the findings of Zong *et al.* where higher mouse TPC1 mRNA expression was observed by northern blotting [307]. Additionally, TPC1 has also been reported as the isoform predominantly expressed in human (SKBR3 cell line), rat (PC12 cell line) and sea urchin (eggs) [39]. Although TPC1 mRNA is more abundant, it remains unclear as to whether this translates into higher protein abundance as discrepancies are often observed between the reported mRNA and protein levels [211]. The discrepancies can arise from the true biological differences between the abundance of mRNA and protein, or from other methodological issues such as the sensitivity of the techniques and sample processing [211].

One item of evidence to support the observation that protein expression of TPC1 is higher than TPC2 comes from western blotting using anti-β-galactosidase antibody to probe for the TPC-β-galactosidase proteins in tissues from TPC gene-trapped mutants. Under the same conditions, the western blots revealed a much more prominent band in TPC1 XG716 than in TPC2 KO (Figure 3.18). The band for TPC2 was barely visible. It is also important to note that not all TPC1 proteins were trapped. The detected expression only indicated a portion of the trapped TPC1 expression; this further suggests that the overall TPC1 expression is higher than TPC2. However, there is always the possibility that the insertion of the gene trap vector might affect the promoter of the

gene, thus affecting the detected trapped expression. Nevertheless, the results reported here strongly suggest that the expression level of endogenous TPC1 protein is higher than TPC2 in mouse tissue types.

A recent study has reported that although both TPCs were expressed in undifferentiated myoblasts and in the earliest embryonic stages of skeletal muscle, only the expression level of TPC2 mRNA was down-regulated during differentiation and skeletal muscle development [5]. As the tissue used in the expression studies was liver from adult mice (∼8 weeks), it is possible that TPC2 expression has already become down-regulated during development similar to skeletal muscle. Therefore, the expression of TPC2 appears to be lower than TPC1 in the adult mouse.

In order to confirm that the endogenous TPC proteins are expressed in a wide range of tissues, our lab has developed anti-sera against mouse and human TPC1. Some TPC1 anti-sera (targeting epitope set A and B, Table 3.1) recognized mouse TPC1 in the TPC1-mCherry-overexpressing membranes in western blotting (Figure 3.12). However, they were unable to detect the endogenous TPC1 protein in hepatic membranes.

Possible explanations for this are that the detection method was not sensitive enough, and/or the endogenous signal is masked by stronger signals from non-specific bands detected by other IgGs in the rabbit serum. These problems might be overcome by purifications of the specific antibodies. Since TPC1 antibodies were from rabbit serum, antibody purification might be needed to enrich TPC1-specific antibodies and thus eliminate non-specific interactions in anti-TPC1 sera (i.e. improve signal to noise ratio). Purification of TPC1 anti-sera might yield antibodies suitable for detecting the endogenous TPC1 protein, and thereby useful to determine which tissue type TPC1 protein is expressed. Alternatively, a more sensitive detection method may need to be used.

Although in-house antibodies were unable to directly detect the endogenous TPC proteins, endogenous expression was identified by the reporter TPC-β-galactoidase fusion protein in the TPC1 XG716. The bands detected for TPC1-β-galactosidase were slightly higher than the predicted size, this may be a result of post-translational modification such as glycosylation. Glycosylation may be tested by endoglycosidases, Peptide: N-Glycosidase F (PNGase-F), which cleaves oligosaccharides from glycoproteins or glycolipids. This should shift the bands to a smaller size.

Consistent with the endogenous expression pattern of TPC1 mRNA (Figure 3.7), TPC1-β-galactosidase protein was shown to be expressed in liver, brain, kidney, and spleen. In liver [52] and brain [215], NAADP has been shown to bind to these tissue membranes. Furthermore, NAADP has been shown to release Ca^{2+} from microsomes in hepatocytes [177]. However, the function of NAADP in kidney has not been investigated. Given the high expression level of TPC1 in liver and kidney, and that NAADP has shown to play a role in liver, it is likely that NAADP also plays a role in kidney.

It is important to understand the tissue expression profiles of different protein isoforms. For instance, ryanodine receptors (RyRs) have three isoforms; RyR1, RyR2, and RyR3. Each isoform has a differential tissue expression: RyR1 is predominantly expressed in skeletal muscle, whereas RyR2 is found in cardiac muscle [93]. Mirroring this principal tissue-expression profile, mutations in those isoforms are intricately linked to several debilitating skeletal or cardiac myopathies in human [149, 175]. Thus, tissue distribution of TPC protein expression should be further explored when specific TPC antibodies become available.

3.3.3 Expression of ΔN-TPC1

Genes with alternative promoters are reported to be more differentially expressed and/or susceptible to diseases such as cancer [164]. The discovery of ΔN-TPC1 raises the question as to whether its expression is tissue-specific. Interestingly, the expression of ΔN-TPC1 was found in all the tissues tested (Figure 3.7B), suggesting potential roles of this variant in a broad range of tissues. This expression pattern is also consistent with the expression pattern of the lower TPC1 bands (i.e. a smaller molecular weight) in the northern blot [307].

Searches in the human cDNA library also revealed homologues of a longer TPC1 variant (e.g. BC150203) and a shorter ΔN-TPC1 (accession number AK296268). Like mouse ΔN-TPC1, human ΔN-TPC1 was also initiated in the long intron 2, possibly from an alternative promoter. Similar to the predicted protein sequence in mice, it had a truncation of 68 amino acid residues in the N-terminus. This suggests that ΔN-TPC1 may be evolutionarily conserved. Interestingly, searches in mouse or human cDNA libraries did not find an equivalent ΔN isoform of TPC2, this might be because *Tpcn2* gene does not

have a long intron near the 5'-end like *Tpcn1*, thereby the chance of having an alternative promoter is reduced.

In this chapter, the characterization of ΔN-TPC1 was only conducted at the mRNA level; whether or not this mRNA can be translated successfully into protein is still unknown. The fact that this mRNA has an alternative start codon suggests that ΔN-TPC1 is not a futile mRNA; it is likely to be translated into a protein. If this indeed is the case, it would be interesting to investigate its role in NAADP-mediated signalling. There are many proteins in the literature that have a N-terminally truncated form attributed to the presence of alternative promoters [147]. Some alternative forms, such as ΔN*p*73 and ΔN*p*63 of *p*73 (tumor protein p73) and *p*63 (tumor protein p63) respectively, function as dominant negatives, whilst others such as DNMT3a2 (ΔN variant of cytosine 5-methyl transferase enzyme) functions the same but its intracellular localization is altered compared to the full length form [147]. Thus, the next key step is to determine whether ΔN-TPC1 mRNA could be successfully translated into protein. This question will be addressed in Chapter 4.

3.3.4 Sex-dependent regulation of TPC expression

Sex-specific differences were observed in the endogenous levels of TPC mRNAs in wild-types. In female, the level of TPC2 mRNA was shown to be higher than the male in two different genetic background strains (Figure 3.21). Similarly, the level of TPC1 mRNA was shown to be higher in female than male in one strain but not in the other. The ERα-binding site found in *Tpcn1* (described above) may help to explain the sex-related differences. Although searches did not find any sex-specific regulatory element in *Tpcn2*, it is speculated that TPC2 gene might also be regulated by sex-specific regulatory elements that have yet been reported. Sex-dependent regulation is not unique to TPCs: many other non-selective cation channels in the TRP (Transient Receptor Potential) family have also been reported to be regulated by sex hormones, including TRPC4 by estrogen [62], TRPM8 by testosterone [32], TRPV4 [132] and TRPV6 [37] by progesterone.

Expression studies in MEFs provided preliminary evidence that regulation of TPC mRNA expression might be sex-dependent. A three-hour incubation of oestradiol (100 nM) significantly up-regulated both TPC1 and TPC2 mRNA expression (Figure 3.24B).

However, the increase was only ∼1.13-fold. Estrogen has been reported to up-regulate expression of other genes, for example, α_{2C}-adrenoceptors in smooth muscle by 2–4-fold [91], and eNOS (endothelial nitric oxide synthase) and iNOS (inducible nitric oxide synthase) in coronary artery by 1.7- and 27-fold, respectively [186]. The extent of up-regulation observed in this study therefore seemed modest. There are two possible reasons for this: MEF cells were originally prepared from a mixture of male and female embryos and additionally this cell type may not exhibit high expression of estrogen receptors. Future expression studies in MEF cells stably transfected with estrogen receptor, or in other cells expressing a high level of estrogen receptors, such as female breast cancer cells, MCF-7, may yield more information on the sex-dependent regulation of TPC expression.

3.3.5 Compensation in TPC KOs

Given that TPCs are likely to be fundamentally important in organisms, it is surprising that in TPC single KOs, mice exhibited no gross phenotypes. In TPC single KOs, the phenotypes arising from the loss of individual proteins were probably alleviated by redundancy and/or compensation by the remaining TPC, and also by compensation by other proteins. Indeed, RT-qPCR in TPC single KOs revealed that the expression of the remaining TPC was up-regulated to compensate for the loss of one isoform (Figure 3.22). Furthermore, the compensation was sex-specific. It is difficult to interpret the observed sex-specific differences, although it can be speculated that the significant increase in the level of TPC1 mRNA in the male and not female TPC2 KO mice was due to a lower basal level of TPC1 mRNA in the male WT2. Thus when TPC2 mRNA was abolished, an up-regulation of TPC1 expression was required for the loss of TPC2 in males to function normally. The basal level of TPC1 mRNA in females was higher, therefore it might be sufficient to compensate for the loss of TPC2.

Interestingly, when TPC1 was knocked out, TPC2 mRNA expression was up-regulated in female TPC1 KOs but not in male. This was not expected. As the basal level of TPC2 is significantly lower in male than in female WT1, a higher degree of TPC2 compensation in the males would be expected. Until more is known about the functions and regulatory elements of individual TPCs in liver, it will be difficult to interpret the results from the RT-qPCR analysis. Despite the difficulty in inferring the physiological function, the data

clearly showed that the expression of the remaining TPC is sex-specifically up-regulated to compensate for the loss of the other isoform in TPC single KOs.

Compensation by the other proteins was also investigated at a global level by microarray analysis. Expression analysis revealed a large number of genes whose expression was either up- or down-regulated in TPC2 KO compared to the WT. The vast numbers of genes involved in compensation for the deletion of a single gene indicates the complexity of cellular expression in restoring normal functions.

In microarray analysis, the gene that was most up-regulated in TPC2 KO was *Accn5* (Figure 3.25), and RT-qPCR also showed that *Accn5* was up-regulated (Figure 3.27). *Accn5* (amiloride-sensitive cation channel 5) belongs to the amiloride-sensitive degenerin/epithelial Na^+ channel (DEG/ENaC) family [288] and is predicted to function in epithelial transport. In mouse, the predominant tissue expression of *Accn5* is in brain, liver, small intestine, kidney, and lung [244]. Based on the localization of its human homologue, *Accn5* is likely to localize to the plasma membrane [247]. Channel electrophysiology has shown that *Accn5* is selective for Na^+ and is constitutively active at physiological extracellular ion concentrations [288]. In TPC2 KO, it is possible that deletion of TPC2 would reduce the NAADP-elicited Ca^{2+} release from acidic stores (the trigger response) and the subsequent Ca^{2+} release from the ER (by CICR). The reduced Ca^{2+} release in the cytosol would then reduce the activity of Na^+/Ca^{2+} electrogenic exchanger (NCX). NCX removes one Ca^{2+} ion from the cytosol in exchange for three Na^+ ions, resulting in net movement of one positive charge [72]. Thus, in TPC2 KO, less Na^+ will be imported into the cytosol as less Ca^{2+} needs to be removed in order to maintain Ca^{2+} homeostasis. However, the membrane potential may become more hyperpolarized as there is a reduced positive charge moving into the cell. *Accn5* would therefore become up-regulated to increase Na^+ influx to maintain the electrochemical gradient.

In microarray analysis, *Klk6* was down-regulated in TPC2 KO male mice. *Klk6* is known as kallikrein 1 (*Klk1*), a tissue kallikrein, and is a serine protease that forms kallidin from kininogen [54, 232]. Kallidin activates kinin receptor type 1 (B_1) but more potently at the type 2 (B_2) [54]. Activation of B_2 kinin receptor is known to lead to endothelium-dependent vasodilatation [281]. NAADP has been reported to play a role in vasoconstriction of pulmonary [36, 138] and coronary [302, 303] arterial smooth muscle

cells. In TPC2 KO, NAADP-mediated vasoconstriction is likely to be reduced, thus *Klk6* may be down-regulated to prevent excessive vasodilatation.

However, determination of the *Klk6* mRNA level using RT-qPCR showed that the level was significantly up-regulated in TPC2 KO (Figure 3.27). Although discrepancies between microarray analysis and RT-qPCR often occur, it is rarely to this extent. In general, RT-qPCR offers a more accurate estimate of the relative expressions. The polarity of the regulation (i.e. up- or down-regulation), however, usually correlates between the two methods [167], but for *Klk6*, the discrepancy was both in extent and direction. This is probably due to the fluorescent probe and primer set used for detecting *Klk6* in RT-qPCR as a high variability was observed across the samples. Future studies with a better set of fluorescent probe and primers are needed to confirm the microarray findings. It is important to emphasize that all expression analyses, by both RT-qPCR and microarray, were conducted only on liver tissue. Since each TPC isoform may have a differential role in different tissues, the degree of redundancy and compensation may therefore vary between tissues.

Although compensatory mechanisms might be complicating the interpretation, the generation of single TPC knockouts has proven highly beneficial in studying endogenous functions of single TPC isoforms. Using TPC2 KO mice, TPC2 has been shown to play a crucial role in NAADP-mediated responses in pancreatic β-cells [52] and bladder smooth muscle [90]. It is possible that in these systems, TPC2 is the dominant channel; or alternatively, that there is not the scope for TPC redundancy here compared to other tissue types in which TPCs are more redundant, and the loss of one isoform can be functionally compensated for by the remaining isoform. It would be interesting to measure the levels of TPC mRNAs in pancreatic β-cells and bladder smooth muscle to determine whether TPC2 is the predominant isoform, and the extent of compensation provided by the remaining TPC. There are two IP_3 receptor subtypes that are important in the mouse pancreatic acinar cells, IP_3R2 and IP_3R3. While knocking out one IP_3R failed to significantly alter agonist-induced Ca^{2+} signalling in pancreatic acinar cells, knocking out both IP_3R2 and IP_3R3 completely abrogated the agonist-induced Ca^{2+} signalling [99].

To circumvent the effects of redundancy and compensation by the remaining isoform in single KOs, TPC1 and TPC2 double KO (TPC DKO) were generated (Figure 3.29).

The TPC DKO will hopefully elucidate important physiological functions governed by the TPC family, in particular, systems where both genes are highly redundant. Furthermore, similar to TPC single KOs, no gross phenotypes were observed in TPC DKO mice. This emphasizes the significance of compensatory mechanisms that are involved to tolerate the deletion of two proteins.

3.4 Conclusions

Expression analysis showed that mouse TPC1 and TPC2 are co-expressed in a broad range of tissue types. This is consistent with the study by Zong *et al.* [307] and implies their fundamental importance in multicellular organisms. Resolving the subcellular localizations of both TPCs will greatly assist further elucidation of their individual roles.

RT-qPCR analysis showed that in mouse liver, the level of TPC1 expression was significant higher than TPC2, supporting the study by findings by Brailoiu *et al.* [39], in which the expression level of TPC1 was found to be higher in sea urchin eggs, rat (PC12) and human (SKBR3) cell lines. The expression of TPCs was also shown to be dependent on the sex and genetic background. Preliminary experiment with oestradiol treatment also supports the finding that the regulation of TPC expression is sex-dependent, possibly by an estrogen promoter.

Table 3.3 shows a set of useful mouse models that has been generated. RT-qPCR analysis demonstrated that the remaining isoform could up-regulate to compensate in TPC single KOs. Microarray analysis in TPC2 KO male mice also showed that compensation could occur by up- or down-regulation of other genes. The occurrence of compensation may help to explain the lack of gross phenotypes observed in these mice mutants.

Although the TPC1 hypomorph was an incomplete knockout, during validation it led to the discovery of an alternative TPC1 mRNA (ΔN-TPC1). Furthermore, the reporter gene in TPC1 hypomorph was useful in providing information such as the expression level and pattern of endogenous TPC1 protein. Using the TPC KO mice generated and characterized in this chapter, it will be exciting to embark on a new era of understanding the endogenous functions of the TPC family.

Mice	**Expression**		**Respective WT**
	TPC1	TPC2	
TPC1 KO	×	✓	WT1
TPC1 H	↓	✓	WT2
TPC2 KO	✓	×	WT2
TPC DKO	×	×	WTD

Table 3.3: Characterization of TPC mutant mice. × indicates no expression, ✓ indicates expression, and ↓ indicates a lower expression. The respective wild-type (WT) indicates the WT mice that shared the same genetic background as the mutant mice. Abbreviations: KO, knockout; H, hypomorph; DKO, double knockout.

3.5 Appendix

Table 3.1: Description of the genes that were up-regulated by at least two fold in TPC2 KO compared to the WT as measured by microarray analysis.

Gene	Accession number	Description
Tnmd	NM022322	Mus musculus tenomodulin (Tnmd), mRNA.
Lias	AK003351	Mus musculus 18-day embryo whole body cDNA, RIKEN full-length enriched library, clone:1110003F10 product:unclassifiable, full
2010321J07Rik	NM028094	Mus musculus RIKEN cDNA 2010321J07 gene (2010321J07Rik), mRNA.
2200002D01Rik	AK008617	Mus musculus adult male stomach cDNA, RIKEN full-length enriched library, clone:2200002D01 product:weakly similar to HAI-2 RELATED
Apip	NM019735	Mus musculus monocyte macrophage 19 (Mmrp19), mRNA.
Cxcl13	NM018866	Mus musculus chemokine (C-X-C motif) ligand 13 (Cxcl13), mRNA.
Asns	NM012055	Mus musculus asparagine synthetase (Asns), mRNA.
Rbp1	NM011254	Mus musculus retinol binding protein 1, cellular (Rbp1), mRNA.
2200001I15Rik	NM183278	Mus musculus RIKEN cDNA 2200001I15 gene (2200001I15Rik), mRNA.
Accn5	NM021370	Mus musculus amiloride-sensitive cation channel 5, intestinal (Accn5), mRNA.
Fpr-rs7	NM177317	Mus musculus formyl peptide receptor, related sequence 7 (Fpr-rs7), mRNA.

Table 3.2: Description of the genes that were down-regulated by at least two fold in TPC2 KO compared to the WT as measured by microarray analysis.

Gene	Accession number	Description
Dpep1	NM007876	Mus musculus dipeptidase 1 (renal) (Dpep1), mRNA.
Tacstd1	NM008532	Mus musculus tumor-associated calcium signal transducer 1 (Tacstd1), mRNA.
Slc6a18	NM011730	Mus musculus solute carrier family 6 (neurotransmitter transporter), member 18 (Slc6a18), mRNA.
Evc	NM021292	Mus musculus Ellis van Creveld gene homolog (human) (Evc), mRNA.
Tmem27	NM020626	Mus musculus transmembrane protein 27 (Tmem27), mRNA.
Lamb1-1	NM008482	Mus musculus laminin B1 subunit 1 (Lamb1-1), mRNA.
Ly6a	NM010738	Mus musculus lymphocyte antigen 6 complex, locus A (Ly6a), mRNA.
Slc1a1	NM009199	Mus musculus solute carrier family 1 (neuronal/epithelial high affinity glutamate transporter, system Xag), member 1 (Slc1a1),
Prss8	NM133351	Mus musculus protease, serine, 8 (prostasin) (Prss8), mRNA.
Inpp5a	NM183144	Mus musculus inositol polyphosphate-5-phosphatase A (Inpp5a), mRNA.
Ly6d	NM010742	Mus musculus lymphocyte antigen 6 complex, locus D (Ly6d), mRNA.
Slc12a1	NM183354	Mus musculus solute carrier family 12, member 1 (Slc12a1), transcript variant 2, mRNA.
D630035O19Rik	NM145932	Mus musculus RIKEN cDNA D630035O19 gene (D630035O19Rik), mRNA.
Akp2	NM007431	Mus musculus alkaline phosphatase 2, liver (Akp2), mRNA.
Amn	NM033603	Mus musculus amnionless (Amn), mRNA.
2010204K13Rik	NM023450	Mus musculus RIKEN cDNA 2010204K13 gene (2010204K13Rik), mRNA.
Nox4	NM015760	Mus musculus NADPH oxidase 4 (Nox4), mRNA.
Igf2bp1	NM009951	Mus musculus insulin-like growth factor 2, binding protein 1 (Igf2bp1), mRNA.
Bicc1	NM031397	Mus musculus bicaudal C homolog 1 (Drosophila) (Bicc1), mRNA.
Slc22a5	NM011396	Mus musculus solute carrier family 22 (organic cation transporter), member 5 (Slc22a5), mRNA.
Slc12a3	NM019415	Mus musculus solute carrier family 12, member 3 (Slc12a3), mRNA.
9130020G10Rik	NM025786	Mus musculus RIKEN cDNA 9130020G10 gene (9130020G10Rik), mRNA.
A330103N21Rik	AK020732	Mus musculus adult male spinal cord cDNA, RIKEN full-length enriched library, clone:A330103N21 product:unclassifiable, full
Slc22a12	NM009203	Mus musculus solute carrier family 22 (organic anion/cation transporter), member 12 (Slc22a12), mRNA.
Atp1b1	NM009721	Mus musculus ATPase, Na+/K+ transporting, beta 1 polypeptide (Atp1b1), mRNA.
Slc5a2	NM133254	Mus musculus solute carrier family 5 (sodium/glucose cotransporter), member 2 (Slc5a2), mRNA.
Mep1a	NM008585	Mus musculus meprin 1 alpha (Mep1a), mRNA.
Timp3	NM011595	Mus musculus tissue inhibitor of metalloproteinase 3 (Timp3), mRNA.
Atp6v1a1	NM007508	Mus musculus ATPase, H+ transporting, V1 subunit A, isoform 1 (Atp6v1a1), mRNA.
Plxdc2	NM026162	Mus musculus plexin domain containing 2 (Plxdc2), mRNA.
0610006O14Rik	NM133764	Mus musculus RIKEN cDNA 0610006O14 gene (0610006O14Rik), mRNA.
Tm7sf1	NM031999	Mus musculus transmembrane 7 superfamily member 1 (Tm7sf1), mRNA.
BC035947	NM178117	Mus musculus cDNA sequence BC035947 (BC035947), mRNA.
Atp6v1b2	NM007509	Mus musculus ATPase, H+ transporting, V1 subunit B, isoform 2 (Atp6v1b2), mRNA.
4933421H10Rik	AK036871	Mus musculus adult female vagina cDNA, RIKEN full-length enriched library, clone:9930020M10 product:similar to CDNA FLJ32111 FIS,
C130037N17Rik	NM198024	Mus musculus RIKEN cDNA C130037N17 gene (C130037N17Rik), mRNA.
Syt11	AK017268	Mus musculus 6 days neonate head cDNA, RIKEN full-length enriched library, clone:5430404N14 product:unknown EST, full insert
Maf	BC041683	Mus musculus avian musculoaponeurotic fibrosarcoma (v-maf) AS42 oncogene homolog, mRNA (cDNA clone IMAGE:4221113), partial cds.
Col4a1	NM009931	Mus musculus procollagen, type IV, alpha 1 (Col4a1), mRNA.
Vil2	NM009510	Mus musculus villin 2 (Vil2), mRNA.
0610009B10Rik	BC030878	Mus musculus RIKEN cDNA 0610009B10 gene, mRNA (cDNA clone MGC:31388 IMAGE:4241631), complete cds.
C030022K24Rik	NM029912	Mus musculus RIKEN cDNA C030022K24 gene (C030022K24Rik), mRNA.
2010001H14Rik	NM027227	Mus musculus RIKEN cDNA 2010001H14 gene (2010001H14Rik), mRNA.
D630029K05Rik	NM175330	Mus musculus RIKEN cDNA D630029K05 gene (D630029K05Rik), mRNA.
Slc16a9	NM025807	Mus musculus solute carrier family 16 (monocarboxylic acid transporters), member 9 (Slc16a9), mRNA.

(Continued overleaf)

Table 3.2: Description of the genes that were down-regulated by at least two fold in TPC2 KO compared to the WT as measured by microarray analysis. *(Continued)*

Gene	Accession number	Description
0610030I09Rik	NM001001444	Mus musculus defensin beta 29 (Defb29), mRNA.
Glb1l	BC021773	Mus musculus galactosidase, beta 1-like, mRNA (cDNA clone MGC:28635 IMAGE:4222994), complete cds.
Phf6	NM027642	Mus musculus PHD finger protein 6 (Phf6), mRNA.
Ndrl	NM008681	Mus musculus N-myc downstream regulated-like (Ndrl), mRNA.
AI467606	NM178901	Mus musculus expressed sequence AI467606 (AI467606), mRNA.
Fhl1	NM010211	Mus musculus four and a half LIM domains 1 (Fhl1), mRNA.
4833439L19Rik	NM133797	Mus musculus RIKEN cDNA 4833439L19 gene (4833439L19Rik), mRNA.
Map17	NM026018	Mus musculus membrane-associated protein 17 (Map17), mRNA.
Slc22a6	NM008766	Mus musculus solute carrier family 22 (organic anion transporter), member 6 (Slc22a6), mRNA.
Rab11fip5	NM177466	synonyms: GAF1, RIP11, C75969, D6Ertd32e, mKIAA0857, 9130206P09Rik; isoform 1 is encoded by transcript variant 1; Mus musculus RAB11 family interacting protein 5 (class I) (Rab11fip5), transcript variant 1, mRNA.; isoform 2 is encoded by transcript variant 2; Mus musculus RAB11 family interacting protein 5 (class I) (Rab11fip5), transcript variant 2, mRNA.
2210404O07Rik	BC036160	Mus musculus RIKEN cDNA 2210404O07 gene, mRNA (cDNA clone IMAGE:4984207), partial cds.
Umod	NM009470	Mus musculus uromodulin (Umod), mRNA.
Lrpap1	NM013587	Mus musculus low density lipoprotein receptor-related protein associated protein 1 (Lrpap1), mRNA.
Gatm	NM025961	Mus musculus glycine amidinotransferase (L-arginine:glycine amidinotransferase) (Gatm), mRNA.
Adra2b	BC055783	Mus musculus adrenergic receptor, alpha 2b, mRNA (cDNA clone IMAGE:6404050), partial cds.
Tacstd2	NM020047	Mus musculus tumor-associated calcium signal transducer 2 (Tacstd2), mRNA.
Ngfa; Klk5	NM010915	Mus musculus kallikrein 5 (Klk5), mRNA.
Pdzk1	NM21517	Mus musculus PDZ domain containing 1 (Pdzk1), mRNA.
Dab2	NM023118	Mus musculus disabled homolog 2 (Drosophila) (Dab2), mRNA.
D630042F21Rik	AK085571	Mus musculus 0 day neonate kidney cDNA, RIKEN full-length enriched library, clone:D630042F21 product:unknown EST, full insert
1700016C15Rik	AK006014	Mus musculus adult male testis cDNA, RIKEN full-length enriched library, clone:1700016C15 product:hypothetical protein, full insert
Tcfcp2l1	NM023755	Mus musculus transcription factor CP2-like 1 (Tcfcp2l1), mRNA.
Gstm5	NM010360	Mus musculus glutathione S-transferase, mu 5 (Gstm5), mRNA.
Cyp2j13	NM145548	Mus musculus cytochrome P450, family 2, subfamily j, polypeptide 13 (Cyp2j13), mRNA.
2810434M15Rik	AK013242	Mus musculus 10, 11 days embryo whole body cDNA, RIKEN full-length enriched library, clone:2810434M15 product:hypothetical protein,
M6B; Gpm6; AI593561	AK020224	Mus musculus 15 days embryo male testis cDNA, RIKEN full-length enriched library, clone:8030496P19 product:glycoprotein m6b, full
Gabrp	NM146017	Mus musculus gamma-aminobutyric acid (GABA-A) receptor, pi (Gabrp), mRNA.
Bsnd	NM080458	Mus musculus Bartter syndrome, infantile, with sensorineural deafness (Barttin) (Bsnd), mRNA.
Slc34a1	NM011392	Mus musculus solute carrier family 34 (sodium phosphate), member 1 (Slc34a1), mRNA.
Scnn1g	NM011326	Mus musculus sodium channel, nonvoltage-gated 1 gamma (Scnn1g), mRNA.
Gpr56	NM018882	Mus musculus G protein-coupled receptor 56 (Gpr56), mRNA.
2410014A08Rik	NM175403	Mus musculus RIKEN cDNA 2410014A08 gene (2410014A08Rik), mRNA.
B130017I01Rik	NM172525	Mus musculus RIKEN cDNA B130017I01 gene (B130017I01Rik), mRNA.
D030060O14Rik	NM153140	Mus musculus RIKEN cDNA D030060O14 gene (D030060O14Rik), mRNA.
Cpe	NM013494	Mus musculus carboxypeptidase E (Cpe), mRNA.
Neu1	NM010893	Mus musculus neuraminidase 1 (Neu1), mRNA.
Nqo1	NM008706	Mus musculus NAD(P)H dehydrogenase, quinone 1 (Nqo1), mRNA.
Defb1	NM007843	Mus musculus defensin beta 1 (Defb1), mRNA.
Uchl1	NM011670	Mus musculus ubiquitin carboxy-terminal hydrolase L1 (Uchl1), mRNA.
Prss35	NM178738	Mus musculus protease, serine, 35 (Prss35), mRNA.
Star	NM011485	Mus musculus steroidogenic acute regulatory protein (Star), mRNA.
Klk6	NM010639	Mus musculus kallikrein 6 (Klk6), mRNA.
Aldoa	NM007438	Mus musculus aldolase 1, A isoform (Aldoa), mRNA.
beta enolase	X70182	M.musculus mRNA for muscle-specific beta enolase.
Gmds	NM146041	Mus musculus GDP-mannose 4, 6-dehydratase (Gmds), mRNA.

(Continued overleaf)

Table 3.2: Description of the genes that were down-regulated by at least two fold in TPC2 KO compared to the WT as measured by microarray analysis. *(Continued)*

Gene	Accession number	Description
Pgam2	NM018870	Mus musculus phosphoglycerate mutase 2 (Pgam2), mRNA.
Vil1	NM009509	Mus musculus villin 1 (Vil1), mRNA.
Saa2	NM011314	Mus musculus serum amyloid A 2 (Saa2), mRNA.
Akr1b7	NM009731	Mus musculus aldo-keto reductase family 1, member B7 (Akr1b7), mRNA.
Gal	NM010253	Mus musculus galanin (Gal), mRNA.
Cgref1	BC023116	Mus musculus cell growth regulator with EF hand domain 1, mRNA (cDNA clone MGC:28551 IMAGE:4206019), complete cds.
A330103N21Rik	BC027571	Mus musculus RIKEN cDNA A330103N21 gene, mRNA (cDNA clone IMAGE:1363058), partial cds.
Calml4	NM138304	Mus musculus calmodulin-like 4 (Calml4), mRNA.
Plscr2	NM008880	Mus musculus phospholipid scramblase 2 (Plscr2), mRNA.
Msi2h	NM054043	Mus musculus Musashi homolog 2 (Drosophila) (Msi2h), mRNA.
Lrrk2	NM025730	Mus musculus RIKEN cDNA 4921513O20 gene (4921513O20Rik), mRNA.
Cubn	AF197159	Mus musculus cubilin mRNA, partial cds.
Kcnj1	NM019659	Mus musculus potassium inwardly-rectifying channel, subfamily J, member 1 (Kcnj1), mRNA.
E130010M05Rik	NM177015	Mus musculus RIKEN cDNA E130010M05 gene (E130010M05Rik), mRNA.
Kl	NM013823	Mus musculus klotho (Kl), mRNA.
Slc5a1	NM019810	Mus musculus solute carrier family 5 (sodium/glucose cotransporter), member 1 (Slc5a1), mRNA.
Slc16a4	NM146136	Mus musculus solute carrier family 16 (monocarboxylic acid transporters), member 4 (Slc16a4), mRNA.
Gsn	NM146120	Mus musculus gelsolin (Gsn), mRNA.
Hexb	NM010422	Mus musculus hexosaminidase B (Hexb), mRNA.
Pkm2	NM011099	Mus musculus pyruvate kinase, muscle (Pkm2), mRNA.
Ckb	NM021273	Mus musculus creatine kinase, brain (Ckb), mRNA.
Sfrp1	NM013834	Mus musculus secreted frizzled-related sequence protein 1 (Sfrp1), mRNA.
Cidec	NM178373	Mus musculus cell death-inducing DFFA-like effector c (Cidec), mRNA.
Avpr2	NM019404	Mus musculus arginine vasopressin receptor 2 (Avpr2), mRNA.
Dnajc12	NM013888	Mus musculus DnaJ (Hsp40) homolog, subfamily C, member 12 (Dnajc12), mRNA.
Runx1	NM009821	Mus musculus runt related transcription factor 1 (Runx1), mRNA.
Fxyd2	NM052824	synonym: Atp1g1; isoform c is encoded by transcript variant c; sodium pump gamma chain; sodium/potassium-transporting ATPase gamma chain; ATPase, Na+/K+ transporting, gamma 1 polypeptide; Mus musculus FXYD domain-containing ion transport regulator 2 (Fxyd2), transcript variant c, mRNA.; isoform a is encoded by transcript variant a; Mus musculus FXYD domain-containing ion transport regulator 2 (Fxyd2), transcript variant a, mRNA.; isoform b is encoded by transcript variant b; Mus musculus FXYD domain-containing ion transport regulator 2 (Fxyd2), transcript variant b, mRNA.
Odc1	NM013614	Mus musculus ornithine decarboxylase, structural 1 (Odc1), mRNA.
Lrp2	Y08566	M.musculus mRNA for gp330.
Hsd3b1	NM008293	Mus musculus hydroxysteroid dehydrogenase-1, delta<5>-3-beta (Hsd3b1), mRNA.
Olfm1	NM019498	Mus musculus olfactomedin 1 (Olfm1), mRNA.
Cyp4b1	NM007823	Mus musculus cytochrome P450, family 4, subfamily b, polypeptide 1 (Cyp4b1), mRNA.
Crat	NM007760	Mus musculus carnitine acetyltransferase (Crat), mRNA.
Cml4	NM023455	Mus musculus camello-like 4 (Cml4), mRNA.
Cyp21a1	NM009995	Mus musculus cytochrome P450, family 21, subfamily a, polypeptide 1 (Cyp21a1), mRNA.
Hsd3b4	NM008294	Mus musculus hydroxysteroid dehydrogenase-4, delta<5>-3-beta (Hsd3b4), mRNA.
BC013476; Cyp4a10	NM201640	synonym: MGC18880; Mus musculus cDNA sequence BC013476 (BC013476), mRNA.; synonyms: RP1, Cyp4a, D4Rp1, AI647584; cytochrome P450, 4a10; Mus musculus cytochrome P450, family 4, subfamily a, polypeptide 10 (Cyp4a10), mRNA.
0610012A11Rik	AK002574	Mus musculus adult male kidney cDNA, RIKEN full-length enriched library, clone:0610012A11 product:hypothetical Serpins containing

Chapter 4

TPC Localization and Sorting Signals

4.1 Introduction

The identity of the Ca^{2+} stores activated by NAADP was first shown to be the reserve granules (lysosome-related organelles) in sea urchin eggs [70], as the Ca^{2+} release evoked by NAADP was inhibited by pharmacological agents that target these acidic stores [70]. Subsequent studies independently verified that NAADP recruits acidic stores such as lysosomes in various mammalian cell types [40, 138, 293]. TPCs were proposed as the NAADP receptor because of their homology to Ca^{2+} channels and their localization in the acidic organelles/endo-lysosomal system [39, 41, 42, 52, 217, 219, 243, 307]. Table 4.1 presents all the localization studies conducted on TPCs to date.

The term "acidic Ca^{2+} stores" refers to a collection of organelles from endosomes, lysosomes, lysosome-related organelles, and secretory vesicles to the Golgi apparatus [216]. These organelles are known to exhibit a range of luminal pH (4–7) and [Ca^{2+}] (μM–mM) [166, 216, 277]. Together with the fact that the luminal pH and [Ca^{2+}] have been reported to regulate TPC2 channel activity [231, 248], this suggests it is important to investigate the subcellular localization of individual TPCs (to specific organelle compartments). This would allow further insight into the roles of individual TPCs and the versatility of NAADP-mediated Ca^{2+} signalling.

Table 4.1: Summary of the reported TPCs localization.

Method	Species	TPC	Tag	Expression system	**Markers**/Organelles	co-localization	References
TT	Sp	1	GFP/mCherry	SKBR3/HEK293	**Lysotracker**/Acidic stores	Full	[41]/[243]
TT	Sp	1	mCherry	HEK293	**LAMP2**/Late endosomes & lysosomes	Some	[243]
TT/I	Sp	1	mCherry	AMO	N/A	Cortex and intracellular puncta	[243]
TT	Sp	2	GFP/mCherry	SKBR3/HEK293	**Lysotracker**/Acidic stores	Full	[41]/[243]
TT	Sp	2	GFP	SKBR3	**LAMP1**/Late endosomes & lysosomes	Full	[41]
TT	Sp	2	mCherry	HEK293	**LAMP2**/Late endosomes & lysosomes	Full	[243]
TT	Sp	2	mCherry	HEK293	**TfR**/Recycling endosomes	Some	[243]
TT/I	Sp	2	mCherry	AMO	N/A	Cortex and intracellular puncta	[243]
TT	Sp	3	GFP/mCherry	SKBR3/HEK293	**Lysotracker**/Acidic stores	Full	[41]/[243]
TT	Sp	3	mCherry	HEK293	**LAMP2**/Late endosomes & lysosomes	Full	[243]
TT	Sp	3	mCherry	HEK293	**TfR**/Recycling endosomes	Some	[243]
E+I	Sp	3	-	Sp eggs	N/A	Cortical and some in deeper puncta	[243]
TT/I	Sp	3	mCherry	AMO	N/A	Cortex and intracellular puncta	[243]
M	Sp	1	GFP	XLO	N/A	Intracellular	[41]
M	Sp	2	GFP	XLO	N/A	Intracellular	[41]
M	Sp	3	GFP	XLO	N/A	Intracellular	[41]
TT	Hs	1	GFP	SKBR3	**LAMP1**/Late endosomes & lysosomes	Substantial	[39]
TT	Hs	1	mRFP	SKBR3	**Endo**/Early & late endosomes	Substantial	[39]
TT	Hs	1	GFP	SKBR3	**KDEL**/ER	No	[39]
M	Hs	1	mRFP	XLO	**RFC**/Plasma membrane	No	[39]
M	Hs	1	GFP	XLO	**RhoB**/Endosome	Partial	[39]
M	Hs	1	GFP	XLO	**LAMP1**/Late endosomes & lysosomes	Partial	[39]
S+I	Hs	1	GFP or His	HEK293	**LAMP2**/Late endosomes & lysosomes	Some	[52]
S+I	Hs	1	GFP or His	HEK293	**M6PR**/Late endosomes	Some	[52]
S+I	Hs	1	GFP or His	HEK293	**EEA1**/Early endosomes	Some	[52]
S+I	Hs	1	GFP or His	HEK293	**Tfn**/Recycling endosomes	Substantial	[52]

(Continued overleaf)

Abbreviations: At, *Arabidopsis thaliana* (Thale cress); AMP, *Arabidopsis* mesophyll protoplasts; AMO, *Asterina miniata* (Starfish) oocytes; CytC, Cytochrome C; E, Endogenous; Gg, *Gallus gallus* (Chicken); GM130, cis-Golgi Matrix protein; Hs, *Homo sapiens* (Human); I, Immunocytochemistry; LAMP1 and LAMP2, Lysosomal-Associated Membrane Protein 1, and 2 respectively; TT, Transient Transfection; M, microinjection; M6PRs, mannose 6-phosphate receptors; Mm, *Mus musculus* (Mouse); PDI, protein disulphide isomerase; RFC, Reduced Folate Carrier; RhoB, Ras homolog gene family, member B; S, Stable cell line; Sp, *Strongylocentrotus purpuratus* (Sea urchin); TfR, Transferrin Receptor; XLO, *Xenopus laevis* (African clawed frog) oocytes.

Table 4.1: Summary of the reported TPCs localization. *(Continued)*

Method	Species	TPC	Tag	Expression system	**Markers**/Organelles	co-localization	References
M	Hs	2	GFP	XLO	**Lysotracker**/Acidic stores	Substantial	[217]
M	Hs	2	mRFP	XLO	**RFC**/Plasma membrane	No	[39]
TT	Hs	2	GFP	SKBR3	**LAMP1**/Late endosomes & lysosomes	Full	[39]
TT	Hs	2	GFP	SKBR3	**KDEL**/ER	No	[39]
TT	Hs	2	mRFP	SKBR3	**Endo**/Early & late endosomes	No	[39]
TT	Hs	2	mRFP	SKBR3	**RFC**/Plasma membrane	No	[42]
S+I	Hs	2	HA	HEK293	**LAMP2**/Late endosomes & lysosomes	Full	[52]
S+I	Hs	2	HA	HEK293	**Lysotracker**/Acidic stores	Substaintial	[52]
S+I	Hs	2	HA	HEK293	**EEA1**/Early endosomes	No	[52]
S+I	Hs	2	HA	HEK293	**M6PR**/Late endosomes	Little	[52]
S+I	Hs	2	HA	HEK293	**PDI**/ER	No	[52]
S+I	Hs	2	HA	HEK293	**GM130**/Golgi apparatus	No	[52]
S+I	Hs	2	HA	HEK293	**CytC**/Mitochondria	No	[52]
E+I	Hs	2	-	HEK293	**LAMP2**/Late endosomes & lysosomes	Full	[52]
TT	At	1	GFP	AMP	Vacuoles (plant lysosomes)	-	[219]
S+I	Gg	3	GFP	HEK293	**LAMP2**/Late endosomes & lysosomes	Partial	[52]
S+I	Gg	3	GFP	HEK293	**M6PR**/Late endosomes	Partial	[52]
TT+I	Mm	1	EGFP	HEK293	Plasma membrane & nuclei	-	[307]
S+I	Mm	2	HA	HEK293	**LAMP1**/Late endosomes & lysosomes	Full	[52]
S+I	Mm	2	HA	HEK293	**LAMP2**/Late endosomes & lysosomes	Full	[52]
S+I	Mm	2	HA	HEK293	**Lysotracker**/Acidic stores	Substantial	[52]
TT+I	Mm	2	EGFP	HEK293	Plasma membrane & nuclei	No	[307]
TT+I	Mm	2	-	COS-7	Plasma membrane	No	[307]
TT+I	Mm	2	-	COS-7	**Calnexin**/ER	Full	[307]
TT+I	Mm	2	-	COS-7	**LAMP1**/Late endosomes & lysosomes	Full	[307]
TT+I	Mm	2	-	COS-7	**Mitotracker**/Mitochondria	No	[307]

Although a study has shown that in mouse, similarly to other species, TPC1 localizes intracellularly [307], the study did not identify specific organelle compartments. From localization studies in human and sea urchin TPC1, it is assumed that mouse TPC1 is localized to acidic stores, specifically the endosomes (and other unidentified compartments) [39, 41, 52]. The localization for mouse TPC2 is better characterized; it is now know that it localizes specifically to late endosomes/lysosomes [52, 307]. This raises an interesting question as to what governs the targeting of these proteins to their required destinations.

Many lysosomal membrane proteins, such as LAP (Lysosomal acid phosphatase) [204], LAMP1 (Lysosomal-Associated Membrane Protein 1) [204] and TRPML [236], are known

to be sorted to late endosomes/lysosomes by two major pathways: the direct pathway, which involves trafficking of the newly synthesized proteins from the trans-Golgi network (TGN) directly to late endosomes/lysosomes; and the indirect pathway, in which the newly synthesized proteins are first transferred from the TGN to the plasma membrane. The protein is then subsequently internalized and delivered to late endosomes/lysosomes by the endocytic pathway [204, 236].

The pathway that proteins employ depends on their sorting signals: short amino acid sequences on the cytosolic domains. Specific proteins or protein domains (Table 4.2) recognize these signals and mediate the different transportation events, such as internalization, lysosomal targeting, basolateral targeting and TGN-to-endosomes sorting, to transport the target proteins to their ultimate destination.

There are two major types of sorting signals that are responsible for sorting of transmembrane proteins to endo-lysosomes: tyrosine-based and dileucine-based (Table 4.2). Their names reflect the critical residues on the consensus motifs. Tyrosine-based sorting signals contain YXXϕ or NPXY consensus motifs, and dileucine-based sorting signals contain [DE]XXXL[LI] or DXXLL consensus motifs (X represents any amino acid, and ϕ represents an amino acid residue that has a bulky hydrophobic side chain).

Signal type	**Putative recognition proteins or protein domains**	**Events**
NPXY	Clathrin terminal domain, μ2 subunit of AP-2, PTB domain of Dab2	Internalization
YXXϕ	μ subunits of AP complexes	Internalization, lysosomal targeting, basolateral targeting
[DE]XXXL[LI]	μ and/or β subunits of AP complexes	Internalization, lysosomal targeting, basolateral targeting
DXXLL	VHS domain of the GGAs	TGN-to-endosomes sorting

Table 4.2: Proposed recognition proteins or protein domains and functions of the endosomal/lysosomal sorting signals. Amino acid residues are denoted by their single letter code. X denotes for any amino acid residue and ϕ denotes for an amino acid residue that contains a bulky hydrophobic side chain. Abbreviations: AP, adaptor protein; Dab2, disabled-2; GGAs, Golgi-localized, γ-ear-containing, ARF-binding proteins; PTB, phosphotyrosine-binding; TGN, trans-Golgi network; VHS domain present in Vps27p, Hrs, Stam. Table is adapted from [38].

Many well-known proteins in the endo-lysosomal system possess YXXϕ motifs, including lysosomal membrane proteins such as LAMP1 and LAMP2, endocytic receptors such as the transferrin receptor, and intracellular sorting receptors such as the mannose 6-phosphate receptors (M6PRs) [38]. Similarly, many transmembrane proteins that localize to late endosomes/lysosomes possess the [DE]XXXL[LI] motifs [38], for example, NPC1 (Niemann-Pick disease, type C1) and LIMP-II (Lysosome membrane protein II). Additionally, some transmembrane proteins in the other specialized compartments of the endo-lysosomal system also possess the [DE]XXXL[LI] motifs such as GLUT4 (Glucose transporter type 4) in stimulus-responsive storage vesicles, and tyrosinase in premelanosomes and melanosomes [38].

Combinations of the motifs leads to multiple transport events (Table 4.2). Additionally, residues that flank the motif and the position of the motif within the cytosolic domains can further fine-tune the strength and specificity of the signals. For most of the YXXϕ motifs that target lysosomes, the motifs tend to have the following features: a glycine (G) before the tyrosine residue, acidic residues (D or E) at the X positions. They are located at the C-terminus and 6–9 residues downstream from the final transmembrane domain. For the [DE]XXXL[LI] motifs, an acidic or serine (S) residue prior to the motif tends to further strengthen the signal. In addition, where the [DE]XXXL[LI] motif is involved in the lysosomal targeting then its position tends to be very near the transmembrane domain (6–11 residues) or at the N- or C-termini [38]. Knowing the importance of the sorting motifs, this chapter will investigate the role of these sorting motifs in mouse TPCs in directing trafficking to the correct destination.

In summary, in many systems, TPCs have been shown to localize intracellularly in the acidic stores — distinct from the ER. However, limited information on the subcellular localization of mouse TPC1 and the discrepancy between reports concerning mouse TPC2 localization prompted the investigation of subcellular localization of mouse TPCs in a mouse cell line. Additionally, lysosomal sorting signals of mouse TPCs have not been studied in detail before. The second part of this chapter reports the investigation of mouse TPC sorting signals. Furthermore, an endogenous truncated TPC1 isoform was identified (Chapter 3), however, it is still not known whether ΔN-TPC1 is just a futile mRNA or it could be translated into a protein. The last part of this chapter addresses this

question, and if it does, the localization of ΔN-TPC1 will be investigated. Additionally, it would be interesting to identify any lysosomal-targeting sorting signals that are absent in the truncated fragment of ΔN-TPC1. If so, how does the loss affect the localization of ΔN-TPC1 compared with FL-TPC1?

As shown in Chapter 3, FL-TPC1, ΔN-TPC1, and TPC2 were all expressed in a broad range of tissue types. This suggests that they may have fundamentally important physiological roles. As TPCs are co-expressed in various tissue types, it is difficult to elucidate the roles of individual TPCs. Thus, by examining the localization profiles of TPCs at a subcellular level, this would hopefully give further insights into the roles of individual TPCs.

4.2 Results

4.2.1 Localization of mouse TPCs

4.2.1.1 Generation and validation of the mouse TPC vectors

While several studies have revealed the localization of mouse TPC2 to be late endosomes/ lysosomes, information on mouse TPC1 localization is limited. Although it is known that it localizes intracellularly, the specific organelle(s) are largely unknown (Table 4.1). Studies on human TPC1 suggest a broad distribution of localization: not only late endosomes/lysosomes but also early and recycling endosomes [39, 52].

In the absence of specific mouse TPC antibodies to detect endogenous TPCs in immunocytochemistry, mCherry-tagged mouse TPC vectors were constructed (Section 2.4.2). TPC1 or TPC2 cDNAs were cloned and fused to mCherry sequence in a mammalian expression vector (pcDNA5/TO, which contains the SV-40 promoter). To validate the recombinant vectors (pcDNA5/TO.TPC.mCherry), the vectors were overexpressed in Human Embryonic Kidney 293 T (HEK293T) cells. The HEK293T cell line stably expresses the large T-antigen; together with the SV-40 promoter this allows episomal replication of the vector DNA. Analysis of the vectors was achieved by western blotting using the membranes of HEK293T cells that had been transfected with the recombinant vectors, and with an antibody against mCherry (α-multi-red (5F8)).

Figure 4.1 shows that two bands were detected for membranes overexpressing TPC1- or TPC2-mCherry in western blotting. The upper bands (black arrows) are likely to represent the fully-glycosylated TPC proteins whereas the lower bands (orange arrows) are likely to represent the core-glycosylated protein [307]. Thus, the differences observed in the bands are possibly due to different degrees of glycosylation.

In membranes from cells overexpressing mouse TPC1-mCherry, the lower band reflects protein at the predicted size of 121 kDa for TPC1-mCherry. In TPC2-mCherry membranes, the lower band was at a much smaller size than the predicted ($\sim$80, compared to 110 kDa). This is consistent with the previous finding of a band lower than the predicted size in western blotting [307].

Western blotting demonstrated that mCherry-tagged TPC proteins can be successfully expressed in mammalian cells that had been transfected with the recombinant vectors

carrying TPC-mCherry cDNA. The proteins expressed also appeared to be stable as the sharp bands suggest little degradation. They were thus considered suitable for localization studies.

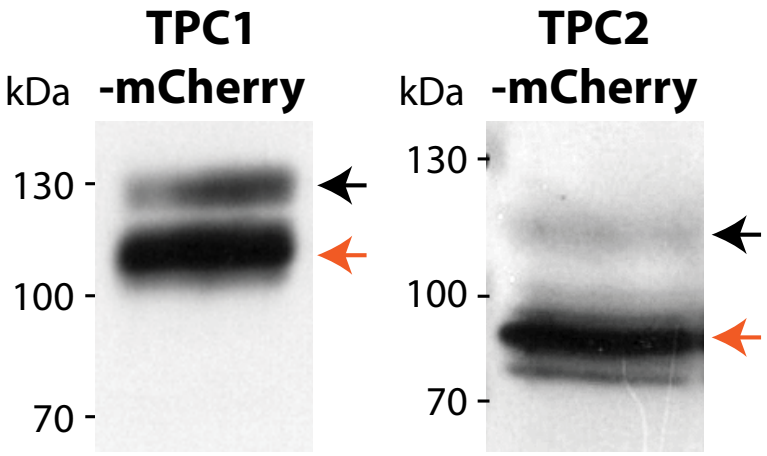

Figure 4.1: Expression vectors pcDNA5/TO.TPC1.mCherry and pcDNA5/TO.TPC2.mCherry produced stable TPC1-mCherry and TPC2-mCherry proteins, respectively, when transiently transfected in HEK293T cells. Western blotting of 25 μg membranes from HEK293T cells transiently transfected with pcDNA5/TO.TPC1.mCherry (10 μg, left) and pcDNA5/TO.TPC2.mCherry (10 μg, right) produced two bands in either membranes when probed with α-multi-red (5F8). The upper (black arrows) and the lower bands (orange arrows) are likely to represent the fully- and the core-glycosylated proteins, respectively [307]. The lower band detected in the TPC1-mCherry membranes was of the expected size of TPC1-mCherry (121 kDa). In line with the previous finding [307], a much lower band (~80 kDa) was detected in the TPC2-mCherry membranes than the predicted size of TPC2-mCherry (110 kDa).

4.2.1.2 Mouse TPC1 localization

To study the subcellular localization of mouse TPC1, mCherry-tagged mouse TPC1 was overexpressed in mouse embryonic fibroblasts (MEF) to enable the intracellular tracking. MEF cells were chosen because they have a larger cytosol to nucleus ratio, allowing organelles to be distinguished more easily. More importantly, the use of MEF cells circumvents potential artefacts that can arise from heterologous TPC expression, as the native machinery directs proteins to the correct locations.

Localization was investigated by comparing the extent of overlapping fluorescence emission from mCherry-tagged TPC1 (red) and GFP-tagged organelle markers (green) co-transfected in MEF cells. Four GFP-tagged organelle markers were used to examine the localization of TPC1 in different compartments of the endo-lysosomal system: Lysosomal-associated membrane protein 1 (LAMP1) for late endosomes/lysosomes, transferrin receptor (TfR) for recycling endosomes and subdomains of endosomes, KDEL retention motif (KDEL) for endoplasmic reticulum (ER), and Early Endosome Antigen 1 (EEA1) for early endosomes.

Figure 4.2 shows representative images for each co-transfection; from these, Pearson's coefficients were calculated for each cell. Analyses of images showed that TPC1 highly co-localized with LAMP1 and TfR (Pearson's coefficient = 0.75 ± 0.02 and 0.71 ± 0.03, respectively), and to a lesser degree with EEA1 and KDEL (Pearson's coefficient = 0.44 ± 0.02 and 0.44 ± 0.05, respectively). This indicates that mouse TPC1 localizes predominantly in late endosomes/lysosomes, and recycling endosomes and subdomains of endosomes, but not in early endosomes, or the ER.

Since TfR identifies both recycling endosomes and subdomains of endosomes, MEF cells that had been transfected with TPC1-mCherry were stained with filipin to distinguish these two compartments. Filipin is a fluorescent antibiotic that binds specifically to the highly enriched cholesterol in recycling endosomes [117]. Figure 4.2 shows that TPC1-mCherry overlapped with filipin minimally (Pearson's coefficient = 0.34 ± 0.03), suggesting that TPC1 is not localized in recycling endosomes. Thus, TPC1 is more likely to be localized in the subdomains of endosomes.

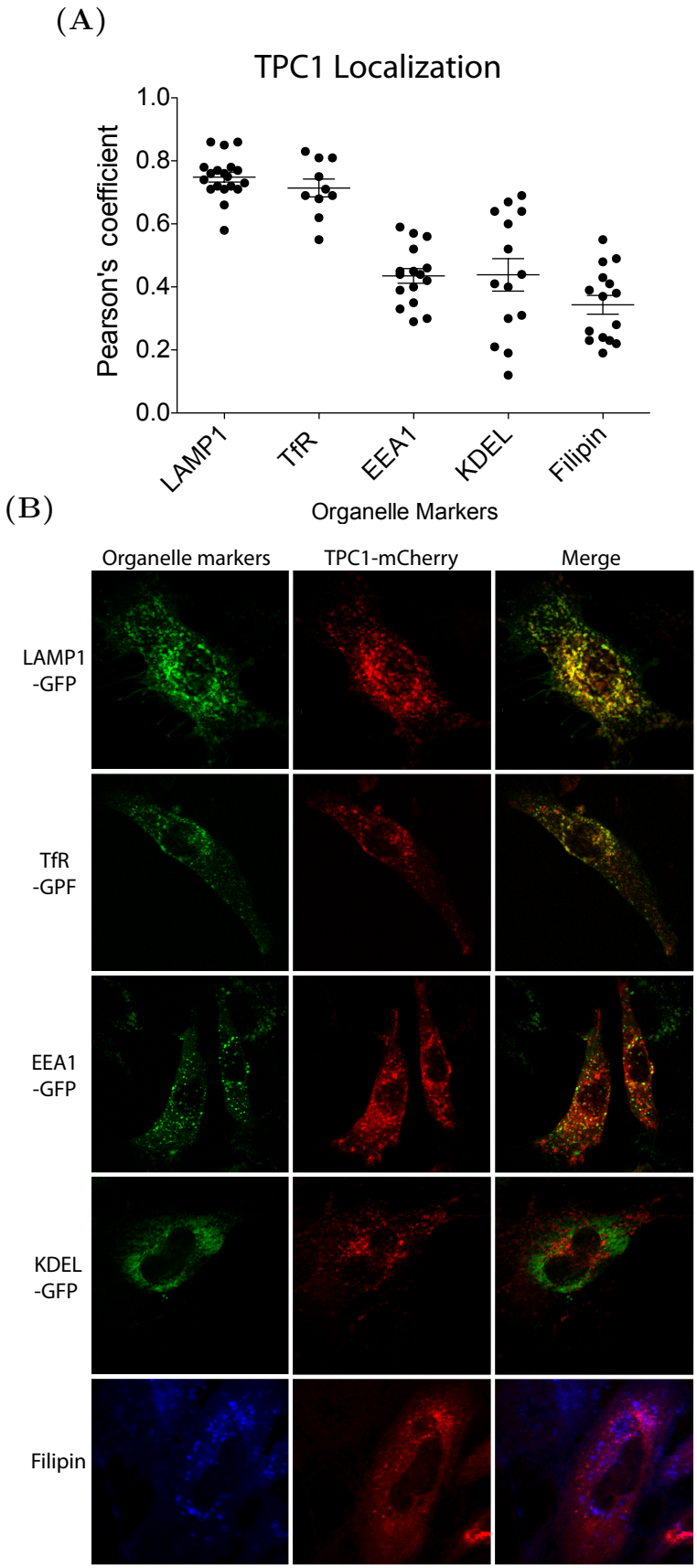

Figure 4.2: (A) The extent of co-localization as measured by Pearson's coefficient of TPC1-mCherry with LAMP1-GFP, TfR-GFP, EEA1-GFP, KDEL-GFP, or filipin in fixed MEF cells. Each cell (n) is indicated by a black dot, n = 10-19. (B) Representative images of organelle markers (left), TPC1-mCherry (centre) and merged images of the organelle markers and TPC1-mCherry (right).

4.2.1.3 Mouse TPC2 localization

To examine the subcellular localization of mouse TPC2, fluorescent emission from mCherry-tagged TPC2 (red) was compared with GFP-tagged organelle markers (green; LAMP1, TfR, KDEL, and EEA1) co-transfected in MEF cells.

Figure 4.3 shows representative images for each co-transfection; from these, Pearson's coefficients were calculated for each cell. Like mouse TPC1, mouse TPC2 overlapped predominantly with LAMP1 (Pearson's coefficient = 0.75 ± 0.02). However, mouse TPC2 showed minimal degree of overlap with TfR, EEA1 or KDEL (Pearson's coefficient = 0.45 ± 0.02, 0.48 ± 0.02, and 0.49 ± 0.04, respectively). This indicates that mouse TPC2 primarily localizes in late endosomes/lysosomes, but not in early or recycling endosomes, or the ER. Filipin staining was not required for TPC2 as there was minimal overlap with TfR.

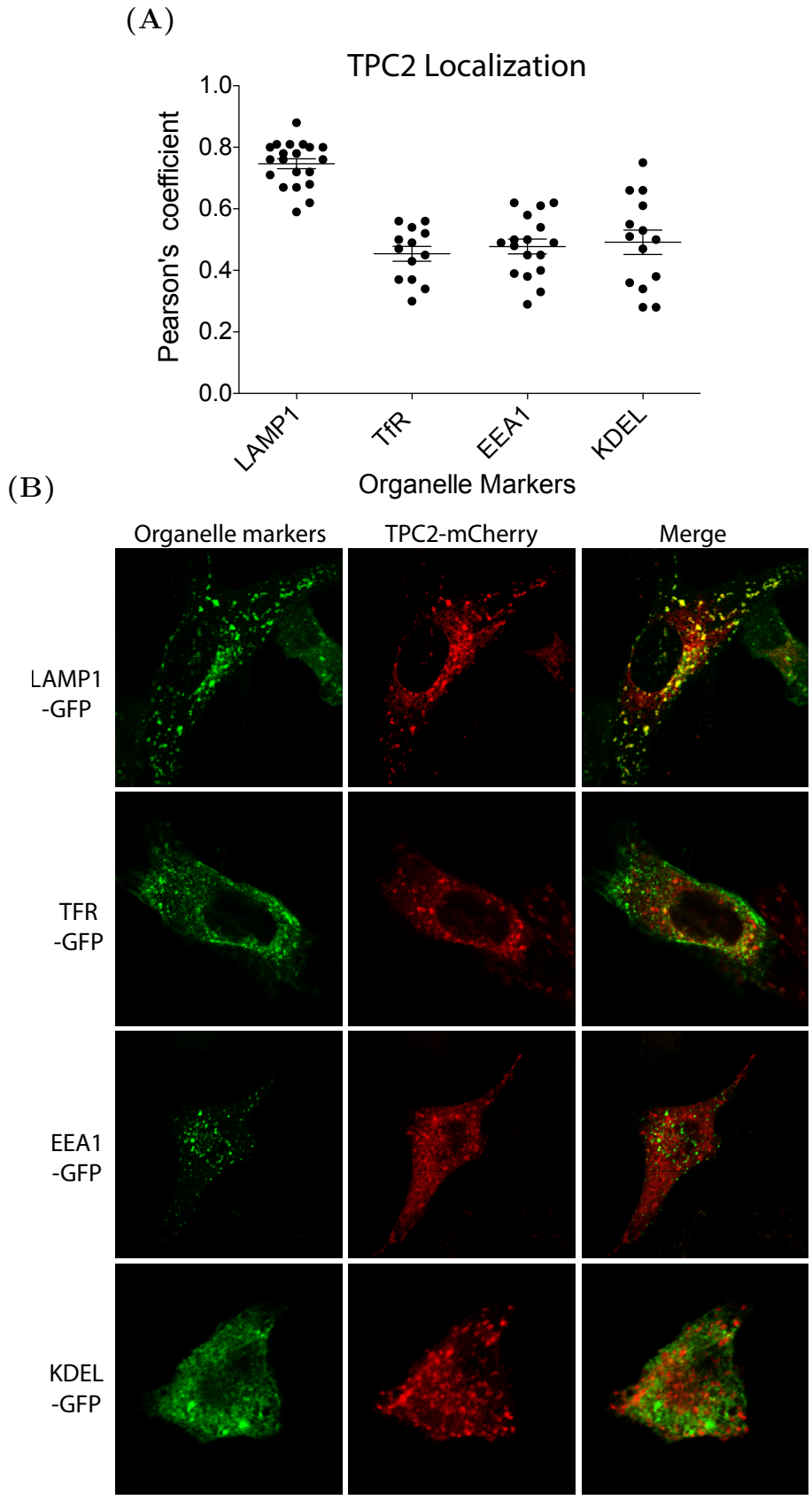

Figure 4.3: (A) The extent of co-localization as measured by Pearson's coefficient of TPC2-mCherry with LAMP1-GFP or TfR-GFP, EEA1-GFP, or KDEL-GFP in fixed MEF cells. Each cell (n) is indicated by a black dot, n = 13-20. (B) Representative images of organelle markers (left), TPC2-mCherry (centre) and merged images of the organelle markers and TPC2-mCherry (right).

4.2.2 Sorting signals of TPCs

4.2.2.1 Searching sorting signals in TPCs

Having established that mouse TPC1 localizes primarily to late endosomes/lysosomes and some unidentified subdomains of endosomes (but not early or recycling), while TPC2 localizes predominantly to late endosomes/lysosomes, the important question arises as to which sorting signals are involved in directing TPCs to their required destinations, resulting in NAADP-evoked spatially organized Ca^{2+} signals.

To understand the sorting signals, the amino acid sequences of mouse TPCs were first examined. There are two main types of endosomal/lysosomal sorting signals: dileucine-based, and tyrosine-based. Dileucine-based motifs are [DE]XXXL[LI] or DXXLL, and tyrosine-based motifs are YXXϕ or NPXY [38]. The results of searches for these four particular motifs in mouse TPC1 and TPC2 amino acid sequence are summarized in Table 4.3.

4.2.2.2 Mapping sorting signals in TPCs

Although a particular motif is detected in the sequence, its position relative to the transmembrane domains, and to the N- or C-termini also affects its functions. Specifically, proteins that are targeted to late endosomes/lysosomes tend to have the [DE]XXXL[LI] motif 6–11 amino acid residues from the transmembrane domain, or very near the N- or C-termini. In order to examine the relative position of the predicted sorting signals to the transmembrane domains of mouse TPCs, the positions of the mouse TPC transmembrane domains were first predicted based on comparison to rat TPC1 [127].

Alignment of mouse TPCs against rat TPC1 protein sequence in Figure 4.4 showed that mouse TPC1 shared ∼96% sequence identity with rat TPC1, and ∼19% with mouse TPC2. Due to the low homology of mouse TPC2 with TPC1, it is not clear whether the putative transmembrane regions of mouse TPC2 can be predicted accurately from the rat TPC1 sequence. Consequently, mouse TPCs and rat TPC1 were further aligned with the putative transmembrane regions of the voltage-gated Ca^{2+} and Na^{+} channels [127]. Figure 4.5 shows that many of the residues conserved in the transmembrane domains of voltage-gated Ca^{2+} and Na^{+} channels, mouse TPC1, and rat TPC1 were also similar,

	Mouse TPC1		Mouse TPC2	
Sorting signal	Position	Amino acid sequence	Position	Amino acid sequence
[DE]XXXL[LI]	7 - 12	**DdvpLI**	4 - 9	EeqpLL
	235 - 240	DillLL	113 - 118	EafcLL
	737 - 742	DvtrLL		
DXXLL	235 - 239	DilLL	440 - 444	DsdLL
YXXϕ	101 - 104	YlfV	43 - 46	YrsI
	304 - 307	YlsI	47 - 50	YhrM
	310 - 313	YfiM	62 - 65	YsnV
	347 - 350	YglL	145 - 148	YfmV
	361 - 364	YrqF	296 - 299	YnqF
	449 - 452	YlvV	322 - 325	YevL
	480 - 483	YlvF	458 - 461	YifI
	534 - 537	YfiV	463 - 466	YylL
	554 - 557	YrnV	519 - 522	YgpL
	579 - 582	YysF	574 - 577	YyvF
	608 - 611	YrfI	656 - 659	YfvL
	625 - 628	YyyL		
	651 - 654	YiiM		
NPXY	-		-	

Table 4.3: Predicted dileucine-based ([DE]XXXL[LI] and DXXLL) and tyrosine-based (YXXϕ and NPXY) sorting signals in the mouse TPC1 and TPC2 amino acid sequences (ExPasy proteomics). The motif in bold is missing from ΔN-TPC1. Amino acid residues are denoted by their single letter code. X denotes any amino acid residue, and ϕ denotes an amino acid residue that contains a bulky hydrophobic side chain. Capital letters refer to the critical residues on the consensus motifs and small letters refer to non-critical residues.

if not, conserved, in mouse TPC2 [127]. This indicates that the putative positions of transmembrane domains in mouse TPC2 could be predicted based on the positions in rat TPC1.

Once positions of the predicted transmembrane domains in mouse TPCs were identified, the positions of the sorting signals in mouse TPCs were then re-examined in relation to the transmembrane domains (Figure 4.4). This revealed that the [DE]XXXL[LI] motifs could be important in directing both TPC1 and TPC2 to endo-lysosomes, as both TPCs possess the [DE]XXXL[LI] motifs near their N- or C-termini, like many late endosomal and lysosomal proteins.

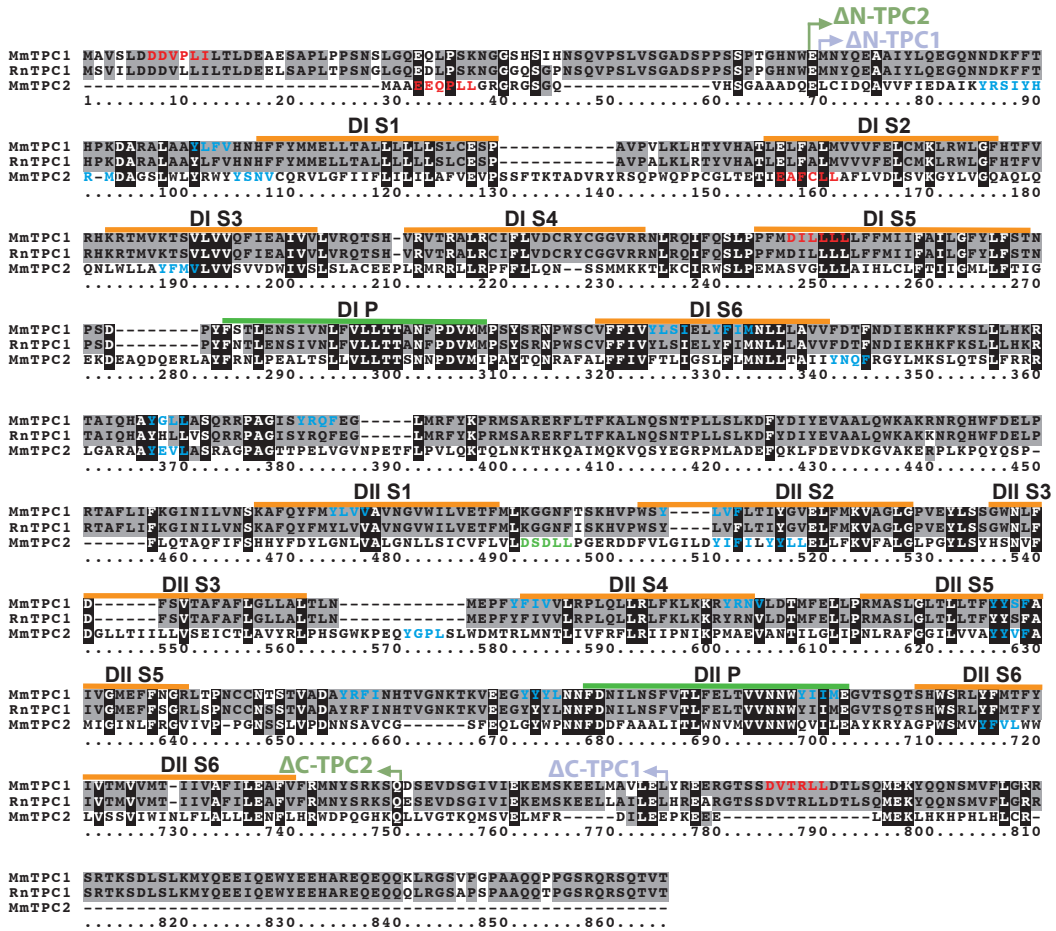

Figure 4.4: Amino acid sequence alignment of mouse TPC1 (AAH58951), TPC2 (AAI41196) and rat TPC1 (AAH62072) using Clustal W2 (http://www.ebi.ac.uk/Tools/msa/clustalw2/). Dileucine-based [DE]XXXL[LI] and DXXLL motifs are coloured in red and green letters, respectively. Tyrosine-based YXXϕ motifs are indicated in blue letters. Orange bars represent putative transmembrane domains I (DI) or II (DII) and segment (S) 1–6. Green bars represent the pore loops (P). The arrows indicate the first amino acid residue of the N-terminal truncated protein (ΔN) and the last amino acid residue of the C-terminal truncated protein (ΔC). Black background indicates conserved residues and the grey background indicate residues, which are the same but not conserved.

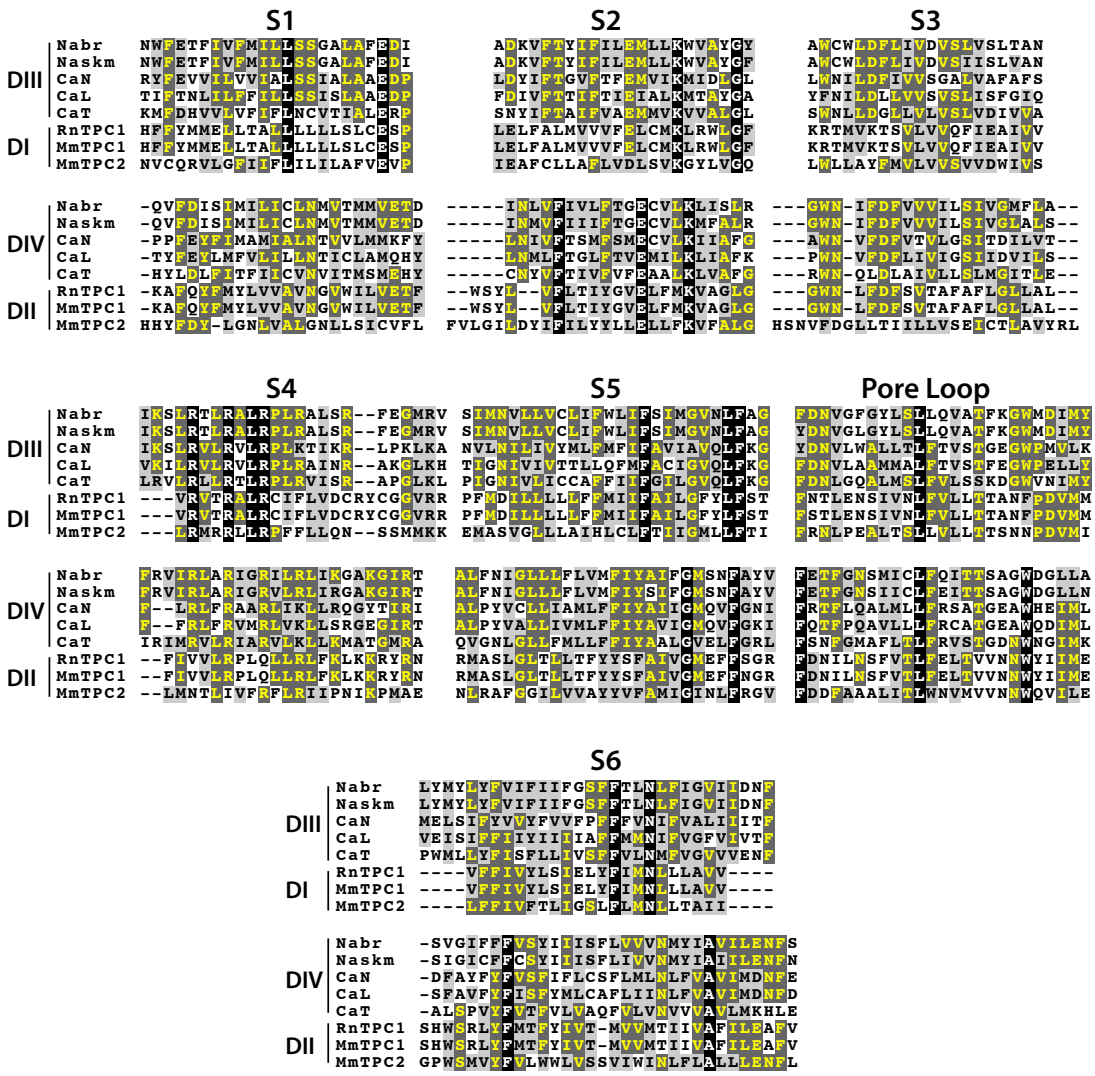

Figure 4.5: Sequence alignment of putative segments (S) 1–6 of the transmembrane domains III (DIII) and IV (DIV) in rat brain sodium channel (Nabr; X03638.1), rat skeletal sodium channel alpha subunit (Naskm; M26643.1), human N-type calcium channel alpha-1 subunit (CaN; M94172.1), human L-type calcium channel alpha-1 subunit (CaL; L04569.1), human T-type calcium channel alpha-1H subunit (CaT; AF051946.3), and S1–6 of the transmembrane domains I (DI) and II (DII) in rat TPC1 (RnTPC1; AAH62072), mouse TPC1 (MmTPC1; AAH58951) and TPC2 (MmTPC2; AAI41196). Alignment was based on the study by Ishibashi *et al.* [127]. Black background indicates conserved residues, dark grey background (with yellow letters) indicates residues which are the same but not conserved, and the light grey background (with black letters) indicate similar residues.

TPC1. Mouse TPC1 has three [DE]XXXL[LI] motifs (red letters in Figure 4.4): the two at the N- and C- termini are likely to be involved in sorting, whereas the third is in the transmembrane domain I segment 5 (DIS5), and is thus unlikely to be involved. Interestingly, there is an acidic D residue prior to the N-terminal motif (DDVPLI) and a serine (S) residue prior to the C-terminal motif (DVTRLL), which may increase the strength of the signal [38]. The presence of the serine residue also raises the possibility of the protein being regulated by serine phosphorylation-dependent internalization (for the subsequent transportation of the protein to lysosomes). The motif (**S**DKQTLL) on CD3-γ has been reported to be involved in serine phosphorylation-dependent internalization of the T-cell antigen receptor (from the cell surface for lysosomal degradation) [38].

In Chapter 3, a native variant of TPC1 mRNA was identified. It is named ΔN-TPC1 because translation of this mRNA predicts a protein of 69-amino acid truncation on the N-terminus relative to FL-TPC1 (purple arrow in Figure 4.4 indicates the start position of ΔN-TPC1). This truncation effectively removes a potential [DE]XXXL[LI] motif (DDVPLI) from the N-terminal as shown in Figure 4.6. The implications of this for ΔN-TPC1 localization will be considered later in this chapter.

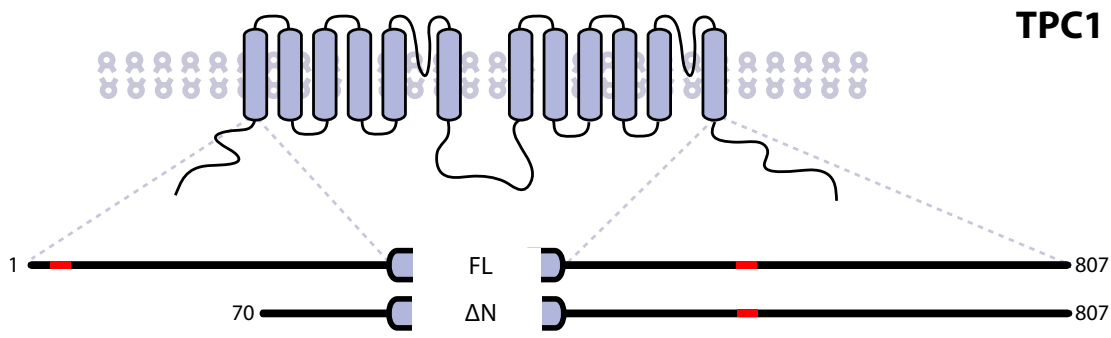

Figure 4.6: Illustration of the terminal [DE]XXXL[LI] motifs (red blocks) in mouse FL-TPC1 and ΔN-TPC1.

Most DXXLL motifs are known to be positioned near the C-terminus, and to mediate its function [38]. Mouse TPC1 has one DXXLL motif, however, it was not positioned near the C-terminus. The DXXLL motif in mouse TPC1 overlaps the [DE]XXXL[LI] motif in the D1S5 (Figure 4.4), so it seems unlikely for this predicted DXXLL motif to play a role in sorting.

Although 13 YXXϕ-type tyrosine motifs were found in TPC1 (blue letters in Figure 4.4),

many were positioned on the putative transmembrane domains, and none were located 6–9 residues from the transmembrane domain, or at the C-terminus. Thus, from analysis of sorting signals position within the protein, it seems that the [DE]XXXL[LI] motifs are the dominant (if not sole) players in directing TPC1 to its final destination.

TPC2. In mouse TPC2, two [DE]XXXL[LI] motifs were found, one at the N-terminal, and the other in segment 2 of transmembrane domain I (DIS2) (red letters in Figure 4.4). However, no signal strengthening residue such as the acidic or serine residue was found prior to the motif. Given the known characteristics of the [DE]XXXL[LI] motifs for lysosomal targeting, it appears that the N-terminal motif is likely to be involved in sorting, whereas the putative motif in DIS2 is non-functional (Figure 4.7).

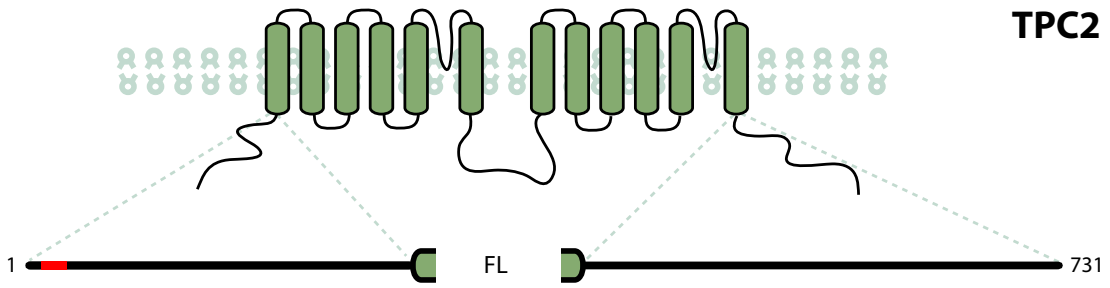

Figure 4.7: Illustration of the terminal [DE]XXXL[LI] motif (red block) in mouse FL-TPC2.

Similar to mouse TPC1, mouse TPC2 has one DXXLL motif; it is not located near the C-terminus, but between DIIS1 and DIIS2 (green letters in Figure 4.4). Therefore, it also seems unlikely that this predicted DXXLL motif in TPC2 plays a role in targeting. Furthermore, there were 11 YXXϕ-type tyrosine motifs identified in TPC2 (blue letters in Figure 4.4); however, many were also positioned on putative transmembrane domains (similar to TPC1). None of the YXXϕ-type tyrosine motifs was located at 6–9 residues from the transmembrane domain, or at the C-terminus.

Overall, like mouse TPC1, it seems that the [DE]XXXL[LI] motifs is the principal element directing TPC2 to its final destination.

4.2.3 Significance of [DE]XXXL[LI] motifs in TPCs

Mapping of the established endo-lysosomal sorting signals in TPCs in relation to structural units has suggested an essential role for the [DE]XXXL[LI] motifs in directing TPCs to lysosomes.

To examine the role of the [DE]XXXL[LI] motifs in a protein to mediate successful sorting, the number and the positions of the motifs are now reviewed. Both TPCs have potential terminal [DE]XXXL[LI] motifs for lysosomal targeting. TPC1 has two, one at each terminus, whereas TPC2 has only a C-terminal motif. Furthermore, predicted translation of ΔN-TPC1 protein revealed that it lacks the N-terminal [DE]XXXL[LI] motif. This immediately raises two questions: are the [DE]XXXL[LI] motifs at the termini crucial in directing TPCs to lysosomes as predicted, and, if so, are both TPC1 motifs required for successful transport to lysosomes? Answering the latter question also helps to know whether the presence of the only C-terminal [DE]XXXL[LI] motif would enable ΔN-TPC1 to be successfully transported to lysosomes.

4.2.3.1 Generation of the truncated mouse TPC vectors

TPC1. To address these questions, TPC1 cDNAs with truncations of either the N-terminus, the C-terminus, or both were generated by PCR using primers designed to exclude the terminal [DE]XXXL[LI] motifs (Section 2.4.2, Figure 4.4). TPC1 with truncated N-terminus, C-terminus, or both termini will be referred to as ΔN-TPC1, ΔC-TPC1, or ΔNC-TPC1, respectively (Figure 4.8).

Since the alternative TPC1 protein has a truncation of the N-terminus that eliminates the [DE]XXXL[LI] motif, the N-terminal truncation of TPC1 (ΔN-TPC1) was generated to match the shorter variant of endogenous TPC1. As there is no commercially available cDNA clone for ΔN-TPC1 (unlike the I.M.A.G.E. clone for FL-TPC1; Section 2.1.2), ΔN-TPC1 cDNA was cloned from mouse kidney total RNA (Section 2.4.1).

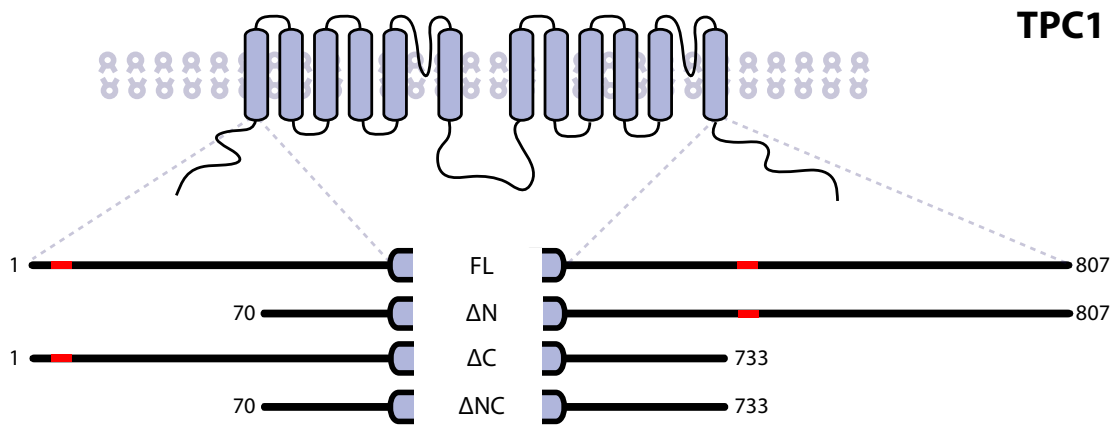

Figure 4.8: Truncations of mouse TPC1 to remove the terminal [DE]XXXL[LI] motifs. The longer variant of endogenous TPC1 is designated the full-length (FL). Truncations of the N-terminus (equivalent of the shorter variant of endogenous TPC1), the C-terminus, or both termini are designated ΔN, ΔC, or ΔNC, respectively. The [DE]XXXL[LI] motifs are indicated by red blocks.

TPC2. TPC2 cDNAs with truncations of the N- or C-terminus were similarly generated (Section 2.4.2). Figure 4.4 shows the truncated regions of the termini. TPC2 with truncations on the N- or C-terminus will be referred to as ΔN-TPC2, and ΔC-TPC2, respectively (Figure 4.9). Although there is no [DE]XXXL[LI] motif on the C-terminus of mouse TPC2, a small part of the C-terminus was still truncated as a control to investigate the effect of truncation without any [DE]XXXL[LI] motif. The wild-type TPC2 (without truncation) will be referred to as the full-length TPC2 (FL-TPC2).

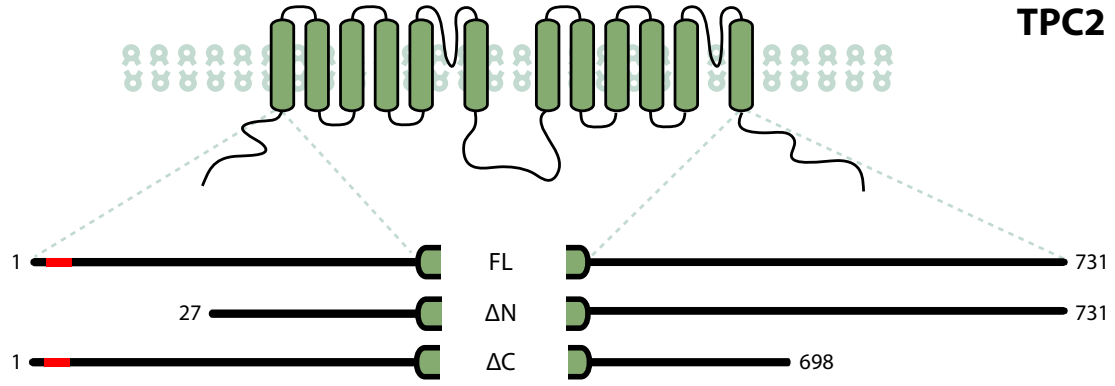

Figure 4.9: Illustration of terminal truncations in mouse TPC2 to remove the [DE]XXXL[LI] motif. The wild-type TPC2 without any truncation is designated as the full-length (FL). Truncations on the N-terminus, or the C-terminus are designated as ΔN, or ΔC, respectively. The [DE]XXXL[LI] motifs are indicated in red blocks.

4.2.3.2 Validation of the truncated mouse TPC vectors

Like FL-TPCs, truncated TPC cDNAs were inserted and fused to mCherry sequence in a mammalian expression vector (pcDNA5/TO) to allow the truncated protein to be expressed and monitored in cells. To ensure that the truncated TPC-mCherry can be expressed in a mammalian system from the recombinant vectors, membranes of HEK293T cells that had been transiently transfected with the recombinant vectors were probed by an antibody against mCherry in western blotting.

TPC1. Figure 4.10 (left) shows pairs of bands detected for membranes overexpressing ΔN-TPC1 by western blotting. Notably, the upper bands in ΔC-TPC1 and ΔNC-TPC1 were extremely faint to almost non-existent. As previously mentioned, the upper bands (black arrows) are likely to represent fully-glycosylated TPC proteins whereas the lower bands (orange arrows) are likely to represent core-glycosylated protein [307]. Thus, the differences observed in the level of the upper bands are possibly caused by different degrees of glycosylation.

In the membranes of TPC1 with single truncations, the lower band reflected proteins at the predicted sizes of 114 and 112 kDa (ΔN-TPC1-mCherry and ΔC-TPC1-mCherry, respectively). In contrast to the sharp bands observed for single truncation in TPC1 constructs, the bands detected in the ΔNC-TPC1-mCherry membranes ranged from the predicted size of ∼100 to less than 50 kDa. This suggests that protein was unstable and subject to degradation in the absence of both N- and C-termini.

TPC2. Figure 4.10 (right) shows the two bands detected for membranes overexpressing ΔC-TPC2 in western blotting. The upper band in membranes overexpressing ΔN-TPC2 was not prominent (Figure 4.10). Similarly to full-length constructs, the differences observed in the level of the upper bands are possibly the result of different degrees of glycosylation.

In line with the previous observation (Figure 4.1), smaller lower bands than the expected size of 108 and 106 kDa were detected in the ΔN- and ΔC-TPC2-mCherry membranes respectively (Figure 4.10).

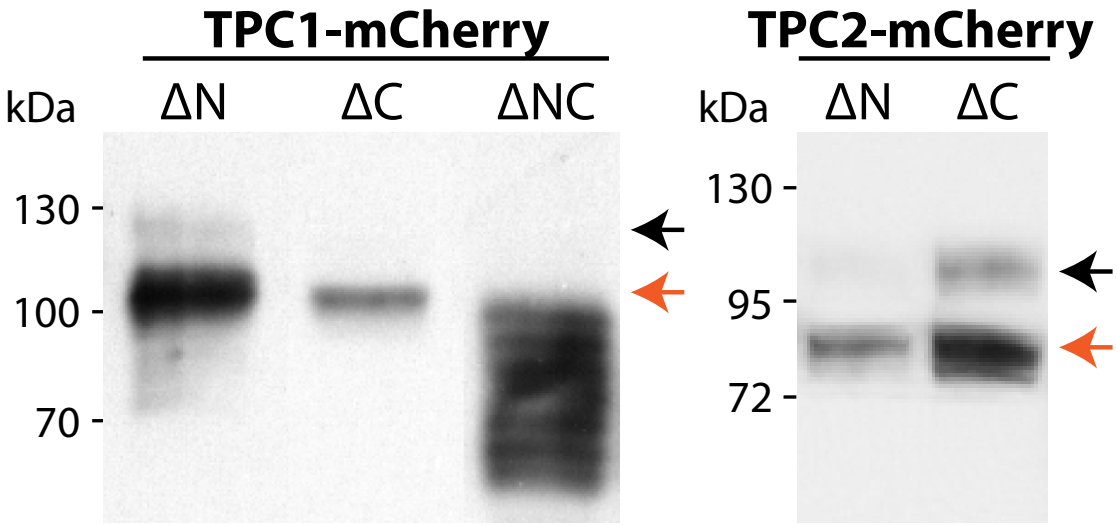

Figure 4.10: Expression vectors bearing truncated TPC-mCherry were able to produce protein when transiently transfected in HEK293T cells. Western blotting of 25 μg membranes from the HEK293T cells overexpressing truncated TPC1-mCherry (10 μg, left) and truncated TPC2-mCherry (10 μg, right) produced one or two bands in the membranes when probed with α-multi-red (5F8) antibody. Upper (black arrows) and lower (orange arrows) bands are likely to represent proteins that are fully- and core-glycosylated respectively [307]. Variation in the level of glycosylation is likely to account for the differences observed in the upper bands. The lower bands detected in the ΔN- and ΔC-TPC1-mCherry membranes were of the predicted size of 114 and 112 kDa respectively. In contrast, the bands detected in the ΔNC-TPC1 membranes ranged from the predicted size of ∼100 to less than 50 kDa, indicating protein degradation. As for full-length constructs (Figure 4.1), bands were detected at a lower apparent molecular mass (∼80 kDa) than predicted for TPC2-mCherry (108 and 106 kDa for ΔN- and ΔC-TPC2-mCherry respectively).

Western blotting demonstrates that truncated TPC-mCherry proteins can be successfully expressed in mammalian cells that had been transfected with the recombinant vectors carrying truncated TPC-mCherry cDNA. This is also the first evidence to demonstrate that the naturally-occurring short variant of TPC1 mRNA (ΔN-TPC1; AK137626) is not a futile mRNA; it could be translated into protein. Furthermore, mCherry-tagged truncated TPC proteins appeared stable only when at least one native terminus was present. Truncations in both termini of TPC1 protein resulted in unstable proteins that was highly susceptible to degradation.

4.2.3.3 Localization of the truncated mouse TPCs

To examine whether deletion of the [DE]XXXL[LI] motif(s) by terminal truncations altered the localization of TPCs specifically in late endosomes/lysosomes, mCherry-tagged truncated TPCs were co-transfected with GFP-LAMP1 in MEF cells. Typical images are shown in Figure 4.11 and 4.12.

TPC1. Deletion of the N- or C-terminal [DE]XXXL[LI] motif on TPC1 did not have a significant effect on the localization to late endosomes/lysosomes relative to FL-TPC1 (Pearson's coefficient = 0.72 ± 0.02 and 0.74 ± 0.02 in ΔN and ΔC, respectively compared to 0.75 ± 0.02 in FL-TPC1; Figure 4.11 and 4.13). This suggests that one [DE]XXXL[LI] motif (on either N- or C-terminus) was sufficient to direct mouse TPC1 to late endosomes/lysosomes.

Co-localization with LAMP1 decreased significantly when both N- and C-terminal [DE]XXXL[LI] motifs were deleted (ΔNC-TPC1; Pearson's coefficient = 0.54 ± 0.02, Figure 4.11 and 4.13). However, western blotting of the ΔNC-TPC1-mCherry membranes showed that truncations at both termini had a detrimental effect on the integrity of the protein. The protein with truncations on both termini appeared to be severely degraded compared to the full-length (Figure 4.1) or single-terminal truncations (Figure 4.10). This may partly explain the reduced co-localization.

TPC2. Surprisingly, removal of the single [DE]XXXL[LI] motif of TPC2 (from N-terminus to produce, ΔN-TPC2) did not significantly affect the overlap with LAMP1 (Pearson's coefficient = 0.75 ± 0.02 for both FL- and ΔN-TPC2, Figure 4.12 and 4.13). This was unexpected as, apart from the [DE]XXXL[LI] motif, no other significant sorting signal was found in the initial searches. It is likely that truncations of these proteins alter their stability. This hypothesis is supported by observation that truncation of the C-terminus of TPC2 (ΔC-TPC2) did not eliminate any sorting signal, but interestingly, the degree of overlapping with LAMP1 was significantly increased (Pearson's coefficient 0.85 ± 0.01, Figure 4.12 and 4.13).

It is possible that the unexpected results of these experiments were artefacts that arose from the extensive truncation rather than just elimination of the targeted signal sequences. To investigate this, an alternative approach was employed to remove the [DE]XXXL[LI] motifs.

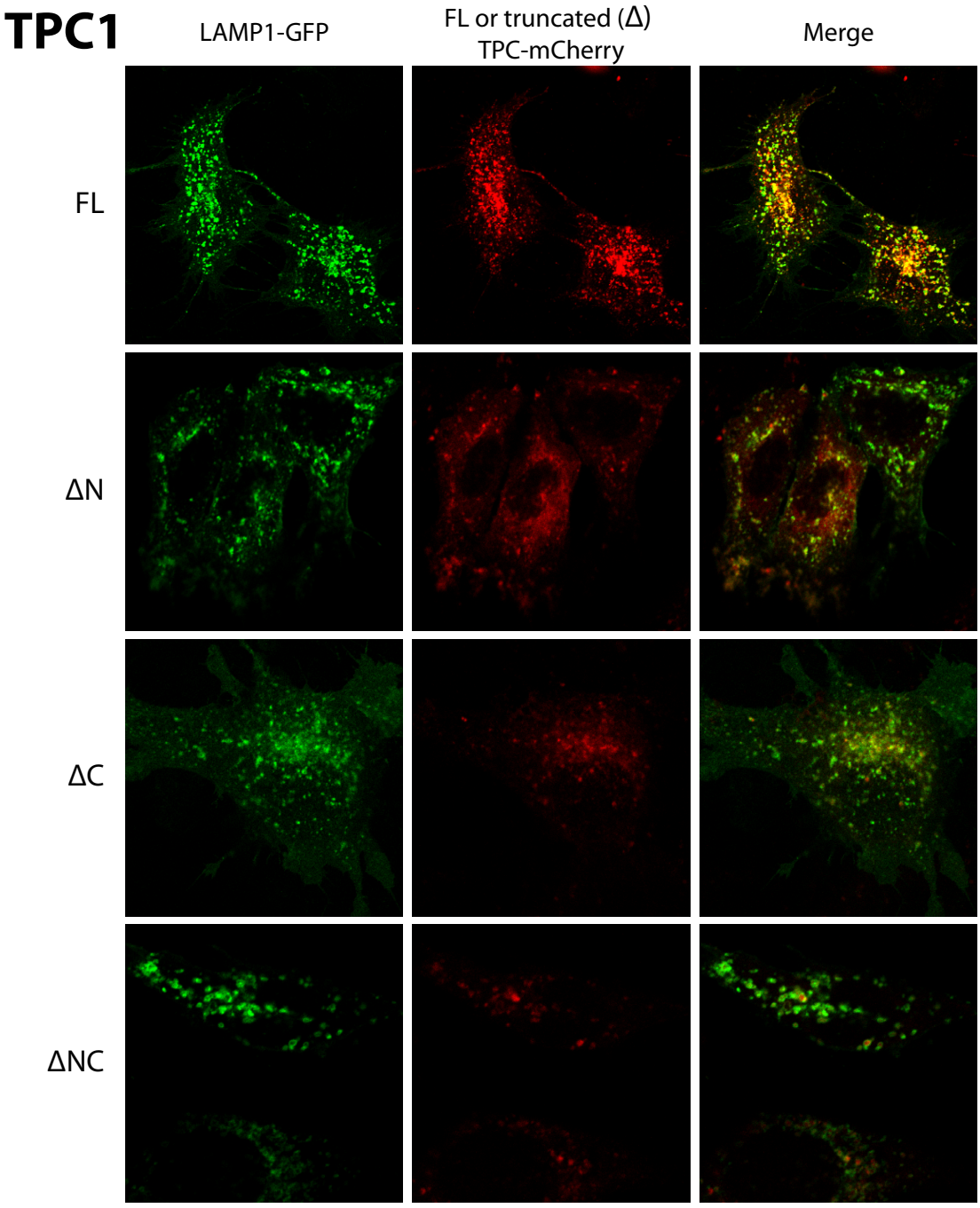

Figure 4.11: Representative images of (left) LAMP1-GFP, (centre) the full-length (FL), the truncated N- (ΔN), C- (ΔC), or both N- and C-terminal (ΔNC) TPC1-mCherry, and (right) merged images of both LAMP1-GFP and the full-length (FL), or the truncated (Δ) TPC1-mCherry in MEF cells.

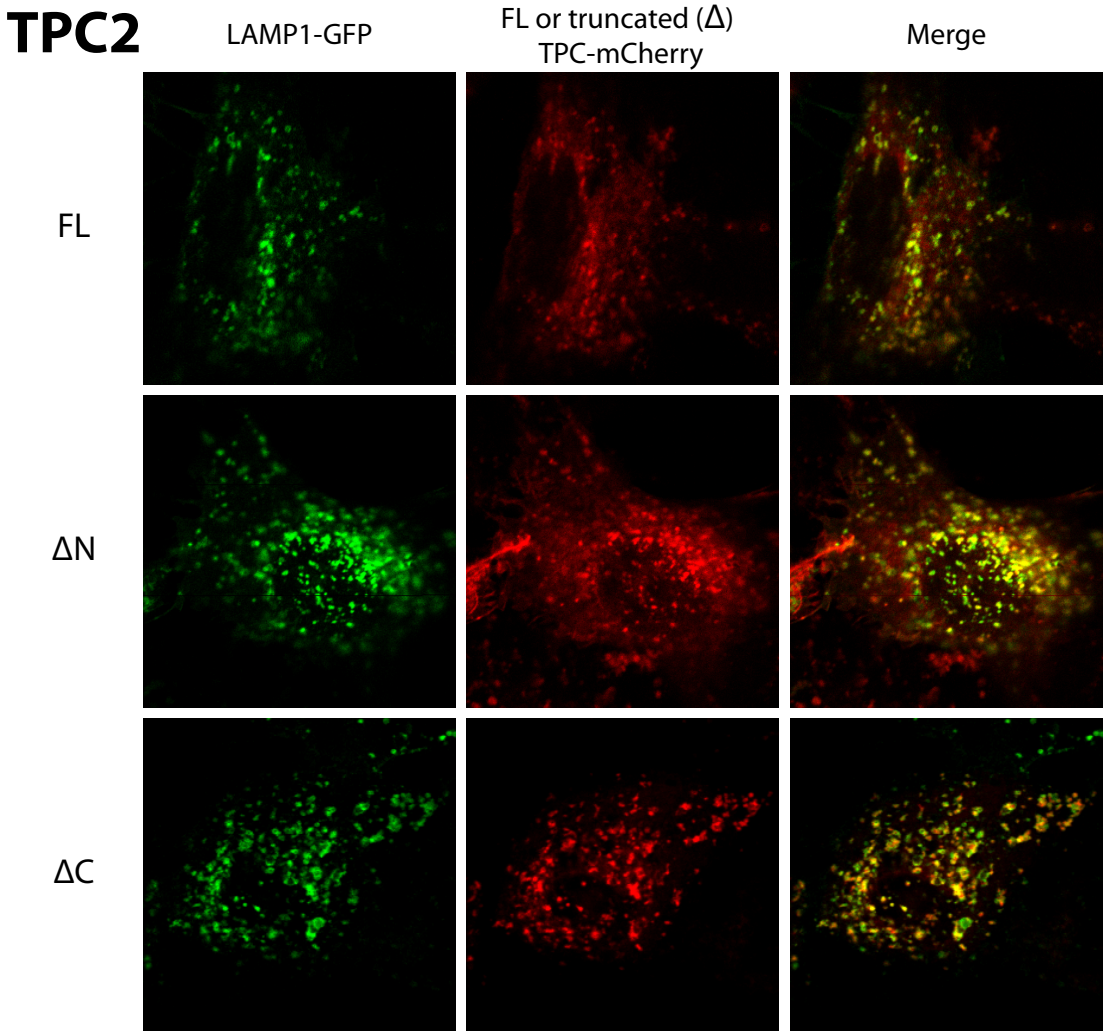

Figure 4.12: Representative images of (left) LAMP1-GFP, (centre) the full-length (FL), the truncated N- (ΔN), or C- (ΔC) TPC2-mCherry, and (right) merged images of both LAMP1-GFP and the full-length (FL), or truncated (Δ) TPC2-mCherry in MEF cells.

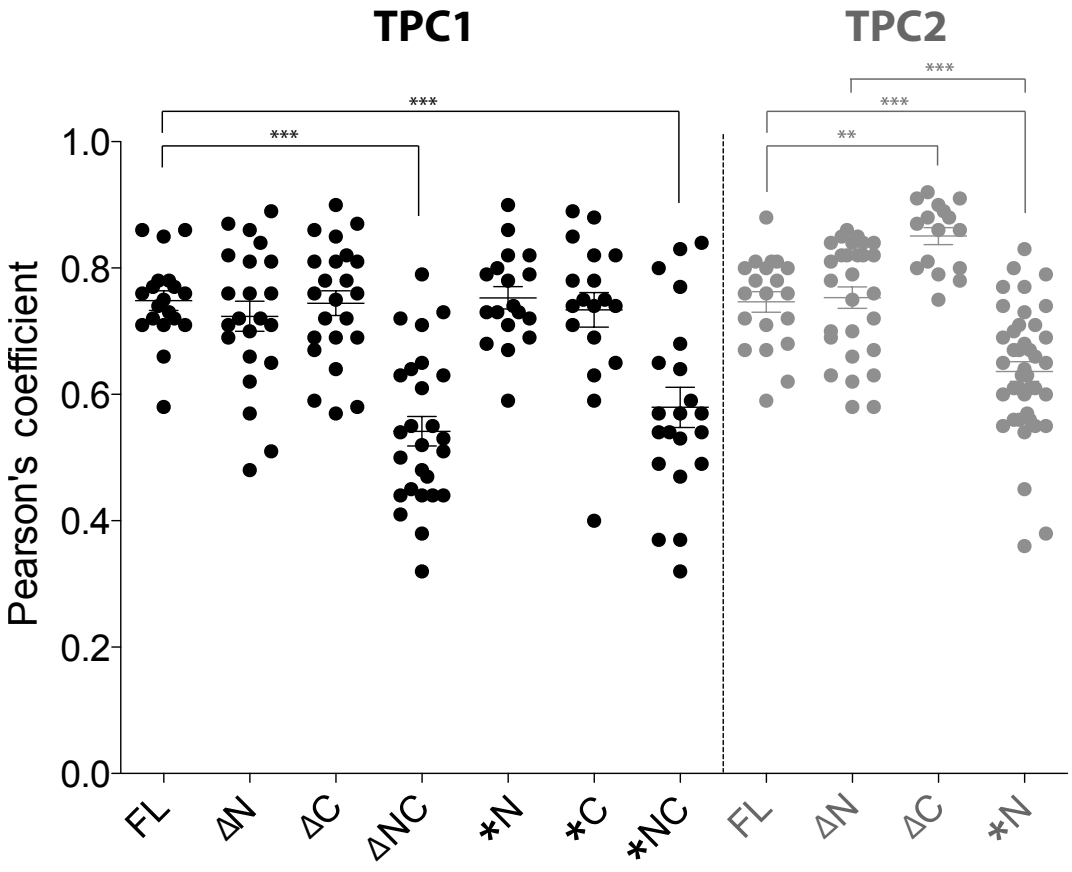

Figure 4.13: The extent of co-localization as measured by Pearson's coefficient of LAMP1-GFP with the full-length (FL), the truncated N- (ΔN), the truncated C- (ΔC), or both the truncated N- and C-terminal (ΔNC) TPC-mCherry, and TPC-mCherry that had mutated [DE]XXXL[LI] motif(s) (to AXXXAA) on the N- (∗N), the C-terminus (∗C), or both the N- and C-termini (∗NC) in MEF cells. Each cell (n) is indicated by the black dot for TPC1 and grey dot for TPC2, n = 19–28, ***P $<$ 0.001 and **P $<$ 0.01.

4.2.3.4 Generation of the mutated mouse TPC vectors

In order to remove the [DE]XXXL[LI] motifs by an alternative method, the motifs were mutated by site-directed mutagenesis (SDM). The resulting constructs are annotated with the prefix ∗. SDM was used to mutate the crucial amino acid residues in the [DE]XXXL[LI] motifs (to AXXXAA; A = alanine), thereby retaining the native protein length. The purpose of this approach was to determine whether the reduced co-localization of ΔNC-TPC1 with LAMP1 was attributable to protein degradations or to the loss of both [DE]XXXL[LI] motifs, and to investigate further why the deletion of only [DE]XXXL[LI] motif in TPC2 appeared to have no significant effect.

Figure 4.14 shows the position of the mutations introduced in TPCs. For TPC1, mutations were introduced to the [DE]XXXL[LI] motifs in the N-terminus, the C-terminus, or both termini; these are termed ∗N-TPC1, ∗C-TPC1 and ∗NC-TPC1, respectively (Figure 4.14A). Similarly, mutation of the N-terminal TPC2 [DE]XXXL[LI] motif produced ∗N-TPC2 (Figure 4.14B).

4.2.3.5 Validation of the mutated mouse TPC vectors

To enable mutated TPC cDNAs to be expressed and monitored in cells, mutant TPC cDNAs were inserted and fused to mCherry sequence in a mammalian expression vector (pcDNA5/TO). The recombinant vectors (pcDNA5/TO.mutated TPC.mCherry) were then transiently transfected into HEK293T cells.

To examine whether the mutated TPC-mCherry can be expressed in a mammalian system from the recombinant vectors, membranes of HEK293T cells that had been transfected with the recombinant vectors were probed by α-multi-red (5F8) in western blots.

TPC1. Figure 4.15 (left) shows the two sharp bands detected in membranes overexpressing mutated TPC1 by western blotting. The upper bands, probably representing the fully-glycosylated ∗N- and ∗C-TPC1, were clearly detected. In contrast, the upper band was not very evident in the ∗NC-TPC1 membranes. Differences observed may be attributable to variations in the extent of glycosylation [307].

The lower bands, which probably represent the core-glycosylated proteins [307], were

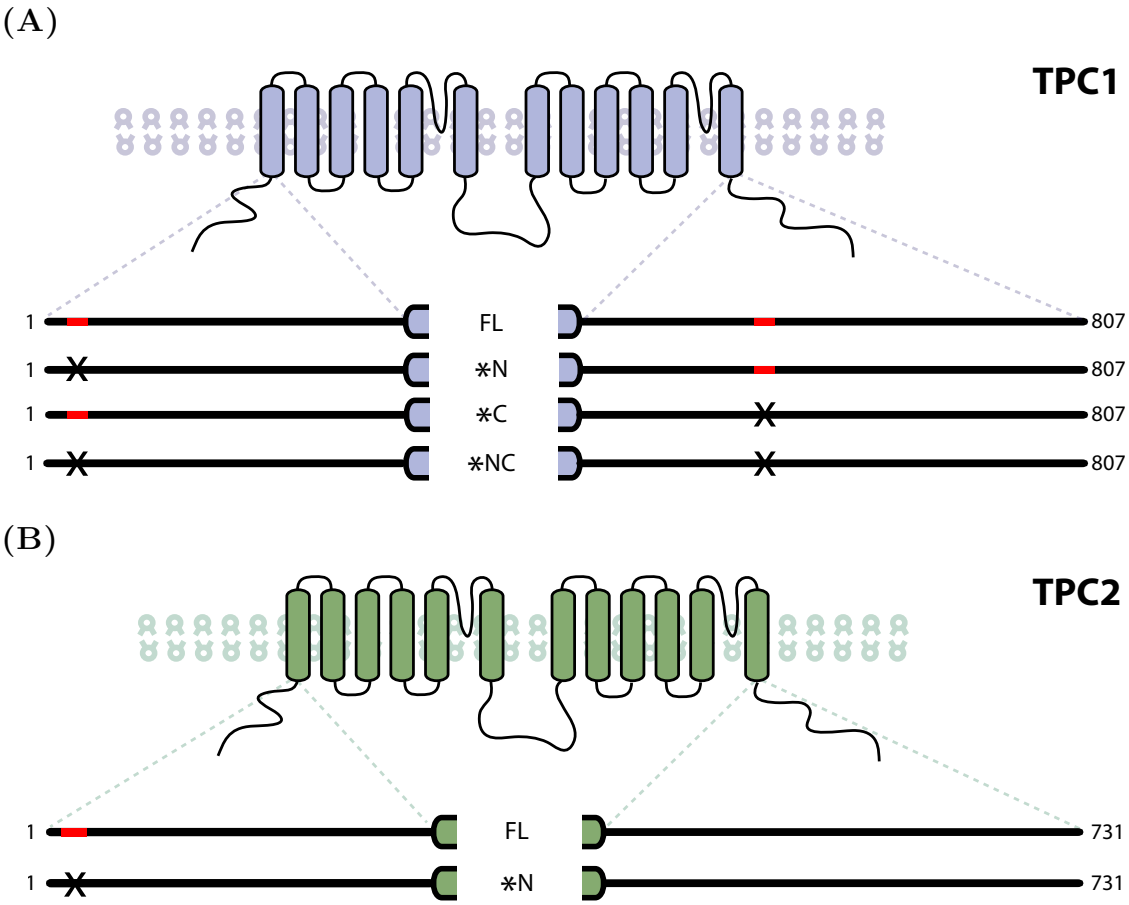

Figure 4.14: Illustration of terminal mutations by site-directed mutagenesis (SDM) of TPC1 and TPC2 to remove the [DE]XXXL[LI] motifs. Mutations at the N-terminus, the C-terminus, or both termini are designated ∗N, ∗C, or ∗NC, respectively. The [DE]XXXL[LI] motifs are indicated in red blocks, and crosses (x) represent the mutations.

detected in all mutated TPC1-mCherry membranes at the predicted size of 121 kDa.

TPC2. Figure 4.15 (right) shows the two sharp bands detected in membranes over-expressing ∗N-TPC2 in western blotting. The upper band (probably representing the fully-glycosylated ∗N-TPC2) was, however, less visible (Figure 4.10). As expected, the lower band (probably representing the core-glycosylated ∗N-TPC2) was smaller than the predicted 110 kDa (Figure 4.15) [307]. Likewise, the differences observed between the level of the upper and lower bands are possibly caused by different extents of glycosylation (full- or core-).

Western blotting confirmed that mutated TPC-mCherry proteins could be expressed in mammalian cells that had been transfected with recombinant vectors carrying the mutated TPC-mCherry cDNA. Furthermore, distinct bands in western blotting provided evidence that the mutated TPC-mCherry proteins were stable.

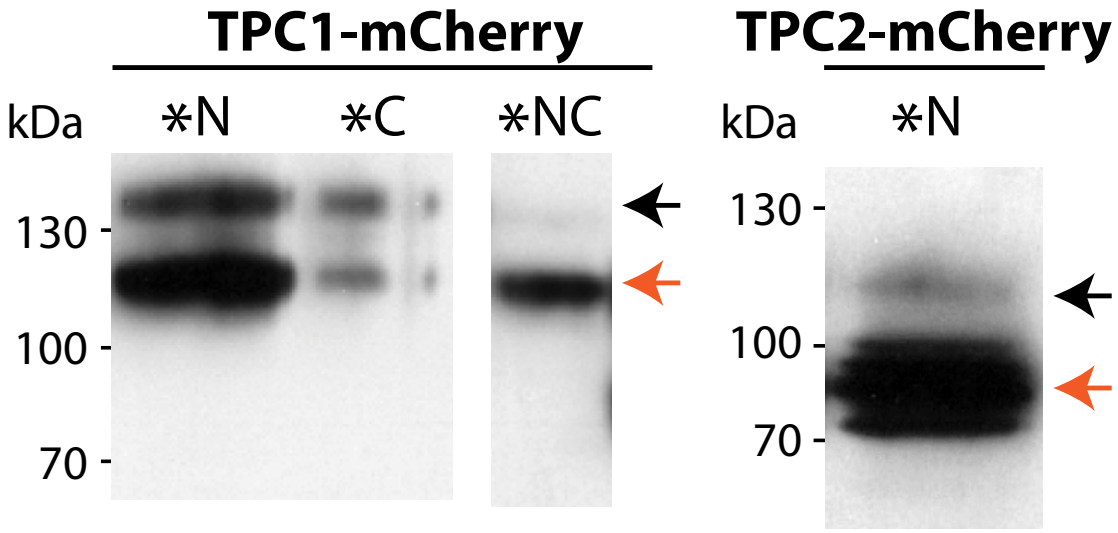

Figure 4.15: Western blotting of 25 μg membranes from HEK293T cells transiently transfected with pcDNA5/TO.mutated (*) TPC1.mCherry (10 μg, left), and pcDNA5/TO.mutated (*) TPC2.mCherry (10 μg, right) produced lower bands at the predicted size of mutated TPC1-mCherry (121 kDa) when probed with antibody α-multi-red (5F8). Similar to the FL-TPC2-mCherry, a lower band ($\sim$80 kDa) was detected that was much smaller than the predicted size of mutated TPC2-mCherry (110 kDa). The upper (black arrows) and lower bands (orange arrows) probably represent proteins that are fully-glycosylated and core-glycosylated, respectively [307]. Variations in the degrees of glycosylation are likely to account for the differences observed in the apparent molecular weights of bands.

4.2.3.6 Localization of the mutated mouse TPCs

To compare the effect of removing the [DE]XXXL[LI] motif(s) by SDM to those by truncation, the localization of TPCs to late endosomes/lysosomes was compared. This was achieved by co-transfection of mCherry-tagged mutant TPCs and GFP-LAMP1 in MEF cells; example images are shown in Figure 4.16.

TPC1. Similarly to the co-localization pattern of truncated TPC1, mutations on the N- or C-terminal [DE]XXXL[LI] motifs in TPC1 resulted in a similar extent of overlapping with LAMP1 compared to the WT full-length TPC1 (Pearson's coefficient = 0.75 ± 0.02 and 0.73 ± 0.03 for ∗N and ∗C-TPC1, respectively; Figure 4.13 and 4.16). Additionally, mutations of the [DE]XXXL[LI] motifs on both N- and C-termini in TPC1 significantly reduced the overlapping with LAMP1 (Pearson's coefficient = 0.58 ± 0.03, Figure 4.13 and 4.16). This verifies the previous hypothesis for TPC1: that one [DE]XXXL[LI] motif is sufficient to direct mouse TPC1 to late endosomes/lysosomes, and mis-sorting only occurs when both dileucine motifs are deleted.

TPC2. In contrast to the previous finding, mutation of the single [DE]XXXL[LI] motif in TPC2 significantly reduced the extent of overlapping with LAMP1 (Pearson's coefficient = 0.64 ± 0.02 compared to the FL-TPC2, and also ΔN-TPC2; Figure 4.13 and 4.16). This indicates that the [DE]XXXL[LI] motif is critical in directing TPC2 to late endosomes/lysosomes. The lack of difference observed between ΔN- and FL-TPC2 is probably attributable to effects caused by the loss of amino acid residues by truncation.

In summary, results from co-localization studies showed that the [DE]XXXL[LI] motifs on the termini are important for directing TPCs to late endosomes/lysosomes. In TPC1, where there are two, the [DE]XXXL[LI] motifs are redundant; even when both terminal [DE]XXXL[LI] motifs were removed (either by truncation or mutation), the extent of co-localization was not completely abolished. The residual co-localization suggests that other sorting motifs such as tyrosine motifs may also play a role in directing TPCs to late endosomes/lysosomes.

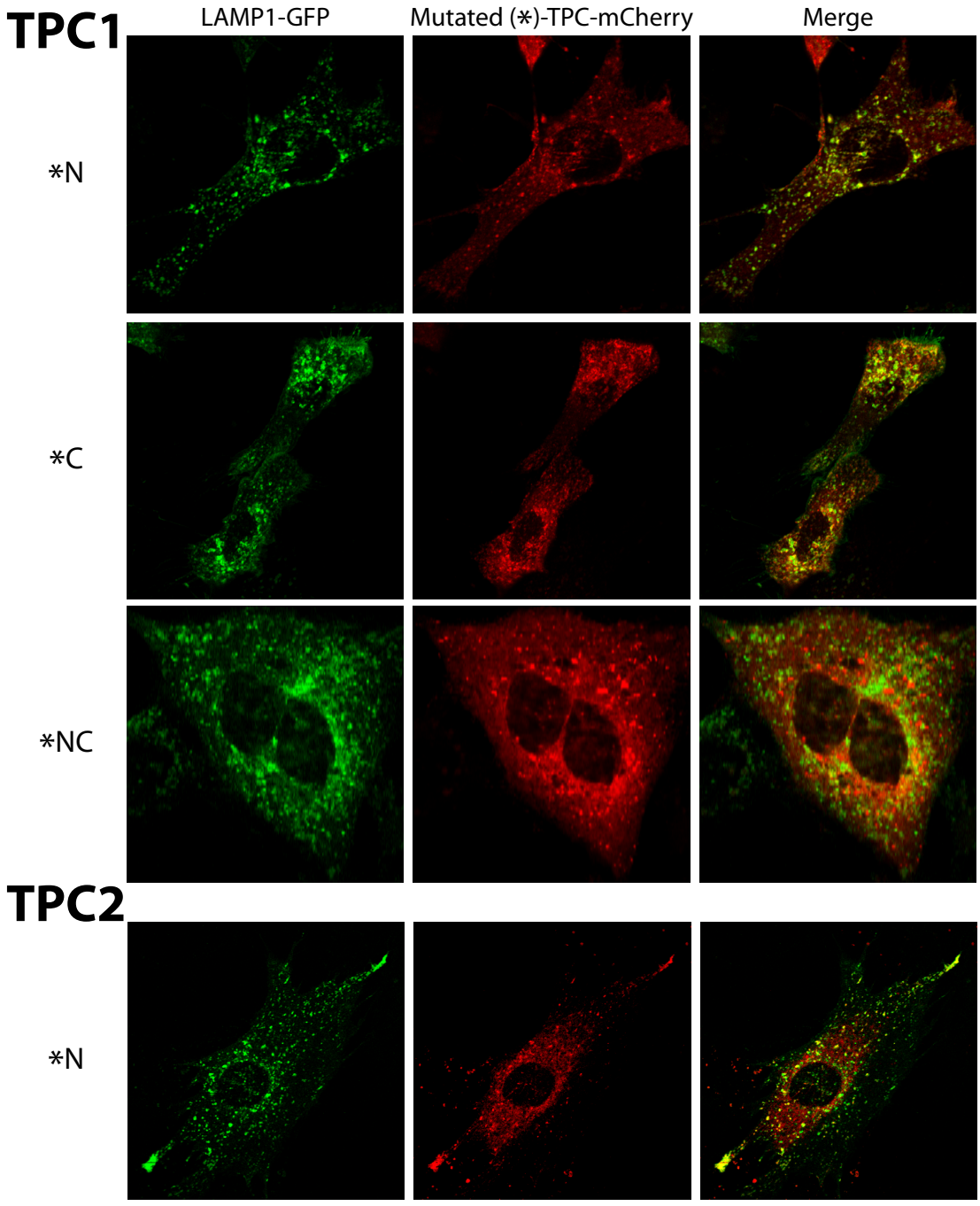

Figure 4.16: Representative images of (left) LAMP1-GFP, (centre) TPC-mCherry that had mutated [DE]XXXL[LI] motif(s) (to AXXXAA) at the N- (∗N), C-terminus (∗C), or both termini (∗NC), and (right) merged images of both LAMP1-GFP and the mutated (∗)-TPC-mCherry in MEF cells.

4.2.4 ΔN-TPC1 Localization

In Chapter 3, the endogenous mRNA of the shorter TPC1 variant (ΔN-TPC1) was shown to be expressed in tissues that also express FL-TPC1 (Figure 3.7). Furthermore, despite the absence of an N-terminal [DE]XXXL[LI] motif in ΔN-TPC1, it nonetheless localized to late endosomes/lysosomes (Figure 4.13). The similarity between FL- and ΔN-TPC1 expression patterns prompted further investigation of their distinct roles by elucidating other subcellular localization of ΔN-TPC1.

Figure 4.17B shows representative examples for each co-transfection, from which Pearson's coefficients were calculated for each cell. Co-transfecting mCherry-tagged ΔN-TPC1 with GFP-tagged organelle markers (TfR, EEA1, and KDEL) in MEF cells showed that the localization of ΔN-TPC1 was significantly lower in recycling endosomes, subdomains of endosomes, and early endosomes compared to the FL-TPC1 (Pearson's coefficient = 0.54 ± 0.03 (TfR) and 0.28 ± 0.03 (EEA1)). In contrast, the localization of ΔN-TPC1 was significantly higher in the ER (Pearson's coefficient = 0.62 ± 0.03, Figure 4.17B) compared to the FL-TPC1 (Figure 4.17A). The lower levels in subdomains of endosomes and early endosomes may be partly explained by an increase in the ER retention caused by the N-terminal truncation.

As TPC channel activities have been reported to be governed by the luminal pH and $[Ca^{2+}]$ [231], the differences in subcellular localization between FL- and ΔN-TPC1 suggest that each variant may exert distinct regulation depending on the acidic stores that it localizes to.

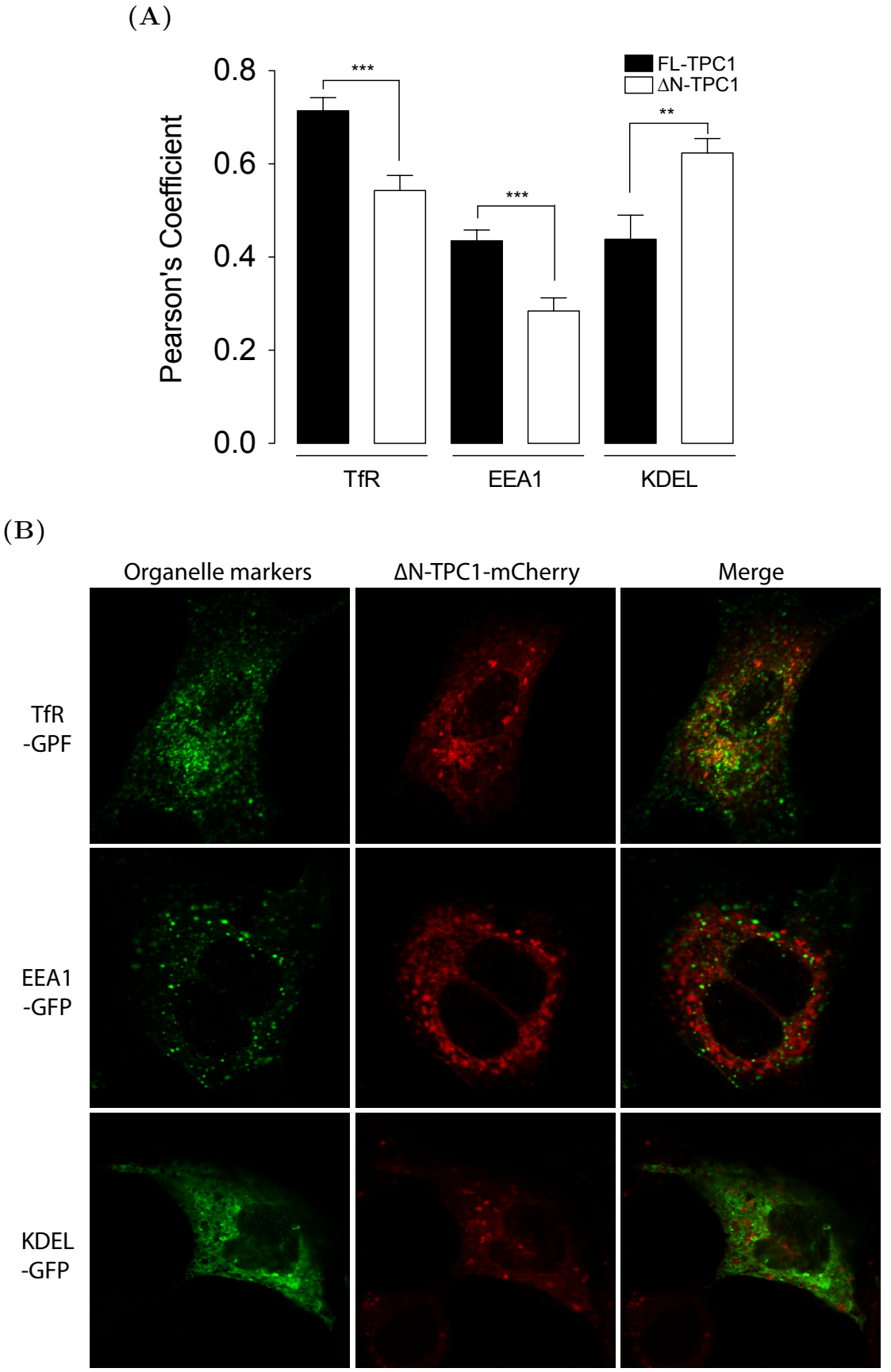

Figure 4.17: (A) Summary of the extent of co-localization as revealed by Pearson's coefficient for the longer (full-length, FL-TPC1), and the shorter (ΔN-TPC1) TPC1-mCherry variants with TfR-GFP, EEA1-GFP, or KDEL-GFP in MEF cells (n = 10–22, ***P < 0.001 and **P < 0.01). (B) Representative images of (left) GFP-tagged organelle markers, (centre) ΔN-TPC1-mCherry, and (right) merged images of both organelle markers and ΔN-TPC1-mCherry in MEF cells.

4.3 Discussion

4.3.1 Localization of TPCs

In this chapter, localization of mouse TPC1, ΔN-TPC1 and TPC2 was studied in detail. This provided the first evidence that the subcellular localization of mouse TPC1 is primarily in late endosomes/lysosomes, and subdomains of endosomes, likely between early and late endosomes (Figure 4.2). This is consistent with observations for human TPC1, which also has the conserved [DE]XXXL[LI] motifs and localizes mainly in endosomes and late endosomes/lysosomes [39, 52]. In contrast to the study by Zong *et al.*, which showed that mouse TPC2 localizes in both late endosomes/lysosomes and in the ER, results here demonstrated that mouse TPC2, similar to human, localizes primarily in late endosomes/lysosomes but not in the ER (Figure 4.3) [217, 307]. Although Zong *et al.* detected mouse TPC2 in the ER, functional studies showed that NAADP-evoked Ca^{2+} release was not significantly altered by 1 μM thapsigargin but by bafilomycin in TPC2-expressing cells. This indicates that the TPC2 channels in the ER were inactive [307].

Functional studies in cells overexpressing human TPC2 showed that NAADP induced Ca^{2+} release in two phases: an initial ramp phase directly from the acidic stores and the second large Ca^{2+} transient phase indirectly from the ER by CICR [52]. It is likely that human TPC2 is localized in late endosomes/lysosomes in proximity to the ER, so the Ca^{2+} trigger induced by NAADP can be amplified by $InsP_3$Rs, or RyRs on the ER by the CICR mechanism [52, 103]. Thus, it is possible that mouse TPC2, like human, is located in late endosomes/lysosomes very near the ER; the resolution of the camera was not sufficient to differentiate the ER staining from that of adjacent lysosomes in the study by Zong *et al.* [307].

Furthermore, Zong *et al.* used a monkey kidney cell line (COS-7) — different from the mouse cell line (MEF cells) that was used in this study. Mouse cell lines are probably more appropriate for investigating mouse protein trafficking as they contains the necessary machinery to direct proteins to the correct localization. The disparate results between Zong *et al.* and this study may therefore be explained by the possibility that mouse TPC2 localizes differently in a heterologous system. Lastly, since all proteins are synthesized in the ER, and the localization study by Zong *et al.* used overexpression, it is likely that the

mouse TPC2 was excessively expressed in their system, resulting in some ER retention.

To further examine whether TPC2 localizes in the ER, additional cell lines and ER markers might be required. It should be noted that both the work of Zong *et al.* and this study have overexpressed the protein to examine its localization. Overexpression of TPCs has been demonstrated to alter the vesicular trafficking and lysosomal distribution [243]. The best solution for identifying physiological localization is probably by using antibodies to probe for the endogenous expression. Unfortunately, there was no available mouse antibody that was able to detect endogenous TPCs by immunocytochemistry. It might be beneficial in the future to generate antibodies for this purpose.

4.3.2 Lysosomal sorting signals & sorting mechanisms of TPCs

4.3.2.1 TPC1

Given that lysosomal-targeting signals tend to be located near the cytosolic termini, and as the N- and C-termini of TPCs were recently confirmed to be cytosolic [122], it is likely that TPCs have the lysosomal-targeting signals. Bioinformatic analysis revealed that mouse TPC1 has two potential lysosomal targeting [DE]XXXL[LI] motifs, one at each terminus. To date, the mechanism by which the [DE]XXXL[LI] motif(s) direct TPC1 to late endosomes/lysosomes is still unclear. Studies have shown that human or mouse TPC1 is localized intracellularly and not in the plasma membrane, even when both [DE]XXXL[LI] motifs were removed [42, 307]. Results from this study agreed with previous findings [42, 307] and further showed that both [DE]XXXL[LI] motifs are important in directing mouse TPC1 to late endosomes/lysosomes. Truncation or mutation of one TPC1 terminal [DE]XXXL[LI] motif had no significant effect on the co-localization with LAMP1; co-localization was only significantly decreased when both [DE]XXXL[LI] motifs were abolished. This provides strong evidence that both terminal [DE]XXXL[LI] motifs are active and mutually redundant as either [DE]XXXL[LI] motif was sufficient to target TPC1 to late endosomes/lysosomes. However, it is not known whether both [DE]XXXL[LI] motifs are recognized by the same molecular machinery for lysosomal targeting or whether each [DE]XXXL[LI] motif is recognized by different molecular machinery, and therefore targeted to lysosomes by different pathways (similar to the system employed by TRPML1).

TRPML1, also referred to as mucolipin-1 or MCOLN1, is a cation channel that

localizes to late endosomes/lysosomes. Its channel activity and regulation is still in debate but the following conducting ions have been reported: Ca^{2+}, K^{+}, Na^{+}, H^{+}, and Fe^{2+} [166, 236]. Like TPC1, TRPML1 has two [DE]XXXL[LI] motifs, each near the N- and the C-termini. Mutation of both [DE]XXXL[LI] motifs in TRPML1 completely eliminated the localization to lysosomes [235, 236, 285]. TRPML1 takes either a direct or indirect pathways to lysosomes. In the direct pathway, TRPML1 migrates from the Golgi apparatus to late endosomes/lysosomes by using interactions between the N-terminal [DE]XXXL[LI] motif and clathrin adaptor AP-1 and AP-3. In the indirect pathway, TRPML1 travels from the Golgi apparatus to the plasma membrane where the C-terminal [DE]XXXL[LI] motif is recognized by clathrin adaptor AP-2 and internalised by the endocytic pathway (from early endosomes and to late endosomes/lysosomes) [236, 285].

It is possible that TPC1, like TRPML1, has two distinct [DE]XXXL[LI] motifs which recruit different sorting mechanisms, thereby similarly travelling by both the direct and indirect pathways (Figure 4.18). One of the ways to determine whether TPC1 takes the indirect pathway is to examine changes in the localization of TPC1 in response to altered AP-2 expression. In addition to the well-established clathrin-dependent endocytosis, endocytosis can also occur independently of the clathrin. With the increasing knowledge of trafficking pathways and their associated proteins it should become easier to test and further distinguish the trafficking pathways that TPCs employ [114].

4.3.3 ΔN-TPC1

The identification of an endogenous alternative TPC1 mRNA, ΔN-TPC1 (Chapter 3) raised the question as to whether the protein has an endogenous function and a role in NAADP-mediated Ca^{2+} signalling, or whether it is merely a futile mRNA. Three lines of enquiry support the hypothesis that ΔN-TPC1 is functional and releases Ca^{2+}: (1) the analysis of cDNA showed that the transmembrane domains of ΔN-TPC1 are unaltered (Figure 4.4), thus ΔN-TPC1 should still form a channel in the membrane allowing passage of Ca^{2+}. Indeed, N-terminal truncated human TPC2, though mis-located due to the loss of the [DE]XXXL[LI] motif, still released Ca^{2+} [42]. It is important to note that in Chapter 3, no endogenous equivalent ΔN version of TPC2 was found. ΔN-TPC2 generated in the study by Brailoiu *et al.* was truncated purposely to mis-locate TPC2 to the plasma membrane in order to measure the channel activity [42]. In contrast, ΔN-TPC1

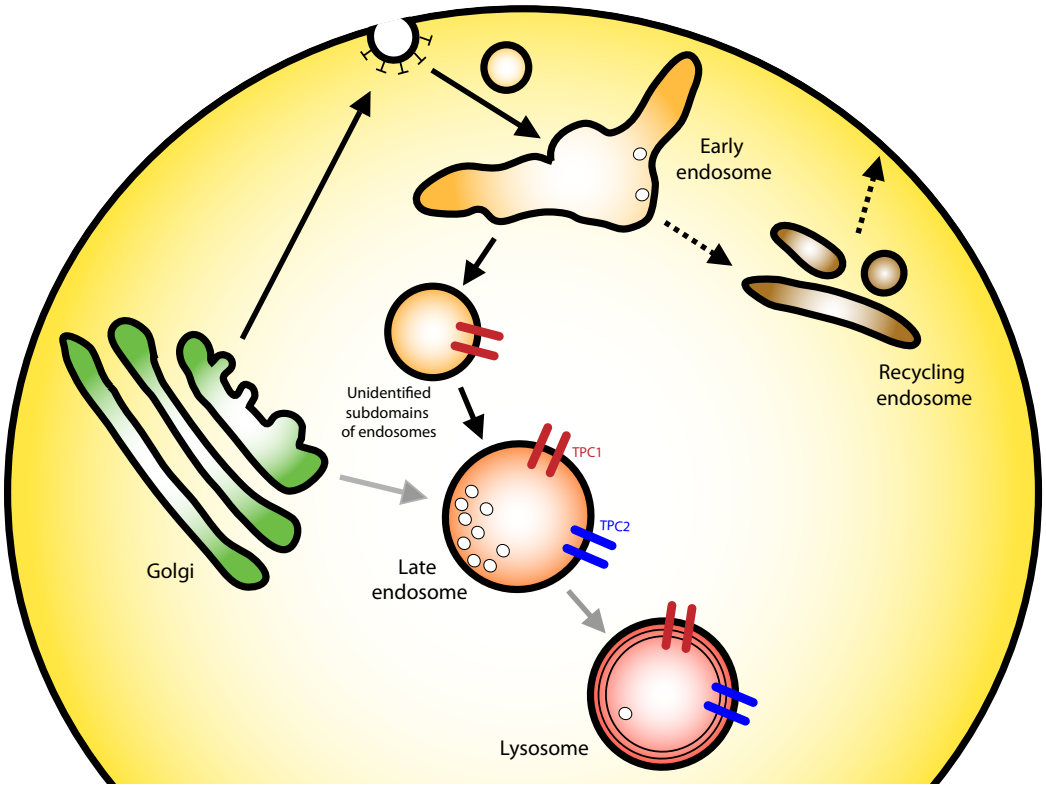

Figure 4.18: Schematic showing the localization of mouse TPC1 (red) and TPC2 (blue) and possible trafficking pathways in the endo-lysosomal system. TPC1 and TPC2 are possibly trafficked by the direct pathway in which proteins in the Golgi apparatus are directly sorted to late endosomes/lysosomes (light arrows). In addition, TPC1 might be trafficked by the indirect pathway in which proteins in the Golgi apparatus are sorted to the plasma membrane and subsequently internalised in the clathrin-coated pits by the endocytic pathway (dark arrows). Dotted arrows represent the recycling pathway where some early endosomes become recycling endosomes. Recycling endosomes receive the cargo proteins from the early endosomes and recycle them back to the plasma membrane.

identified in Chapter 3 is expressed endogenously in both human and mouse. (2) Western blotting demonstrated that the ΔN-TPC1 mRNA (AK137626) was not futile; it was translated into protein possibly from the alternative endogenous ATG start codon. In addition, the loss of 69 amino acid residues in the N-terminus of TPC1 did not result in any noticeable protein degradation (Figure 4.10). (3) The localization study showed the typical TPC1 punctate pattern in late endosomes/lysosomes, even though more protein was retained in the ER (Figure 4.17B). Alternatively, it is possible that some ΔN-TPC1 is localized in the ER, however, whether or not this ER-localized ΔN-TPC1 would function needs to be tested in future. Different localization pattern of the FL- and ΔN-TPC1 may reflect distinct channel activities and regulations as acidic stores possess different luminal pH and $[Ca^{2+}]$ [166, 216, 277]; these environment parameters are known to alter channel

activities [231].

In western blotting analysis, two proteins bands were detected for each mouse TPC-mCherry protein. Previous studies had attributed the two bands to different glycosylation of TPC proteins. The upper band represents the fully-glycosylated form whereas the lower band represents the core-glycosylated protein. The glycosylation was asparagine (N)-linked as two bands were shifted lower after endoglycosidase treatment by Peptide: N-Glycosidase F (PNGase-F) [122, 307]. Different ratios between the upper and the lower band in FL-TPC1 and ΔN-TPC1 suggest that proteins were glycosylated to different levels. Since N-linked glycosylation has been reported to regulate NAADP-elicited Ca^{2+} release [122], this supports the theory that FL-TPC1 and ΔN-TPC1 have distinctive roles in NAADP-mediated Ca^{2+} signalling. However, it is important to note that N-linked glycosylation (for both TPCs) occurs at the pore loop region. The study that reported the regulation by N-linked glycosylation in NAADP-elicited Ca^{2+} release was done by mutating asparagine to glutamine. Thus, the enhanced NAADP-evoked Ca^{2+} release in the N-linked glycosylation TPC mutant may result from an alteration to the ion-conducting pore rather than from the loss of N-linked glycosylation [122].

The likelihood of an endogenous function for ΔN-TPC1 raised the question of how it would differ from FL-TPC1. One possible hypothesis is that FL-TPC1 and ΔN-TPC1 are targeted by different molecular machinery and therefore reach late endosomes/lysosomes by different pathways. Cells that exclusively use one particular pathway may employ ΔN-TPC1 more readily than FL-TPC1, and vice versa. Alternatively, if both FL- and ΔN-TPC1 are sorted by the same pathway, ΔN-TPC1 might act as a dominant negative to FL-TPC1, in the same way as Δ$Np73$ functioning as the dominant negative to $p73$ (tumor suppressor protein p73) [147].

Furthermore, ΔN-TPC1 might serve to interfere with dimer formation and thus down-regulate the Ca^{2+} release via FL-TPC1. TPCs have two homologous six-transmembrane domains, and are predicted to be an evolutionary intermediate between voltage-gated Ca^{2+} or Na^{+} channels and TRP channels, which have four homologous domains and one six-transmembrane domain, respectively. Since TRP channels assemble in tetramers, TPCs are predicted to form dimers. The N-terminus of TRPC4 has been shown to contain domains that are important for the TRP channels assembly [157]. It is possi-

ble that ΔN-TPC1 still interacts at the C-terminus but is unable to form a functional channel with FL-TPC1 as the N-terminus is missing, rather forming dysfunctional TPC1 dimers. Alternatively, given that both ΔN-TPC1 and FL-TPC2 are localized to late endosomes/lysosomes, there is a possibility that ΔN-TPC1 might form a heterodimer with FL-TPC2 to regulate its function.

4.3.4 TPC2

Bioinformatic analysis revealed that mouse TPC2 has a single [DE]XXXL[LI] motif at the N-terminus. This [DE]XXXL[LI] motif was shown to be important in directing mouse TPC2 to late endosomes/lysosomes, as the co-localization of TPC2 with LAMP1 was significantly reduced when the single [DE]XXXL[LI] motif was removed. This is consistent with human ΔN-TPC2, where the removal of the sole [DE]XXXL[LI] motif abolished lysosomal localization [42]. Surprisingly, the co-localization of mouse TPC2 with LAMP1 was only significantly reduced when the [DE]XXXL[LI] motif was removed by mutation, and not by truncation. One likely explanation is that truncation removes other amino acid residues in addition to the target [DE]XXXL[LI] motif. This may result in a non-specific effect that masks the true effect mediated by the loss of [DE]XXXL[LI] motif. This interpretation is supported by the analysis of ΔC-TPC2 where truncation interfered with the co-localization with LAMP1 even though the truncation region did not contain any [DE]XXXL[LI] motif (Figure 4.13). Furthermore, excessive truncations might decrease the stability of the protein and facilitate degradation as observed in the case of ΔNC-TPC1 (Figure 4.10). Truncated proteins may be more susceptible to proteolysis or ubiquitination pathways, and thus be more susceptible to degradation.

Localization studies showed that both mouse TPCs remained intracellularly located, even after removal of all terminal [DE]XXXL[LI] motifs. It would be interesting to discover where the proteins reside, if not targeted to late endosomes/lysosomes, (retained in the ER, or mis-targeted to other organelles?) This would broaden our understanding the trafficking pathways employed by TPCs.

In human TPC2, removal of the [DE]XXXL[LI] motif resulted in protein mis-location from lysosomes to the plasma membrane [42]. Surprisingly, the localization of mouse TPC2 was still punctate and not peripheral after the [DE]XXXL[LI] motif removal. The intracellular localization is consistent with a previous finding [307], suggesting that mouse

TPC2 is not mis-located to the plasma membrane. However, this will need to be confirmed using a plasma membrane marker. It is interesting though that, given the sequence similarity between mouse and human TPC2, they do not necessarily behave the same. The retained intracellular localization after the [DE]XXXL[LI] motif removal can be explained if mouse TPC2 travels exclusively by the direct pathway and never to the plasma membrane (Figure 4.18). With this pathway, mouse TPC2 would not accumulate in the plasma membrane when the [DE]XXXL[LI] motif is deleted. Human TPC2, however, might travel by the indirect pathway, so the loss of the [DE]XXXL[LI] motif in ΔN-TPC2 prevents the interaction with, for example, AP-2 that is involved in the internalization, thus resulting in accumulation in the plasma membrane.

Even when all terminal TPC [DE]XXXL[LI] motifs had been removed, TPCs did not completely lose their localization to late endosomes/lysosomes. Some residual TPCs were still targeted to late endosomes/lysosomes. This suggests that other sorting signals such as tyrosine motifs may also play a role in the lysosomal targeting of TPCs. Although no evident candidate tyrosine motifs were found in the initial searches (Table 4.3), the possible involvement of these motifs should be investigated.

4.3.5 Role of TPCs in endo-lysosomal system

In the endo-lysosomal system, luminal Ca^{2+} is essential for vesicle fusion [172, 230]. Fusion occurs either homotypically between early and late endosomes, or heterotypically between late endosomes and lysosomes in order to convey their contents and membrane proteins to the pathway for degradation or ubiquintination. Luminal Ca^{2+} is also required for condensing luminal content to form lysosomes after heterotypic fusion [172, 230]. An imbalance in the intracellular Ca^{2+} homeostasis can lead to lysosomal storage diseases such as mucolipidosis type IV or Niemann-Pick Type C [142, 165, 286]. A recent study has shown that alterations in sea urchin TPC expression affect vesicular trafficking, and lysosomal size, distribution, and storage, this indicates involvement of TPCs in lysosomal biogenesis and lysosomal storage disorders [243].

TPC1 has a broader subcellular distribution than TPC2, suggesting that they may employ different trafficking pathways. Thus, TPC1 might be more involved in vesicular trafficking as it has a broader distribution, whereas TPC2 (predominantly localized in

late endosomes/lysosomes) might be more involved in heterotypic fusion and luminal content condensation. Furthermore, if ΔN-TPC1 is functional, it might serve to expand the armoury in regulating the complex endo-lysosomal system.

Although there are still many issues remaining to be solved in the endo-lysosomal field, recent discoveries of NAADP-gated Ca^{2+} release via TPCs in the endo-lysosomal system have accelerated our understanding of the role of Ca^{2+} in endo-lysosomes. Given the mobility and fast turnover of the endocytic vesicles, Ca^{2+} release from endo-lysosomes may function not only locally, but also globally, for example, by travelling to the ER to facilitate Ca^{2+} release by CICR, or to the plasma membrane to regulate Ca^{2+}-sensitive channels to alter the membrane excitability [103]. An understanding of the subcellular distribution and the trafficking pathway of TPCs will help to gain further insight into the spatial organization of NAADP-mediated Ca^{2+} signalling.

4.4 Conclusions

Work from this chapter provided the first evidence that a shorter variant of TPC1 (ΔN-TPC1) is not a futile mRNA; it could be translated into a protein. It is possible that this protein serves as an additional NAADP-gated Ca^{2+} channel to increase the diversity of NAADP signals.

The localization of fluorescently-tagged mouse TPC isoforms/variants also showed for the first time that mouse TPC1 is predominantly expressed in both subdomains of endosomes and late endosomes/lysosomes, while ΔN-TPC1 and TPC2 are primarily expressed in late endosomes/lysosomes. These results are consistent with human TPCs [39, 52]. The differential localization observed may yield insight into the spatial organization of NAADP-evoked Ca^{2+} signals, and may reflect the distinct roles of TPC isoforms/variants in regulating specific cellular events.

Investigation into the sorting signals of TPCs demonstrated that the [DE]XXXL[LI] motifs are important for the lysosomal targeting of TPCs. In the case of TPC1, where there are two [DE]XXXL[LI] motifs, these motifs are mutually redundant. The removal of all [DE]XXXL[LI] motifs in TPC variants/isoforms, however, did not completely abolish their localization to late endosomes/lysosomes. This suggests that other lysosomal targeting motifs, such as tyrosine-based sorting signals, may also be involved.

Chapter 5

NAADP Binding in Mouse Hepatic Membranes

5.1 Introduction

Biochemical, pharmacological and functional studies over the past two years have established that both TPC1 and TPC2 are NAADP-gated channels [39, 42, 52, 231, 307]. However, the exact mechanism of action underlying NAADP-induced TPC activation is still unknown.

In human TPC2-overexpressing membranes, the specific binding of NAADP was shown to increase with biphasic affinities in the nM and μM range, mirroring that of endogenous mammalian binding (summarized in Table 5.1). Furthermore, specific binding of NAADP was shown to be retained in immunopurified endogenous sea urchin TPC complexes, with the affinities, as well as the characteristic K^+-dependent irreversible binding [87, 243], similar to those of the native system. These binding properties of NAADP in TPC-overexpressing systems, and immunopurified TPCs (similar to the endogenous behaviour) established that NAADP indeed binds to TPC complexes.

Although persuasive evidence has demonstrated that NAADP binds to a component of TPC complexes, it is possible that the NAADP target is not TPC itself but an accessory protein that is tightly bound to TPC. The increased specific binding observed in the TPC-overexpressing system may just be a consequence of enhanced binding complex formations. Identification of the NAADP-binding protein would yield insight into the mechanisms underlying NAADP-induced TPC activation. It would also facilitate the

	K_d (high affinity, nM)	K_d (low affinity, μM)	References
Human TPC2	5.0	7.2	[52]
Rat brain microsomes	200	-	[215]
Rabbit heart microsomes	0.13 and 4	∼1	[16]
MIN6	130	12	[178]
Mouse liver	6.6	4.6	[52]

Table 5.1: Summary of NAADP K_d values in different mammalian systems. MIN6 is a mouse insulinoma cell line.

design of future drugs to target the NAADP signalling pathway.

There is also the question as to whether NAADP binds differently to complexes formed from the different TPC isoforms? Different NAADP affinities to the different complexes may lead to differential sensitivity of Ca^{2+} stores to NAADP. In light of the distinct subcellular localization profiles of TPCs (for example, mouse TPC1 has a broader subcellular distribution compared to TPC2 as shown in Chapter 4), this would offer more versatility in response to NAADP-evoked Ca^{2+} release.

To address the above questions, hepatic membranes were extracted from TPC KO mice to study the effect of knocking out one or both TPC isoforms on NAADP binding. Hepatic membranes were chosen as northern blotting has shown that TPC mRNAs are highly expressed in liver [52, 127, 307]. Additionally, TPCs are localized in the endo-lysosomal compartments, which are enriched in liver [306], and liver is a large organ so provides a reasonable sample volume/animal. Furthermore, NAADP binding has been previously characterized in this system [52].

Prior to testing the effect of knocking out TPCs on NAADP binding, the binding assay conditions were optimized. Binding conditions had been previously studied in the sea urchin [87] but not in mammals. In the mammalian system, the buffers used to study NAADP binding were either Glu-IM (intracellular-like medium containing gluconate, see below) [52] or 20 mM HEPES [16, 178, 215]. Glu-IM is a physiologically relevant sea urchin buffer whereas 20 mM HEPES has a low osmolarity.

The ionic composition of the buffer is highly significant (for example, K^+ concentration in sea urchins affects the kinetics of NAADP binding [87]), so choosing a suitable buffer is essential. The binding kinetics of NAADP in the improved buffers were also examined to confirm that the new buffers would be suitable for the subsequent NAADP binding studies.

5.2 Results

5.2.1 Optimizing experimental conditions

For studying NAADP binding in mouse hepatic membranes, Calcraft *et al.* used Glu-IM for both the binding and the wash buffer [52]. Glu-IM, used for sea urchin egg, comprises 250 mM potassium gluconate, 250 mM *N*-methyl D-glucamine, 20 mM HEPES and 1 mM $MgCl_2$ (pH 7.2, with acetic acid). This buffer is not an ideal mimic of the intracellular medium of mammalian systems: this typically contains 140 mM K^+, 5–10 mM Na^+, 1 mM Mg^{2+}, and other ions such as Cl^- and Ca^{2+}. Glu-IM is also viscous due to the presence of gluconate; it is therefore more difficult to separate bound and unbound radioligand by rapid filtration. Although Glu-IM gave a workable signal to noise ratio (i.e. total to non-specific binding) for NAADP binding in the mouse hepatic membranes [52], optimizations were carried out on various components of Glu-IM in order to obtain a more suitable mammalian buffer.

Calcraft *et al.* used 200 pM [^{32}P]NAADP in their binding studies [52]. In this study, a threefold lower concentration of [^{32}P]NAADP was used in the new buffers because the initial material for synthesizing [^{32}P]NAADP was [^{32}P]ATP rather than [^{32}P]NAD. [^{32}P]ATP has threefold higher specific activity, so the lower concentration minimises radiation exposure. Additionally, [^{32}P]NAADP synthesis is expensive and labour intensive, so reducing the amount of radioligand used is desirable.

5.2.1.1 Wash buffer

To optimize the wash buffer Glu-IM, mouse hepatic membranes (5 mg/ml) were incubated with 66 pM [^{32}P]NAADP in Glu-IM in the presence or absence of unlabelled NAADP (1 mM) for 1 h before separating bound from unbound [^{32}P]NAADP in one of the five wash buffers (summarized in Table 5.2). These buffers were designed to test the components of Glu-IM, and the importance of each ion was determined by different combinations of ionic components.

Buffer H (77 ± 5.9%) and buffer HM (69 ± 5.4%) significantly increased the % specific binding of NAADP compared to Glu-IM (32 ± 4.8%), whereas buffers HK_{250} and $HK_{250}M$ did not show enhanced specific binding (33 ± 7.4 and 32 ± 2.2% respectively; Figure 5.1).

Buffer H was chosen over HM as the wash buffer for the subsequent binding assays because of its superior total binding performance.

Buffer	Ionic composition
Glu-IM	250 mM potassium gluconate, 250 mM *N*-methyl D-glucamine, 20 mM HEPES, and 1 mM $MgCl_2$
H	20 mM HEPES
HK_{250}	20 mM HEPES, and 250 mM potassium acetate
$HK_{250}M$	20 mM HEPES, 250 mM potassium acetate, and 1 mM $MgCl_2$
HM	20 mM HEPES, and 1 mM $MgCl_2$

Table 5.2: Buffers used for binding and washing showing its ionic composition.

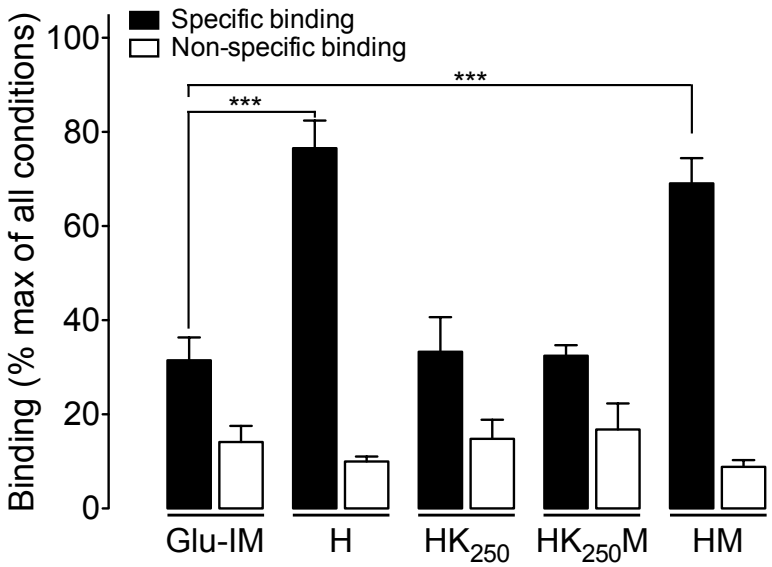

Figure 5.1: Effect of wash buffer ionic compositions on the [^{32}P]NAADP binding in the mouse hepatic membranes. Total binding was determined by incubating mouse hepatic membranes with 66 pM [^{32}P]NAADP in Glu-IM for 1 h before separating bound [^{32}P]NAADP from unbound by rapid filtration in one of the five wash buffers: Glu-IM, H, HK_{250}, HK_{250}M and HM (n = 2 of 3 replicas). Non-specific binding (white bars) was determined by pre-incubating the membranes with 1 mM unlabelled NAADP for 10 min before the addition of [^{32}P]NAADP to the reaction. Specific binding (black bars) was derived by subtracting non-specific binding from total binding. Results are normalized to the highest total binding value, ***P < 0.001 (1way ANOVA; post test: Dunnett's Multiple comparison Test).

5.2.1.2 Binding buffer

To optimize the binding buffer, mouse hepatic membranes (5 mg/ml) were incubated with 66 pM [^{32}P]NAADP in each of the buffers indicated in Table 5.2 for 1 h before separating bound from unbound by rapid filtration in wash buffer H. Buffers HK_{250} (63 ± 4.1%), HM (66 ± 4.3%), and $HK_{250}M$ (67 ± 4.8%) showed significantly increased % specific binding compared to Glu-IM (33 ± 2.3%; Figure 5.2A). A slight increase in % specific binding was also observed for buffer H (47 ± 1.4%), though this was not significant. Interestingly, despite a higher total binding observed in buffer HM compared to buffer $HK_{250}M$, the non-specific binding was also significantly increased (∼20%), resulting in similar % specific binding (Figure 5.2A).

Although buffer $HK_{250}M$ gave the highest % specific binding, the presence of $MgCl_2$ also increased non-specific binding, so buffer HK_{250} was chosen. However, 250 mM K^+ is 1.8-fold higher than that in the intracellular mammalian medium (∼140 mM), so a binding buffer consisting 20 mM HEPES and 140 mM potassium acetate (HK_{140}) was therefore tested against buffer HK_{250} to assess the effect of K^+ concentration on specific binding. Figure 5.2B shows that % specific binding was significantly higher (9%) in buffer HK_{140} relative to buffer HK_{250}. Thus, buffer HK_{140} was selected as the binding buffer for subsequent binding assays as it gave a high % specific binding and its ionic composition is more mammalian friendly.

Buffer optimization for the mammalian system has not been reported before. Results from this section revealed that by altering the composition of the wash and binding buffers, the specific binding of NAADP could be increased by at least 50%.

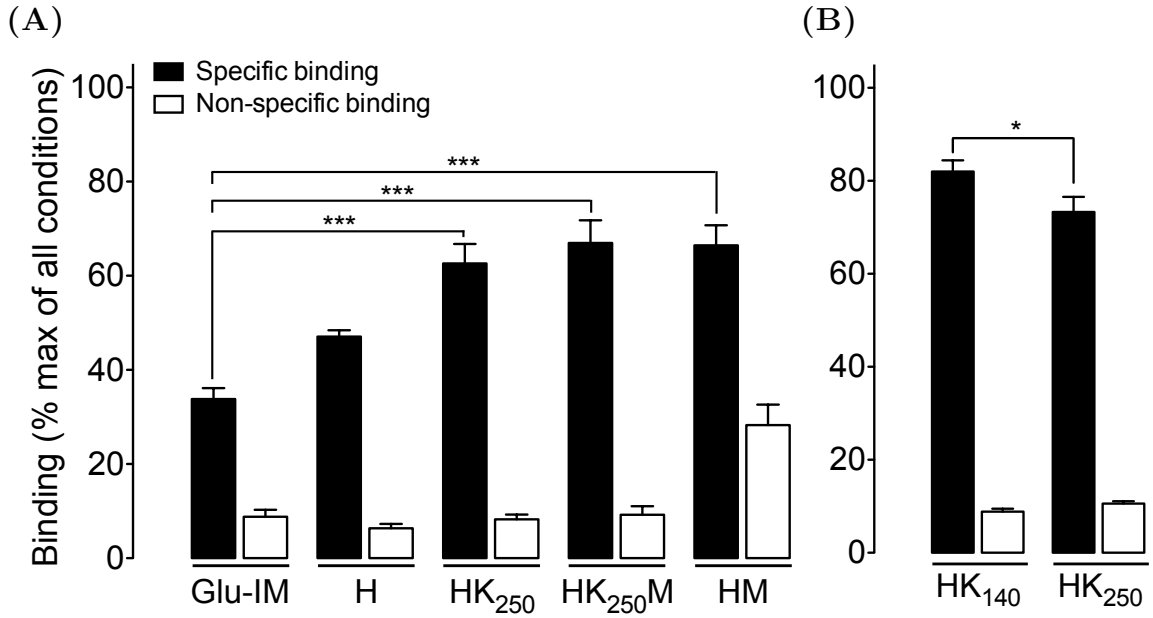

Figure 5.2: Effect of binding buffer ionic compositions on [^{32}P]NAADP binding in mouse hepatic membranes. Total binding was determined by incubating mouse hepatic membranes with 66 pM [^{32}P]NAADP in (A) the five binding buffers: Glu-IM, H, HK_{250}, HK_{250}M and HM for 1 h prior to rapid filtration with wash buffer H (n = 2 of 3 replicas). (B) Effect of lowering K^+ concentration in HK_{250} binding buffer from a non-mammalian-physiological concentration of 250 mM to 140 mM in HK_{140} (n = 3 of 3 replicas). Non-specific binding (white bars) was determined by pre-incubating membranes with 1 mM unlabelled NAADP for 10 min before the addition of [^{32}P]NAADP. Specific binding (black bars) was derived by subtracting non-specific binding from total binding. Results are normalized to the highest total binding value, ***P < 0.001 and *P $<$ 0.05 (1way ANOVA; post test: Dunnett's Multiple comparison Test).

5.2.2 Kinetic binding studies

Analyses of radioligand binding experiments were based on the law of mass action: the rate of a reaction is proportional to the product of the concentrations of the reactants. Thus, the rate of association = k_{on}·[Ligand]·[Receptor] and the rate of dissociation = k_{off}·[Ligand·Receptor] where k_{on} and k_{off} are the association and dissociation rate constants:

$$[Ligand] + [Receptor] \underset{k_{off}}{\overset{k_{on}}{\rightleftharpoons}} [Ligand \cdot Receptor] \tag{5.1}$$

At equilibrium, the rate of association equals the rate of dissociation:

$$[Ligand] \cdot [Receptor] \cdot k_{on} = [Ligand \cdot Receptor] \cdot k_{off} \tag{5.2}$$

and the equilibrium dissociation constant (K_d) which measures the affinity of a ligand to the receptor can then be determined by rearranging Equation 5.2:

$$\frac{[Ligand] \cdot [Receptor]}{[Ligand \cdot Receptor]} = \frac{k_{off}}{k_{on}} = K_d \tag{5.3}$$

Thus, by obtaining k_{on} and k_{off} from kinetic binding studies, K_d can be evaluated.

The Glu-IM binding and wash buffers were improved to increase signal-to-noise ratio (Section 5.2.1). To assess the binding kinetics of [^{32}P]NAADP in the new buffers, dissociation and association binding assays were conducted.

5.2.2.1 Dissociation binding

Dissociation binding assays characterizes the interaction of [^{32}P]NAADP with the receptor and determine whether the binding of NAADP to its receptor is reversible. This also establishes the rate at which [^{32}P]NAADP dissociates from the receptor. Mouse hepatic membranes (5 mg/ml) were incubated with 66 pM [^{32}P]NAADP in buffer HK_{140} for 1 h to allow receptor·[^{32}P]NAADP complexes to form before dissociating [^{32}P]NAADP from the receptor by adding unlabelled NAADP (1 mM) at various time points.

Comparison of fitting models in GraphPad Prism suggested that the binding dissociated in two phases - a fast and a slow phase. 50% of bound [^{32}P]NAADP dissociated in 0.62 min for the fast and 72 min for the slow phase (Figure 5.3). The dissociation rate constant

of the fast phase ($k_{off.fast}$) was 1.118 ± 0.562 min^{-1} and of the slow phase ($k_{off.slow}$) was 0.0097 ± 0.0255 min^{-1}. After 90 min from the initial dissociation, 20% remained bound, possibly representing the % non-specific binding. It is important to note that $k_{off.fast}$ was greater than 1, indicating a low affinity of the ligand for the receptor. The fast dissociation suggests that NAADP binding complexes might dissociate during rapid filtration, which can potentially compromise subsequent data.

Overall, results revealed that in the new buffers, the binding of NAADP to the receptor was reversible, and that at least 50% of NAADP dissociated from the receptor in 60 min. This validated the use of the new buffers for the following competition binding assays.

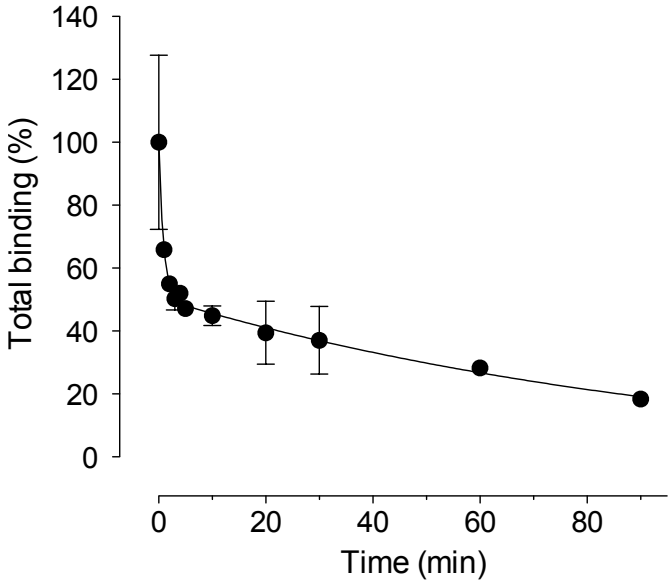

Figure 5.3: Dissociation binding of [^{32}P]NAADP in the mouse hepatic membranes using the new buffers. Mouse hepatic membranes (5 mg/ml) were incubated with 66 pM [^{32}P]NAADP in buffer HK_{140} for 1 h before initiating dissociation by addition of 1 mM unlabelled NAADP. Bound [^{32}P]NAADP was determined by rapid filtration with ice-cold buffer H after dissociating for the indicated times; n = 1 of 2 replicas.

5.2.2.2 Association binding

Association binding assays yield k_{on} values for further characterization of the interaction of [^{32}P]NAADP with the receptor. Mouse hepatic membranes (5 mg/ml) were incubated with 66 pM [^{32}P]NAADP in buffer HK_{140} at various time points in the presence or absence of unlabelled NAADP (1 mM).

Comparison of one- and two-site binding fits in GraphPad Prism suggests that NAADP binds to the receptor at two sites rather than at one. [^{32}P]NAADP reached half-maximal of the first phase at around 1.04 min, and of the second phase at around 24.8 min. The observed rate constants were 0.664 ± 0.173 min^{-1} for the fast phase ($k_{ob.fast}$), and 0.0279 ± 0.0092 min^{-1} for the slow phase ($k_{ob.slow}$) (Figure 5.4).

These results indicate that an incubation time of 60 min is likely to be sufficient for the subsequent saturation and competition binding assays.

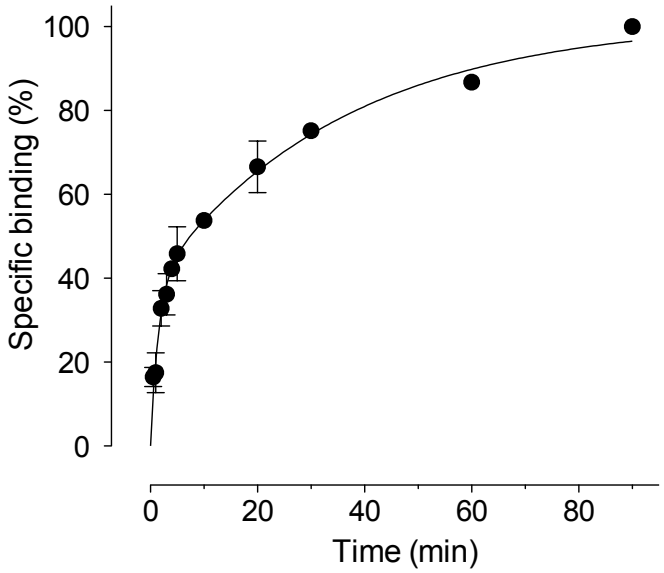

Figure 5.4: Association binding of [^{32}P]NAADP in mouse hepatic membranes using the new buffers. Mouse hepatic membranes (5 mg/ml) were incubated with 66 pM [^{32}P]NAADP in buffer HK_{140} for indicated times before rapid filtration with ice-cold buffer H. Non-specific binding was determined by addition of 1 mM unlabelled NAADP in the reaction. Specific binding was derived by subtracting non-specific binding from total binding; n = 1 of 2 replicas.

5.2.2.3 Calculation of k_{on} from k_{ob} obtained in association studies

The observed rate constant (k_{ob}) values obtained from the association assay (Section 5.2.2.2) together with the k_{off} values obtained from the dissociation assay (Section 5.2.2.1) allow the calculation of k_{on} values using:

$$k_{on} = \frac{k_{ob} - k_{off}}{[[^{32}P]NAADP]} \tag{5.4}$$

rearranged from:

$$k_{ob} = k_{on} \times [[^{32}P]NAADP] + k_{off} \tag{5.5}$$

In the dissociation assay, [^{32}P]NAADP was shown to dissociate in two phases. If [^{32}P]NAADP has a high affinity for the receptor, it should have a fast association and slow dissociation rate constant. However, the $k_{off.fast}$ obtained from the previous section was 1.12 min^{-1} which is greater than the $k_{ob.slow}$ (0.028 min^{-1}) and even than the $k_{ob.fast}$ (0.664 min^{-1}), thus k_{on} can not be derived from Equation 5.4. When $k_{off.slow}$ was used instead, $k_{on.fast}$ and $k_{on.slow}$ were determined to be 9.91 x 10^9 and 2.76 x 10^8 M^{-1}min^{-1}, respectively (Table 5.3).

Table 5.3 shows a summary of the k_{on} values derived, and the previously obtained k_{ob} and k_{off} values.

Rate constant	Value
Dissociation ($k_{off.fast}$)	1.118 min^{-1}
Dissociation ($k_{off.slow}$)	0.0097 min^{-1}
Observed ($k_{ob.fast}$)	0.664 min^{-1}
Observed ($k_{ob.slow}$)	0.0279 min^{-1}
Association ($k_{on.fast}$)	9.91 x 10^9 M^{-1}min^{-1}
Association ($k_{on.slow}$)	2.76 x 10^8 M^{-1}min^{-1}

Table 5.3: Binding kinetic summary of [^{32}P]NAADP for the receptor in optimised buffers determined by experimental data, and by calculation from Equation 5.5.

5.2.2.4 Evaluating K_d from association and dissociation rate constants

Using the obtained k_{on} and k_{off} values, K_d of NAADP to its receptor was calculated by using Equation 5.3. Where there were two k_{off} values, high affinity K_d was calculated from $k_{off.slow}$ and $k_{on.fast}$:

$$\text{High affinity } K_d = \frac{k_{off.slow}}{k_{on.fast}} \tag{5.6}$$

and low affinity K_d was calculated from $k_{off.fast}$ and $k_{on.slow}$:

$$\text{Low affinity } K_d = \frac{k_{off.fast}}{k_{on.slow}} \tag{5.7}$$

Using equations 5.6 and 5.7, the K_d value for the high affinity site was determined to be 0.98 pM, and for the low affinity site, 4.05 nM. Compared to the other reported affinities in mammalian systems (summarized in Table 5.1), these affinities are 1000-fold higher.

5.2.3 Saturation binding

Given the gross disparity between the K_d values derived from kinetic studies (above) and reported K_d values, it was decided to obtain directly K_d values by an alternative method, saturation binding. Saturation binding also allows determination of the number of binding sites (i.e. receptor density (B_{max}) in mouse hepatic membranes).

Saturation binding was conducted by incubating 5 mg/ml of the mouse hepatic membranes at various concentrations of [^{32}P]NAADP for 1 h to reach equilibrium in the presence or absence of unlabelled NAADP (1 mM). From the literature, NAADP binds biphasically in the nM and μM range. In order to saturate the low affinity site, the concentration of [^{32}P]NAADP would need to be $\geq$100 μM. However, the high level of specific activity at this concentration exceeds the departmental limitations.

Unsurprisingly, at 70 nM (the maximum permissible concentration to comply with regulations), the binding sites for NAADP were not saturated after 1 h incubation (Figure 5.5). This suggests that an alternative method is needed to determine the K_d of NAADP.

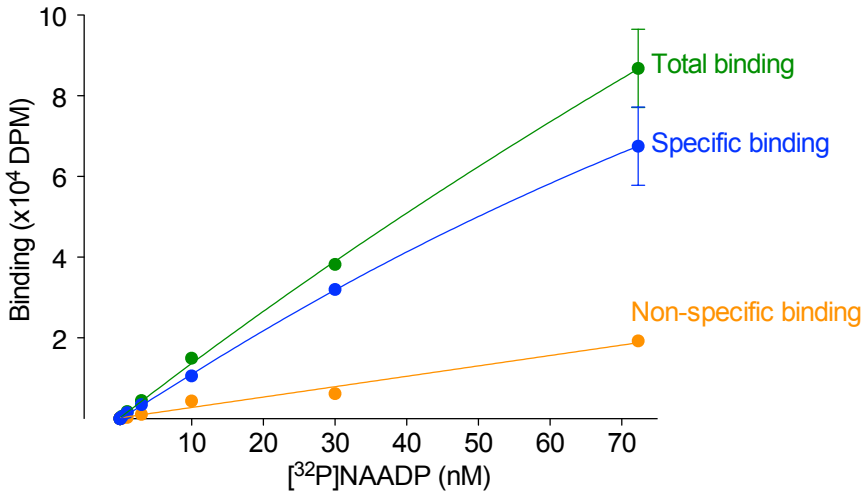

Figure 5.5: Saturation binding of [^{32}P]NAADP in the mouse hepatic membranes. Mouse hepatic membranes (5 mg/ml) were incubated with various concentrations of [^{32}P]NAADP in Glu-IM for 1 h before rapid filtration in ice-cold Glu-IM. Non-specific binding (orange) was determined by preincubating the membranes with 1 mM unlabelled NAADP for 10 min in the reaction before [^{32}P]NAADP addition. Specific binding (blue) was derived from subtracting non-specific binding from total binding (green); n = 1 of 2 replicas.

5.2.4 Competition binding of NAADP in the mouse hepatic membranes

The saturation binding study showed that in order for the K_d to be determined accurately by this technique, a concentration of greater than 70 nM [^{32}P]NAADP would be required. An alternative method, which overcomes this limitation, is to determine NAADP K_d by competition binding assays. Competition binding determines the affinities of unlabelled compounds indirectly, through quantifying the interference unlabelled ligand imposes on the binding of radioligand to the receptor. Even if the K_d could be obtained from the saturation binding, it still requires a substantial amount of [^{32}P]NAADP per experiment. Thus, competition binding offers a significant cost advantage over saturation binding.

5.2.4.1 Competition binding in the wild-type (WT) membranes

In competition binding assays, the K_d of NAADP to its receptor is determined by homologous competition binding in which [^{32}P]NAADP competes with increasing concentrations of unlabelled NAADP. Studies of NAADP binding in mammalian membranes indicated that NAADP binds to multiple sites. Although in some studies, data were fitted to a one-site model, in the others, a two-site model was used (summarized in Table 5.1, [16, 52, 178, 215]). In a standard implementation [^{32}P]NAADP would compete with unlabelled NAADP at twelve different concentrations. However, it is sometimes difficult to conclude whether there are two binding sites with curve from just twelve data points. So far, the most convincing evidence for the multiple binding sites was shown in mouse hepatic membranes; in this, two phases of NAADP binding were clearly observed [52].

To confirm that the curve is truly biphasic in this system, a competition binding assay with 24 concentrations of unlabelled NAADP was conducted. Competition binding of [^{32}P]NAADP to the WT mouse hepatic membranes revealed a distinct biphasic curve with K_d of 7.97 $\pm$ 2.47 nM for the high and 30.5 $\pm$ 11.3 μM for the low affinity site. Additionally, the amounts of NAADP binding to the high and the low affinity sites were roughly equal (Figure 5.6). This result clearly suggests that NAADP binding is indeed biphasic. Furthermore, consistent with the reported affinities from the two-site model [52, 178], the high and low affinities were in the nM and μM ranges, respectively.

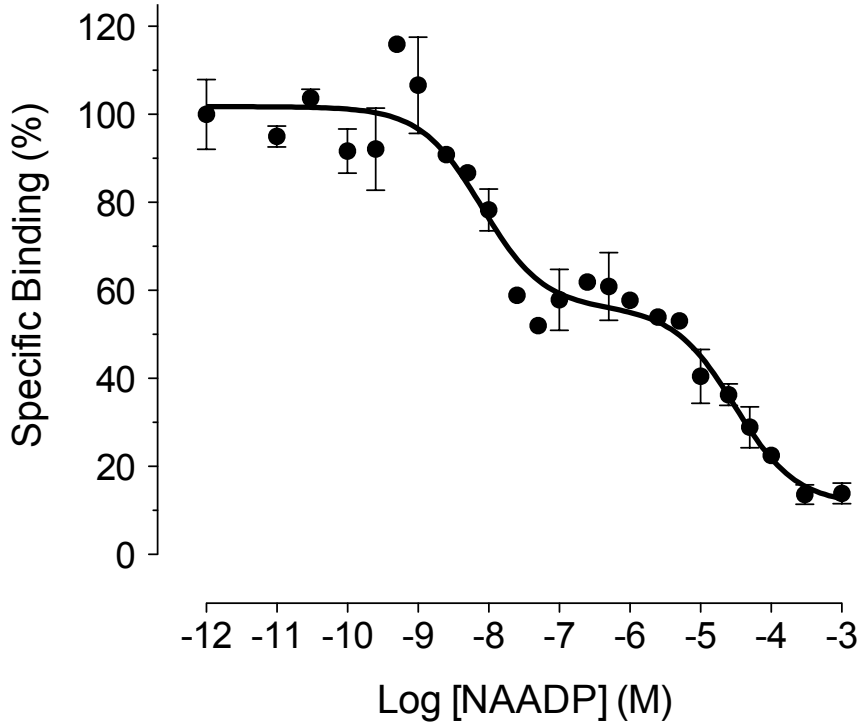

Figure 5.6: Competition binding of [^{32}P]NAADP in the WT mouse hepatic membranes. Mouse hepatic membranes (5 mg/ml) were incubated with 24 concentrations of unlabelled NAADP in buffer HK_{140} for 10 min prior to the addition of 66 pM [^{32}P]NAADP. The reaction was incubated for 1 h before rapid filtration with ice-cold buffer H; n = 1 of 2 replicas.

5.2.4.2 Specificity of NAADP-binding protein for NAADP in WT membranes

To examine the specificity of the NAADP-binding protein for NAADP, [^{32}P]NAADP was competed with an established NAADP antagonist (Ned-19) [200], its derivatives (NAD, NAAD (Nicotinic Acid Adenine Dinucleotide), NADP), and other intracellular Ca^{2+} mobilizing messengers (cADPR, $InsP_3$, and ryanodine).

Ned-19 is a hydrophobic compound and at high concentrations, Ned-19 must be dissolved in 10% DMSO. Interestingly, Ned-19 did not compete with [^{32}P]NAADP in the mouse hepatic membranes (Figure 5.7A) despite the similarity of its three-dimensional shape and electrostatic properties to NAADP, and the fact that it has been shown to compete with NAADP in sea urchin homogenate [200]. This is the first evidence of Ned-19 not competing with NAADP in a mammalian system. It should be noted that unlabelled NAADP in 10% DMSO still competed with [^{32}P]NAADP biphasically; however, the K_d was approximately 10-fold higher than previous reports (high affinity: 36.3 ± 11.18 nM and low affinity: 47.5 ± 28.6 μM).

Consistent with previous findings [16, 52, 215], of all the compounds tested, only NADP competed with [^{32}P]NAADP (Figure 5.7B and 5.7C). Instead of binding biphasically (like NAADP), NADP only bound to the low affinity site, with K_d of 4.07 ± 0.48 μM. This suggests that the high affinity site of the NAADP-binding protein was selective for NAADP, in contrast, the low affinity site was non-selective and likely to bind to other nucleotides. Alternatively, this may be due to the contamination with NAADP in the commercial sources of NADP [153].

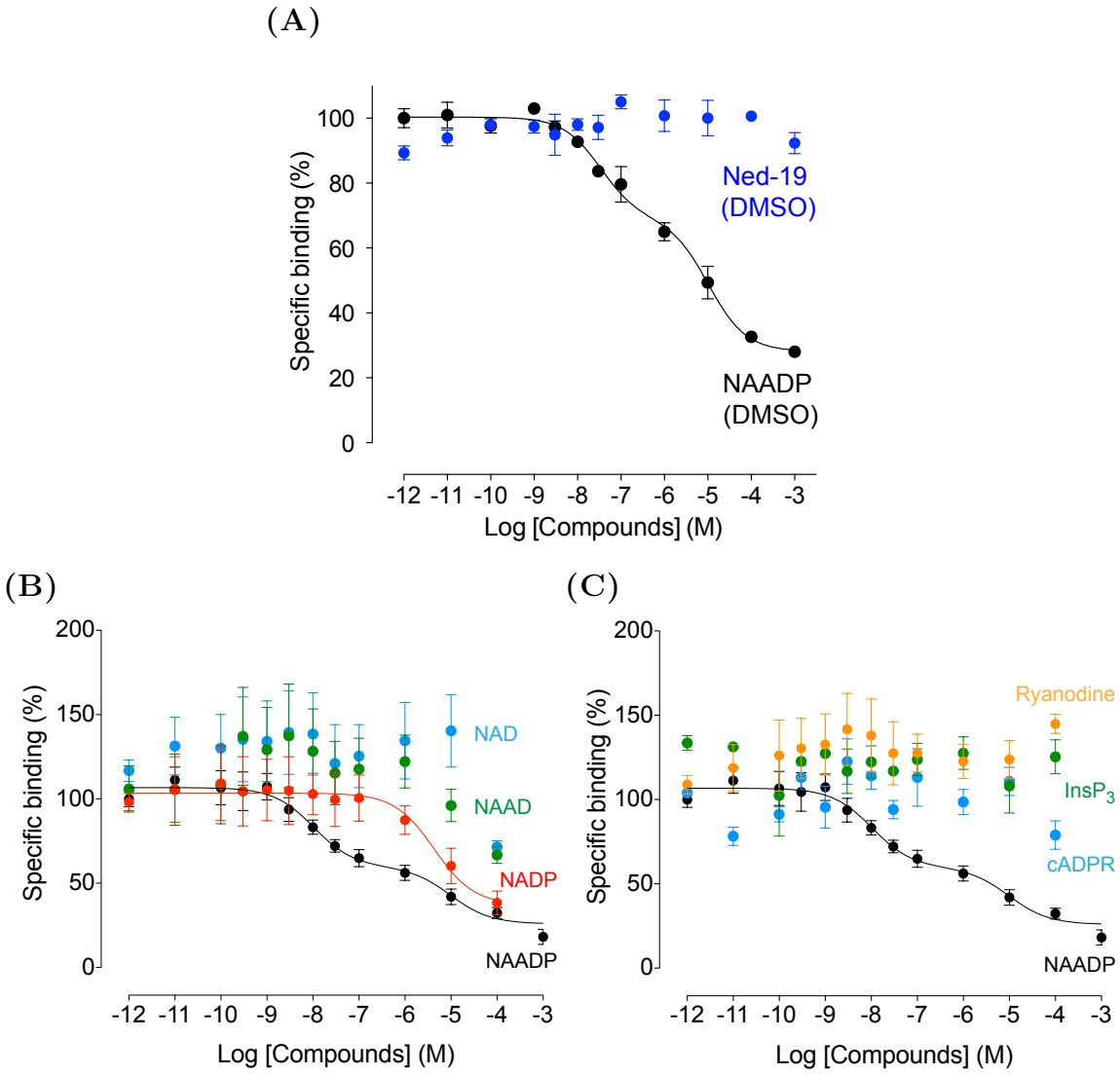

Figure 5.7: Competition binding of [^{32}P]NAADP with various concentrations of (A) unlabelled NAADP (black), and an established NAADP antagonist, Ned-19 (blue) in 10% DMSO, (B) unlabelled NAADP (black), its derivatives (NAD (blue), NAAD (green), NADP (red)), and (C) unlabelled NAADP and other intracellular Ca^{2+} mobilizing messengers (cADPR (blue), $InsP_3$ (green), and ryanodine (orange)) in WT mouse hepatic membranes. WT mouse hepatic membranes were incubated with unlabelled compounds for 10 min before an addition of 200 pM [^{32}P]NAADP in Glu-IM. The reaction was incubated for 1 h before rapid filtration in ice-cold Glu-IM. Non-specific binding was determined by pre-incubating the membranes with 1 mM unlabelled NAADP in the reaction before [^{32}P]NAADP addition. Specific binding was determined by subtracting non-specific binding from total binding; n = 1-3 of 2 replicas.

5.2.4.3 Competition binding in TPC single knockout (KO) membranes

Although both TPC1 and TPC2 have been shown to be NAADP-gated Ca^{2+} channels [39, 41, 42, 52, 217, 243, 307], the molecular identity of the NAADP-binding protein remains unclear. In the previous sections, assay buffers were improved, and it was established that mouse hepatic membranes constitute a good system for investigating mammalian NAADP binding. By applying this assay technique to TPC KO mice (characterized in Chapter 3), it is possible to examine the binding property of individual TPCs to NAADP in an endogenous system, and to examine the effect of knocking out one TPC on the specific binding of NAADP.

TPC1 KO. Incubation of the mouse hepatic membranes with 66 pM [^{32}P]NAADP in the presence and absence of unlabelled NAADP (1 mM) showed that in the TPC1 KO membranes, specific binding was 46% higher than WT (Figure 5.8A, left); however, this increase was not statistically significant.

The increased specific binding of [^{32}P]NAADP in the TPC single KO membranes raises the question as to whether the K_d of NAADP to its receptor has altered. Competition binding of radioligand [^{32}P]NAADP with various concentrations of unlabelled NAADP showed that knocking out TPC1 did not have a significant effect on the K_d of NAADP. NAADP still bound biphasically to the TPC1 KO membranes with similar K_d (1.39 ± 0.59 nM for the high and 10.4 ± 4.29 μM for the low affinity site) to the WT (2.14 ± 0.86 nM and 5.53 ± 1.47 μM for the high and low affinity sites, respectively; Figure 5.8A, right). Interestingly, the high affinity fraction was increased from 0.32 ± 0.03 in the WT to 0.44 ± 0.05 in the TPC1 KO, which correlates well with the slight increase in specific binding observed in the TPC1 KO membranes.

TPC2 KO. In TPC2 KO, there was also no significant difference in the specific binding of NAADP between the TPC2 KO and WT membranes (96.3 ± 12.8 and 100 ± 0.00 %, respectively; Figure 5.8B, left).

Knocking out TPC2 also did not alter the K_d of NAADP. NAADP bound biphasically to the TPC2 KO membranes with similar K_d (1.69 ± 1.07 nM for the high and 4.88 ± 2.30 μM for the low affinity site) as the WT (2.88 ± 1.33 nM and 6.85 ± 2.80 μM for the

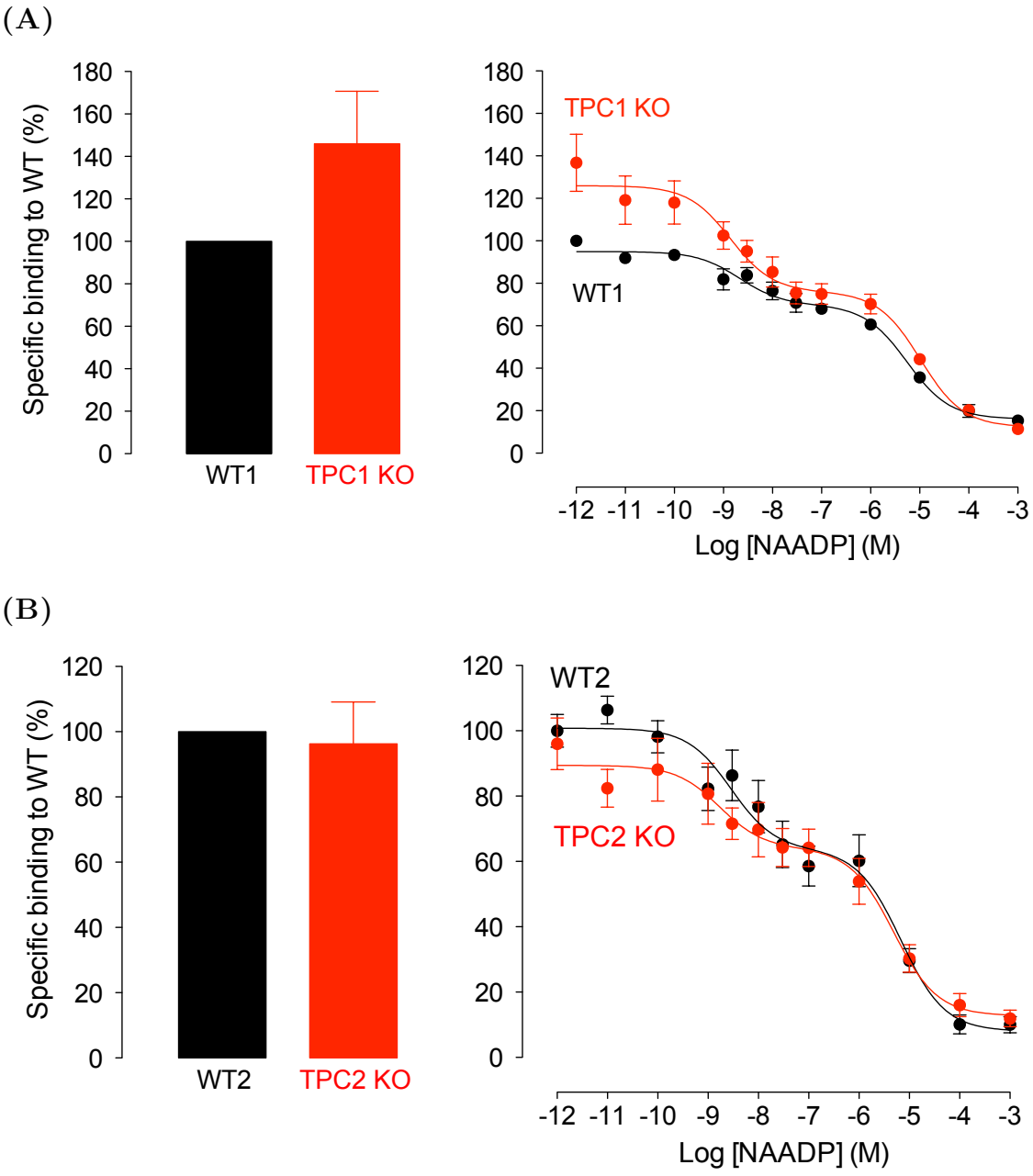

Figure 5.8: Left, specific binding of [^{32}P]NAADP in the (A) WT1 and TPC1 KO, and the (B) WT2 and TPC2 KO mouse hepatic membranes. Right, competition binding of 66 pM [^{32}P]NAADP in (A) WT and TPC1 KO, and (B) WT and TPC2 KO mouse hepatic membranes with various concentrations of unlabelled NAADP. Black bars or traces represent the WT whereas red bars or traces represent TPC single KOs. The reaction was incubated for 1 h in buffer HK_{140} before rapid filtration in ice-cold buffer H. Non-specific binding was determined by pre-incubating the membranes with 1 mM unlabelled NAADP in the reaction for 10 min before [^{32}P]NAADP addition. Specific binding was determined by subtracting non-specific binding from total binding. Results are normalized to the WT maximal specific binding; n = 4 of 2 replicas.

high and low affinity sites, respectively; Figure 5.8B, right). The high affinity fraction was also not significantly altered (WT: 0.40 ± 0.05, TPC2 KO: 0.33 ± 0.07).

Overall, these results revealed that knocking out one TPC isoform in the mouse hepatic membranes did not alter the binding affinity to NAADP; NAADP still bound specifically with the K_d as reported in the literature. As mouse liver expresses both TPC1 and TPC2 (Figure 3.7A and 3.17A), it is possible that NAADP binds to the remaining TPC in the TPC single KO membranes. Alternatively, it is possible that NAADP might bind to the accessory protein in TPC complexes, in which case knocking out TPCs would not affect binding. The increased level of specific binding in the TPC1 KO membranes may be due to compensatory mechanisms (e.g. up-regulating TPC2 or accessory protein(s)).

5.2.4.4 Competition binding in the TPC double knockout (DKO) membranes

To ascertain whether the NAADP binding observed in TPC single KOs was due to compensation by the remaining TPC or the accessory protein in the TPC complexes, NAADP binding in the TPC double knockout (DKO) membranes was studied. Incubation of the membranes with 66 pM [^{32}P]NAADP in the presence or absence of 1 mM unlabelled NAADP revealed that NAADP still bound to the TPC DKO membranes. The binding was specific with no significant difference to WT (108 ± 14.6 and 100 ± 0.0%, respectively; Figure 5.9, left).

Competition bindings showed no significant change in either NAADP affinity for its receptor (K_d of 3.52 ± 1.16 and 3.32 ± 1.46 nM for the high and 6.56 ± 2.50 and 3.41 ± 1.98 μM for the low affinity site in WT and TPC DKO, respectively), or in the binding fractions for the high affinity sites (0.485 ± 0.043 compared to 0.536 ± 0.069, for WT and TPC DKO, respectively; Figure 5.9, right). Results of NAADP binding in all WT and TPC single and double KO mouse hepatic membranes are summarized in Table 5.4.

Studies in TPC DKO membranes provide the first direct evidence that TPC is not the binding protein for NAADP. Thus, NAADP is likely to bind to an accessory protein in TPC complexes.

	K_d (high affinity, nM)	K_d (low affinity, μM)	High affinity fraction
WT1	2.14 ± 0.86	5.53 ± 1.47	0.32 ± 0.03
TPC1 KO	1.39 ± 0.59	10.4 ± 4.29	0.44 ± 0.05
WT2	2.88 ± 1.33	6.85 ± 2.80	0.40 ± 0.05
TPC2 KO	1.69 ± 1.07	4.88 ± 2.30	0.33 ± 0.07
WTD	3.52 ± 1.16	6.56 ± 2.50	0.49 ± 0.04
TPC DKO	3.32 ± 1.46	3.41 ± 1.98	0.54 ± 0.07

Table 5.4: Summary of the K_d values of NAADP for the binding complexes in the WT, and TPC single and double KO mouse hepatic membranes.

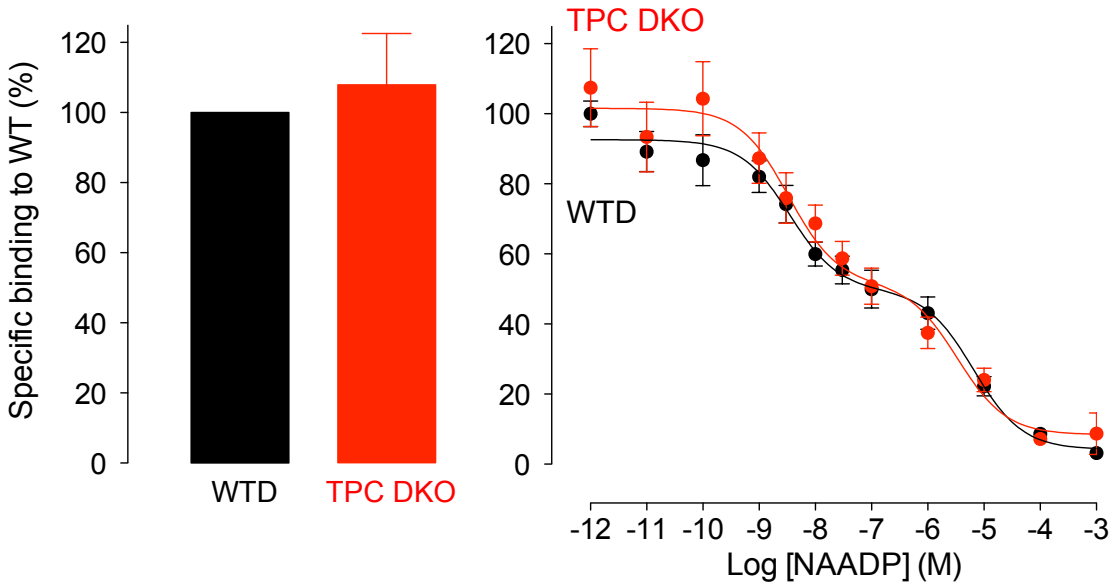

Figure 5.9: Left, specific binding of [^{32}P]NAADP in the WTD and TPC DKO mouse hepatic membranes. Right, competition binding of 66 pM [^{32}P]NAADP in WTD and TPC DKO mouse hepatic membranes with various concentrations of unlabelled NAADP. The black bar and trace represent the WT whereas the red bar and trace represent TPC DKO. The reaction was incubated for 1 h in buffer HK_{140} before rapid filtration in ice-cold buffer H. Non-specific binding was determined by pre-incubating the membranes with 1 mM unlabelled NAADP in the reaction before [^{32}P]NAADP addition. Specific binding was determined by subtracting non-specific binding from total binding. Results are normalized to the WT maximal specific binding; n = 4 of 2 replicas.

5.3 Discussion

Prior to elucidating whether TPCs are the *bona fide* NAADP binding-protein, the buffers (based on Glu-IM) was improved. Buffer tests showed that a combination of 20 mM HEPES and 140 mM potassium acetate (HK_{140}) as the binding buffer, and 20 mM HEPES (H) as the wash buffer, significantly improved the signal-to-noise ratio (Figures 5.1 and 5.2). Different ionic composition in buffers can enhance or inhibit binding and can also increase or decrease the affinity of the radioligand for the receptor [50]. In this study, Mg^{2+} was shown to enhance the binding of [^{32}P]NAADP both specifically and non-specifically when binding buffer HM was used compared to H (Figure 5.2).

5.3.1 Kinetic binding studies in the improved buffers

Kinetic binding studies in the new buffers demonstrated that NAADP binding was still reversible, thereby validating the use of the new buffers for the subsequent binding studies. In this study, the binding of NAADP to its binding protein was shown to dissociate in pH 7.2 buffers. However, in the single-channel study, NAADP-activated channel opening in immunopurified TPC2 complexes was shown to be irreversible at pH 7.2, but reversible at pH 4.8 [231]. The conflicting results may be explained by the duration of the experiments. In the single channel studies, the dissociation was examined within seconds, whereas in radioligand binding studies, the dissociation was examined over minutes/hours. If dissociation is slow, it might not be observed within the timescale of the single channel studies.

Association studies showed that NAADP associates in two phases, and that an incubation of 60 min was probably sufficient for the subsequent binding studies. The time required for NAADP to bind to half of the binding sites in the fast phase in the mouse hepatic membranes (1.04 min for 66 pM [^{32}P]NAADP) is comparable to a previously reported time, 0.6 min in rabbit cardiac microsomes, with 150 pM [^{32}P]NAADP [16]. Binding (i.e. Ligand·Receptor complex) occurs when a ligand randomly collides with the receptor with sufficient energy and in the correct orientation. Equilibrium is reached when the rate of formation ([Ligand]·[Receptor]·k_{on}) equals the rate of dissociation ([Ligand·Receptor]·k_{off}) Ligand·Receptor (Equation 5.2). A higher concentration of [^{32}P]NAADP increases the number of random collisions, and in theory, the rate of association would also increase

(i.e. by 2.27-fold for 150 pM instead of 66 pM [^{32}P]NAADP·[Receptor]·k_{on}), and a shorter time would be required to reach the equilibrium.

With an increase in rate by 2.27-fold, one would expect the half-life to be 0.46 min rather than 0.6 min for 150 pM [^{32}P]NAADP. The longer time required may be explained by the fact that the experiment was performed on ice, and therefore the rate of association would be slower. Furthermore, the association occurred in one phase, rather than two, in rabbit cardiac microsomes [16], possibly due to the differences in species and/or tissue type. Surprisingly, the half-life for NAADP to associate in the rat brain membranes was 10-fold longer, although the binding was done with a higher concentration of [^{32}P]NAADP (1 nM) and at a higher temperature (37 °C) [215]. With a higher concentration and temperature, one would expect binding to occur at a much higher rate. It is possible that the first phase was reached within the first minute, and this cannot be detected accurately by rapid filtration. Thus, the study mainly measured the slow phase of NAADP association.

The rate constants obtained from the kinetic studies (Table 5.3) can be useful in characterizing the interaction between NAADP and its binding protein. If the law of mass action is obeyed then the K_d of NAADP to its receptor can be accurately calculated by k_{off} over k_{on} (Equation 5.3). The calculated K_d (Section 5.2.2.4), however, did not match previously reported values well (Table 5.1 and Section 5.2.4.1). The apparent discrepancies might suggest that the binding of NAADP to its receptor did not follow all the assumptions inherent in the law of mass action (which includes: all receptors are equally accessible to ligands; all receptors are either free or bound to ligand; neither ligand nor receptor are altered by binding; and reversible binding [196]). Alternatively, the dissociation studies may have underestimated the $k_{off.fast}$. Assuming the $k_{on.slow}$ was accurate, $k_{off.fast}$ would need to be $\sim$300 min^{-1} to obtain a K_d in the μM range. This rate is probably too high to be accurately determined by rapid filtration. Furthermore, as the rate constants were derived from duplicates of a single experiment, future studies with more repeats are necessary to confirm accurate values.

5.3.2 TPCs are not the direct NAADP-binding proteins

It has already been established that NAADP binds to TPC complexes [52, 243]. The most important question now is whether NAADP binds directly to TPCs, or to accessory proteins in TPC complexes to activate the channels? Competition binding of NAADP to TPC DKO hepatic membranes provided the first direct evidence that TPC is not the binding target for NAADP. Knocking out both TPCs had no effect on the magnitude of specific binding, the K_d, or the binding fractions of each affinity compared to WT (Figure 5.9). If TPC is the binding protein for NAADP, knocking out either TPC isoform would have reduced the total level of specific binding, and the binding fraction of the higher affinity site. However, the level was not significantly altered in membranes of TPC1 and TPC2 single KO compared to the WT (Figure 5.8).

The fact that NAADP binds to an accessory protein tightly associated in the TPC complexes, rather than directly to TPCs, explains why the specific binding in the membranes overexpressing human TPC2 increased by only 3-fold while there was a more than 250-fold increase in TPC2 mRNA [52]. The limiting factor was the NAADP-binding protein and not TPC itself. When TPCs are overexpressed, the accessory protein that NAADP binds to may also become up-regulated. If the up-regulation was 3-fold compared to the WT (as implied by the increase in specific binding), this might suggest that more TPCs are activated by NAADP, and consequently there would be sufficient Ca^{2+} release from endo-lysosomes to initiate CICR. This would explain why a much larger Ca^{2+} response was observed in the TPC-overexpressing systems, despite the fact that TPC is not the binding protein.

5.3.3 Multiple binding sites for NAADP in mammalian systems

In this chapter, the observation of two prominent fractions in competition binding with unlabelled NAADP at 24 various concentrations clearly demonstrated that NAADP binds biphasically with both a high (nM) and a low (μM) affinity (Figure 5.6). This is consistent with some previous findings [52, 178], but not with studies that suggested at least three sites [16]. In all previous NAADP binding studies, only twelve concentrations of unlabelled NAADP were used to cover a wide range (eight log units) and for multiple-phase fittings. The low number of data points over a large scale might introduce ambiguity

when attempting to infer the number of binding sites.

The study by Bak *et al.* reported at least three binding sites [16], two with high affinity (130 pM and 4 nM) and one low (μM) affinity. As the magnitudes of the two high affinity sites were very similar, and so it is not entirely clear that these were truly distinct sites. Although the biphasic model appears to be the most suitable for NAADP binding, it is possible that NAADP binds with different numbers of phases (affinities) depending on the tissue types and species.

5.3.4 Biphasic binding models

How does NAADP bind to the accessory protein in TPC complexes and thus induce TPC activation? It may be assumed that NAADP binds biphasically to its binding protein in TPC complexes. The biphasic binding could be due to either a single binding site with two conformational stages, or two separate binding sites. Each biphasic binding model will be discussed in the following sections.

5.3.4.1 Scenarios of one binding site with two conformational stages

In the literature, two possible scenarios have been proposed for singe-site binding with two conformational stages: the GTP-dependent regulatory protein (G protein) interaction scenario, and the receptor isomerization scenario.

1. The G protein interaction scenario describes the interaction of a G protein-coupled receptor (GPCR) with a G protein after agonist stimulation:

$$[Agonist]+[Receptor] \rightleftarrows [Agonist{\cdot}Receptor]+[G] \rightleftarrows [Agonist{\cdot}Receptor{\cdot}G] \quad (5.8)$$

   In the case of NAADP-induced TPC activation, TPC is assumed to act like the G protein (see below; Equation 5.9).

When the GPCR is activated, agonist binding to the GPCR (Agonist + Receptor) alters the interaction of the receptor (Agonist·Receptor) with its coupled G protein (G). In the first part of the equilibrium where [Agonist] + [Receptor] $\rightleftarrows$ [Agonist·Receptor], when Agonist·Receptor binds to the G protein, the Agonist·Receptor is effectively 'lost' in the first equilibrium. The reaction will now be driven to the right to form more

Agonist·Receptor complexes, resulting in a higher rate k_{ob} and therefore k_{on}, providing that the [Agonist] and k_{off} remain constant. A higher k_{on} and a constant k_{off} lead to a lower K_d (i.e. a higher affinity; Equation 5.3).

Figure 5.10A shows that addition of G protein increases the affinity by a factor of 600 if there is no limitation in the ratio of receptors to G proteins [95, 134]. Additionally, Figure 5.10B shows that if the availability of G proteins is limiting (for example, in recombinant systems where the number of receptors exceeds the number of G proteins), a biphasic competition curve would be observed. The high affinity site represents the binding of Agonist·Receptor to the G proteins, and the lower affinity site measures the true affinity of the agonist to the receptor in the absence of the binding to G proteins [63, 134]. The high affinity phase arises from the formation of ternary complexes (Agonist·Receptor·G) that can sometimes be misinterpreted as another binding site.

In the case of NAADP-induced TPC activation, binding of NAADP to the accessory protein would change its interaction with TPC, and result in channel activation:

$$[NAADP] + [Protein] \rightleftarrows [NAADP \cdot Protein] + [TPC] \rightleftarrows [NAADP \cdot Protein \cdot TPC] \tag{5.9}$$

The high affinity state of the biphasic curve would reflect the binding of NAADP·Protein to TPC, and the lower affinity state would reflect the binding of NAADP to the protein (solid line in Figure 5.10C). Thus, in TPC DKO (dotted line in Figure 5.10C), the absence of TPCs should mirror the absence of G protein and the high affinity state should no longer exist. However, the results showed that NAADP still binds biphasically to the TPC DKO membranes (Figure 5.9), so this scenario is rejected.

2. The other scenario involves binding at one site with two conformational stages and is termed the receptor isomerization mechanism. This is where the binding of an agonist to the receptor alone induces a conformational change that induces the signal:

$$[Agonist] + [Receptor] \rightleftarrows [Agonist \cdot Receptor] \rightleftarrows [Agonist \cdot Receptor^*] \tag{5.10}$$

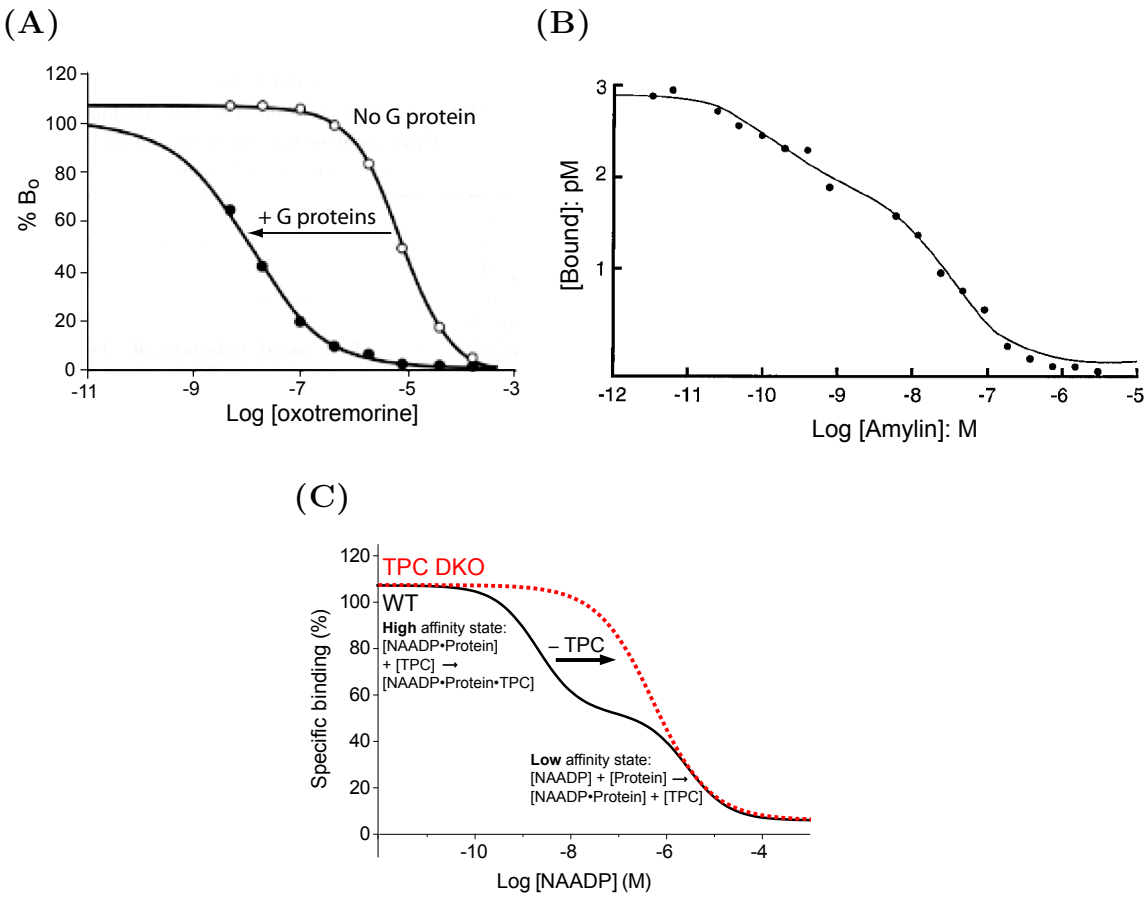

Figure 5.10: Effect of G proteins on the affinity of the compounds for GPCRs in the competition binding assays. (A) Competition binding of the antagonist [^{3}H]quinuclidinyl benzylate by the agonist oxotremorine for bovine muscarinic receptors in the presence (•) and absence (○) of G proteins. The addition of G proteins shifted the curve to the left i.e. increased the affinity by a factor of 600. The graph is taken from [134]. (B) Competition binding of the antagonist [^{125}I]AC512 by the agonist amylin for human calcitonin receptors in MCF-7 cells in a G protein limited system. Overexpression of the receptors diminished the available G proteins in the system and the resulting affinity of agonist for the receptor becomes biphasic. The graph is taken from [63]. (C) Hypothetic biphasic binding of NAADP to its target protein based on the G protein interaction scenario (Equation 5.9). It is hypothesized that binding of NAADP to the protein changes its interaction with TPC, and results in channel activation. In the WT (solid line), the high affinity state is represented by the binding of NAADP·Protein to TPC, and the low affinity state is represented by the binding of NAADP to the protein. This hypothesis is unlikely to be the case for NAADP-induced TPC activation, as the loss of TPC in TPC DKO (dotted line) would shift the affinity of NAADP significantly to the right.

Nicotinic acetylcholine receptor channels have been reported to isomerize (between R and R* states), and depending on its conformation, has either a high or a low affinity for acetylcholine [13]. Specifically, R* has a high affinity for acetylcholine (predicted K_d of ∼20 nM) and R has a low affinity (predicted K_d of ∼140 μM) [13].

Figure 5.11 shows that NAADP-induced TPC activation is better described by the receptor isomerization mechanism:

$$[NAADP]+[Protein{-}TPC] \rightleftarrows [NAADP{\cdot}Protein{-}TPC] \rightleftarrows [NAADP{\cdot}Protein^{*}{-}TPC] \tag{5.11}$$

The NAADP-binding protein appears to be very tightly bound to TPCs [52, 243], such that binding of NAADP to Protein–TPC induces conformational changes and consequent activation of the channel. The low affinity site reflects the initial binding of NAADP to Protein–TPC complexes to form NAADP·Protein–TPC, while the high affinity site reflects the binding of NAADP to the isomerized Protein*–TPC. The binding of NAADP to the isomerized complexes leads to channel activation.

In TPC DKO, the NAADP binding profile was almost identical to that of the WT (Figure 5.9); this might be because NAADP could still bind with low affinity to the accessory protein (NAADP·Protein), and with high affinity to the isomerized accessory protein (NAADP·Protein*). This isomerization, however, does not lead to channel activation as there is no TPC. This scenario is depicted in Figure 5.11B.

5.3.4.2 Scenarios of two separate binding sites

In addition to the receptor isomerization scenario, the biphasic binding may be due to two separate binding sites on the same binding protein, as shown in Figure 5.12.

In sea urchin, NAADP has been proposed to bind at two sites: a high-affinity inhibitory allosteric site at subthreshold NAADP concentrations (inactivation), and a low-affinity orthosteric site for the Ca^{2+} release (Figure 1.11) [214, 241]. Based on the models in sea urchin [214, 241], Figure 5.12 shows a proposed model for the mammalian system. At low concentrations, NAADP binds at the high-affinity orthosteric site on the binding protein, which opens the channel, while at high concentrations, NAADP binds at the low-affinity allosteric site on the binding protein, and thus closes the channel.

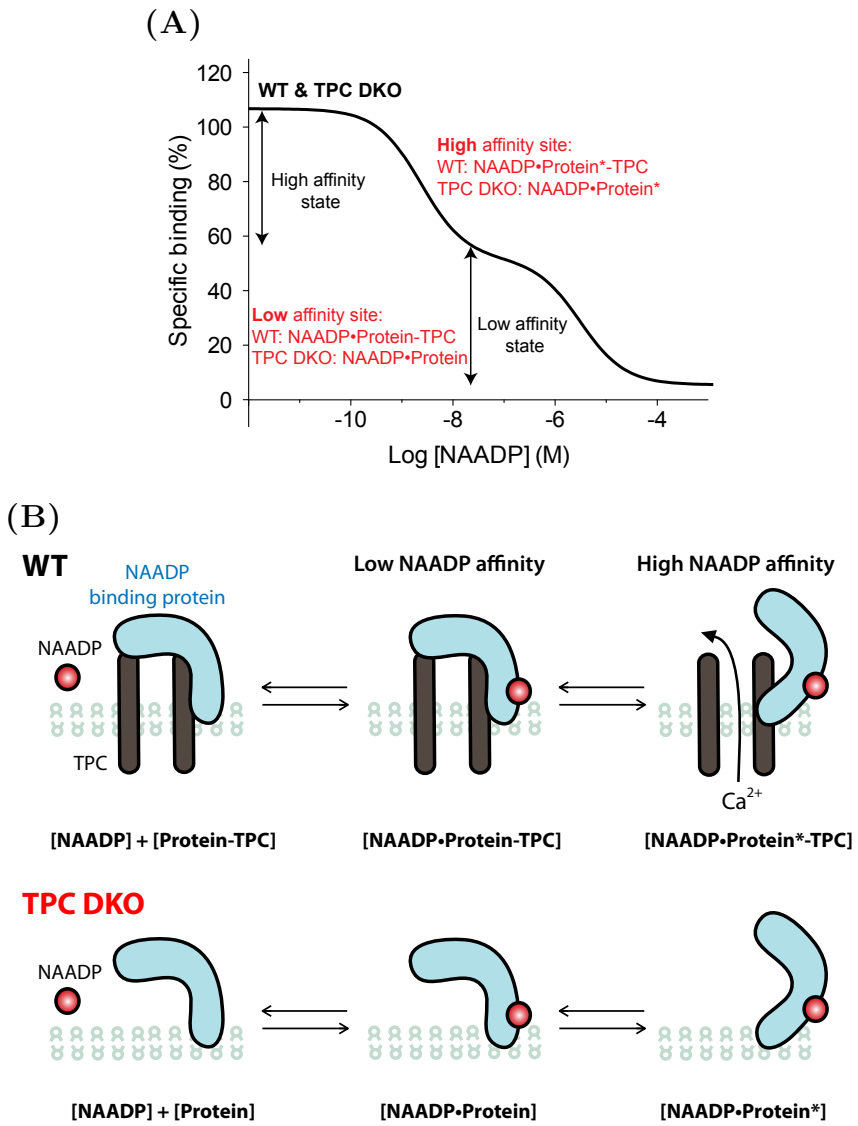

Figure 5.11: (A) Hypothetic model of the biphasic binding of NAADP to its receptor based on the receptor isomerization mechanism (Equation 5.11). (B) In this scenario, the binding of NAADP to the tightly associated Protein-TPC complex (NAADP·Protein–TPC) induces the isomerization of this complex (NAADP·Protein*–TPC) and leads to the channel opening. The two affinities observed in competition binding may be explained by the complex formation. The low affinity state is represented by NAADP·Protein–TPC whereas the high affinity state is represented by NAADP·Protein*–TPC. A similar binding profile was observed in TPC DKO, as NAADP still bound with low affinity to the binding protein (NAADP·Protein), and with high affinity to the isomerized binding protein (NAADP·Protein*), even in the absence of TPC.

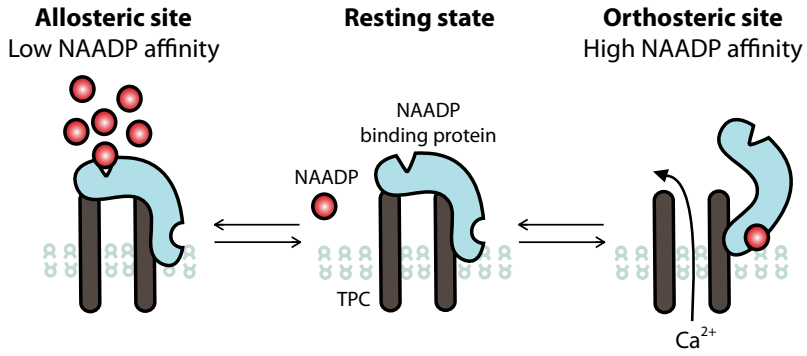

Figure 5.12: Schematic depicting the biphasic binding of NAADP at two separate binding sites on the same binding protein.

In summary, few models have been hypothesized to explain how TPCs may be activated by NAADP, even though TPCs were proposed not to be the NAADP-binding protein. As discussed above, the G protein interaction scenario is unlikely to apply in this case. Rather, models based on the isomerization scenario, together with the two separate binding site model are likely to accurately represent the mechanisms underlying NAADP-induced TPC activation.

5.3.5 NAADP-binding protein

The molecular identity of the NAADP-binding protein is unknown. However, it is known that the binding is conducted in membrane preparations, so the protein is predicted to be a membrane-integral or -peripheral protein. Additionally, the binding site is specific to NAADP, as the NAADP derivatives, cADPR, $InsP_3$, and ryanodine, did not compete with NAADP, consistent with previous finding [16]. Although NADP competed with NAADP with μM affinity, this may be attributable to the contamination with NAADP in the commercial sources of NADP [153]. Alternatively, the low affinity site on the binding protein might not be specific for NAADP.

5.3.6 Ned-19 binding

At low concentrations (1–100 nM), Ned-19 has been shown to directly activate TPC2 channels and also potentiate NAADP-evoked TPC2 channel opening, while at high concentrations ($\geq$1 μM), Ned-19 inhibited NAADP-evoked TPC2 opening [231]. This classic bell-shaped behaviour resembles that of NAADP-mediated Ca^{2+} release, suggesting

that Ned-19 may act on the same site as NAADP. However, the competition study in this chapter provided the first evidence that Ned-19 does not compete with NAADP in the mammalian system. This is in contrast to the situation with sea urchin egg homogenate in which Ned-19 was shown to compete with NAADP [200]. These apparently conflicting results could be explained as species-specific differences, and this might also help to explain why the NAADP concentration-response is different in the mammalian system (bell-shaped) compared to the sea urchin egg homogenate (high-affinity desensitization) (Section 1.5.1).

It is unclear where Ned-19 binds in the mammalian TPC complexes to exert its stimulatory and inhibitory actions; since Ned-19 does not compete with NAADP, it may or may not act on the NAADP-binding protein. Competition binding with Ned-19 analogues that do not compete with [^{32}P]NAADP in the sea urchin such as Ned-19.4 [241] may perhaps be useful in investigating the mechanisms of NAADP binding in mammalian system. Given the species differences, it might be that these Ned-19 analogues can compete with [^{32}P]NAADP in a mammalian system.

5.4 Conclusions

In radioligand binding assays, improvement of buffers from Glu-IM to more mammalian friendly buffers significantly increased the signal-to-noise ratio in mouse hepatic membranes. Using the improved conditions, competition binding with unlabelled NAADP at 24 various concentrations clearly showed that NAADP binds biphasically with a high (nM) and a low (μM) affinity to mouse hepatic membranes. This is consistent with previous findings on NAADP binding in mammalian systems [52, 178].

Preliminary experiment using Ned-19 showed that Ned-19 does not compete with NAADP in the mammalian system in contrast to the reported binding in the sea urchin egg membranes [200].

The most exciting discoveries were the findings that TPCs are not the direct binding protein for NAADP. This suggests that NAADP activates TPCs via binding to an accessory protein in the TPC complexes. The next crucial step to unravel the mechanisms underlying TPC activation is to identify the binding protein for NAADP.

Chapter 6

Role of TPCs in pancreatic acinar cells

6.1 Introduction

As discussed in Section 1.6, pancreatic acinar cells provide an ideal model system for studying intracellular Ca^{2+} release. They were also the first mammalian cell type to demonstrate that NAADP can evoke Ca^{2+} responses at low concentrations, and that it can self-inactivate at high concentrations. Furthermore, the concept that NAADP acts as a trigger was also hypothesized based on studies in pancreatic acinar cells [57]. It would therefore seem ideal to use this cell type as a model to study the endogenous role of TPCs.

By using its self-inactivating properties, it has been shown that various agonists employ different Ca^{2+} mobilizing messengers to evoke specific Ca^{2+} signals [57, 90, 103, 153, 178]. In pancreatic acinar cells, inactivating (high) concentrations of NAADP inhibited CCK- and NAADP-evoked Ca^{2+} spikes, but not those evoked by ACh, cADPR, or $InsP_3$. This strongly suggested that CCK, but not ACh, employs NAADP to evoke Ca^{2+} spikes [56, 57, 59]. Table 6.1 summarises the pharmacology of agonist-evoked Ca^{2+} spikes in pancreatic acinar cells.

The pharmacology shown in Table 6.1 is consistent with theory that different Ca^{2+} mobilizing messengers are produced in response to different secretagogue stimulations. CCK stimulation has been shown to increase NAADP and cADPR [294] but not $InsP_3$ levels [179]. Furthermore, and supporting the trigger hypothesis [36, 57, 58, 138], NAADP

	CCK	NAADP (nM)	cADPR	ACh	$InsP_3$
NAADP (100 μM)	●[57]	●[57]	○[57]	○[59]	○[57]
Bafilomycin A1 (150 nM [185] or 3 μM [293])	●[293]	●[293]	○[293]	○[293]/●[185]	○[293]/●[185]
GPN (50 μM [293] or 200 μM [185])	●[293]	●[293]	○[293]	○[293]/●[185]	○[293]

Table 6.1: Pharmacology of agonist (column)-evoked Ca^{2+} spikes in pancreatic acinar cells. Filled circles (●) indicate inhibition by various pharmacological agents (row), and open circles (○) indicate no effect.

was synthesized rapidly and transiently in response to CCK; more importantly, this synthesis occurred before the onset of Ca^{2+} signals [294]. Stimulation by the other secretagogue ACh, however, did not increase the NAADP, but rather cADPR and $InsP_3$ levels [289, 294].

It has been suggested that CD38 is the mammalian ADP-ribosyl cyclase (ARC) that is responsible for the synthesis of cADPR and NAADP [2, 74, 237]. In the pancreatic acinar cells of CD38 KO mice, CCK could no longer stimulate NAADP or cADPR production [74]. Additionally, CCK was not able to evoke Ca^{2+} oscillations in the absence of extracellular Ca^{2+} [74]. This suggests that the intracellular Ca^{2+} signalling pathway has been markedly remodelled and that the primary source of Ca^{2+} oscillations was now external Ca^{2+}.

To gain further insight into NAADP-mediated Ca^{2+} signalling, there is need for more chemical tools to inhibit NAADP signalling mechanisms beyond just NAADP self-activation. Although NAADP (at high concentrations) is specific and reliable in inhibiting mammalian NAADP-mediated Ca^{2+} signalling, it has the major disadvantage of not being cell-permeant. Sophisticated labour-intensive techniques, such as whole cell patching, microinjection, or tissue permeabilization, are therefore required to deliver NAADP into cells, so cell-permeant drugs would be highly beneficial.

NAADP-evoked Ca^{2+} release could potentially be inhibited at the Ca^{2+} store level (cf. thapsigargin for ER SERCA inhibitor), or at the receptor level (cf. heparin for $InsP_3R$, and 8-NH_2-cADPR for RyR). The discovery of reserve granules (lysosome-related organelles) in sea urchin eggs used as Ca^{2+} stores recruited by NAADP [70], led to subsequent findings that acidic stores are indeed the Ca^{2+} stores targeted by NAADP in mammals [40, 138, 293]. This discovery expanded the range of target sites for inhibitors of NAADP-mediated Ca^{2+} signalling. Pharmacological agents such as bafilomycin A1 (an

inhibitor of vacuolar H^+-ATPase) and GPN (osmotically lyses acidic stores) have been frequently used to differentiate Ca^{2+} release mediated by NAADP from that mediated by $InsP_3$ or cADPR (which primarily release Ca^{2+} from the ER).

The fact that in pancreatic acinar cells, Ca^{2+} spikes evoked by CCK and ACh are mediated by different Ca^{2+} mobilizing messengers implies that different Ca^{2+} stores are associated with different agonist-evoked Ca^{2+} signals. Indeed, Yamasaki *et al.* showed that bafilomycin A1 and GPN were able to inhibit Ca^{2+} spikes in response to photolysis of microinjected caged NAADP but not to caged $InsP_3$ or cADPR [293]. Yamasaki *et al.* further showed that CCK-mediated Ca^{2+} oscillations were dependent on acidic stores, as oscillations were abolished by bafilomycin A1 and GPN. In contrast, ACh-mediated Ca^{2+} oscillations persisted in the presence of these two drugs, thereby suggesting that ACh does not release Ca^{2+} from the acidic stores [293].

Interestingly, another study demonstrated that $InsP_3$-induced spiking was sensitive to bafilomycin A1 but not to GPN in whole-cell patched pancreatic acinar cells. In this study, the authors concluded that $InsP_3$ also releases Ca^{2+} from the acidic stores (most likely zymogen granules) but not from lysosomes, as GPN had no significant effect [185] (Table 6.1). Zymogen granules are acidic stores that can contribute to Ca^{2+} spiking [273], and are therefore susceptible to bafilomycin A1, which collapses the proton gradient. GPN only targets cathepsin-C containing lysosome-related organelles, so it is unlikely to affect zymogen granules.

Although bafilomycin A1 and GPN inhibit NAADP-mediated Ca^{2+} signalling, the discovery that other Ca^{2+} mobilizing messengers also recruit acidic stores prompted the need to develop tools to inhibit NAADP-evoked Ca^{2+} release at the receptor level. There are two such strategies: use of a drug that acts as an NAADP antagonist, and knockout (or knockdown) of the NAADP-gated Ca^{2+} channel.

Recently, a cell-permeant NAADP antagonist, Ned-19, was discovered by virtual screening [200]. Although Ned-19 and NAADP have quite distinct chemical structures, they share a remarkably similar three dimensional structure and electrostatic surface pattern, as shown in Figure 6.1 [200]. Ned-19 has been reported to possess both inhibitory and stimulatory effects depending on its concentration [231]: at high concentrations, Ned-19 inhibited NAADP-evoked responses in many cell and tissue types (Table 6.2),

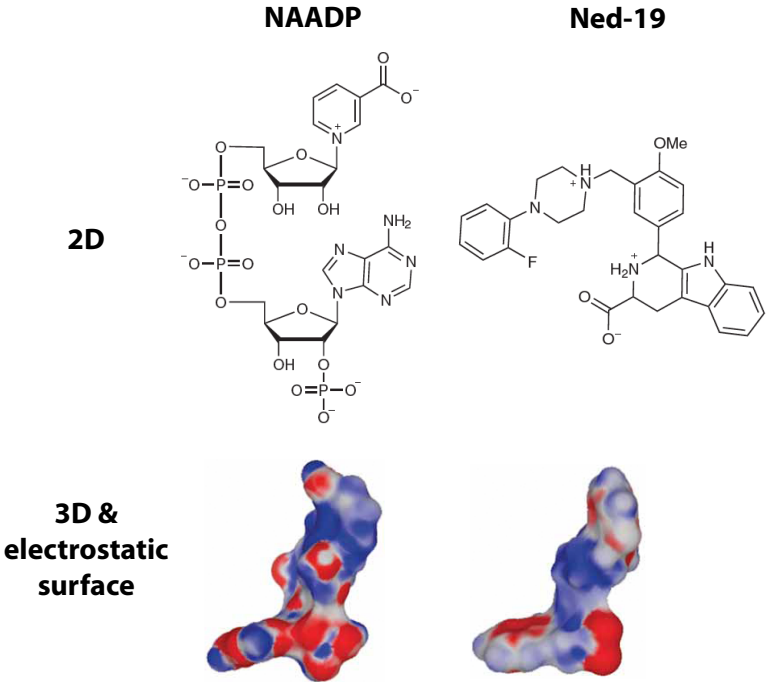

Figure 6.1: Top, two-dimensional chemical structure of NAADP and Ned-19. Bottom, three-dimensional structure and electrostatic surfaces of NAADP and Ned-19. The diagram is taken from [200].

Model system	**Cell type/TPC studied**	**[Ned-19] used/μM**	**Inhibition of NAADP -evoked responses**
Lipid bilayer	Immunopurified human TPC2 channel [231]	1	Channel activation
Homogenates	Sea urchin egg [200]	100	Ca^{2+} release
Cells	Intact sea urchin eggs [200]	100	Ca^{2+} release
	Primary mouse pancreatic β-cells [200]	10–100	Ca^{2+} release
	Primary rat uterine smooth muscle cells [6]	0.1–5	Ca^{2+} release
	Skeletal muscle C2C12 cells [5]	100	Differentiation
	Primary murine myoblasts [5]	100	Differentiation
	Human aortic endothelial cells [44]	1	Ca^{2+} release
	HEK293 cells overexpressing sea urchin TPCs [243]	10	Ca^{2+} release
	Primary rat cortical astrocytes [19]	100	Ca^{2+} release
Tissues	Whole rat uterine strips [6]	1	Contraction

Table 6.2: Inhibitory effect of Ned-19 in NAADP-evoked responses in various biological model systems.

while at low concentrations (1–100 nM), Ned-19 was reported to act as an NAADP agonist, activating channel opening of immunopurified TPC2 in a lipid bilayer.

To date, persuasive evidence supports the hypothesis that TPCs are the NAADP-gated Ca^{2+} channels; however, most studies have been conducted in heterologous systems [39, 41, 52, 231, 243, 248, 307]. To enable the study of the endogenous role of TPCs in NAADP signalling pathways, TPC mutant mice (Chapter 3) provide a practical experimental system (Table 3.3).

This laboratory has used TPC KO mice to demonstrate a key role of endogenous TPC in NAADP-mediated Ca^{2+} signalling. The first major discovery was that dialysing NAADP into pancreatic β-cells via a patch pipette evoked Ca^{2+}-induced oscillatory inward currents in the wild-type (WT) but not in the TPC2 KO mice [52]. Later studies showed that in WT pancreatic β-cells, glucose-evoked Ca^{2+} spiking is dependent on NAADP, and that these Ca^{2+} spikes are significantly reduced in TPC single KOs (TPC1 KO and TPC2 KO; Arredouani *et al.*, unpublished data). Furthermore, it has been shown that in bladder from WT mice, NAADP led to smooth muscle contraction, and that this was abolished in bladder from TPC2 KO mice [90].

With the availability of Ned-19 and TPC mutant mice, these new tools will hopefully shed light on the most critical link missing in CCK-mediated Ca^{2+} signalling in pancreatic acinar cells: molecular identity of the channel that mediates NAADP-evoked Ca^{2+} release. The first part of this chapter reports the validation of Ned-19 in pancreatic acinar cells, and the second part reports examination of the role of endogenous TPCs in CCK-evoked Ca^{2+} oscillations in TPC mutant mice.

6.2 Results

6.2.1 Effect of Ned-19 at a high concentration on ACh- and CCK-evoked Ca^{2+} oscillations

It has been established that in pancreatic acinar cells, NAADP is involved selectively in CCK- and not ACh-induced Ca^{2+} oscillations. Therefore, if Ned-19 is indeed an NAADP antagonist, it should selectively inhibit CCK- and not ACh-induced Ca^{2+} oscillations. As Ned-19 has never been used in pancreatic acinar cells, the inhibitory effect was first investigated at a high concentration of Ned-19.

6.2.1.1 Effect of Ned-19 on ACh-evoked Ca^{2+} oscillations

Based on the data shown in Table 6.2, a concentration of 10 μM Ned-19 was initially selected. As expected, Ca^{2+} oscillations evoked by physiological concentrations of ACh (25–50 nM) were unaffected by Ned-19; this is consistent with its supposed predominant involvement of the $InsP_3$-mediated signalling pathway (Figure 6.2A and 6.2B). Physiological concentrations of ACh evoked Ca^{2+} oscillations in 100% of cells (Figure 6.2C), and this persisted in 91 $\pm$ 5.9% of cells following Ned-19 addition (Figure 6.2C).

6.2.1.2 Effect of Ned-19 on CCK-evoked Ca^{2+} oscillations

There is a possibility that the sensitivity of pancreatic acinar cells to CCK could vary between preparations. Generally, physiological concentrations of CCK (5–25 pM) were able to evoke Ca^{2+} oscillations. For all experiments, low concentrations of CCK (just above threshold level) were used. To investigate whether Ned-19 is inhibitory at 10 μM, cells were preincubated with Ned-19 for approximately 15 min before the addition of CCK. At this concentration, Ned-19 dramatically reduced or completely abolished Ca^{2+} oscillations elicited by physiological concentrations of CCK (Figure 6.3A).

Similarly, when Ned-19 was added to cells exhibiting Ca^{2+} oscillations evoked by a suprathreshold concentration of CCK, the oscillations were abruptly terminated (Figure 6.3B), although occasionally, the oscillations persisted (Figure 6.3C). The peak height and ISP (interspike period) of CCK-evoked Ca^{2+} oscillations before and after Ned-19 addition were analysed (described in Section 2.9.4). The amplitude threshold for peak

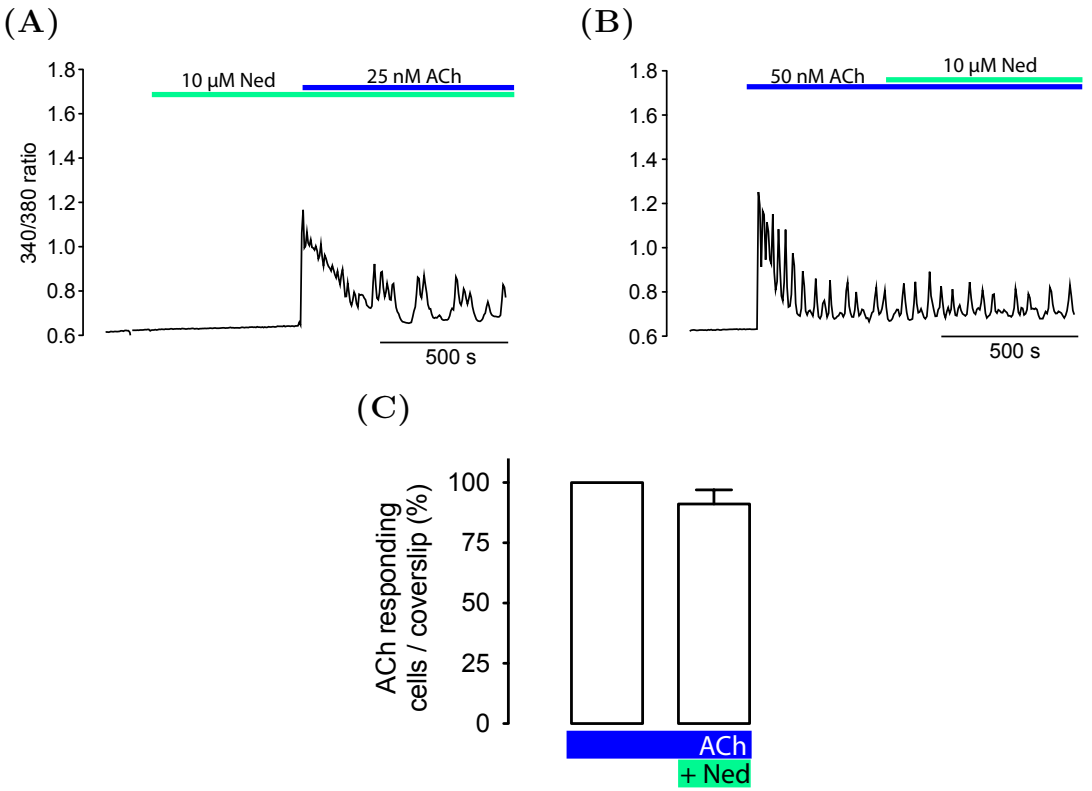

Figure 6.2: Representative traces showing the effect of (A) pre-treatment and (B) post-treatment with 10 μM Ned-19 on Ca^{2+} oscillations evoked by physiological concentrations of ACh. (C) % of cells responding to ACh in the presence and absence of Ned-19 (post-treatment). n = 39, experiments were performed in 6–9 coverslips. Green and blue bars represent the presence of Ned-19, and ACh, respectively.

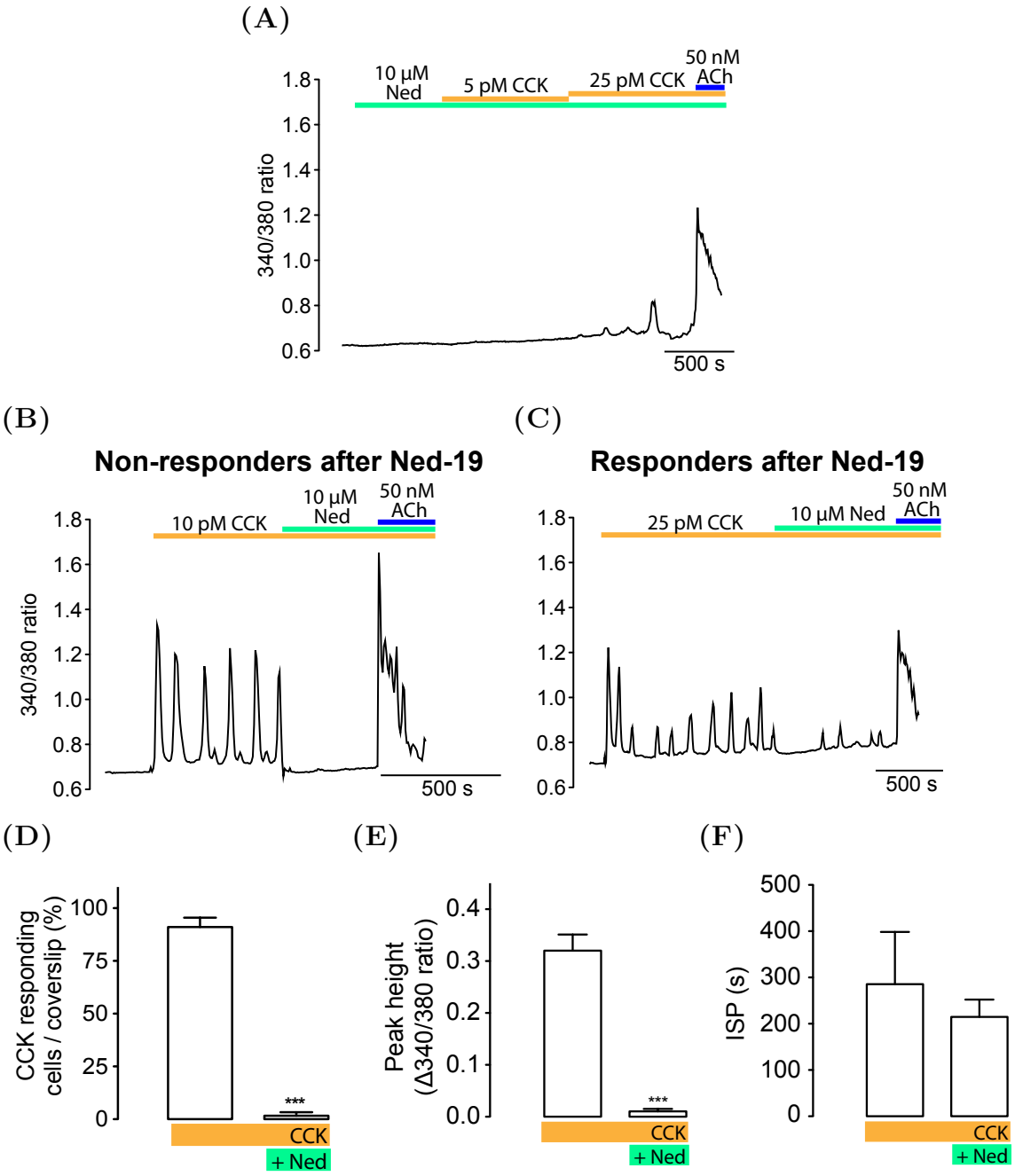

Figure 6.3: Effect of 10 μM Ned-19 on CCK-evoked Ca^{2+} oscillations. (A) The effect of Ned-19 pre-treatment on Ca^{2+} oscillations evoked by physiological concentrations of CCK (5–25 pM). (B) and (C) The effect of Ned-19 addition on Ca^{2+} oscillations evoked by physiological CCK concentrations. Summary of the effect of Ned-19 (post-treatment) on (D) the % of cells responding to CCK, (E) the peak height and (F) ISP of CCK-evoked Ca^{2+} oscillations. The analysis was conducted by comparing the peak height and ISP of CCK-evoked Ca^{2+} oscillations before and after Ned-19 addition in the same cells using a paired student's t-test. Number of cells (n) analysed for responding cells = 44, peak height = 29, and ISP = 3, experiments were performed in 6–8 coverslips. ***P $<$ 0.001. Orange, green, and blue bars represent the presence of CCK, Ned-19 (Ned), and ACh, respectively.

inclusion was 0.05 Δ340/380 ratio. Analysis showed that the peak height was significantly reduced after Ned-19 addition (Figure 6.3E).

For the ISP analysis, only cells that continued to oscillate after the Ned-19 addition were included; this allowed ISP after Ned-19 to be compared (as a pair) to ISP before Ned-19 in the same cell. After Ned-19 addition, only a few cells continued to oscillate; but for those that did, the ISP of oscillations was not significantly altered. As Ned-19 was shown to have minimal inhibition on ACh-evoked Ca^{2+} oscillations, ACh was added at the end of the experiment to ensure that the cells were still viable.

Overall, >90% of WT cells showed Ca^{2+} oscillations in response to stimulation of physiological concentrations of CCK (Figure 6.3D). The addition of Ned-19 abruptly impaired such Ca^{2+} oscillations: <2% of cells responded to CCK in the presence of Ned-19 (Figure 6.3D).

This study shows for the first time that Ned-19 is able to selectively inhibit CCK-evoked, but not ACh-evoked Ca^{2+} oscillations in pancreatic acinar cells. This selectivity of Ned-19 resembles that of other established pharmacological drugs that inhibit NAADP signalling (Table 6.1), consistent with its action as an NAADP antagonist.

6.2.2 Investigation of the stimulatory effect of Ned-19

Recently, Ned-19 at low concentrations (1–100 nM) was shown to activate immunopurified TPC2 channel-opening in a lipid bilayer. This unexpected behaviour suggests that Ned-19 can act as an agonist to TPCs, similarly to NAADP [231]. To examine whether low concentrations of Ned-19 can be used as an NAADP alternative (to trigger Ca^{2+} release in mouse pancreatic acinar cells), cells were treated with various concentrations of Ned-19 (1 nM to 10 μM) for 15 min.

Figure 6.4 shows that there is no significant difference in the % increase of the 340/380 ratio, and shows also a similar slope between Ned-19 (at various concentrations) and the control (0.1% DMSO) after 15 min incubation. This suggests that Ned-19 does not act as an agonist at low concentrations in mouse pancreatic acinar cells.

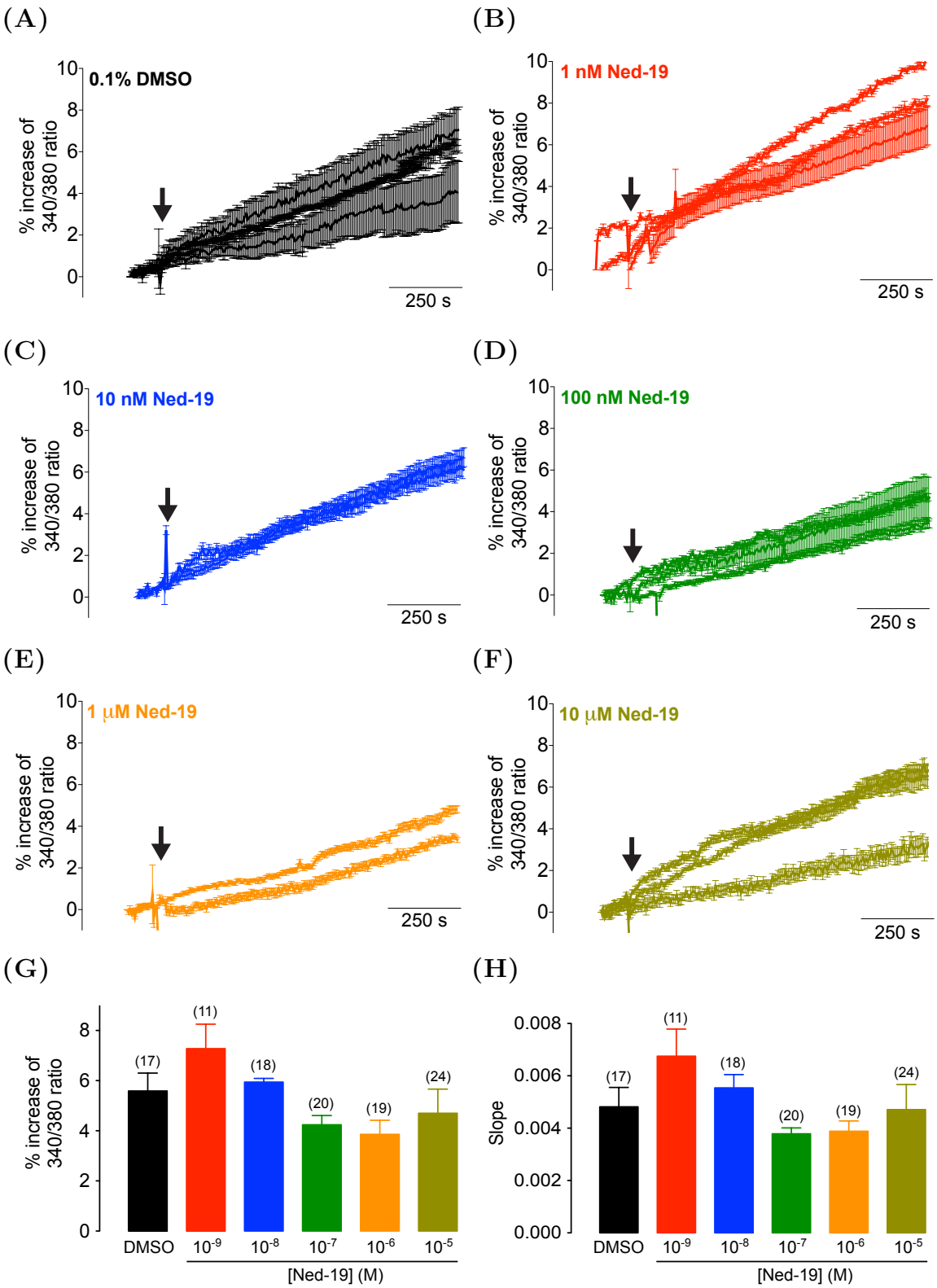

Figure 6.4: (A)-(F) Traces showing the % increase in the 340/380 ratio following Ned-19 addition. Each line and error bar represent the % mean ± S.E.M. increase at particular time points per coverslip. Arrows indicate the time of Ned-19 addition. (G) and (H) Summary of the % increase of 340/380 ratio and the slope after 15 min incubation with various concentrations of Ned-19, respectively. The total number of cells are indicated in the bracket, experiments were performed in 2–4 coverslips. % increase in the 340/380 ratio of different concentrations of Ned-19 were compared using one-way ANOVA.

6.2.3 Investigation of the endogenous role of TPCs in CCK-mediated Ca^{2+} signalling

As NAADP is known to play a role in the CCK-mediated Ca^{2+} signalling, and TPCs have been shown to be NAADP-gated Ca^{2+} channels, it is likely that TPCs play the central role in the CCK-mediated Ca^{2+} signalling. To examine the role of endogenous TPCs, CCK-induced Ca^{2+} oscillations were assessed in various TPC mutant mice (Chapter 3, summarized in Table 3.3).

It would be expected that if TPCs are not redundant, CCK-evoked Ca^{2+} oscillations would be abolished in TPC single KOs. Surprisingly, in TPC single KOs, 5 pM CCK was still able to evoke Ca^{2+} oscillations (Figure 6.5A, 6.5B), suggesting that the remaining TPC had possibly compensated for the deleted TPC.

Since NAADP has been proposed to act as a trigger, it is possible that it triggers each spike in the oscillation. The abrogation of one TPC subtype expression might therefore decrease the overall probability of NAADP triggering in CCK-mediated signalling pathway (i.e. result in slower oscillations). The peak height of Ca^{2+} spikes, however, should not be affected as it is determined by the properties of CICR. Unexpectedly, no significant difference in the ISP of Ca^{2+} oscillations was observed between TPC single KOs and their respective WTs (Figure 6.5A, 6.5B and 6.5E). Neither was a significant difference observed in the peak height of Ca^{2+} spikes evoked by 5 pM CCK (Figure 6.5A, 6.5B and 6.5D).

The most striking differences were observed with TPC1 H (hypomorph), the mutant in which mRNA expression of TPC1 was only partially knocked down. As expected, 5 pM CCK was able to evoke Ca^{2+} oscillations in TPC1 H (Figure 6.5B), but, interestingly, the ISP was significantly longer than for WT (Figure 6.5E); also, the peak height of the spikes was significantly decreased (Figure 6.5D).

Assuming that TPCs are necessary for CCK signalling, CCK-evoked Ca^{2+} oscillations observed in TPC single KOs are likely to have been generated by the remaining TPC. Thus, it is possible that abrogation of both TPCs is required to observe a difference in the CCK-evoked Ca^{2+} oscillations.

Surprisingly, 5 pM CCK was still able to elicit Ca^{2+} oscillations in TPC DKO cells. The spiking frequency was significantly decreased (as assessed by the ISP of the Ca^{2+} oscillations) in TPC DKO compared to WT. However, the peak height of the oscillations

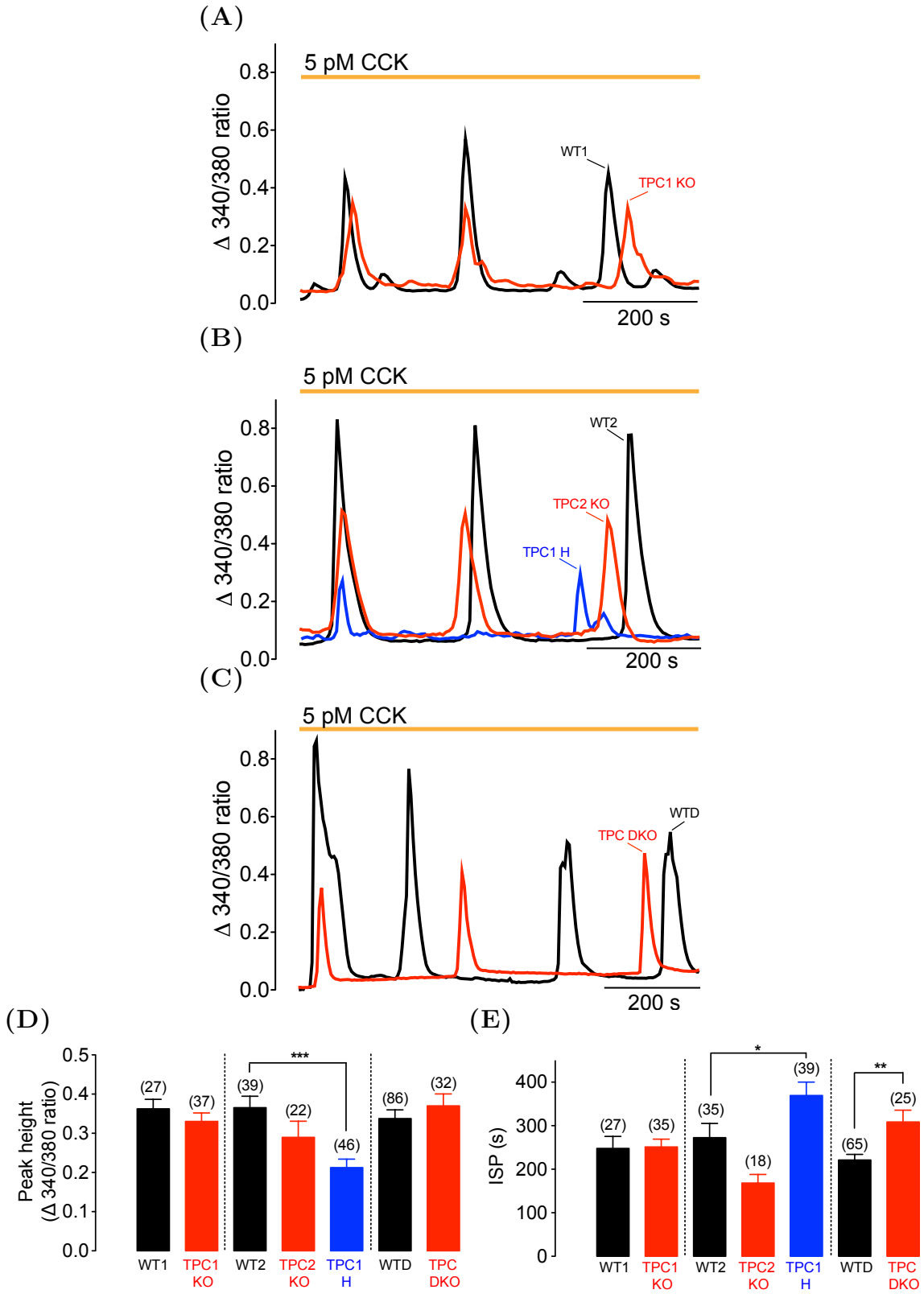

Figure 6.5: Traces of Ca^{2+} oscillations evoked by 5 pM CCK in (A) TPC1 KO (red), (B) TPC2 KO (red), TPC1 H (blue), and (C) TPC DKO (red) in comparison to their respective WT (black). Summary of (D) the peak height and (E) the interspike period (ISP) of Ca^{2+} oscillations evoked by CCK (5 pM) in TPC mutant mice and their respective WT. Total number of cells are indicated in the bracket, experiments were performed in 3–11 coverslips; ***P < 0.001, **P < 0.01, and *P < 0.05.

Mice	Expression		5 pM CCK-induced Ca^{2+} oscillations		
	TPC1	TPC2	ISP	Frequency	Peak height
TPC1 KO	×	✓	–	–	–
TPC1 H	↓	✓	↑	↓	↓
TPC2 KO	✓	×	–	–	–
TPC DKO	×	×	↑	↓	–

Table 6.3: Summary of 5 pM CCK-induced Ca^{2+} oscillations in pancreatic acinar cells of TPC mutant mice (see Chapter 3). ×: no expression; ✓: expression; ↓: reduction; ↑: elevation; –: no difference. Abbreviations: KO, knockout; H, hypomorph; DKO, double knockout.

was not significantly different between the TPC DKO and WT (Figure 6.5C). Table 6.3 summaries the relative TPC mRNA levels and properties of 5 pM CCK-induced Ca^{2+} oscillations in TPC mutant mice relative to WT.

There are three possible explanations for the oscillations evoked by CCK in TPC DKO: TPCs are not involved (NAADP acts on another channel to mediate Ca^{2+} release); or, in WT cells TPCs are involved in CCK signalling but in TPC DKO cells CCK recruits $InsP_3$ or cADPR instead of NAADP to trigger Ca^{2+} release; or in TPC DKO, CCK still recruits NAADP but (to compensate for the deletion of TPCs) the NAADP-binding protein of the TPC signalling complex forms a complex with alternative homologous Ca^{2+} channels (e.g. TRPs). In the last of these models, NAADP would still bind to its binding protein (Chapter 5) in the new complex, and continue to elicit Ca^{2+}. To test these hypotheses, various pharmacological agents were used to dissect the CCK signalling pathway (see below).

6.2.4 Pharmacology of CCK-mediated Ca^{2+} signalling in TPC1 KO

6.2.4.1 Effect of Ned-19

Since CCK still elicited Ca^{2+} oscillations in TPC1 KO cells (Figure 6.5), it is possible that in TPC1 KO cells, NAADP releases Ca^{2+} via the remaining TPC and thus triggers Ca^{2+} oscillations. If this is the case, Ned-19 should still inhibit CCK-evoked oscillations if NAADP is recruited. On the other hand, if $InsP_3$ or cADPR signalling pathways are recruited, then Ned-19 should a minimal effect [6, 200].

When this was tested, CCK evoked Ca^{2+} oscillations in the majority of WT and TPC1 KO cells, and it was seen that Ned-19 indeed inhibited CCK-evoked oscillations and significantly reduced the % of cells responding to CCK (Figure 6.6C) and the peak height of CCK-evoked oscillations (Figure 6.6D) in both TPC1 KO (Figure 6.6B) and its respective WT (Figure 6.6A). ACh (50 nM) was added after Ned-19 inhibition to confirm that the cells were still viable.

Although Ned-19 significantly reduced the peak height of CCK-evoked Ca^{2+} oscillations in both WT and TPC1 KO cells, the change in peak oscillation height after Ned-19 treatment was not significantly different between these two cells (Figure 6.6D). No WT cells continued to oscillate after Ned-19 treatment, and only a handful of TPC1 KO cells continued. For these, the ISP was not significantly affected by Ned-19 treatment (Figure 6.6E).

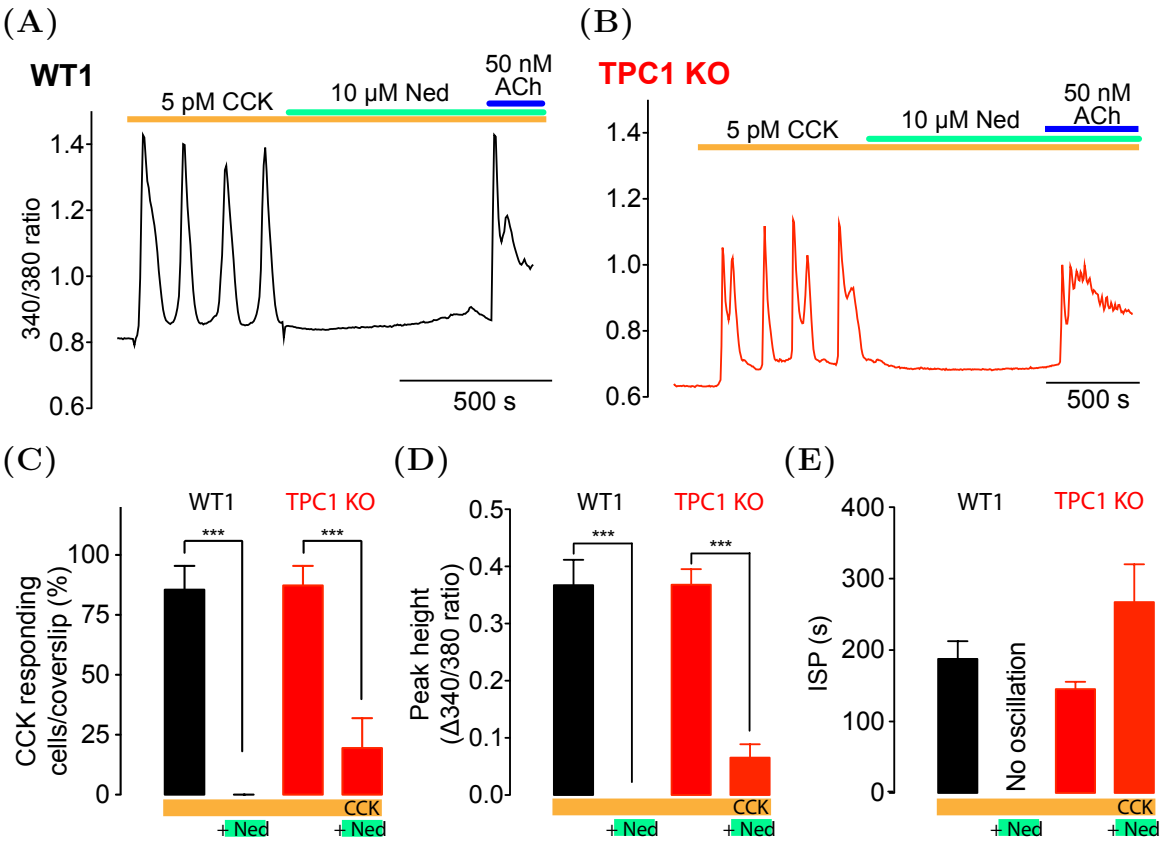

Figure 6.6: Ned-19 (green bar) inhibition of Ca^{2+} oscillations evoked by CCK (orange bar) in (A) WT and (B) TPC1 KO. ACh (blue bar) was added following Ned-19 treatment to confirm cell viability. Summary of the effect of Ned-19 (10–20 μM) on (C) the % of cells responding to CCK, (D) the peak height, and (E) the ISP of Ca^{2+} oscillations evoked by CCK (5–25 pM) in TPC1 KO and its respective WT. The analysis was conducted by comparing the peak height and ISP of CCK-evoked Ca^{2+} oscillations before and after Ned-19 addition in the same cells using a paired student's t-test. Number of cells (n) analysed for responding cells = 23 (WT1) and 25 (TPC1 KO), peak height = 19 (WT1) and 23 (TPC1 KO), and ISP = 17 (WT1) and 3 (TPC1 KO), experiments were performed in 3–6 coverslips; ***P $<$ 0.001.

6.2.4.2 Effect of GPN

CCK is known to recruit acidic stores for the release of Ca^{2+} by NAADP in mouse pancreatic acinar cells [185, 293, 294]. If NAADP is still involved in CCK signalling in TPC1 KO cells, lysing of the acidic stores by GPN should inhibit the CCK-evoked Ca^{2+} oscillations.

Consistent with previous findings [185, 293], GPN (100 μM) significantly diminished CCK-evoked Ca^{2+} oscillations in WT (Figure 6.7A and 6.7B). In TPC1 KO, GPN also significantly inhibited the CCK-evoked Ca^{2+} oscillations (Figure 6.7C and 6.7D). However, unlike Ned-19 (with which only a few cells continued to oscillate), inhibition by GPN was less absolute: a higher proportion of cells continued oscillating, although with a reduced peak height. Example traces of cells that were still responsive after GPN treatment are shown in Figure 6.7B and 6.7D.

GPN significantly reduced the % of TPC1 KO cells responding to CCK, similar to the situation with WT cells (Figure 6.7E). Again, 50 nM ACh was able to elicit Ca^{2+} response from both the WT and TPC1 KO cells whose CCK-evoked oscillations had been inhibited by GPN, suggesting that cells were still viable. Furthermore, the peak height of Ca^{2+} oscillations was significantly reduced after GPN treatment but to a similar extent in both WT and the TPC1 KO cells (Figure 6.7F). Only a few WT and TPC1 KO cells continued to oscillate after GPN treatment. For these, the ISP appeared to be longer although statistical analysis could not be conducted due to the small number of oscillating cells (Figure 6.7G).

In summary, in TPC1 KO cells, CCK-evoked Ca^{2+} oscillations were still sensitive to both Ned-19 and GPN. This suggests that in the absence of TPC1, NAADP is still likely to be involved in CCK-evoked Ca^{2+} oscillations to release Ca^{2+} from acidic stores, specifically, cathepsin-C containing lysosome-related organelles.

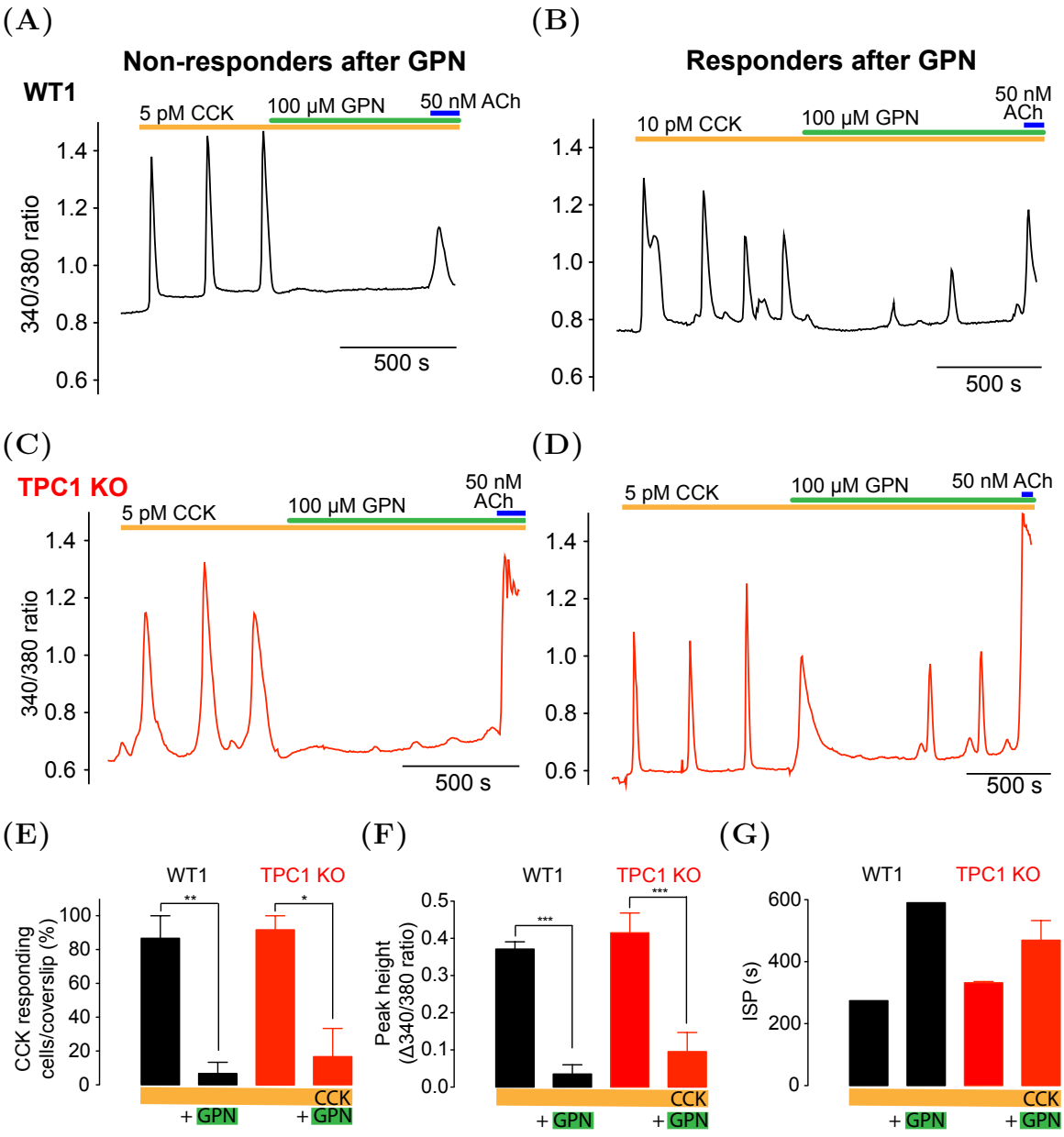

Figure 6.7: GPN (green bar) inhibition of Ca^{2+} oscillations evoked by CCK (orange bars) in (A) and (B) WT, and (C) and (D) TPC1 KO. ACh (blue bar) was added at the end to confirm cell viability. The effect of GPN (100 μM) on (E) the % of cells responding to CCK, (F) the peak height, and (G) the ISP of Ca^{2+} oscillations evoked by CCK (5–10 pM) in TPC1 KO and its respective WT. The analysis was conducted by comparing the peak height and ISP of CCK-evoked Ca^{2+} oscillations before and after GPN addition in the same cells using a paired student's t-test. Number of cells (n) analysed for responding cells = 16 (WT1) and 9 (TPC1 KO), peak height = 14 (WT1) and 8 (TPC1 KO), and ISP = 1 (WT1) and 2 (TPC1 KO), experiments were performed in 2–3 coverslips; ***P < 0.001, **P < 0.01, and *P < 0.05.

6.2.5 Pharmacology of CCK-mediated Ca^{2+} signalling in TPC2 KO

In Section 6.2.3, it was shown that CCK elicited Ca^{2+} oscillations in TPC2 KO cells, and it was suggested that this might due to the compensation by TPC1. However, it is possible that TPC1 is not involved in CCK-evoked Ca^{2+} oscillations: perhaps TPC2 has an essential role. This may explain why pharmacological intervention had a similar effect in TPC1 KO compared to WT cells. If TPC2 is essential, CCK-evoked Ca^{2+} oscillations may be dramatically remodelled in TPC2 KO.

6.2.5.1 Effect of Ned-19

An addition of Ned-19 at a high concentration completely abolished CCK-evoked Ca^{2+} oscillations in TPC2 KO cells (Figure 6.8B), similar to WT (Figure 6.8A). Analysis showed that the % of cells responding to CCK after Ned-19 treatment (Figure 6.8C) and the peak height of CCK-evoked Ca^{2+} oscillations (Figure 6.8D) were significantly reduced in TPC2 KO, similar to the response of its respective WT. Additionally, none of the TPC2 KO and WT cells continued to oscillate after Ned-19 treatment (Figure 6.8E).

6.2.5.2 Effect of GPN

GPN also inhibited CCK-evoked Ca^{2+} oscillations (Figure 6.9C and 6.9D) in TPC2 KO cells; inhibition was comparable to that with its respective WT (Figure 6.9A and 6.9B). After GPN treatment, the % of TPC2 KO cells responding to CCK (Figure 6.9E) and the peak height of Ca^{2+} oscillations in TPC2 KO cells (Figure 6.9F) were significantly decreased, to a similar extent as with WT cells. However, in those cells that did continue to oscillate after GPN addition, the ISP was unaltered in WT cells, a significantly longer ISP was observed in TPC2 KO cells (Figure 6.9G).

In summary, similarly to the situation with TPC1 KO cells, CCK-evoked Ca^{2+} oscillations were still sensitive to both Ned-19 and GPN in TPC2 KO cells. This suggests that in the absence of TPC2, NAADP is still likely to be involved in CCK signalling, possibly by releasing Ca^{2+} from cathepsin-C containing lysosome-related organelles.

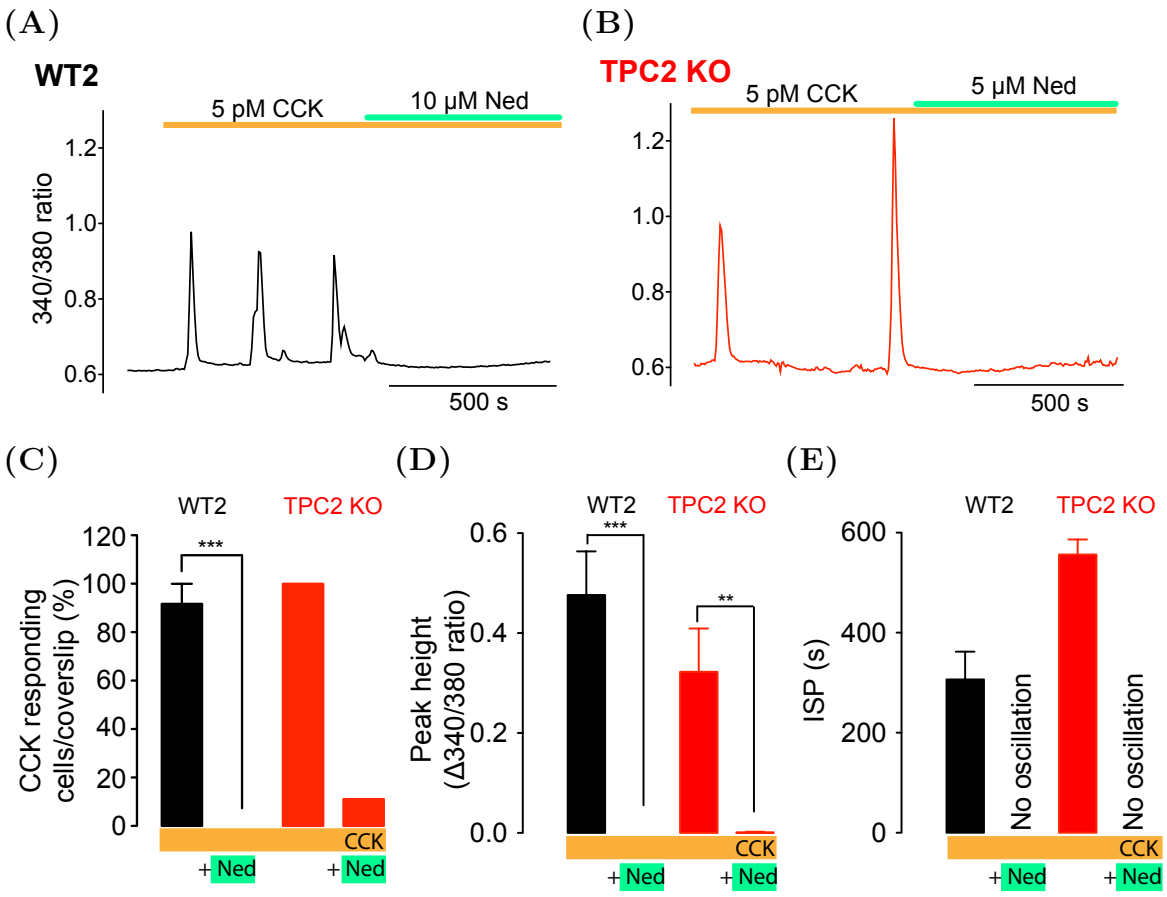

Figure 6.8: Ned-19 (green bar) inhibition of Ca^{2+} oscillations evoked by CCK (orange bar) in (A) WT and (B) TPC2 KO. Summary of the effect of Ned-19 (5–10 μM) on (C) the % of cells responding to CCK, (D) the peak height, and (E) the ISP of Ca^{2+} oscillations evoked by CCK (5–20 pM) in TPC2 KO and its respective WT. The analysis was conducted by comparing the peak height and ISP of CCK-evoked Ca^{2+} oscillations before and after Ned-19 addition in the same cells using a paired student's t-test. Number of cells (n) analysed for responding cells = 12 (WT2) and 9 (TPC2 KO), peak height = 11 (WT2) and 9 (TPC2 KO), and ISP = 8 (WT2) and 2 (TPC2 KO), experiments were performed in 1–3 coverslips; ***P $<$ 0.001, and **P $<$ 0.01.

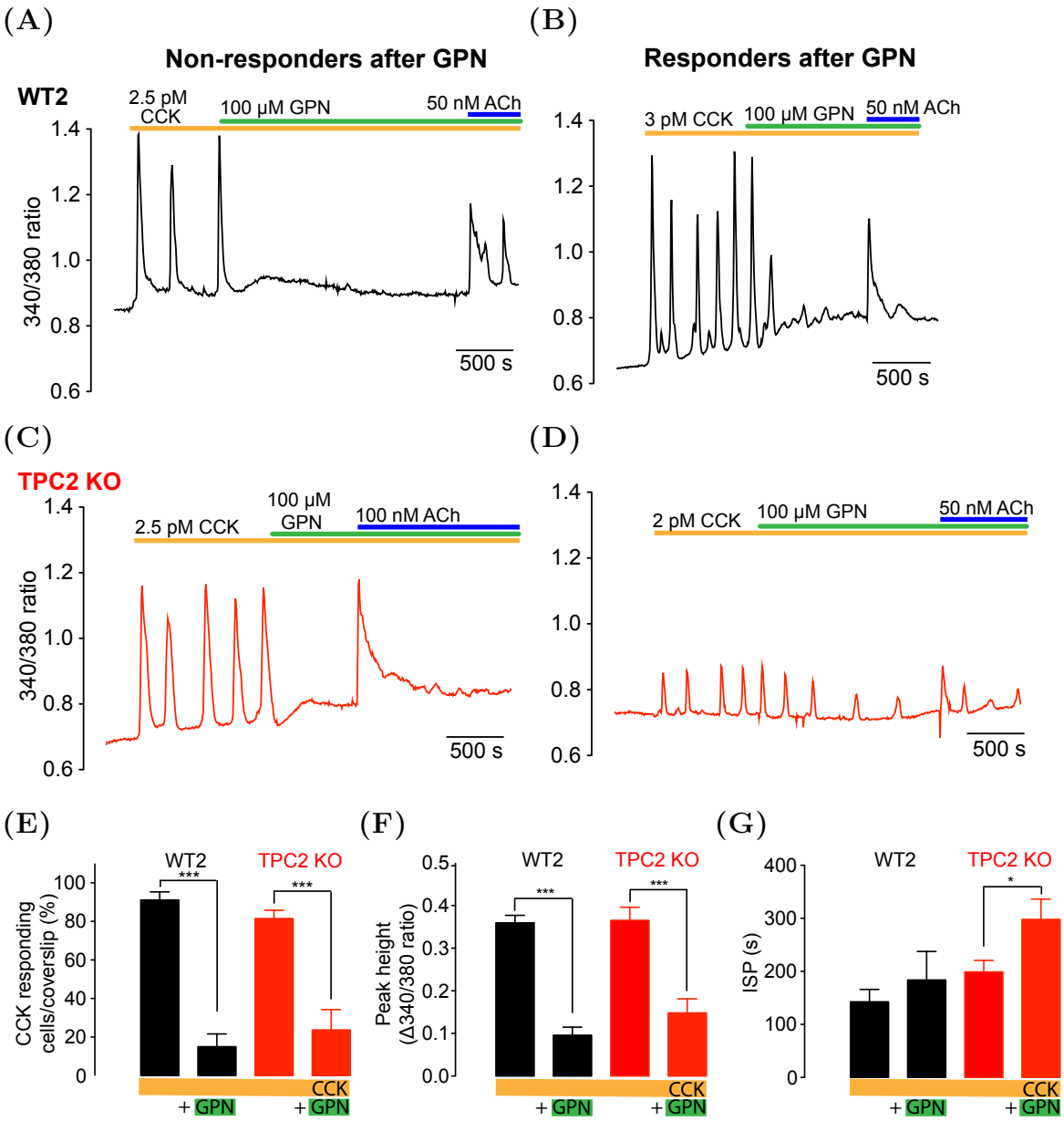

Figure 6.9: GPN (green bar) inhibition of Ca^{2+} oscillations evoked by CCK (orange bars) in (A) and (B) WT, and (C) and (D) TPC2 KO. ACh (blue bar) was added at the end to confirm cell viability. The effect of GPN (100–200 μM) on (E) the % of cells responding to CCK, (F) the peak height, and (G) the ISP of Ca^{2+} oscillations evoked by CCK (2–5 pM) in TPC2 KO and its respective WT. The analysis was conducted by comparing the peak height and ISP of CCK-evoked Ca^{2+} oscillations before and after GPN addition in the same cells using a paired student's t-test. Number of cells (n) analysed for responding cells = 52 (WT2) and 72 (TPC2 KO), peak height = 49 (WT2) and 68 (TPC2 KO), and ISP = 7 (WT2) and 15 (TPC2 KO), experiments were performed in 5–7 coverslips; ***P $<$ 0.001, and *P $<$ 0.05.

6.2.6 Pharmacology of CCK-mediated Ca^{2+} signalling in TPC DKO

The likelihood for NAADP involvement in CCK-evoked Ca^{2+} oscillations in TPC single KOs suggests that TPCs are mutually redundant: the loss of one TPC isoform can be compensated by the action of the other isoform. Thus, the TPC DKO, in which no TPCs are expressed, will prove highly valuable in examining the role of the TPC family in the CCK-mediated signalling pathway. Based on the above results, it would be predicted that the signal transduction pathway of CCK-evoked responses in TPC DKO would be reconfigured, switching to $InsP_3$ and cADPR to transduce Ca^{2+} signals.

6.2.6.1 Effect of Ned-19

Surprisingly, Ned-19 still inhibited CCK-evoked Ca^{2+} oscillations in TPC DKO (Figure 6.10A and 6.10B). In particular, Ned-19 significantly reduced the % of cells responding to CCK (Figure 6.10C) and the peak height of Ca^{2+} oscillations in TPC DKO cells (Figure 6.10D), to a similar extent as that for WT cells. Additionally, in the few WT and TPC DKO cells that continued to oscillate after Ned-19 treatment, the ISP was not significantly different between TPC DKO and its respective WT (Figure 6.10E).

6.2.6.2 TPC DKO morphology and acidic store sensitivity to GPN

Since TPCs have been reported to be important in lysosome biogenesis — in particular, vesicle fusion and trafficking [165, 243] — prior to testing GPN in TPC DKO, it is necessary to account for potential compensatory mechanisms in lysosomal physiology. If compensation alters the lysosomal physiology in TPC DKO, the sensitivity of the acidic stores to GPN is likely to be altered. It is therefore important to confirm that the acidic stores are still sensitive to GPN before using GPN to investigate CCK signalling in TPC DKO.

First, the morphology of TPC DKO and the WT cells was examined. Pancreatic acinar cells isolated from TPC DKO (Figure 6.11A) exhibited the hallmark polarized secretary poles; these were indistinguishable from WT cells (Figure 6.11B). To investigate whether TPC DKO lysosomal physiology is also unaltered from WT, lysotracker red was used to label acidic stores. Staining from lysotracker red showed that the acidic stores were still present in TPC DKO (Figure 6.11A), similar to WT cells (Figure 6.11B).

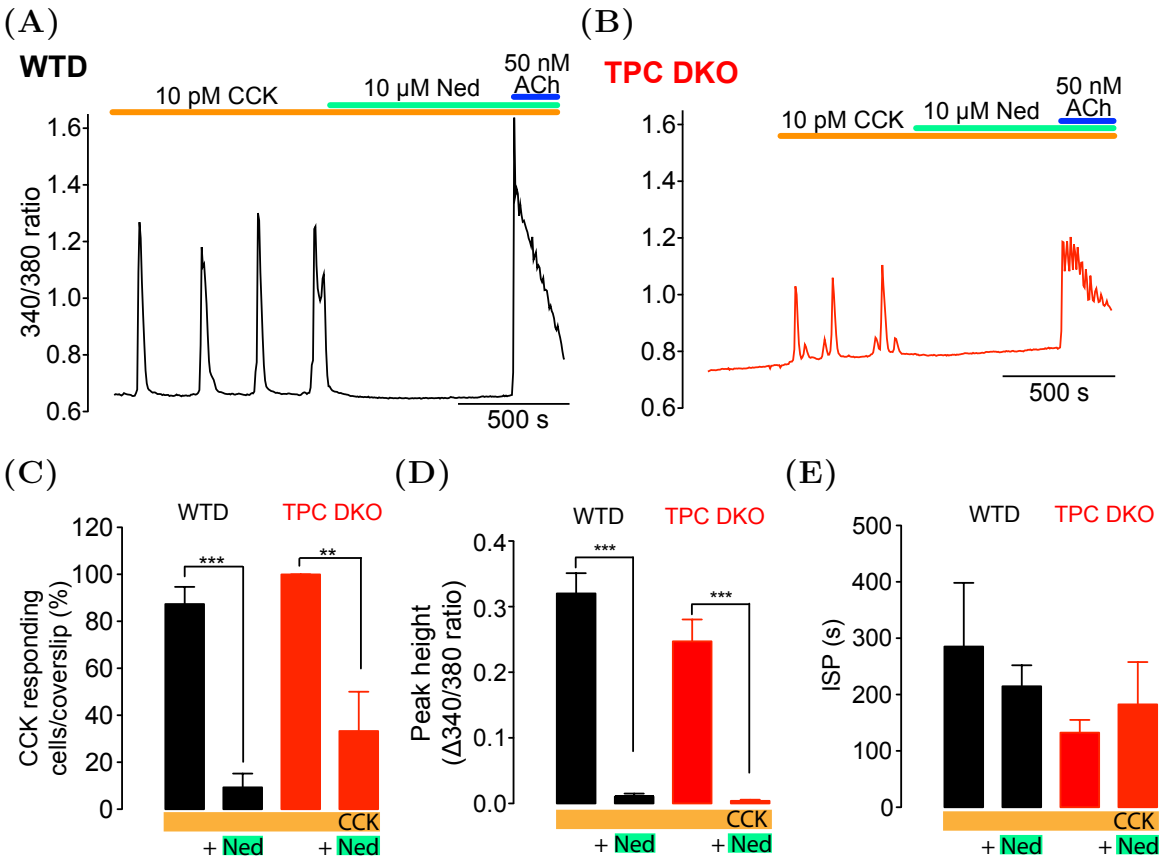

Figure 6.10: Ned-19 (green bar) inhibition of Ca^{2+} oscillations evoked by CCK (orange bar) in (A) WT, and (B) TPC DKO. ACh (blue bar) was added at the end to confirm cell viability. The effect of Ned-19 (10 μM) on (C) the % of cells responding to CCK, (D) the peak height, and (E) the ISP of Ca^{2+} oscillations evoked by CCK (5–50 pM) in TPC DKO and its respective WT. The analysis was conducted by comparing the peak height and ISP of CCK-evoked Ca^{2+} oscillations before and after Ned-19 addition in the same cells using a paired student's t-test. Number of cells (n) analysed for responding cells = 53 (WTD) and 37 (TPC DKO), peak height = 29 (WTD) and 35 (TPC DKO), and ISP = 3 (WTD) and 5 (TPC DKO), experiments were performed in 7–8 coverslips; ***P $<$ 0.001, and **P $<$ 0.01.

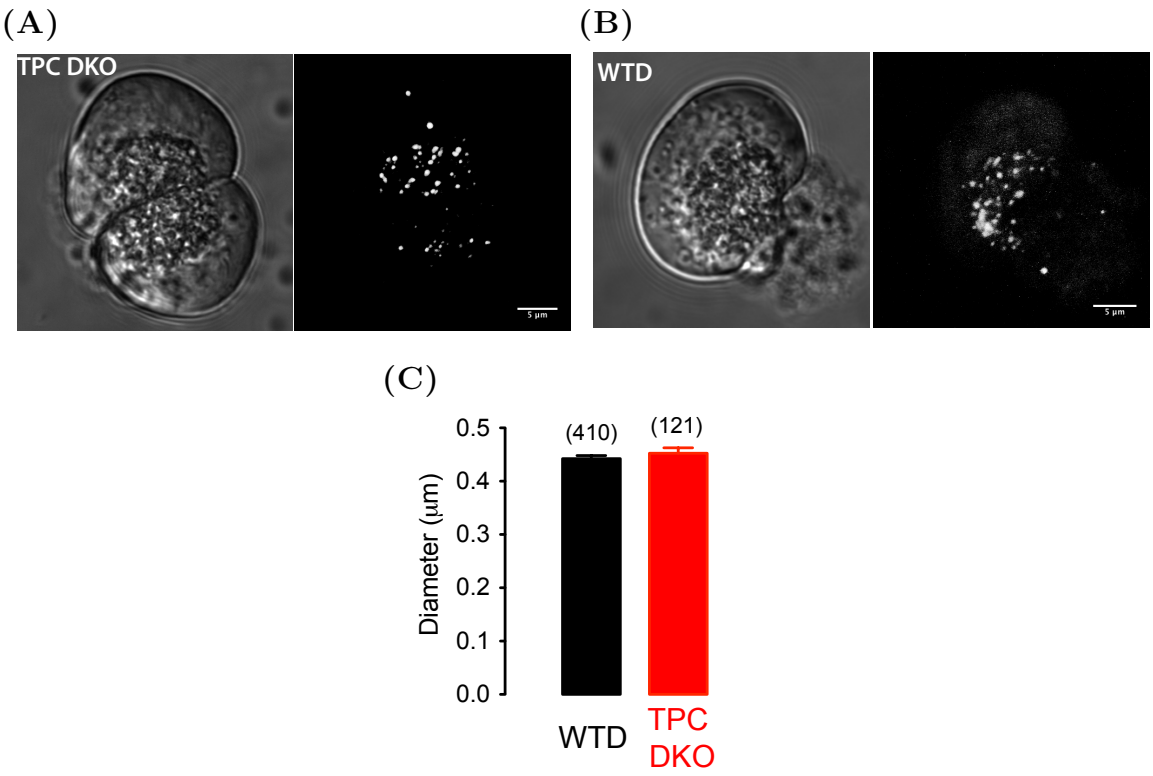

Figure 6.11: (A) TPC DKO exhibited normal polarity (left) and contained acidic stores (detected by lysotracker red staining, right). These were indistinguishable from the respective WT (B). Images of lysotracker staining were generated by Z-stacking. (C) Diameter of ≥10 randomly chosen acidic vesicles in each TPC DKO and WT cells. Total number of vesicles measured are indicated in the bracket in 11–33 cells.

As the lysosomes have been reported to be enlarged in HEK293 cells overexpressing sea urchin TPCs [243], it is possible that the lysosomal size is also altered in TPC DKO. However, analysis of the diameter of the acidic stores staining showed that TPC DKO and the WT diameters were essentially identical (Figure 6.11C).

Next, the sensitivity of the acidic stores to GPN in TPC DKO was studied. The preliminary results show that the lysotracker staining decreased rapidly after an addition of GPN (50 or 200 μM) and was abolished within 10 min in both TPC DKO and WT cells (Figure 6.12), suggesting that lysosomes in TPC DKO cells are still sensitive to GPN. A difference was observed in the rate of decrease in fluorescence between WT and TPC DKO cells, and future investigations may be required to confirm this finding. However, as the acidic stores are still present and sensitive to GPN in TPC DKO, GPN was used to test whether acidic stores are recruited in CCK-evoked Ca^{2+} oscillations in TPC DKO.

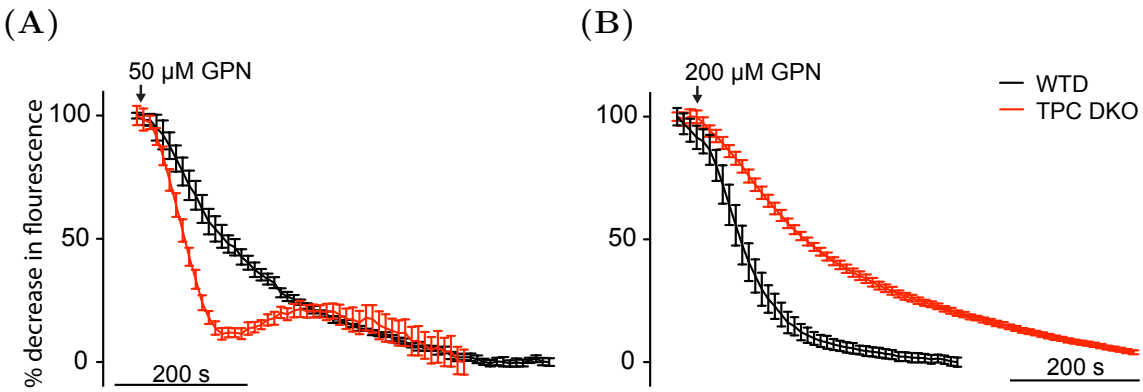

Figure 6.12: Staining of the acidic stores by lysotracker red was rapidly abolished upon GPN addition (50 or 200 μM) in both TPC DKO (red trace) and WT (black trace). The fluorescence data reflect the total red fluorescence exhibited in one cell. The fluorescence at each time point was normalized to fluorescence at time = 0, n = 3–6 cells.

6.2.6.3 Effect of GPN

In TPC DKO, GPN inhibited CCK-evoked Ca^{2+} oscillations (Figure 6.13C and 6.13D) similar to WT cells (Figure 6.13A and 6.13B). Furthermore, analysis showed that after GPN treatment, the % of cells responding to CCK (Figure 6.13E) and also the peak height of Ca^{2+} oscillations (Figure 6.13F) were significantly decreased in TPC DKO to a similar extent as that for WT cells. Interestingly, while in WT cells that continued to oscillate after GPN addition the ISP was unchanged, in TPC DKO cells that continued to oscillate the ISP was, however, significantly longer (Figure 6.13F).

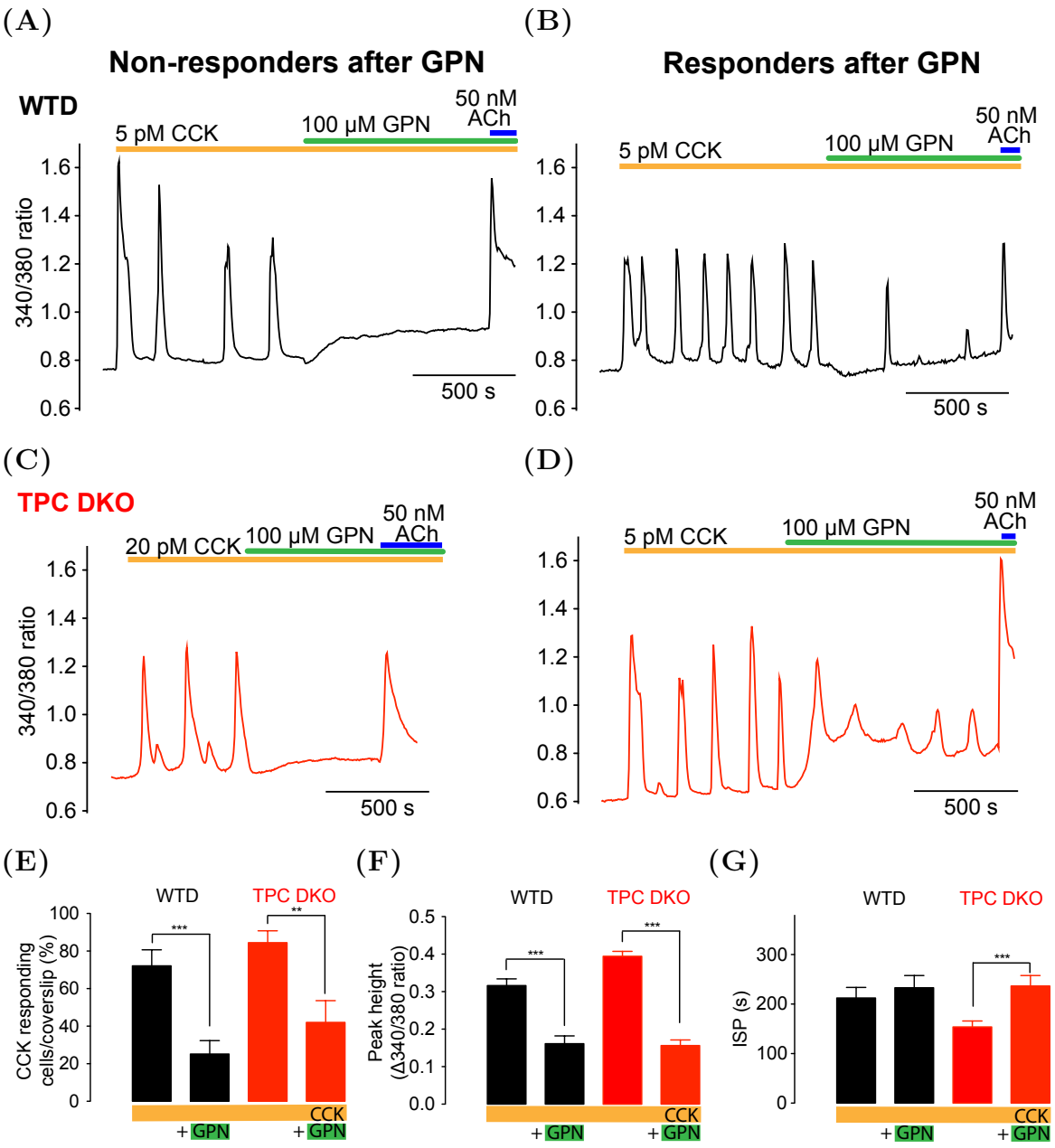

Figure 6.13: GPN (green bar) inhibition of Ca^{2+} oscillations evoked by CCK (orange bars) in (A) and (B) WT, and (C) and (D) TPC DKO. ACh (blue bar) was added at the end to confirm cell viability. The effect of GPN (50–200 μM) on (E) the % of cells responding to CCK, (F) the peak height, and (G) the ISP of Ca^{2+} oscillations evoked by CCK (5–25 pM) in TPC DKO and its respective WT. The analysis was conducted by comparing the peak height and ISP of CCK-evoked Ca^{2+} oscillations before and after GPN addition in the same cells using a paired student's t-test. Number of cells (n) analysed for responding cells = 131 (WTD) and 95 (TPC DKO), peak height = 112 (WTD) and 89 (TPC DKO), and ISP = 32 (WTD) and 44 (TPC DKO), experiments were performed in 13 coverslips; ***P < 0.001 and **P < 0.01.

6.2.6.4 Effect of bafilomycin A1

Bafilomycin A1 is another pharmacological agent that inhibits NAADP-mediated Ca^{2+} signalling by interfering with acidic stores. Bafilomycin A1 targets a broader range of acidic stores than GPN, which specifically inhibits cathepsin-C containing lysosome-related organelles.

As expected, CCK-evoked Ca^{2+} oscillations were sensitive to bafilomycin A1 in WT (Figure 6.14A). It is worth noting that the inhibitory action of bafilomycin A1 is different from GPN. After the addition of bafilomycin A1, the cells tended to continue oscillating with decreasing amplitude. This is unlike GPN, where the oscillation tended to terminate abruptly. Bafilomycin A1 might act slower than GPN as its action is dependent on the leakiness of Ca^{2+} from the stores.

In TPC DKO, CCK-evoked Ca^{2+} oscillations were also sensitive to bafilomycin A1 (Figure 6.14B), confirming the results from GPN studies. Like GPN, bafilomycin A1 decreased the % of responding cells (Figure 6.14C) and the peak height of Ca^{2+} oscillations (Figure 6.14D) in TPC DKO cells to a similar extent as that for WT cells. Additionally, in the WT cells that continued to oscillate, no significant change was observed in the ISP of Ca^{2+} oscillations; however, the ISP was significantly longer in the TPC DKO cells that continued to oscillate after GPN addition (Figure 6.14E).

In summary, CCK-evoked Ca^{2+} oscillations were still sensitive to Ned-19, GPN and bafilomycin A1 in TPC DKO cells. This suggests that even in the absence of TPCs, CCK might still depend on NAADP to release Ca^{2+} from the acidic stores to evoke Ca^{2+} oscillations.

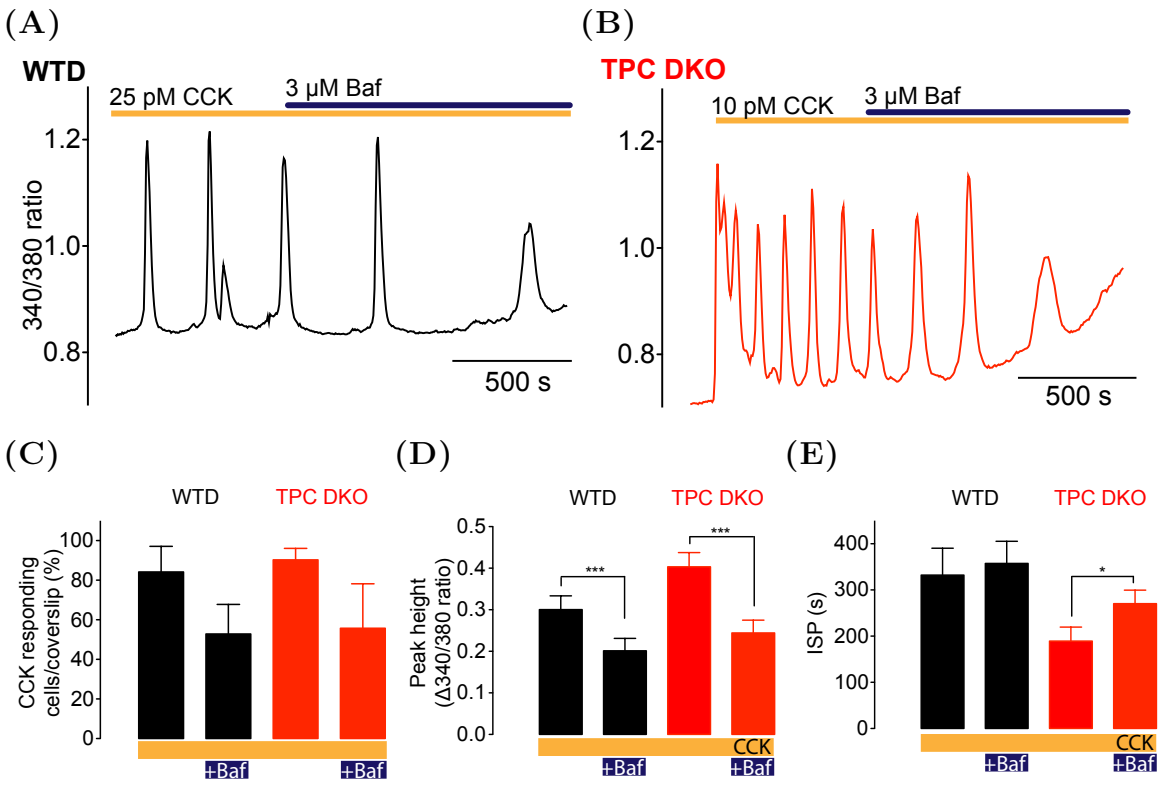

Figure 6.14: Bafilomycin A1 (blue bar) inhibition of Ca^{2+} oscillation evoked by CCK (orange bars) in (A) WT, and (B) TPC DKO. The effect of bafilomycin A1 (3 μM) on (C) the % of cells responding to CCK, (D) the peak height, and (E) the ISP of Ca^{2+} oscillations evoked by CCK (5–25 pM) in TPC DKO and its respective WT. The analysis was conducted by comparing the peak height and ISP of CCK-evoked Ca^{2+} oscillations before and after GPN addition in the same cells using a paired student's t-test. Number of cells (n) analysed for responding cells = 29 (WTD) and 19 (TPC DKO), peak height = 26 (WTD) and 18 (TPC DKO), and ISP = 26 (WTD) and 18 (TPC DKO), experiments were performed in 3–5 coverslips; ***P $<$ 0.001, and *P $<$ 0.05.

6.2.6.5 Effect of extracellular Ca^{2+}

All of the above studies had been conducted in the Ca^{2+}-containing buffer. Although CCK-evoked Ca^{2+} oscillations were shown to recruit internal acidic stores in TPC DKO (Figure 6.13 and 6.14), it is still possible that the Ca^{2+} entry from the extracellular medium is altered due to remodelling as has been reported for CD38 KO mice [74]: in WT cells, CCK-evoked Ca^{2+} oscillations are less sensitive to extracellular Ca^{2+}, and oscillation can persist for minutes in the absence of extracellular Ca^{2+} [188, 297]. However, in CD38 KO cells, CCK-evoked Ca^{2+} oscillations were significantly dependent on extracellular [Ca^{2+}], as CCK was not able to evoke oscillation in the absence of extracellular Ca^{2+}.

Stimulation of cells with 10 pM CCK in the extracellular buffer containing either Ca^{2+} or no Ca^{2+} with 100 μM EGTA (Ca0) showed that CCK was able to evoke Ca^{2+} oscillations in both WT and TPC DKO cells regardless of extracellular Ca^{2+} (Figure 6.15A and 6.15B). Furthermore, in both cell types, the % of cells responding to CCK (Figure 6.15C) and the peak height of Ca^{2+} spikes (Figure 6.15D) were independent of extracellular Ca^{2+}. Unexpectedly, the removal of extracellular Ca^{2+} significantly decreased the ISP of Ca^{2+} oscillations (i.e. higher frequency) in the WT, but had no effect on TPC DKO cells.

In summary, Ca^{2+} entry in CCK-evoked Ca^{2+} oscillations appeared to be unaffected by the presence or absence of TPCs. In the absence of extracellular Ca^{2+}, the ISP of CCK-evoked Ca^{2+} oscillations was significantly decreased in the WT cells; however, the number of cells tested was too small to draw a firm conclusion.

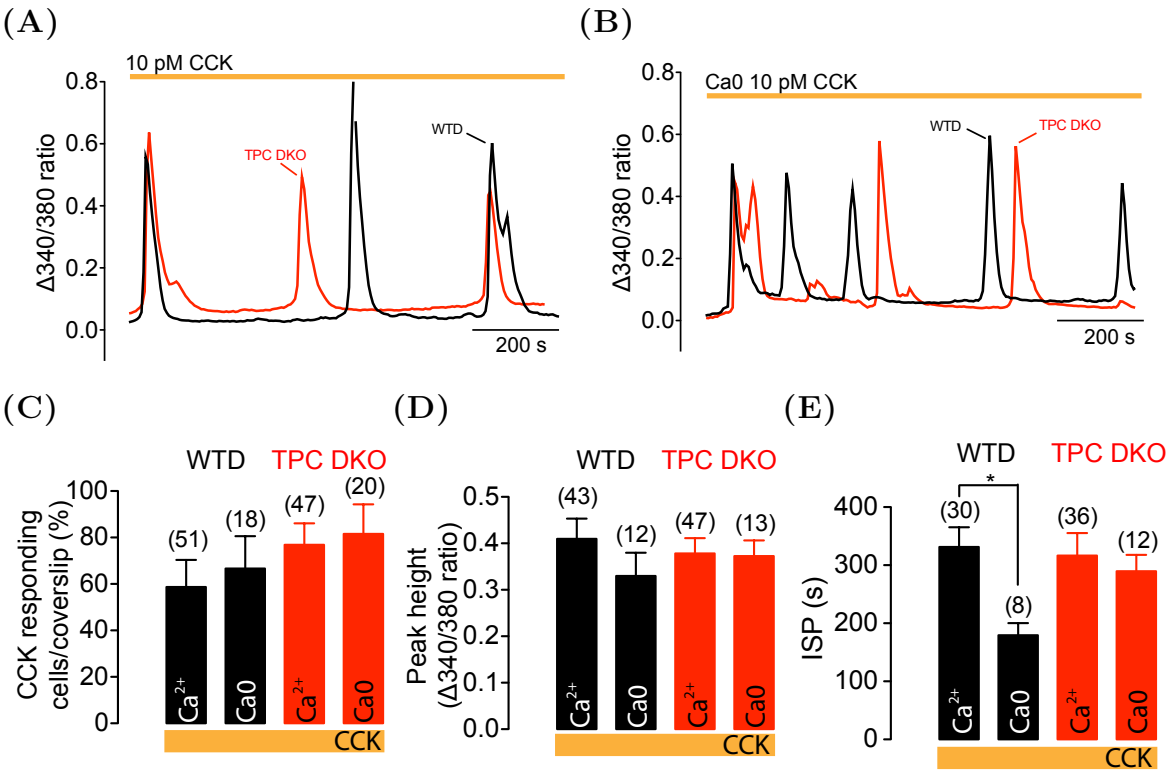

Figure 6.15: Representative traces of Ca^{2+} oscillations evoked by 10 pM CCK in (A) the presence of external Ca^{2+} and (B) the absence of external Ca^{2+} with 100 μM EGTA (Ca0) in TPC DKO (red trace) and its respective WT (black trace). Summary of the effect of Ca^{2+} free in combination with 100 μM EGTA in the extracellular buffer on (C) the % of cells responding to CCK (10 pM), (D) the peak height, and (E) the ISP of 10 pM CCK-evoked Ca^{2+} oscillations. An unpaired student's t-test was used to compare WT from TPC DKO cells. Total number of cells are indicated in the bracket, experiments were done in 3–7 coverslips; *P $<$ 0.05.

6.3 Discussion

The main function of pancreatic acinar cells is to secrete fluid and digestive enzymes in response to agonist stimulations. Remarkable progress has been made over the past 30 years in elucidating the details of this sophisticated stimulus–secretion signalling pathway. Cancela *et al.* clearly demonstrated the recruitment of NAADP by CCK [57, 59]. Subsequent studies by Yamasaki *et al.* identified the Ca^{2+} stores that NAADP uses [293], as well as confirming the selectivity of the agonists for different messengers by measuring changes in NAADP, cADPR, and $InsP_3$ levels [294]. More recently, Cosker *et al.* showed that CD38 is likely the enzyme responsible for the synthesis of NAADP [74]. Currently, the outstanding question is the molecular identity of the channel that is gated by NAADP to mediate Ca^{2+} release. Of these, TPC is perhaps the most credible candidate.

6.3.1 Ned-19

There are two approaches to investigate the role of TPCs in NAADP signalling in CCK-mediated Ca^{2+} oscillations: first, by using an NAADP antagonist, and second, by knocking TPCs down or out. Ned-19 is the first established cell-permeant antagonist of NAADP [200]. It is a relatively new drug and to date, it has been shown to selectively inhibit NAADP-mediated Ca^{2+} signalling pathway in sea urchin homogenate [200] and rat uterine smooth muscle cells [6].

The inhibitory action of Ned-19 in mammalian cells was observed at high concentrations (Table 6.2). In this chapter, the potential use of Ned-19 in pancreatic acinar cells as an NAADP antagonist has been investigated. 10 μM Ned-19 selectively inhibited the CCK-mediated Ca^{2+} signalling pathway that is known to employ NAADP but not ACh, which is NAADP-independent (Figure 6.2 and 6.3). Furthermore, in agreement with the trigger hypothesis whereby NAADP-induced Ca^{2+} release is amplified by CICR to generate Ca^{2+} oscillations [57, 70, 138, 185, 293], Ned-19 had the tendency to interrupt Ca^{2+} oscillations abruptly. However, whether or not Ned-19 can act as a true NAADP antagonist in pancreatic acinar cells needs to be empirically tested by using NAADP-AM (a membrane permeant ester that is broken down by cytosolic esterases to release NAADP) or by direct intracellular dialysis of NAADP. As Ned-19 has been shown to inhibit NAADP-evoked responses in many mammalian cell types (Table 6.2), it is likely

that Ned-19 could also serve as an NAADP antagonist in pancreatic acinar cells.

Interestingly, at low concentrations Ned-19 has been reported to act as an agonist in the mammalian system [231]. Although studies here could not detect any differences between low concentrations of Ned-19 and DMSO (control), one cannot discount the possibility that the amount of Ca^{2+} release was undetectable. The inability to detect the response may either be due to the fact that the pure NAADP-dependent response may be very small in pancreatic acinar cells, as the release is primarily from endosomes/lysosomes [226], or that the high affinity dye, Fura-2, is buffering and repressing responses. If the latter, then using a lower affinity dye (which buffers more weakly) might improve resolution. Furthermore, the small Ca^{2+} release evoked by low concentrations of Ned-19 may not be amplified because the $InsP_3$ and cAPDR were at the basal level. In order to observe an amplified response in future studies, CICR channels could perhaps be 'tickled' by treating cells with either low concentrations of $InsP_3$/cADPR or else by sensitizing their cognate receptors with the sulphydryl agent thimerosal (a sulphydryl-group-oxidising agent [270]).

6.3.2 Why knocking out one TPC isoform affects some systems and not the others?

The difficulties of transfection and maintaining primary cells such as pancreatic acinar cells prompted the decision to generate TPC KO mice. TPC mutant mice characterized in Chapter 3 provide a selection of powerful tools to examine the role of TPCs in CCK-evoked Ca^{2+} signalling. Given the importance of NAADP in CCK-evoked Ca^{2+} oscillations, and the fact that TPCs are the NAADP-gated Ca^{2+} channels, it was surprising that CCK was still able to evoke Ca^{2+} oscillations in TPC single KOs with oscillatory properties and pharmacology similar to wild-type.

This contrasts with other NAADP-dependent systems, such as glucose-stimulated mouse pancreatic β-cells [52], [Arredouani et al, 2011, unpublished], and carbachol-stimulated mouse bladder smooth muscle [90], where knocking out TPC2 alone had a profound effect on agonist and NAADP-mediated responses. This suggests that in these systems, TPCs are not redundant and that TPC2 is the predominant or important isoform.

It is possible that different systems have different spatial organization (i.e. proximity) of acidic stores to the ER, thereby explaining the apparent discrepancies. There is

precedent for different organelles to tether to each other in a juxtaposition for effective communication during Ca^{2+} signalling; for example, it has been shown that mitochondria tether to the ER via mitofusin 2 for effective mitochondrial Ca^{2+} uptake [46]. In pulmonary arterial smooth muscle cell, the close proximity of lysosomes to the SR in the lysosome-SR (trigger) zone has been proposed to underlie amplification of lysosomal Ca^{2+} release evoked by NAADP and its agonist (vasoconstrictor hormone endothelin-1) via RyRs on the SR [138]. Although in a different smooth muscle, it is possible that the trigger zone also exists in bladder smooth muscle, and as TPC2 has a restricted localization to late endosomes/lysosomes (albeit in MEF cells, Figure 4.3), it may be more involved than TPC1 in the 'trigger zone'.

On the other hand, the spatial organization of TPC-localized acidic stores in relation to the ER may be different in pancreatic acinar cells (cf. TPCs with the SR in the bladder smooth muscle). In pancreatic acinar cells, although the majority of the ER has been shown to be distributed in the basolateral region, some ER terminals extend into the apical region and appeared to surround acidic stores [112, 113, 225]. Additionally, the ER extensions and the acidic stores have been reported to be extremely close ($<$ a few hundred nanometers) in the apical region [110]. This close proximity of the acidic stores to the ER may form the trigger zone in pancreatic acinar cells. Furthermore, in pancreatic acinar cells, $InsP_3Rs$ have been shown to be predominantly localized to the apical region, while the localization of RyRs are more broadly distributed to the basolateral region [126, 156]. Thus, Ca^{2+} release evoked by NAADP in the trigger zone is likely to be amplified by $InsP_3Rs$ in pancreatic acinar cells.

It is possible that in pancreatic acinar cells, the area of the trigger zone is larger than that in pulmonary arterial smooth muscle cells, and that both TPCs are localized at the trigger zone, thus causing the redundancy of TPCs in CCK signalling (compensation by the remaining TPC in TPC single KOs). It would therefore be pertinent to study the localization of TPCs in pancreatic acinar cells, in particular, its relation to amplifiers such as $InsP_3Rs$ and RyRs. Furthermore, a similar redundancy was observed in $InsP_3R2$ or $InsP_3R3$ single KOs; ACh and CCK were still able to elicit Ca^{2+} responses in pancreatic acinar cells of single KOs, while the Ca^{2+} responses were completely abolished in the absence of both $InsP_3R2$ and $InsP_3R3$ [99].

6.3.3 Acidic stores in pancreatic acinar cells

In pancreatic acinar cells, acidic stores comprise the members of the endo-lysosomal system (such as endosomes and lysosomes) and also the secretory (zymogen) granules [226, 228] that are predominantly localized in the apical region [74, 92, 185, 269, 293]. The results from TPC single KO experiments showed that both TPC single KOs were sensitive to GPN suggesting that TPC1 and TPC2 are localized in cathepsin-C containing lysosome-related organelles. This supports the previous finding that both mouse TPC1 and TPC2 are localized in late endosomes/lysosomes (Figure 4.2 and 4.3).

Interestingly, GPN did not completely abolish CCK-evoked Ca^{2+} signalling in some TPC single KO cells; the residual response may be explained by the fact that mouse TPC1 was shown to have a broader subcellular distribution than mouse TPC2 in MEF cells. It is possible that in TPC2 KO pancreatic acinar cells, mouse TPC1 is also localized to non-lysosomal stores (such as endosomes) which are not targeted by GPN. It is also possible that the localization of TPC2 in TPC1 KO may have extended to endosomes in order to compensate for the loss of TPC1 in those acidic stores. Alternatively, the residual response may simply due to cell variations in the activity of cathepsin-C, or lysosomal luminal pH (as the activity of cathepsin-C is pH-dependent [71]).

6.3.4 Mechanisms underlying Ca^{2+} oscillations

6.3.4.1 Frequency of oscillations

In view of the importance of NAADP signalling in CCK-evoked Ca^{2+} oscillations in WT cells, it would be predicted that in the absence of TPCs, CCK would not to elicit any oscillations. Quite unexpectedly, CCK was still able to elicit oscillations in TPC DKO albeit with a lower frequency than with WT (Figure 6.5C). Interestingly, CCK-evoked oscillations were also slower in TPC1 H (Figure 6.5B). This suggests that TPCs may be important for CCK-evoked oscillations.

In pancreatic acinar cells, the trigger response induced by NAADP from endosomes/lysosomes may be too small to be detected; the observed oscillations evoked by CCK probably reflects CICR amplification, as NAADP-evoked Ca^{2+} release from acidic stores have been shown to be dependent on CICR [110, 226]. Several factors have

been proposed to play a role in determining the frequency of Ca^{2+} oscillations: the stimulus intensity [222, 223]; the filling of the ER store [27, 275]; and Ca^{2+} feedback on the messenger production or degradation [89, 254], or at the intracellular channel level [221].

It has been suggested that the frequency of Ca^{2+} oscillations is regulated by combined contributions of SERCA, $InsP_3Rs$, cytosolic and the luminal ER Ca^{2+} concentration [27, 195, 221, 275]. It is believed that during ISP, the refilling of the ER via SERCA is important for determining the $InsP_3R$ sensitivity to cytosolic $InsP_3$ and Ca^{2+} [27, 267], and thereby the initiation of the next spike. The sensitivity of $InsP_3Rs$ increases with luminal $[Ca^{2+}]$ [27, 267]. Thus, the faster the store is refilled, the shorter the delay to the next spike [27, 267]. Upon spike initiation, the slope of the rising edge reflects the CICR amplification [27, 221], and when the cytosolic $[Ca^{2+}]$ reaches a certain level, further release becomes inhibitory to $InsP_3Rs$ [221, 267], reflected in the falling edge of the spike. This process repeats to drive oscillations.

In TPC1 H and TPC DKO cells, the process of ER refilling may be altered; it is possible that in these cells, there is less Ca^{2+} released from the acidic stores because there are less (in TPC1 H) or no TPC channels (in TPC DKO). This reduced release may lead to less Ca^{2+} being taken up into the ER store (to prime the ER store). Additionally, the reduced Ca^{2+} may also reduce the Ca^{2+} trigger to sensitise the $InsP_3Rs$/RyRs to initiate CICR. A combination of both scenarios may help to explain why the ISP is longer in these cells.

Alternatively, Ca^{2+} oscillations in pancreatic acinar cells have been suggested to depend on oscillatory $InsP_3$ concentrations [254] as a result of Ca^{2+} feedback on the production of $InsP_3$ by phospholipase C (PLC) and degradation of $InsP_3$ by $InsP_3$ 3-kinase. Both PLC, specifically, PLCδ and $InsP_3$ 3-kinase are known to be stimulated by Ca^{2+} [7, 28, 89]. Knowing the importance of messenger level on regulating Ca^{2+} oscillations, it is possible that Ca^{2+} oscillations in pancreatic acinar cells are also dependent on the oscillatory NAADP levels.

NAADP has been reported to be synthesized by CD38 [74] and catabolized by a Ca^{2+}-dependent 2'-phosphatase [26, 159]. It is not known whether CD38 is regulated by Ca^{2+}, however, an NAADP synthase in sea urchin sperm has been reported to be

regulated by Ca^{2+} [282, 283], thus it is possible that CD38 is Ca^{2+}-sensitive. Rather than the direct regulation by Ca^{2+}, CD38 may be indirectly regulated by Ca^{2+} by cAMP. It has been suggested that sea urchin ADP-ribosyl cyclases (ARCs) are activated by cAMP resulting in NAADP production [291]. It is possible that the mammalian homologue of ARCs, CD38 is also activated by cAMP via Ca^{2+} stimulation on specific adenylyl cyclases (AC) isoforms [290]. In pancreas, AC isoform 8 (AC8) has been reported to be the predominant isoform and this isoform is also known to be stimulated by Ca^{2+} [290]. Thus, in pancreatic acinar cells, AC8 may perhaps play a role in Ca^{2+} feedback on the NAADP production. Generation of oscillatory NAADP levels may thereby depend on the Ca^{2+} feedback on CD38 (directly or indirectly by cAMP crosstalk) and Ca^{2+}-dependent 2'-phosphatase.

As mentioned above, it is possible that the Ca^{2+} release from the acid stores is reduced in TPC1 H and TPC DKO cells. This reduction in Ca^{2+} may reduce the overall rate of NAADP production and degradation, resulting in a lower frequency of oscillatory NAADP levels. Consequently, this may lead to a lower frequency of Ca^{2+} oscillations. This hypothesis could be tested by directly adding more NAADP to these cells to examine whether the frequency of oscillations is indeed dependent on NAADP concentration.

Rather than the reduced number of channels, the reduced Ca^{2+} release in TPC1 H may result from the pH change in the acidic stores of these cells. Ca^{2+} and pH appear to exhibit a profound interdependence in the acidic stores; it has been shown that Ca^{2+} filling in acidic stores depends on the proton gradient [67], and conversely, NAADP-induced Ca^{2+} release has been shown to alkalinize the acid stores [74, 192, 193]. It is possible that a reduction in the TPC expression on the acidic stores may alter the pH of the acidic stores. However, a study showed that the luminal lysosomal pH remained unaltered in cells overexpressing sea urchin TPCs [243]. Nevertheless, if pH has increased, this may help to explain the reduced Ca^{2+} release from the acidic stores (a whole-lysosome patching study of mouse TPC2 has shown that NAADP-activated cation currents were abolished when the luminal pH was increased from 4.6 to 7.2 [248]). Thus, it would be informative to examine whether the vesicular pH is altered in TPC mutant cells in the future studies.

6.3.4.2 Amplitude of oscillations

In addition to the longer ISP, CCK-evoked Ca^{2+} oscillations in TPC1 H cells also had smaller peak heights. It is possible that the luminal ER [Ca^{2+}] in these cells is reduced (possibly due to less ER Ca^{2+} uptake as mentioned above), so the maximum amount of Ca^{2+} released during CICR would be reduced. This could be tested by direct measurement of the luminal ER [Ca^{2+}], or by studying the amount of Ca^{2+} release from the ER store by using ionomycin or by direct dialysis of $InsP_3$.

6.3.5 TPC1 KO versus TPC1 H

It is interesting that the parameters of the CCK-evoked Ca^{2+} oscillations were more significantly altered in TPC1 H than in TPC1 KO. A hypomorphic mouse is normally generated when the homozygous knockout is embryonic/neonatal lethal [97, 144] and when the heterozygous knockout has no significant phenotype. It is unclear why TPC1 H has a more significant phenotype than TPC1 KO even though its level of TPC1 protein is reduced but not completely abolished. RT-qPCR and microarray analysis (Chapter 3) showed that the remaining TPC and other genes could become up- or down-regulated to compensate for the loss of one TPC isoform. It is possible that TPC1 H experiences less compensatory mechanisms than TPC1 KO, thus explaining why its phenotype is not masked to the same extent.

6.3.6 CCK signalling in TPC DKO

The CCK signalling pathway in TPC DKO was examined by using various established pharmacological agents that inhibit the NAADP-mediated signalling pathway. The results yielded were unexpected; they showed that in the absence of TPCs, CCK-evoked Ca^{2+} oscillations were still sensitive to GPN (Figure 6.13), bafilomycin A1 (Figure 6.14) and Ned-19 (Figure 6.10). This implies that the pathway is still dependent on the Ca^{2+} release from the acidic stores, possibly by NAADP, in the absence of TPCs.

Although $InsP_3$, cADPR and NAADP have all been reported to release Ca^{2+} from the acidic stores in pancreatic acinar cells [110, 185, 293], Ned-19 has been shown to inhibit NAADP- but not $InsP_3$- or cADPR-mediated Ca^{2+} release in sea urchin egg homogenate [200]. In the mammalian system (rat uterine smooth muscle cells), Ned-19

has also been shown to inhibit Ca^{2+} release evoked by injection of NAADP, but not by $InsP_3$ [6]. In line with this, this study showed that Ned-19 selectively inhibited CCK- and not ACh-evoked Ca^{2+} oscillations (Figure 6.2). This selectivity suggests that NAADP is likely to act as a trigger to release Ca^{2+} from the acidic stores in response to CCK, even in the absence of TPCs. Furthermore, this also suggests that $InsP_3$ signalling pathway is not involved in CCK-evoked oscillations in TPC DKO, as the responses were inhibited by Ned-19.

Although Ned-19 appeared to be selective in inhibiting NAADP signalling in mammalian systems, future studies should confirm its selectivity against the direct responses evoked by NAADP, cADPR and $InsP_3$ in pancreatic acinar cells. Furthermore, in pancreatic acinar cells, it is known that $InsP_3$ signalling is involved in stimulation by non-physiological concentrations of CCK in pancreatic acinar cells [249], if Ned-19 does not target $InsP_3$ signalling, it should also not inhibit oscillations evoked by non-physiological CCK concentrations.

As NAADP is not involved in the ACh signalling pathway [59, 294], it was hypothesis that ACh signalling would not be altered in TPC DKO cells, so this study focused on CCK signalling. However, it would be informative to examine the pharmacology of the ACh signalling pathway in TPC DKO cells to confirm this hypothesis.

The possibility that CCK still recruits NAADP to mediate Ca^{2+} release from the acidic stores in the absence of TPCs should be further tested by using NAADP-AM or by direct dialysis of NAADP via a patch pipette. If similar results are obtained then the phenomenon may be explained by one of two scenarios (Figure 6.16). In the first, TPC is not involved, and in the CCK-mediated signalling pathway NAADP activates another channel on the acidic stores to release Ca^{2+} (Figure 6.16). Ned-19 would have multiple sites of action in addition to the reported TPC complexes [231, 243] as it was shown to be able to inhibit CCK-evoked responses via another channel in the absence of TPCs. This channel (targeted by Ned-19 but not in the TPC complexes) would play a role in the CCK- but not in the ACh-mediated signalling pathway, as Ned-19 showed a minimal effect in inhibiting ACh-evoked Ca^{2+} oscillations (Figure 6.2 and 6.3). Since Ned-19 was only developed two years ago, more information needs to be obtained concerning its mechanism of actions in inhibiting NAADP-mediated signalling.

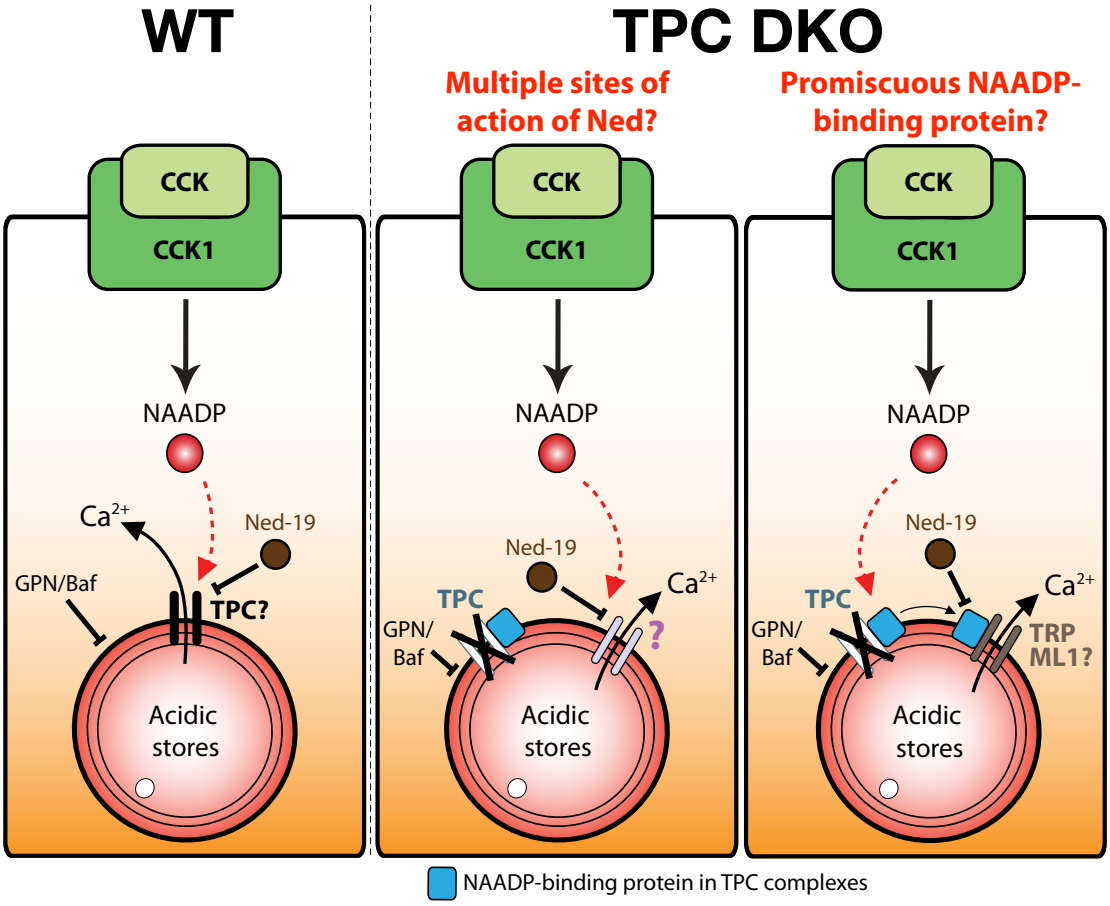

Figure 6.16: Schematics of the possible signalling pathway in CCK-evoked Ca^{2+} oscillations in TPC DKO. In WT, CCK recruits NAADP to release Ca^{2+} from the acidic stores as the CCK-evoked Ca^{2+} response is inhibited by Ned-19, GPN, and bafilomycin A1 (Baf). TPC is the most convincing candidate for the NAADP-gated Ca^{2+} channel, but it is still not known whether TPC plays a role in the CCK-evoked Ca^{2+} response. Studies with TPC DKO showed that in the absence of TPC, CCK-evoked Ca^{2+} oscillations were still inhibited by Ned-19, suggesting that the $InsP_3$- and cADPR-signalling pathways were not recruited [200] and that NAADP is the major player. Additionally, CCK-evoked Ca^{2+} oscillations in TPC DKO were sensitive to GPN, and Baf, suggesting two possible scenarios. Firstly (central panel), NAADP gates other Ca^{2+} channels to mediate Ca^{2+} release from the acidic stores in response to CCK. However, the fact that Ned-19 still inhibited this response suggesting Ned-19 has other sites of action in addition to the reported TPC complex [231, 243]. Secondly (right panel), NAADP-binding protein in TPC complexes becomes promiscuous to compensate for the loss of both TPCs. These proteins start forming new complexes with Ca^{2+} channels that have similar structure to TPCs in the acidic stores, such as TRPML1. Ned-19 is still able to inhibit the response by acting on proteins of the original TPC complexes.

The second scenario is based on compensatory mechanisms in TPC DKO mice. Here, the NAADP-binding protein is promiscuous, and the loss of TPCs prompts the binding protein to form complexes with another Ca^{2+} channel (Figure 6.16). In the previous chapter, it was suggested that TPCs are not the direct binding targets of NAADP. NAADP is likely to bind to an accessory protein on the membrane tightly associated with TPC in a complex. The molecular identity of this binding protein is still unknown, but it could become promiscuous to compensate for the loss of TPCs. It is possible that in the absence of TPCs, the NAADP-binding protein forms new complexes with other Ca^{2+} channels that have shared structural homology with TPCs (e.g. TRP channels) on the acidic stores. This newly formed complex would bind to and respond to NAADP, and consequently release Ca^{2+}. Ned-19 would still inhibit Ca^{2+} release by targeting the components from the original TPC complexes in this newly formed complex. Perhaps, Ned-19 binds to an allosteric site (as Ned-19 does not compete with NAADP in mammalian systems, Section 5.2.4.2) on the NAADP-binding protein to inhibit Ca^{2+} release. Alternatively, Ned-19 might bind to other accessory proteins that are tightly associated in a complex with the promiscuous binding protein.

One candidate to form the alternative complex with the NAADP-binding protein is TRPML1. TRPML1 is a nonselective cation channel that is localized predominantly to late endosomes/lysosomes. Several studies have reported that NAADP is able to activate TRPML1 channel opening [300, 303] while a role of TRPML1 in NAADP-mediated Ca^{2+} signalling has been ruled out by others [166, 235, 292]. In particular, direct dialysis of NAADP via patch clamping elicited Ca^{2+} spikes in TRPML1 KO pancreatic acinar cells [292]. This strongly suggests that NAADP does not normally target TRPML1 channel to release Ca^{2+}. The study also showed that although TRPML1 does not release Ca^{2+} in response to NAADP, TRPML1 and TPCs exist in the same complex [292]. This supports the idea that in the absence of TPCs, the NAADP-binding protein that was associated with TPCs may recruit TRPML1 in the same complex to release Ca^{2+}.

Many voltage-gated Ca^{2+} channels comprise a pore-forming subunit and auxiliary subunits that modulate trafficking and the biophysical properties (such as current kinetics and amplitude) of the pore-forming subunit [9, 203]. TPCs may well have auxiliary subunits that contribute to channel regulation. It is therefore crucial to identify the

molecular components of the TPC complex to further understand the signalling pathway mediated by NAADP.

The major limitation in using knockout animals is the issue of compensation. Compensation occurs often in knockout animals to maintain near-normal function [75, 86, 176, 212, 229]. In addition to the protein promiscuity (mentioned above), there is also the possibility that the NAADP synthesis pathway is altered. It is possible that NAADP is not synthesized upon CCK stimulation in TPC DKO, and Ca^{2+} oscillations are evoked by other unknown compensatory mechanisms that are sensitive to Ned-19 and GPN/bafilomycin A1. Future studies should examine the levels of NAADP in TPC DKO.

It is also possible that in TPC DKO cells, the Ca^{2+} signals evoked by CCK are perhaps initiated from the basolateral region rather than the apical region as in the WT [56, 57, 59, 272]. It would therefore be interesting to study the spatial-temporal pattern of Ca^{2+} oscillations evoked by CCK and NAADP in TPC DKO.

6.4 Conclusions

Thus far, although ample evidence has demonstrated that TPCs are the NAADP-gated Ca^{2+} channel, results from this chapter suggest that TPCs are perhaps not as crucial to CCK-mediated Ca^{2+} oscillations in pancreatic acinar cells as anticipated. In the absence of TPCs, CCK was still able to evoke Ca^{2+} oscillations and the pharmacology of Ca^{2+} oscillations was similar to the wild-type. Future studies should confirm these results by using NAADP-AM or by direct dialysis of NAADP via a patch pipette.

However, the effect of compensation in TPC DKO must not be discarded. Compensation is suggested to occur throughout the development of many knockout mice, such as for mice with knockout of the transient receptor potential vanilloid receptor (TRPV1) [212], mitogen-activated protein kinase (MAPKs) [8], and prion protein (PrP) [176]. It is equally possible that the true phenotype of TPC KOs is similarly masked by compensatory mechanisms. This could be overcome by generating more sophisticated mouse models, for example, tissue-specific or conditional knockouts, to circumvent developmental compensation [229].

Furthermore, if it emerges that TPCs do not have a pivotal role here, it indicates that there are other ion channels that are activated by NAADP in the acidic stores for the subsequent Ca^{2+} release. This versatility of NAADP-mediated signalling requires elucidation.

Chapter 7

General discussion

In the preceding chapters the implications of the experimental results were discussed within the context of the chapters' investigative approaches. This chapter collates the individual strands of this research and reviews them within the broader field of Ca^{2+} signalling. This discussion focuses on the physiological and pathophysiological roles of TPCs, the contribution of KO/mutant mice to NAADP-signalling research, and directions for future investigations of TPC roles in NAADP-signalling pathways.

7.1 Roles of individual TPC isoforms

A major focus of this research was the investigation of the physiological roles of individual mouse TPCs. This allows further insight into the versatility of NAADP-signalling pathways. An important discovery here was that in addition to the two isoforms of mouse TPCs (TPC1 and TPC2), there exists a shorter TPC1 variant (ΔN-TPC1). Although these TPC isoforms and the TPC1 variant were shown to be expressed in all the tissue types tested (Chapter 3), it was also clearly demonstrated that each TPC isoform and the TPC1 variant has a distinct subcellular distribution pattern (Chapter 4). The longer variant of TPC1 has a broader subcellular distribution, predominately in some unidentified subdomains of endosomes and in late endosomes/lysosomes. The subcellular distributions of ΔN-TPC1 and TPC2 are more restricted to late endosomes/lysosomes, with ΔN-TPC1 appearing to be localized more to the ER than TPC2.

The function of ΔN-TPC1 is currently unknown; if ΔN-TPC1 does release Ca^{2+} like

its longer variant, this adds a hitherto unrecognised pathway for NAADP-mediated Ca^{2+} signalling. Thus, it would be key to investigate whether ΔN-TPC1 is sensitive to NAADP; this could be done by overexpressing ΔN-TPC1 in cells to test whether Ca^{2+} is released upon NAADP stimulation, and if so, whether the release is from the acidic stores. If cells overexpressing ΔN-TPC1 do not release Ca^{2+} upon NAADP stimulation, there is a possibility that ΔN-TPC1 acts as a dominant negative to TPC channels. If this is the case, ΔN-TPC1 could be co-expressed with TPC1 or TPC2 to test whether the NAADP-evoked responses in cells overexpressing TPC1 or TPC2 are altered.

The distinct subcellular localization of TPCs implies considerable versatility of NAADP-mediated signalling. Local Ca^{2+} release from the acidic stores elicited by NAADP has been proposed to: facilitate vesicle fusion in the endo-lysosomal system [103, 172]; to activate Ca^{2+}-sensitive ion channels on the plasma membrane in order to modulate membrane excitability and ion flux; and to act as a trigger to initiate a global response via CICR in the ER/SR [100, 103] (Chapter 1, Figure 1.9).

Sea urchin TPCs has been shown to localize differentially in acidic stores; sea urchin TPC2 and TPC3 localize predominantly in late endosomes/lysosomes and some in recycling endosomes, while sea urchin TPC1 only localizes partly in late endosomes/lysosomes [243]. Differential effects upon endo-lysosomal trafficking and functions were also observed when cells were overexpressed with different sea urchin TPCs; HEK293 cells overexpressing sea urchin TPC1 exhibited the severest defect in endo-lysosomal trafficking and the largest increase in lysosomal size compared to those cells ovexpressing sea urchin TPC2 and TPC3 [243]. Interestingly, HEK293 cells overexpressing sea urchin TPC3 exhibited no enlarged lysosomes but had defect in endo-lysosomal trafficking [243]. Specific TPC isoforms/variants might therefore be involved in regulating vesicular fusion and trafficking in specific sections of the endo-lysosomal pathway depending on their localization (Figure 7.1). The longer variant of mouse TPC1 may play a role in vesicular fusion and trafficking of both endosomes and lysosomes, as it has a broader distribution, while ΔN-TPC1 and TPC2 may be more involved in lysosomal fusion, as their predominant localization are in late endosomes/lysosomes. Additionally, the endosome-localized TPC1 may be involved in modulating membrane excitability, as the spatial organization of endosomes is nearer to the plasma membrane than late endosomes/lysosomes.

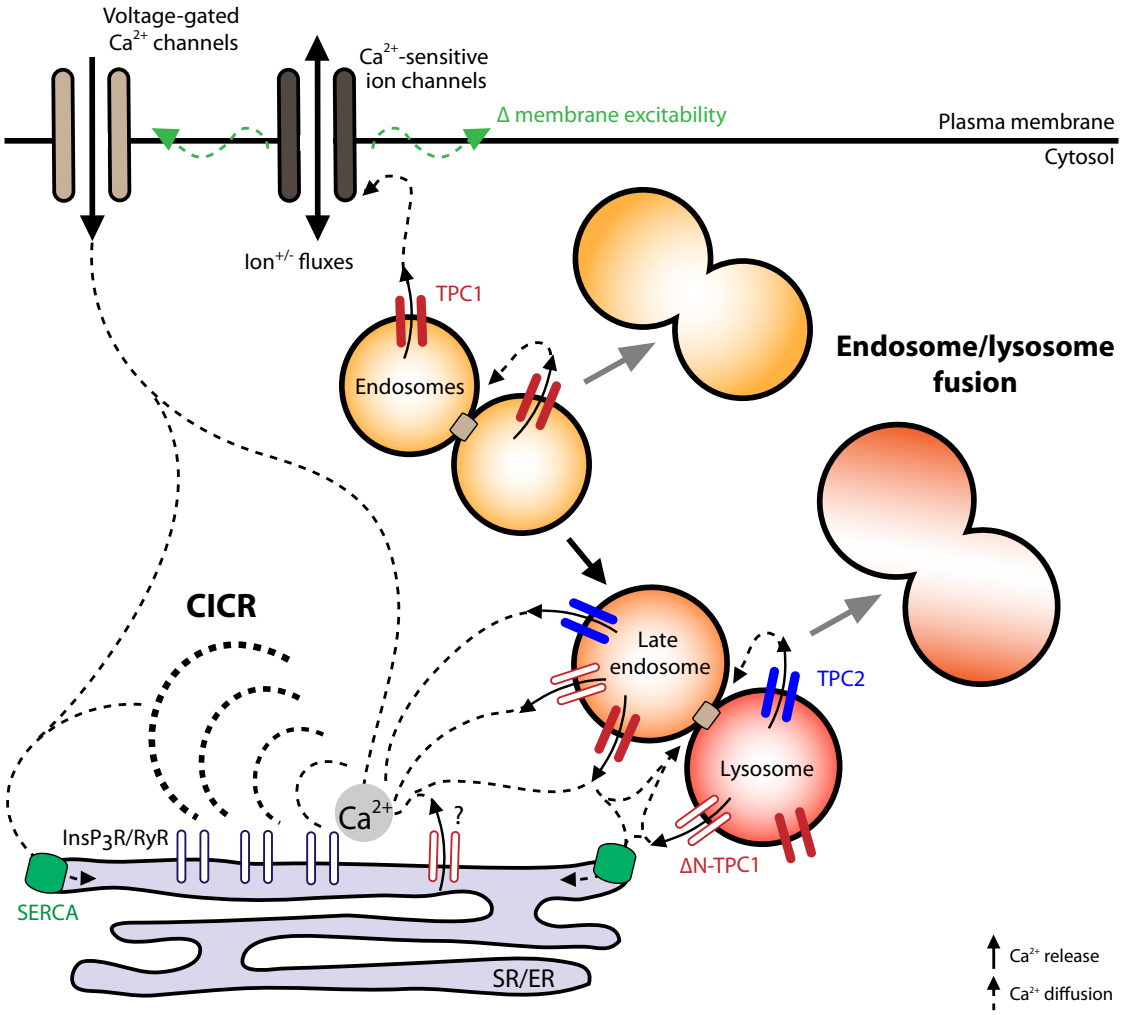

Figure 7.1: Differential localization of TPCs may underlie the diverse spatial organization of NAADP-mediated Ca^{2+} signals and thereby the regulation of specific cellular events.

7.1.1 TPCs in the NAADP trigger hypothesis

In HEK293 cells overexpressing human TPC2, NAADP elicited a biphasic Ca^{2+} response: an initial ramp due to trigger Ca^{2+} release from the acidic stores, and the large Ca^{2+} transient that results from CICR via $InsP_3Rs$ [52].

Interestingly, while NAADP-elicited Ca^{2+} release was highly localized in HEK293 cells overexpressing human TPC1 (supplementary data of [52]), the release was global in SKBR3 cells overexpressing human TPC1, and for the latter the globalization of the Ca^{2+} signal was due to CICR via coupling to the RyRs [39]. These disparate results may be partly explained by the localization of human TPC1 in different expression systems. In HEK293 cells, human TPC1 had minimal localization in late endosomes/lysosomes

(supplementary data of [52]), while in SKBR3 cells, human TPC1 has a substantial distribution in late endosomes/lysosomes [39]. Lysosomes have been shown to co-localize with sections of the SR; this lysosome–SR junction is the trigger zone for amplification of NAADP-elicited Ca^{2+} release via CICR [138, 139]. The higher proportion of human TPC1 in lysosomes therefore implies an increased probability the trigger at this locus.

It is interesting why lysosomes and not endosomes form the trigger zone with the ER/SR; in addition to the localization, the luminal environment (Ca^{2+} and pH) might also contribute to the formation of the trigger zone. A lower luminal [Ca^{2+}] has been shown to reduce NAADP-evoked currents via TPC channels and TPC channel opening probability [231, 248]. Together with the fact that lysosomes (∼500 μM) have a higher luminal [Ca^{2+}] than endosomes (∼40 μM) [166, 251], this suggests that TPC channel activity may be reduced in endosomes compared to that in lysosomes. Although the mechanism underlying the regulation of TPCs by luminal pH is currently unclear; an increase in luminal pH (from 4.6 to 7.2) has been shown to abolish NAADP-evoked currents via TPC channels [248]. As the pH in endosomes and lysosomes have been reported to be approximately 6 [166, 251] and 4.5 [166, 277], respectively, it is possible that the NAADP-evoked responses via TPCs are reduced in endosomes as a result of a higher pH. Thus, the regulation of TPCs by luminal Ca^{2+} and pH might help to explain why the endosome-localized TPCs are less likely to generate a trigger for CICR amplification.

As mouse TPC1, ΔN-TPC1 and TPC2 were shown to be localized in late endosomes/lysosomes (in MEF cells, Chapter 4), it is likely that NAADP-elicited Ca^{2+} release via these channels would act as a local trigger for CICR amplification from the SR/ER. However, it has been shown that NAADP was not able to elicit a large Ca^{2+} response in HEK293 cells overexpressing mouse TPC1 [307]. Although the authors claimed that mouse TPC1 is insensitive to NAADP, it might be that the increase in Ca^{2+} is small and localized, and thus evaded detection in that study. Additionally, it is possible that the localization of mouse TPC1 in HEK293 cells differs from that in MEF cells, such that mouse TPC1 does not localize in late endosomes/lysosomes; this too might explain why the responses were not amplified.

In HEK293 cells overexpressing mouse TPC2, NAADP was indeed able to elicit Ca^{2+} release; the release was not sensitive to thapsigargin, thus indicating that CICR

amplification from the ER was not recruited in this system [307]. Interestingly, mouse TPC2 has been shown to localize predominantly in late endosomes/lysosomes when overexpressed in HEK293 cells, so it would be expected that the responses would have been amplified similar to human TPC2 in HEK293 cells. This unexpected response is therefore likely to be attributable to the use of heterologous expression systems. Thus far, heterologous overexpression of mouse TPCs has not supported the model in which NAADP acts as a trigger. Future functional studies using a mouse cell line could be useful in resolving these inconsistencies.

As mentioned above, overexpression of TPCs in cells could disrupt the endo-lysosomal trafficking and functions [243]. It is possible that overexpression of mouse TPCs in the study by Zong *et al.* severely altered lysosomal functions; this might also explain the discrepancies. A better transfection method is required to express the gene at physiological levels [35, 143]; bacterial artificial chromosomes could be potentially useful, as the vector is large and allows the entire genomic sequence of the gene with its endogenous promoters and regulatory elements, as well as fluorescent tag to be inserted [35, 143].

Furthermore, it would be highly informative to study elementary Ca^{2+} signals arising from TPC channels to shed light on their triggering properties. It is possible that the elementary signals arise from mouse TPCs are smaller and shorter than those from the human homologues; thus, although the localization of mouse TPC2 resembles that of human TPC2, their Ca^{2+} signals may not be large enough to trigger CICR.

7.2 Accessory proteins in TPC complexes

Many ion channels, for example, voltage-gated Na^+, K^+, and Ca^{2+} channels [190, 203], RyRs [149, 284], and $InsP_3Rs$ [279], are known to form macromolecular signalling complexes, these comprise a pore-forming subunit with associated auxiliary subunits and/or regulatory proteins (such as protein kinases, phosphatases and calmodulin).

The evidence here suggests that NAADP activates TPC by binding to an unknown accessory protein in the TPC complexes (Chapter 5). There are precedents for nucleotide-binding accessory proteins to regulate channel activities, for example, the binding of cADPR to FKBP12.6 in RyR complexes [202, 304]. The fact that NAADP was bound to immunopurified sea urchin TPC complexes with the same affinity as the native system [243]

suggests that the NAADP-binding protein is tightly associated in TPC complexes. Furthermore, in Chapter 5, it was shown that NAADP was bound to the TPC DKO membranes in the absence of TPCs, thus indicating that the binding protein is membrane-integral or -peripheral protein.

A transmembrane auxiliary $\alpha_2\delta$ subunit of voltage-gated Ca^{2+} channels has been reported to exist independently of its channel complex, and it was hypothesized that association/dissociation of the $\alpha_2\delta$ subunit with the channel complex modulates the channel conductance. It is possible that NAADP-binding protein behaves in a similar manner with TPCs (Figure 7.2). This model would explain the NAADP binding observed with TPC DKO membrane preparation (Chapter 5), and also for immunopurified TPC complexes [243].

Interestingly, truncation or mutation of the N-terminal dileucine motif in human TPC2 has been shown to result in redirection from late endosomes/lysosomes to the plasma membrane [42]. This plasma membrane-localized human TPC2 mutant could still be activated by nanomolar NAADP. An interesting question arises as to how the

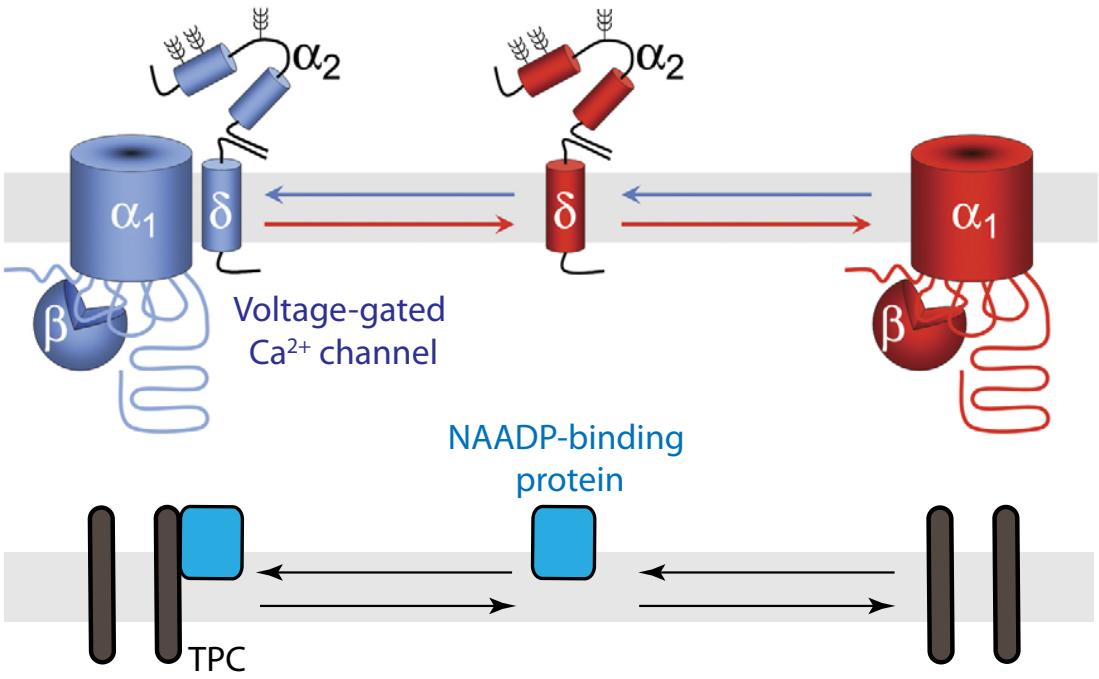

Figure 7.2: Top, a voltage-gated Ca^{2+} channel is comprised of the pore-forming $\alpha 1$ subunit and auxiliary β and $\alpha_2\delta$ subunits. $\alpha_2\delta$ subunit may modulate the channel by association and dissociation. The diagram is taken from [203]. Bottom, an NAADP-binding protein may also have the ability (like the $\alpha_2\delta$ subunit) to associate and dissociate from TPC complexes.

NAADP-binding protein fits with this scenario. It is possible that some NAADP-binding proteins form complexes with TPC shortly after protein synthesis in the ER, and that these binding protein-TPC complexes are transported to their destination according to the sorting signals on TPCs. Those binding proteins that do not couple to TPCs might be directed to late endosomes/lysosomes (assuming that this is where they are normally localized).

Specific auxiliary subunits or regulatory proteins have been reported to regulate more than one class of channel. For example, the Neto1 auxiliary subunit has been shown to regulate both *N*-Methyl-D-aspartate (NMDAR) and kainate receptor (KAR) classes of ionotropic glutamate receptors [264]; protein kinase A (PKA) and Ca^{2+}/calmodulin-dependent protein kinase (CaMKII) can regulate both RyRs [149] and $InsP_3Rs$ [279]. This dual-role capability might also apply for the NAADP-binding protein (i.e. regulate other channels in addition to TPCs) and is consistent with the model of 'promiscuous' binding protein in the absence of TPCs in pancreatic acinar cells (Figure 6.16). As TPCs are not found in acidic stores in pancreatic acinar cells, the NAADP-binding protein may thereby become associated to a neighbouring channel on the acidic stores, such as TRPML1. It has recently been reported that TRPML1 can exist in a complex with TPCs [292], as TRPML1 was shown to co-localize and co-immunoprecipitate with TPC2, and to a lesser extent with TPC1 [292]. This helps to explain why in TPC DKO cells, CCK was still able to evoke Ca^{2+} oscillations (as NAADP could still bind to the binding protein that regulates another channel on the acidic stores), and the oscillations were still sensitive to Ned-19 (assuming Ned-19 acts on the NAADP-binding protein) and GPN/bafilomycin A1 (Figure 6.16).

Channels that exist in multiple isoforms, for example RyRs, have been reported to incorporate different components in their complexes [284]. Additionally, different auxiliary subunit isoforms have shown to have distinct tissue distribution profiles [9]. This may help to explain why in some cell types such as pancreatic acinar cells, TPCs exhibit mutual redundancy (Chapter 6) whereas in others, such as in bladder smooth muscle [90] and pancreatic β-cells [52], they do not. Perhaps in bladder smooth muscle and pancreatic β-cells, only one NAADP-binding protein isoform is expressed, and this only associates with TPC2, whereas in pancreatic acinar cells, two NAADP-binding protein isoforms are

expressed and each associates with just one of the isoforms.

Finally, some accessory proteins have been shown to modulate the affinity of agonist binding to the receptor, for example, an accessory protein for interleukin-1 receptor (IL-1R AcP) [76]. This type of accessory protein may help to explain the two distinct activation/inactivation mechanisms of NAADP (see Section 1.5.1); it is possible that two distinct regulatory proteins are associated with the NAADP-binding protein resulting in differential NAADP affinity and activation profiles.

As TPCs have been shown to play an important role in many physiological functions [52, 90, 220, 243], it would not be surprising to discover that TPCs are regulated by a range of accessory proteins. Future studies to identify the NAADP-binding protein and other accessory proteins (for example, by immunopurification of TPC complexes, or affinity chromatography followed by mass spectrometry) will be essential to gain insight into the mechanisms underlying NAADP-induced TPC activation, and to further understand the versatility of TPC signalling.

7.3 Mutant mice to elucidate the physiological roles of NAADP signalling

Mouse models represent a powerful tool to study a vast range of proteins for their significance in human physiology and disease, for example, knockout/mutant mice for $InsP_3Rs$ and RyRs (detailed in Section 1.3.3 and 1.4.4, respectively) and p53 (tumour suppressor protein p53); p53 KO mice have shown to be an important model for human Li-Fraumeni syndrome, a disorder in which cancer susceptibility is dramatically increased [88].

In this section the use of mouse models will be discussed from four aspects: a review of the NAADP-signalling discoveries achieved using KO mice; the problems of compensatory mechanisms in KO mice, and approaches to overcome these; the application of these KO mice in further NAADP research; and finally, some observations on the relative merits of gene-trapping and gene-targeting as techniques in KO mouse generation.

7.3.1 Using knockout/mutant mice for functional analysis

7.3.1.1 Smooth muscle

NAADP has been shown to play a role in muscle contraction in many types of smooth muscle, for example, pulmonary arterial [36, 138], coronary arterial [302, 303], testicular peritubular [104], renal arteriolar [268], bladder detrusor [90] and uterine [6, 255].

Using CD38 KO mice, a study showed that the basal and the histamine-induced NAADP level was not dependent on CD38 and also the base-exchange reaction in myometrial cells [255]. This work suggests that in this cell type, CD38 is not an NAADP synthase [255].

Using the TPC2 KO mice described in Chapter 3, another study has provided further evidence for the role of TPC in smooth muscle contraction: NAADP-evoked contraction in bladder detrusor smooth muscle was completely abolished; in addition, agonist (carbachol)-evoked contraction became insensitive to pharmacological inhibitors of NAADP signalling pathway in the TPC2 KO tissue [90].

Although NAADP signalling was not involved in mediating carbachol-evoked contraction in TPC2 KO, the level of agonist-evoked contraction appeared not to be significantly reduced compared to the WT [90]. This indicates that compensation may have occurred in TPC2 KO mice. Indeed, the carbachol-evoked response appeared to be more dependent on RyRs in TPC2 KO [90]. Microarray analysis of male TPC2 KO liver tissue (Section 3.2.6) showed that a vast number of genes had been up- or down-regulated; perhaps because liver and not bladder muscle was analyzed, RyR did not appear to be one of the up- or down-regulated genes.

7.3.1.2 Pancreatic β-cells

NAADP has also been shown to mediate Ca^{2+} release in response to agonists such as glucose, insulin, and glucagon-like peptide-1 (GLP-1) in pancreatic β-cells [4, 10, 52, 131, 136, 178, 189, 293].

A study using CD38 KO has shown that GLP-1-stimulated NAADP production is partly dependent on CD38 in pancreatic β-cells [136]. Furthermore, another study showed that NAADP-evoked Ca^{2+} release was completely abolished in pancreatic β-cells from

TPC2 KO mice [52] (validated in Chapter 3), thereby confirming the role of TPC2 in NAADP-mediated Ca^{2+} release in pancreatic β-cells. In TPC2 KO pancreatic β-cells, it is not known whether any compensation has occurred in the agonist-evoked signalling pathway in which NAADP is involved.

7.3.1.3 Pancreatic acinar cells

Accumulated evidence over the past few years has demonstrated a role of NAADP-mediated Ca^{2+} release in pancreatic acinar cells, and that this is specifically in CCK- and not ACh-signalling pathway [57, 59, 74, 185, 293, 294].

CD38 KO mice have proved useful in determining that CD38 is the NAADP synthase in response to CCK stimulation in pancreatic acinar cells [74]. In the absence of CD38, CCK could no longer stimulate NAADP production, and it was also shown that CCK-evoked Ca^{2+} oscillations were insensitive to GPN [74]. However, the fact that CCK could still evoke Ca^{2+} oscillations in CD38 KO cells suggested that compensatory mechanisms may have occurred. Indeed, CCK-evoked Ca^{2+} oscillations in CD38 KO mice appeared to have become remodelled such that the oscillations were heavily dependent on Ca^{2+} influx from the extracellular medium [74].

Surprisingly, CCK was still able to evoke Ca^{2+} oscillations in TPC single and double KO cells with similar pharmacological profiles to that of WT cells (Chapter 6). As mentioned in Section 6.3, it is suspected that compensation may have occurred here as well. However, unlike the case with the CD38 KO mice, the exact compensatory mechanisms underlying CCK-evoked oscillations in TPC KO mice remain unclear as the oscillations were still sensitive to Ned-19, GPN, bafilomycin A1 and were not affected by the extracellular Ca^{2+}. In contrast to carbachol-evoked contraction in bladder smooth muscle (where a residual NAADP-response was observed after $InsP_3R$ or RyR inhibition), pharmacological inhibitors of $InsP_3Rs$ and RyRs are unlikely to be helpful in investigations with pancreatic acinar cells, as CCK-evoked oscillations tend to be completely abolished by these inhibitors [59]. Direct application of NAADP in TPC DKO cells is required to confirm unambiguously that TPCs play a role in CCK signalling. Whether or not TPCs are involved in NAADP signalling in pancreatic acinar cells, the TPC DKO mice will be useful in providing novel insights into the mechanism of action of NAADP signalling.

7.3.2 Ways to overcome compensation

As mentioned above, compensatory mechanisms are likely to be occurring in the KO mice; this perhaps underlines the importance of NAADP signalling and may further provide a route to identifying proteins that are involved with NAADP/TPC in shaping the agonist-evoked response. In cases like TPC DKO pancreatic acinar cells, compensation during development may mask the true phenotype resulting from impaired signalling (caused by the absence of TPCs). A more sophisticated mouse model would be highly beneficial. Models such as tissue-specific or conditional KOs may help to overcome these limitations as gene deletion could be scheduled in specific tissue and/or at a defined time [116, 229]. Alternatively, siRNA knockdown of TPC expression could also circumvent the masking by developmental compensation. A combination of sophisticated mouse models with siRNA would hopefully unravel the function of TPCs in pancreatic acinar cells.

7.3.3 Using knockout/mutant mice for other analyses

Despite the absence of a distinct phenotype due to functional compensation, important information was obtained from analysis of these mutant mice. The use of gene-trapped mutant mice allowed the identification of mRNA/protein expression patterns of endogenous TPCs (Chapter 3). In addition to the self-evident benefits of using TPC KO mice to provide a TPC-null background for functional studies, they also served as negative controls to test antibody specificities (Chapter 3) and were essential to demonstrate that TPCs are not themselves the NAADP-binding proteins (Chapter 5).

As an alternative to knocking out TPCs, the TPC genes could be genetically modified by fusing to fluorescent proteins. This would allow TPCs to be monitored in a native system in real time, and thus avoid the expression artefact resulting from heterologous or overexpression systems.

7.3.4 Gene trapping versus gene targeting

There are currently over 460,000 trapped genes in the knockout consortia but only around ∼10,000 targeted ES cell lines [116]. Thus, the chance of obtaining a mutant ES cell line for a target gene (in this case TPCs) is significantly higher. Even though the number

of trapped cell lines far exceeds the number of mouse genes (∼20,000), only 50–70% of genes have been trapped. This is because some genes have been trapped more than once, while some vectors have been inserted into non-coding regions [116]. Additionally, because gene trapping is a random process, certain regions of the genome are not susceptible to trapping [116]. In the case of a TPC mutant ES cell line, in order to generate a true loss-of-function (i.e. KO) mice, not only does the vector need to have been inserted in the coding region, but the insertion site needs to be in the region upstream (near 5'-end) of the gene.

Fortunately, ES cell lines that contain gene trap mutation near 5'-end of TPC1 and TPC2 genes were found (Chapter 3). However, while the TPC2 mutant ES cell line successfully generated a true TPC2 KO, TPC1 mutant ES cell line generated a hypomorph. For this reason it was necessary to generate a TPC1 KO from an ES cell line that has been mutated by gene targeting. This time-consuming process to generate a TPC1 KO highlights the fact that although there is a vast number of mutant ES cell lines, the best approach is often to generate knockout mice by gene targeting where gene-targeted ES cell lines are available.

In conclusion, the TPC KOs have provided critical insights into the physiological role of TPCs in NAADP signalling in particular cell types. Although compensation occurs in certain cell types, tissue-specific and/or conditional TPC KOs are likely to be the best solution to overcome this. In addition to the above cell/tissue types mentioned, NAADP has been reported to play a role in a myriad of cell types including white blood cells (T-lymphocytes [24] and lymphokine-activated killer (LAK) cells [237]), platelets [168, 169], cardiac muscle [174], astrocytes [220], endothelium [44], and neuron [40]. Future studies in these cell types in TPC KOs would accelerate our understanding of the role of TPC family in human physiology.

7.4 Implications of TPCs in human diseases

7.4.1 Lysosomal Storage Diseases (LSDs)

TPCs are important for the regulation of Ca^{2+} homeostasis in the endo-lysosomal system [243], and thus dysfunction of TPCs could be responsible for lysosomal storage

diseases (LSDs). LSDs are caused by the impairment of lysosome capability to uptake, sort, or metabolise the material obtained during endocytosis, or autophagy due to defective enzyme activity, resulting in accumulation of undigested material [142, 210].

7.4.1.1 Gaucher disease

Gaucher disease the most common LSD, is characterized by a defective glucocerebrosidase activity resulting in glucosylceramide accumulation [250]. A study has shown that the L-type Ca^{2+} channel blockers (diltiazem and verapamil) were able to alleviate symptoms derived from fibroblasts in Gaucher patient [197]. As these drugs have been shown to diminish NAADP-mediated Ca^{2+} release [107, 300, 301], it suggests that TPC defects may be involved in Gaucher disease. Furthermore, the activity of glucocerebrosidase has been shown to become reduced at pH >5 [278]. A possible interpretation is that in Gaucher disease, NAADP-mediated Ca^{2+} release via TPCs is up-regulated and the pH of the acidic stores is more alkalinized (NAADP has been shown to alkalinize the acid stores concomitant with Ca^{2+} release [74, 192, 193]), thus contributing to defective glucocerebrosidase activities. It would be interesting to confirm the above hypothesis by using Ned-19 in Gaucher patient-derived fibroblasts to see whether inhibition of NAADP-induced Ca^{2+} release via TPCs [231] alleviates symptoms.

Another symptom associated with Gaucher disease is auditory abnormalities [18, 55]. It is possible that TPC2 may also be involved in this abnormality, as the TPC2 gene has been located to an autosomal recessive nonsyndrommic deafness locus (chromosome location 11q13.2-q13.4) [133, 135]. However, no disease-causing mutation was found in the TPC2 gene from an affected individual [133]. Rather, the auditory abnormality may be a result of increased TPC2 expression [305]: TPC2 overexpression has been shown to confer excessive mechanosensitive Ca^{2+} signals [305]; this might impede hair cell mechanotransduction, resulting in deafness [115].

7.4.1.2 Niemann-Pick disease type C1 (NPC1)

TPC dysfunction might also be involved in another LSD, Niemann-Pick disease type C1 (NPC1), which is characterized by the storage of multiple lipids including sphingomylin, cholesterol, glycosphingolipids, and sphingosine [165]. In NPC disease, it is believe the

storage of sphingosine reduces the available lysosomal Ca^{2+} content and thereby reduces NAADP-mediated Ca^{2+} release. In NPC1 mutant cells, NAADP-evoked Ca^{2+} release is reduced by around 70%. This causes impediment to vesicle fusion and trafficking, and the subsequent elevated storage of cholesterol and glycosphingolipids [165]. It would be interesting to assess the effect of sphingosine storage on TPC channel activity; it is likely that the reduction in luminal [Ca^{2+}] resulting from sphingosine storage would lead to a decrease in the sensitivity of TPC to NAADP, and thus the probability of TPC channel opening [231]. This could explain the reduced NAADP-evoked Ca^{2+} release in NPC1-mutant cells.

It would be interesting to further investigate the role of TPCs in NPC1 by isolating cells (for example, macrophages) from TPC KO mice and treated with U18666A (a drug used to induce an NPC disease cellular phenotype [165]). It is possible that the NPC1 disease phenotype will be exacerbated by the deletion of TPCs.

7.4.2 Diabetes mellitus type 2

As mentioned in Section 7.3.1.2, TPC is the key player in NAADP-evoked Ca^{2+} release in pancreatic β-cells [52]. Recently, NAADP signalling has been linked to glucose-evoked Ca^{2+} oscillations in this cell type [200]. Together with the fact that glucose mediates insulin secretion [25, 119], this suggests that NAADP-mediated Ca^{2+} release via TPCs is likely to play a role in glucose-mediated insulin secretion. Dysfunction of TPCs may therefore precipitate type 2 diabetes, as defective Ca^{2+} oscillations and insulin secretion would lead to an imbalance in glucose homeostasis [10, 173].

7.4.3 Smooth muscle dysfunction

7.4.3.1 Bladder

As mentioned in Section 7.3.1.1, using TPC2 KO mice, TPC was shown to play a role in ACh-evoked detrusor smooth muscle contraction [90]. Thus, TPC dysfunction might contribute to bladder dysfunctions, such as unstable bladder, which is characterized urodynamically by spontaneous or provoked involuntary contraction of detrusor, resulting in an increase in pressure during filling [47, 276].

7.4.3.2 Vascular

Finally, endothelin-1 has been suggested to be associated with basal vasoconstrictor tone and the pathogenesis of hypertension [20]. Together with the fact that NAADP is important in arteriole smooth muscle in response to endothelin-1 [36, 138, 268, 303], this suggests that TPC mis-regulation (perhaps by a constant elevated channel activity) may result in increased basal vascular tone and thereby precipitate hypertension. Furthermore, it would be interesting to investigate whether NAADP-evoked arterial smooth muscle contraction is abolished in TPC KO mice, and whether in these mice there is a decreased basal vascular tone and possibly a lower blood pressure.

7.4.4 Pigmentation disorders

Single nucleotide polymorphisms in the human TPC2 gene has been shown to be associated with hair colour in northern Europeans [260]; two nonsynonymous coding variants of TPC2 gene are associated with blond versus brown hair [260]. The process of pigmentation is believed to involve the melanin production (melanogenesis) in lysosome-related organelles, melanosomes, in melanocytes [82, 218, 274]. After maturation, melanosomes could either stay in melanocytes or be transferred to the surrounding keratinocytes by an unclear mechanism [82].

As NAADP has been shown to release Ca^{2+} from lysosome-related organelles [240], and melanosomes have been reported to contain high [Ca^{2+}] [245], it is possible that TPC2 may be localized to melanosomes and that melanosomes may act as NAADP-sensitive Ca^{2+} stores. Thus, TPC2 may be involved in regulating melanogenesis by altering the melanosomal pH, as melanogenesis has been shown to be regulated by pH [128], and NAADP has been shown to alkalinize acidic stores [74, 192, 193]. Alternatively, TPC2 may be involved in the trafficking of melanosomes to keratinocytes [218]; TPCs have been suggested to play a role in trafficking of acidic vesicles [243].

TPC2 dysfunction in melanosomes may thus lead to impairment of melanosome transfer to keratinocytes, or abnormalities in melanin synthesis, resulting in pigmentation disorders.

7.5 Final conclusions

This chapter has reviewed the findings of the current research, hypothesised over the potential role of TPCs (and their regulation) in cellular processes, and speculated on the effects of TPC dysfunction on human disease. In the future, a thorough understanding of the spatial and temporal regulation of Ca^{2+} signals via TPCs, and the molecular mechanisms by which localized signal are amplified globally will be central to elucidating how NAADP regulates a myriad of physiological processes.

The studies reported in the thesis have characterized TPC KO mice and mouse TPCs at various levels including expression, subcellular, NAADP binding, and functional. Such studies greatly increase our understanding of the diverse Ca^{2+} signals evoked by the NAADP pathway. In the future, the speculation of the diseases that TPCs are implicated in may soon be confirmed with the availability of TPC KO mice, moreover, the identification of proteins in TPC complexes would accelerate the design of therapeutic drugs to target the diseases in which TPCs are likely to be involved.

References

[1] R. Aarhus, D. M. Dickey, R. M. Graeff, K. R. Gee, T. F. Walseth, and H. C. Lee. Activation and inactivation of ca2+ release by naadp+. *The Journal of biological chemistry*, 271(15):8513–6, Apr 1996.

[2] R. Aarhus, R. M. Graeff, D. M. Dickey, T. F. Walseth, and H. C. Lee. Adp-ribosyl cyclase and cd38 catalyze the synthesis of a calcium-mobilizing metabolite from nadp. *The Journal of biological chemistry*, 270(51):30327–33, Dec 1995.

[3] P. Aksoy, T. A. White, M. Thompson, and E. N. Chini. Regulation of intracellular levels of nad: a novel role for cd38. *Biochemical and Biophysical Research Communications*, 345(4):1386–92, Jul 2006.

[4] E. U. Alejandro, T. B. Kalynyak, F. Taghizadeh, K. S. Gwiazda, E. K. Rawstron, K. J. Jacob, and J. D. Johnson. Acute insulin signaling in pancreatic beta-cells is mediated by multiple raf-1 dependent pathways. *Endocrinology*, 151(2):502–12, Feb 2010.

[5] P. K. Aley, A. M. Mikolajczyk, B. Munz, G. C. Churchill, A. Galione, and F. Berger. Nicotinic acid adenine dinucleotide phosphate regulates skeletal muscle differentiation via action at two-pore channels. *Proc Natl Acad Sci USA*, 107(46):19927–32, Nov 2010.

[6] P. K. Aley, H. J. Noh, X. Gao, A. A. Tica, E. Brailoiu, and G. C. Churchill. A functional role for nicotinic acid adenine dinucleotide phosphate in oxytocin-mediated contraction of uterine smooth muscle from rat. *J Pharmacol Exp Ther*, 333(3):726–35, Jun 2010.

[7] V. Allen, P. Swigart, R. Cheung, S. Cockcroft, and M. Katan. Regulation of inositol lipid-specific phospholipase cdelta by changes in ca2+ ion concentrations. *Biochem J*, 327 (Pt 2):545–52, Oct 1997.

[8] M. Aouadi, B. Binetruy, L. Caron, Y. L. Marchand-Brustel, and F. Bost. Role of mapks in development and differentiation: lessons from knockout mice. *Biochimie*, 88(9):1091–8, Sep 2006.

[9] J. Arikkath and K. P. Campbell. Auxiliary subunits: essential components of the voltage-gated calcium channel complex. *Curr Opin Neurobiol*, 13(3):298–307, Jun 2003.

[10] A. Arredouani, A. M. Evans, J. Ma, J. Parrington, M. X. Zhu, and A. Galione. An emerging role for naadp-mediated ca2+ signaling in the pancreatic Îš-cell. *Islets*, 2(5):323–30, Jan 2010.

[11] M. C. Ashby, C. Camello-Almaraz, O. V. Gerasimenko, O. H. Petersen, and A. V. Tepikin. Long distance communication between muscarinic receptors and ca2+ release channels revealed by carbachol uncaging in cell-attached patch pipette. *The Journal of biological chemistry*, 278(23):20860–4, Jun 2003.

[12] M. C. Ashby, O. H. Petersen, and A. V. Tepikin. Spatial characterisation of ryanodine-induced calcium release in mouse pancreatic acinar cells. *Biochem J*, 369(Pt 3):441–5, Feb 2003.

[13] A. Auerbach. The gating isomerization of neuromuscular acetylcholine receptors. *The Journal of Physiology*, 588(Pt 4):573–86, Feb 2010.

[14] C. P. Austin, J. F. Battey, A. Bradley, M. Bucan, M. Capecchi, F. S. Collins, W. F. Dove, G. Duyk, S. Dymecki, J. T. Eppig, F. B. Grieder, N. Heintz, G. Hicks, T. R. Insel, A. Joyner, B. H. Koller, K. C. K. Lloyd, T. Magnuson, M. W. Moore, A. Nagy, J. D. Pollock, A. D. Roses, A. T. Sands, B. Seed, W. C. Skarnes, J. Snoddy, P. Soriano, D. J. Stewart, F. Stewart, B. Stillman, H. Varmus, L. Varticovski, I. M. Verma, T. F. Vogt, H. von Melchner, J. Witkowski, R. P. Woychik, W. Wurst, G. D. Yancopoulos, S. G. Young, and B. Zambrowicz. The knockout mouse project. *Nature Genetics*, 36(9):921–4, Sep 2004.

[15] J. Bak, R. A. Billington, and A. A. Genazzani. Effect of luminal and extravesicular ca2+ on naadp binding and release properties. *Biochemical and Biophysical Research Communications*, 295(4):806–11, Jul 2002.

[16] J. Bak, R. A. Billington, G. Timar, A. C. Dutton, and A. A. Genazzani. Naadp receptors are present and functional in the heart. *Curr Biol*, 11(12):987–90, Jun 2001.

[17] J. Bak, P. White, G. Timár, L. Missiaen, A. A. Genazzani, and A. Galione. Nicotinic acid adenine dinucleotide phosphate triggers ca2+ release from brain microsomes. *Curr Biol*, 9(14):751–4, Jul 1999.

[18] D. E. Bamiou, P. Campbell, A. Liasis, J. Page, T. Sirimanna, S. Boyd, A. Vellodi, and C. Harris. Audiometric abnormalities in children with gaucher disease type 3. *Neuropediatrics*, 32(3):136–41, Jun 2001.

[19] M. Barceló-Torns, A. M. Lewis, A. Gubern, D. Barneda, D. Bloor-Young, F. Picatoste, G. C. Churchill, E. Claro, and R. Masgrau. Naadp mediates atp-induced ca(2+) signals in astrocytes. *FEBS Lett*, 585(14):2300–6, Jul 2011.

[20] M. Barton and M. Yanagisawa. Endothelin: 20 years from discovery to therapy. *Can. J. Physiol. Pharmacol.*, 86(8):485–98, Aug 2008.

[21] J. M. Baughman, F. Perocchi, H. S. Girgis, M. Plovanich, C. A. Belcher-Timme, Y. Sancak, X. R. Bao, L. Strittmatter, O. Goldberger, R. L. Bogorad, V. Koteliansky, and V. K. Mootha. Integrative genomics identifies mcu as an essential component of the mitochondrial calcium uniporter. *Nature*, Jun 2011.

[22] A. Beck, M. Kolisek, L. A. Bagley, A. Fleig, and R. Penner. Nicotinic acid adenine dinucleotide phosphate and cyclic adp-ribose regulate trpm2 channels in t lymphocytes. *FASEB J*, 20(7):962–4, May 2006.

[23] M. Bengtsson, A. Ståhlberg, P. Rorsman, and M. Kubista. Gene expression profiling in single cells from the pancreatic islets of langerhans reveals lognormal distribution of mrna levels. *Genome Research*, 15(10):1388–92, Oct 2005.

[24] I. Berg, B. V. Potter, G. W. Mayr, and A. H. Guse. Nicotinic acid adenine dinucleotide phosphate (naadp(+)) is an essential regulator of t-lymphocyte ca(2+)-signaling. *J Cell Biol*, 150(3):581–8, Aug 2000.

[25] P. Bergsten. Role of oscillations in membrane potential, cytoplasmic ca2+, and metabolism for plasma insulin oscillations. *Diabetes*, 51 Suppl 1:S171–6, Feb 2002.

[26] G. Berridge, R. Cramer, A. Galione, and S. Patel. Metabolism of the novel ca2+-mobilizing messenger nicotinic acid-adenine dinucleotide phosphate via a 2'-specific ca2+-dependent phosphatase. *Biochem J*, 365(Pt 1):295–301, Jul 2002.

[27] M. J. Berridge. Inositol trisphosphate and calcium signalling mechanisms. *Biochimica et biophysica acta*, 1793(6):933–40, Jun 2009.

[28] M. J. Berridge, M. D. Bootman, and H. L. Roderick. Calcium signalling: dynamics, homeostasis and remodelling. *Nat Rev Mol Cell Biol*, 4(7):517–29, Jul 2003.

[29] M. J. Berridge, P. Lipp, and M. D. Bootman. The versatility and universality of calcium signalling. *Nat Rev Mol Cell Biol*, 1(1):11–21, Oct 2000.

[30] D. M. Bers. Cardiac excitation-contraction coupling. *Nature*, 415(6868):198–205, Jan 2002.

[31] F. Bertocchini, C. E. Ovitt, A. Conti, V. Barone, H. R. Schöler, R. Bottinelli, C. Reggiani, and V. Sorrentino. Requirement for the ryanodine receptor type 3 for efficient contraction in neonatal skeletal muscles. *EMBO J*, 16(23):6956–63, Dec 1997.

[32] G. Bidaux, M. Roudbaraki, C. Merle, A. Crépin, P. Delcourt, C. Slomianny, S. Thebault, J.-L. Bonnal, M. Benahmed, F. Cabon, B. Mauroy, and N. Prevarskaya. Evidence for specific trpm8 expression in human prostate secretory epithelial cells: functional androgen receptor requirement. *Endocr Relat Cancer*, 12(2):367–82, May 2005.

[33] R. A. Billington and A. A. Genazzani. Characterization of naadp(+) binding in sea urchin eggs. *Biochemical and Biophysical Research Communications*, 276(1):112–6, Sep 2000.

[34] P. Bimboese, C. J. Gibson, S. Schmidt, W. Xiang, and B. E. Ehrlich. Isoform-specific regulation of the inositol 1,4,5-trisphosphate receptor by o-linked glycosylation. *The Journal of biological chemistry*, 286(18):15688–97, May 2011.

[35] A. W. Bird and A. A. Hyman. Building a spindle of the correct length in human cells requires the interaction between tpx2 and aurora a. *J Cell Biol*, 182(2):289–300, Jul 2008.

[36] F.-X. Boittin, A. Galione, and A. M. Evans. Nicotinic acid adenine dinucleotide phosphate mediates ca2+ signals and contraction in arterial smooth muscle via a two-pool mechanism. *Circ Res*, 91(12):1168–75, Dec 2002.

[37] K. A. Bolanz, M. A. Hediger, and C. P. Landowski. The role of trpv6 in breast carcinogenesis. *Mol Cancer Ther*, 7(2):271–9, Jan 2008.

[38] J. S. Bonifacino and L. M. Traub. Signals for sorting of transmembrane proteins to endosomes and lysosomes. *Annu Rev Biochem*, 72:395–447, Jan 2003.

[39] E. Brailoiu, D. Churamani, X. Cai, M. G. Schrlau, G. C. Brailoiu, X. Gao, R. Hooper, M. J. Boulware, N. J. Dun, J. S. Marchant, and S. Patel. Essential requirement for two-pore channel 1 in naadp-mediated calcium signaling. *J Cell Biol*, 186(2):201–9, Jul 2009.

[40] E. Brailoiu, J. L. Hoard, C. M. Filipeanu, G. C. Brailoiu, S. L. Dun, S. Patel, and N. J. Dun. Nicotinic acid adenine dinucleotide phosphate potentiates neurite outgrowth. *The Journal of biological chemistry*, 280(7):5646–50, Feb 2005.

[41] E. Brailoiu, R. Hooper, X. Cai, G. C. Brailoiu, M. V. Keebler, N. J. Dun, J. S. Marchant, and S. Patel. An ancestral deuterostome family of two-pore channels mediates nicotinic acid adenine dinucleotide phosphate-dependent calcium release from acidic organelles. *J Biol Chem*, 285(5):2897–901, Jan 2010.

[42] E. Brailoiu, T. Rahman, D. Churamani, D. L. Prole, G. C. Brailoiu, R. Hooper, C. W. Taylor, and S. Patel. An naadp-gated two-pore channel targeted to the plasma membrane uncouples triggering from amplifying ca2+ signals. *The Journal of biological chemistry*, 285(49):38511–6, Dec 2010.

[43] G. C. Brailoiu, E. Brailoiu, R. Parkesh, A. Galione, G. C. Churchill, S. Patel, and N. J. Dun. Naadp-mediated channel 'chatter' in neurons of the rat medulla oblongata. *Biochem J*, 419(1):91–7, 2 p following 97, Apr 2009.

[44] G. C. Brailoiu, B. Gurzu, X. Gao, R. Parkesh, P. K. Aley, D. I. Trifa, A. Galione, N. J. Dun, M. Madesh, S. Patel, G. C. Churchill, and E. Brailoiu. Acidic naadp-sensitive calcium stores in the endothelium: agonist-specific recruitment and role in regulating blood pressure. *The Journal of biological chemistry*, 285(48):37133–7, Nov 2010.

[45] R. Brenner, G. J. Peréz, A. D. Bonev, D. M. Eckman, J. C. Kosek, S. W. Wiler, A. J. Patterson, M. T. Nelson, and R. W. Aldrich. Vasoregulation by the beta1 subunit of the calcium-activated potassium channel. *Nature*, 407(6806):870–6, Oct 2000.

[46] O. M. D. Brito and L. Scorrano. Mitofusin 2 tethers endoplasmic reticulum to mitochondria. *Nature*, 456(7222):605–10, Dec 2008.

[47] P. Bulmer and P. Abrams. The unstable detrusor. *Gynecol Obstet Invest*, 72(1):1–12, Jan 2004.

[48] D. Burdakov, O. H. Petersen, and A. Verkhratsky. Intraluminal calcium as a primary regulator of endoplasmic reticulum function. *Cell Calcium*, 38(3-4):303–10, Jan 2005.

[49] K. T. Bush, R. O. Stuart, S. H. Li, L. A. Moura, A. H. Sharp, C. A. Ross, and S. K. Nigam. Epithelial inositol 1,4,5-trisphosphate receptors. multiplicity of localization, solubility, and isoforms. *The Journal of biological chemistry*, 269(38):23694–9, Sep 1994.

[50] D. B. Bylund and M. L. Toews. Radioligand binding methods: practical guide and tips. *Am J Physiol*, 265(5 Pt 1):L421–9, Nov 1993.

[51] X. Cai and S. Patel. Degeneration of an intracellular ion channel in the primate lineage by relaxation of selective constraints. *Molecular biology and evolution*, 27(10):2352–9, Oct 2010.

[52] P. J. Calcraft, M. Ruas, Z. Pan, X. Cheng, A. Arredouani, X. Hao, J. Tang, K. Rietdorf, L. Teboul, K.-T. Chuang, P. Lin, R. Xiao, C. Wang, Y. Zhu, Y. Lin, C. N. Wyatt, J. Parrington, J. Ma, A. M. Evans, A. Galione, and M. X. Zhu. Naadp mobilizes calcium from acidic organelles through two-pore channels. *Nature*, 459(7246):596–600, May 2009.

[53] C. Camello, R. Lomax, O. H. Petersen, and A. V. Tepikin. Calcium leak from intracellular stores–the enigma of calcium signalling. *Cell Calcium*, 32(5-6):355–61, Jan 2002.

[54] D. J. Campbell. The kallikrein-kinin system in humans. *Clin Exp Pharmacol Physiol*, 28(12):1060–5, Dec 2001.

[55] P. E. Campbell, C. M. Harris, C. M. Harris, T. Sirimanna, and A. Vellodi. A model of neuronopathic gaucher disease. *J Inherit Metab Dis*, 26(7):629–39, Jan 2003.

[56] J. M. Cancela. Specific ca2+ signaling evoked by cholecystokinin and acetylcholine: the roles of naadp, cadpr, and ip3. *Annu Rev Physiol*, 63:99–117, Jan 2001.

[57] J. M. Cancela, G. C. Churchill, and A. Galione. Coordination of agonist-induced ca2+-signalling patterns by naadp in pancreatic acinar cells. *Nature*, 398(6722):74–6, Mar 1999.

[58] J. M. Cancela, F. V. Coppenolle, A. Galione, A. V. Tepikin, and O. H. Petersen. Transformation of local ca2+ spikes to global ca2+ transients: the combinatorial roles of multiple ca2+ releasing messengers. *EMBO J*, 21(5):909–19, Mar 2002.

[59] J. M. Cancela, O. V. Gerasimenko, J. V. Gerasimenko, A. V. Tepikin, and O. H. Petersen. Two different but converging messenger pathways to intracellular ca(2+) release: the roles of nicotinic acid adenine dinucleotide phosphate, cyclic adp-ribose and inositol trisphosphate. *EMBO J*, 19(11):2549–57, Jun 2000.

[60] J. M. Cancela and O. H. Petersen. The cyclic adp ribose antagonist 8-nh2-cadp-ribose blocks cholecystokinin-evoked cytosolic ca2+ spiking in pancreatic acinar cells. *Pflugers Arch*, 435(5):746–8, Apr 1998.

[61] E. Carafoli, L. Santella, D. Branca, and M. Brini. Generation, control, and processing of cellular calcium signals. *Crit Rev Biochem Mol Biol*, 36(2):107–260, Apr 2001.

[62] A. S. Chang, S. M. Chang, R. L. Garcia, and W. P. Schilling. Concomitant and hormonally regulated expression of trp genes in bovine aortic endothelial cells. *FEBS Lett*, 415(3):335–40, Oct 1997.

[63] W. J. Chen, S. Armour, J. Way, G. Chen, C. Watson, P. Irving, J. Cobb, S. Kadwell, K. Beaumont, T. Rimele, and T. Kenakin. Expression cloning and receptor pharmacology of human calcitonin receptors from mcf-7 cells and their relationship to amylin receptors. *Mol Pharmacol*, 52(6):1164–75, Dec 1997.

[64] H. Cheng, M. R. Lederer, W. J. Lederer, and M. B. Cannell. Calcium sparks and [ca2+]i waves in cardiac myocytes. *Am J Physiol*, 270(1 Pt 1):C148–59, Jan 1996.

[65] H. Cheng, W. J. Lederer, and M. B. Cannell. Calcium sparks: elementary events underlying excitation-contraction coupling in heart muscle. *Science*, 262(5134):740–4, Oct 1993.

[66] E. N. Chini, K. W. Beers, and T. P. Dousa. Nicotinate adenine dinucleotide phosphate (naadp) triggers a specific calcium release system in sea urchin eggs. *The Journal of biological chemistry*, 270(7):3216–23, Feb 1995.

[67] K. A. Christensen, J. T. Myers, and J. A. Swanson. ph-dependent regulation of lysosomal calcium in macrophages. *J Cell Sci*, 115(Pt 3):599–607, Feb 2002.

[68] D. Churamani, M. J. Boulware, T. J. Geach, A. C. R. Martin, G. W. Moy, Y.-H. Su, V. D. Vacquier, J. S. Marchant, L. Dale, and S. Patel. Molecular characterization of a novel intracellular adp-ribosyl cyclase. *PLoS ONE*, 2(8):e797, Jan 2007.

[69] G. C. Churchill and A. Galione. Naadp induces ca2+ oscillations via a two-pool mechanism by priming ip3- and cadpr-sensitive ca2+ stores. *EMBO J*, 20(11):2666–71, Jun 2001.

[70] G. C. Churchill, Y. Okada, J. M. Thomas, A. A. Genazzani, S. Patel, and A. Galione. Naadp mobilizes ca(2+) from reserve granules, lysosome-related organelles, in sea urchin eggs. *Cell*, 111(5):703–8, Nov 2002.

[71] B. Cigic and R. H. Pain. Location of the binding site for chloride ion activation of cathepsin c. *Eur J Biochem*, 264(3):944–51, Sep 1999.

[72] D. E. Clapham. Calcium signaling. *Cell*, 131(6):1047–58, Dec 2007.

[73] D. L. Clapper, T. F. Walseth, P. J. Dargie, and H. C. Lee. Pyridine nucleotide metabolites stimulate calcium release from sea urchin egg microsomes desensitized to inositol trisphosphate. *The Journal of biological chemistry*, 262(20):9561–8, Jul 1987.

[74] F. Cosker, N. Cheviron, M. Yamasaki, A. Menteyne, F. E. Lund, M.-J. Moutin, A. Galione, and J.-M. Cancela. The ecto-enzyme cd38 is a nicotinic acid adenine dinucleotide phosphate (naadp) synthase that couples receptor activation to ca2+ mobilization from lysosomes in pancreatic acinar cells. *The Journal of biological chemistry*, 285(49):38251–9, Dec 2010.

[75] J. N. Crawley. Unusual behavioral phenotypes of inbred mouse strains. *Trends Neurosci*, 19(5):181–2; discussion 188–9, May 1996.

[76] E. B. Cullinan, L. Kwee, P. Nunes, D. J. Shuster, G. Ju, K. W. McIntyre, R. A. Chizzonite, and M. A. Labow. Il-1 receptor accessory protein is an essential component of the il-1 receptor. *J Immunol*, 161(10):5614–20, Nov 1998.

[77] P. C. A. da Fonseca, S. A. Morris, E. P. Nerou, C. W. Taylor, and E. P. Morris. Domain organization of the type 1 inositol 1,4,5-trisphosphate receptor as revealed by single-particle analysis. *Proc Natl Acad Sci USA*, 100(7):3936–41, Apr 2003.

[78] W. Dammermann and A. H. Guse. Functional ryanodine receptor expression is required for naadp-mediated local ca2+ signaling in t-lymphocytes. *The Journal of biological chemistry*, 280(22):21394–9, Jun 2005.

[79] W. Dammermann, B. Zhang, M. Nebel, C. Cordiglieri, F. Odoardi, T. Kirchberger, N. Kawakami, J. Dowden, F. Schmid, K. Dornmair, M. Hohenegger, A. Flügel, A. H. Guse, and B. V. L. Potter. Naadp-mediated ca2+ signaling via type 1 ryanodine receptor in t cells revealed by a synthetic naadp antagonist. *Proc Natl Acad Sci USA*, 106(26):10678–83, Jun 2009.

[80] P. J. Dargie, M. C. Agre, and H. C. Lee. Comparison of ca2+ mobilizing activities of cyclic adp-ribose and inositol trisphosphate. *Cell Regul*, 1(3):279–90, Feb 1990.

[81] L. C. Davis, A. J. Morgan, M. Ruas, J. L. Wong, R. M. Graeff, A. J. Poustka, H. C. Lee, G. M. Wessel, J. Parrington, and A. Galione. Ca(2+) signaling occurs via second messenger release from intraorganelle synthesis sites. *Curr Biol*, 18(20):1612–8, Oct 2008.

[82] E. C. Dell'Angelica, C. Mullins, S. Caplan, and J. S. Bonifacino. Lysosome-related organelles. *FASEB J*, 14(10):1265–78, Jul 2000.

[83] O. Dellis, S. G. Dedos, S. C. Tovey, Taufiq-Ur-Rahman, S. J. Dubel, and C. W. Taylor. Ca2+ entry through plasma membrane ip3 receptors. *Science*, 313(5784):229–33, Jul 2006.

[84] O. Dellis, A. M. Rossi, S. G. Dedos, and C. W. Taylor. Counting functional inositol 1,4,5-trisphosphate receptors into the plasma membrane. *The Journal of biological chemistry*, 283(2):751–5, Jan 2008.

[85] S. Derveaux, J. Vandesompele, and J. Hellemans. How to do successful gene expression analysis using real-time pcr. *Methods*, 50(4):227–30, Apr 2010.

[86] B. N. Desai and D. E. Clapham. Trp channels and mice deficient in trp channels. *Pflugers Arch*, 451(1):11–8, Oct 2005.

[87] G. D. Dickinson and S. Patel. Modulation of naadp (nicotinic acid-adenine dinucleotide phosphate) receptors by k+ ions: evidence for multiple naadp receptor conformations. *Biochem J*, 375(Pt 3):805–12, Nov 2003.

[88] L. A. Donehower, M. Harvey, B. L. Slagle, M. J. McArthur, C. A. Montgomery, J. S. Butel, and A. Bradley. Mice deficient for p53 are developmentally normal but susceptible to spontaneous tumours. *Nature*, 356(6366):215–21, Mar 1992.

[89] G. Dupont, L. Combettes, G. S. Bird, and J. W. Putney. Calcium oscillations. *Cold Spring Harb Perspect Biol*, 3(3), Mar 2011.

[90] N. T. Durlu-Kandilci, M. Ruas, K.-T. Chuang, A. Brading, J. Parrington, and A. Galione. Tpc2 proteins mediate nicotinic acid adenine dinucleotide phosphate (naadp)- and agonist-evoked contractions of smooth muscle. *The Journal of biological chemistry*, 285(32):24925–32, Aug 2010.

[91] A. H. Eid, K. Maiti, S. Mitra, M. A. Chotani, S. Flavahan, S. R. Bailey, C. S. Thompson-Torgerson, and N. A. Flavahan. Estrogen increases smooth muscle expression of 2c-adrenoceptors and cold-induced constriction of cutaneous arteries. *AJP: Heart and Circulatory Physiology*, 293(3):H1955–H1961, Jun 2007.

[92] M. A. Falkowski, D. D. H. Thomas, S. W. Messenger, T. F. Martin, and G. E. Groblewski. Expression, localization, and functional role for synaptotagmins in pancreatic acinar cells. *AJP: Gastrointestinal and Liver Physiology*, 301(2):G306–16, Aug 2011.

[93] M. Fill and J. A. Copello. Ryanodine receptor calcium release channels. *Physiol Rev*, 82(4):893–922, Oct 2002.

[94] A. D. Flora, E. Zocchi, L. Guida, L. Franco, and S. Bruzzone. Autocrine and paracrine calcium signaling by the cd38/nad+/cyclic adp-ribose system. *Annals of the New York Academy of Sciences*, 1028:176–91, Dec 2004.

[95] V. A. Florio and P. C. Sternweis. Mechanisms of muscarinic receptor action on go in reconstituted phospholipid vesicles. *The Journal of biological chemistry*, 264(7):3909–15, Mar 1989.

[96] J. K. Foskett, C. White, K.-H. Cheung, and D.-O. D. Mak. Inositol trisphosphate receptor ca2+ release channels. *Physiol Rev*, 87(2):593–658, Apr 2007.

[97] A. Fritsch, S. Loeckermann, J. S. Kern, A. Braun, M. R. Bösl, T. A. Bley, H. Schumann, D. V. Elverfeldt, D. Paul, M. Erlacher, D. B. V. Rautenfeld, I. Hausser, R. Fässler, and L. Bruckner-Tuderman. A hypomorphic mouse model of dystrophic epidermolysis bullosa reveals mechanisms of disease and response to fibroblast therapy. *J Clin Invest*, 118(5):1669–79, May 2008.

[98] T. Furuichi, K. W. Cunningham, and S. Muto. A putative two pore channel attpc1 mediates ca(2+) flux in arabidopsis leaf cells. *Plant Cell Physiol*, 42(9):900–5, Sep 2001.

[99] A. Futatsugi, T. Nakamura, M. K. Yamada, E. Ebisui, K. Nakamura, K. Uchida, T. Kitaguchi, H. Takahashi-Iwanaga, T. Noda, J. Aruga, and K. Mikoshiba. Ip3 receptor types 2 and 3 mediate exocrine secretion underlying energy metabolism. *Science*, 309(5744):2232–4, Sep 2005.

[100] A. Galione. Naadp receptors. *Cold Spring Harb Perspect Biol*, Nov 2010.

[101] A. Galione and G. C. Churchill. Interactions between calcium release pathways: multiple messengers and multiple stores. *Cell Calcium*, 32(5-6):343–54, Jan 2002.

[102] A. Galione, H. C. Lee, and W. B. Busa. Ca(2+)-induced ca2+ release in sea urchin egg homogenates: modulation by cyclic adp-ribose. *Science*, 253(5024):1143–6, Sep 1991.

[103] A. Galione, A. J. Morgan, A. Arredouani, L. C. Davis, K. Rietdorf, M. Ruas, and J. Parrington. Naadp as an intracellular messenger regulating lysosomal calcium-release channels. *Biochem Soc Trans*, 38(6):1424–31, Dec 2010.

[104] G. Gambara, R. A. Billington, M. Debidda, A. D'Alessio, F. Palombi, E. Ziparo, A. A. Genazzani, and A. Filippini. Naadp-induced ca(2+ signaling in response to endothelin is via the receptor subtype b and requires the integrity of lipid rafts/caveolae. *J Cell Physiol*, 216(2):396–404, Aug 2008.

[105] H. Gao, S. Fält, A. Sandelin, J.-A. Gustafsson, and K. Dahlman-Wright. Genome-wide identification of estrogen receptor alpha-binding sites in mouse liver. *Mol Endocrinol*, 22(1):10–22, Jan 2008.

[106] A. A. Genazzani, R. M. Empson, and A. Galione. Unique inactivation properties of naadp-sensitive ca2+ release. *The Journal of biological chemistry*, 271(20):11599–602, May 1996.

[107] A. A. Genazzani, M. Mezna, D. M. Dickey, F. Michelangeli, T. F. Walseth, and A. Galione. Pharmacological properties of the ca2+-release mechanism sensitive to naadp in the sea urchin egg. *Br J Pharmacol*, 121(7):1489–95, Aug 1997.

[108] J. Gerasimenko, Y. Maruyama, A. Tepikin, O. H. Petersen, and O. Gerasimenko. Calcium signalling in and around the nuclear envelope. *Biochem Soc Trans*, 31(Pt 1):76–8, Feb 2003.

[109] J. V. Gerasimenko, Y. Maruyama, K. Yano, N. J. Dolman, A. V. Tepikin, O. H. Petersen, and O. V. Gerasimenko. Naadp mobilizes ca2+ from a thapsigargin-sensitive store in the nuclear envelope by activating ryanodine receptors. *J Cell Biol*, 163(2):271–82, Oct 2003.

[110] J. V. Gerasimenko, M. Sherwood, A. V. Tepikin, O. H. Petersen, and O. V. Gerasimenko. Naadp, cadpr and ip3 all release ca2+ from the endoplasmic reticulum and an acidic store in the secretory granule area. *J Cell Sci*, 119(Pt 2):226–38, Jan 2006.

[111] J. V. Gerasimenko, A. V. Tepikin, O. H. Petersen, and O. V. Gerasimenko. Calcium uptake via endocytosis with rapid release from acidifying endosomes. *Curr Biol*, 8(24):1335–8, Dec 1998.

[112] O. V. Gerasimenko, J. V. Gerasimenko, R. R. Rizzuto, M. Treiman, A. V. Tepikin, and O. H. Petersen. The distribution of the endoplasmic reticulum in living pancreatic acinar cells. *Cell Calcium*, 32(5-6):261–8, Jan 2002.

[113] F. Gorelick and J. Jamieson. The pancreatic acinar cells: structure-function relationships. *Physiology of the Gastrointestinal Tract, 4th ed.*, pages 1313–1335, Jan 2006.

[114] B. D. Grant and J. G. Donaldson. Pathways and mechanisms of endocytic recycling. *Nat Rev Mol Cell Biol*, 10(9):597–608, Sep 2009.

[115] L. Grant and P. A. Fuchs. Auditory transduction in the mouse. *Pflugers Arch*, 454(5):793–804, Aug 2007.

[116] C. Guan, C. Ye, X. Yang, and J. Gao. A review of current large-scale mouse knockout efforts. *Genesis*, 48(2):73–85, Feb 2010.

[117] M. Hao, S. X. Lin, O. J. Karylowski, D. Wüstner, T. E. McGraw, and F. R. Maxfield. Vesicular and non-vesicular sterol transport in living cells. the endocytic recycling compartment is a major sterol storage organelle. *The Journal of biological chemistry*, 277(1):609–17, Jan 2002.

[118] M. R. Hellmich and F. Strumwasser. Purification and characterization of a molluscan egg-specific nadase, a second-messenger enzyme. *Cell Regul*, 2(3):193–202, Mar 1991.

[119] J. C. Henquin. Triggering and amplifying pathways of regulation of insulin secretion by glucose. *Diabetes*, 49(11):1751–60, Nov 2000.

[120] Y. Hirata, N. Kimura, K. Sato, Y. Ohsugi, S. Takasawa, H. Okamoto, J. Ishikawa, T. Kaisho, K. Ishihara, and T. Hirano. Adp ribosyl cyclase activity of a novel bone marrow stromal cell surface molecule, bst-1. *FEBS Letters*, 356(2-3):244–8, Dec 1994.

[121] M. Hohenegger, J. Suko, R. Gscheidlinger, H. Drobny, and A. Zidar. Nicotinic acid-adenine dinucleotide phosphate activates the skeletal muscle ryanodine receptor. *Biochem J*, 367(Pt 2):423–31, Oct 2002.

[122] R. Hooper, D. Churamani, E. Brailoiu, C. W. Taylor, and S. Patel. Membrane topology of naadp-sensitive two-pore channels and their regulation by n-linked glycosylation. *The Journal of biological chemistry*, 286(11):9141–9, Mar 2011.

[123] U. C. Hoppe. Mitochondrial calcium channels. *FEBS Letters*, 584(10):1975–81, May 2010.

[124] M. Howard, J. C. Grimaldi, J. F. Bazan, F. E. Lund, L. Santos-Argumedo, R. M. Parkhouse, T. F. Walseth, and H. C. Lee. Formation and hydrolysis of cyclic adp-ribose catalyzed by lymphocyte antigen cd38. *Science*, 262(5136):1056–9, Nov 1993.

[125] C. L.-H. Huang, L. Sun, J. A. Fraser, A. A. Grace, and M. Zaidi. Similarities and contrasts in ryanodine receptor localization and function in osteoclasts and striated muscle cells. *Annals of the New York Academy of Sciences*, 1116:255–70, Nov 2007.

[126] S. Z. Husain, P. Prasad, W. M. Grant, T. R. Kolodecik, M. H. Nathanson, and F. S. Gorelick. The ryanodine receptor mediates early zymogen activation in pancreatitis. *Proc Natl Acad Sci USA*, 102(40):14386–91, Oct 2005.

[127] K. Ishibashi, M. Suzuki, and M. Imai. Molecular cloning of a novel form (two-repeat) protein related to voltage-gated sodium and calcium channels. *Biochemical and Biophysical Research Communications*, 270(2):370–6, Apr 2000.

[128] S. Ito and K. Wakamatsu. Human hair melanins: what we have learned and have not learned from mouse coat color pigmentation. *Pigment Cell Melanoma Res*, Sep 2010.

[129] M. Itoh, K. Ishihara, H. Tomizawa, H. Tanaka, Y. Kobune, J. Ishikawa, T. Kaisho, and T. Hirano. Molecular cloning of murine bst-1 having homology with cd38 and aplysia adp-ribosyl cyclase. *Biochemical and Biophysical Research Communications*, 203(2):1309–17, Sep 1994.

[130] M. Iwai, T. Michikawa, I. Bosanac, M. Ikura, and K. Mikoshiba. Molecular basis of the isoform-specific ligand-binding affinity of inositol 1,4,5-trisphosphate receptors. *The Journal of biological chemistry*, 282(17):12755–64, Apr 2007.

[131] J. D. Johnson and S. Misler. Nicotinic acid-adenine dinucleotide phosphate-sensitive calcium stores initiate insulin signaling in human beta cells. *Proc Natl Acad Sci USA*, 99(22):14566–71, Oct 2002.

[132] C. Jung, C. Fandos, I. M. Lorenzo, C. Plata, J. Fernandes, G. G. Gené, E. Vázquez, and M. A. Valverde. The progesterone receptor regulates the expression of trpv4 channel. *Pflugers Arch*, 459(1):105–13, Oct 2009.

[133] E. Kalay, R. Caylan, A. F. Kiroglu, T. Yasar, R. W. J. Collin, J. G. A. M. Heister, J. Oostrik, C. W. R. J. Cremers, H. G. Brunner, A. Karaguzel, and H. Kremer. A novel locus for autosomal recessive nonsyndromic hearing impairment, dfnb63, maps to chromosome 11q13.2-q13.4. *J Mol Med*, 85(4):397–404, Apr 2007.

[134] T. Kenakin. A pharmacology primer: theory, applications, and methodsâĂŐ. *A Pharmacology Primer: Theory, Application and Methods, 1st ed.*, pages 63–64, Dec 2003.

[135] S. Y. Khan, S. Riazuddin, M. Tariq, S. Anwar, M. I. Shabbir, S. A. Riazuddin, S. N. Khan, T. Husnain, Z. M. Ahmed, T. B. Friedman, and S. Riazuddin. Autosomal recessive nonsyndromic deafness locus dfnb63 at chromosome 11q13.2-q13.3. *Hum Genet*, 120(6):789–93, Feb 2007.

[136] B.-J. Kim, K.-H. Park, C.-Y. Yim, S. Takasawa, H. Okamoto, M.-J. Im, and U.-H. Kim. Generation of nicotinic acid adenine dinucleotide phosphate and cyclic adp-ribose by glucagon-like peptide-1 evokes ca2+ signal that is essential for insulin secretion in mouse pancreatic islets. *Diabetes*, 57(4):868–78, Apr 2008.

[137] E. Kim, A. Magen, and G. Ast. Different levels of alternative splicing among eukaryotes. *Nucleic Acids Res*, 35(1):125–31, Jan 2007.

[138] N. P. Kinnear, F.-X. Boittin, J. M. Thomas, A. Galione, and A. M. Evans. Lysosome-sarcoplasmic reticulum junctions. a trigger zone for calcium signaling by nicotinic acid adenine dinucleotide phosphate and endothelin-1. *J Biol Chem*, 279(52):54319–26, Dec 2004.

[139] N. P. Kinnear, C. N. Wyatt, J. H. Clark, P. J. Calcraft, S. Fleischer, L. H. Jeyakumar, G. F. Nixon, and A. M. Evans. Lysosomes co-localize with ryanodine receptor subtype 3 to form a trigger zone for calcium signalling by naadp in rat pulmonary arterial smooth muscle. *Cell Calcium*, 44(2):190–201, Aug 2008.

[140] Y. Kirichok, G. Krapivinsky, and D. E. Clapham. The mitochondrial calcium uniporter is a highly selective ion channel. *Nature*, 427(6972):360–4, Jan 2004.

[141] K. Kiselyov, G. A. Mignery, M. X. Zhu, and S. Muallem. The n-terminal domain of the ip3 receptor gates store-operated htrp3 channels. *Mol Cell*, 4(3):423–9, Sep 1999.

[142] K. Kiselyov, S. Yamaguchi, C. W. Lyons, and S. Muallem. Aberrant ca2+ handling in lysosomal storage disorders. *Cell Calcium*, 47(2):103–11, Feb 2010.

[143] R. Kittler, L. Pelletier, C. Ma, I. Poser, S. Fischer, A. A. Hyman, and F. Buchholz. Rna interference rescue by bacterial artificial chromosome transgenesis in mammalian tissue culture cells. *Proc Natl Acad Sci USA*, 102(7):2396–401, Feb 2005.

[144] H. Koutnikova, T.-A. Cock, M. Watanabe, S. M. Houten, M.-F. Champy, A. Dierich, and J. Auwerx. Compensation by the muscle limits the metabolic consequences of lipodystrophy in ppar gamma hypomorphic mice. *Proc Natl Acad Sci USA*, 100(24):14457–62, Nov 2003.

[145] E. Krause, A. Gobel, and I. Schulz. Cell side-specific sensitivities of intracellular ca2+ stores for inositol 1,4,5-trisphosphate, cyclic adp-ribose, and nicotinic acid adenine dinucleotide phosphate in permeabilized pancreatic acinar cells from mouse. *The Journal of biological chemistry*, 277(14):11696–702, Apr 2002.

[146] G. D. Lamb. Excitation-contraction coupling in skeletal muscle: comparisons with cardiac muscle. *Clin Exp Pharmacol Physiol*, 27(3):216–24, Mar 2000.

[147] J.-R. Landry, D. L. Mager, and B. T. Wilhelm. Complex controls: the role of alternative promoters in mammalian genomes. *Trends Genet*, 19(11):640–8, Nov 2003.

[148] M. F. Langhorst, N. Schwarzmann, and A. H. Guse. Ca2+ release via ryanodine receptors and ca2+ entry: major mechanisms in naadp-mediated ca2+ signaling in t-lymphocytes. *Cell Signal*, 16(11):1283–9, Nov 2004.

[149] J. T. Lanner, D. K. Georgiou, A. D. Joshi, and S. L. Hamilton. Ryanodine receptors: structure, expression, molecular details, and function in calcium release. *Cold Spring Harb Perspect Biol*, 2(11):a003996, Nov 2010.

[150] H. C. Lee. Multiplicity of ca2+ messengers and ca2+ stores: a perspective from cyclic adp-ribose and naadp. *Curr Mol Med*, 4(3):227–37, May 2004.

[151] H. C. Lee. Nicotinic acid adenine dinucleotide phosphate (naadp)-mediated calcium signaling. *The Journal of biological chemistry*, 280(40):33693–6, Oct 2005.

[152] H. C. Lee and R. Aarhus. Adp-ribosyl cyclase: an enzyme that cyclizes nad+ into a calcium-mobilizing metabolite. *Cell Regul*, 2(3):203–9, Mar 1991.

[153] H. C. Lee and R. Aarhus. A derivative of nadp mobilizes calcium stores insensitive to inositol trisphosphate and cyclic adp-ribose. *The Journal of biological chemistry*, 270(5):2152–7, Feb 1995.

[154] H. C. Lee, T. F. Walseth, G. T. Bratt, R. N. Hayes, and D. L. Clapper. Structural determination of a cyclic metabolite of nad+ with intracellular ca2+-mobilizing activity. *The Journal of biological chemistry*, 264(3):1608–15, Jan 1989.

[155] M. F. Leite, A. D. Burgstahler, and M. H. Nathanson. Ca2+ waves require sequential activation of inositol trisphosphate receptors and ryanodine receptors in pancreatic acini. *Gastroenterology*, 122(2):415–27, Feb 2002.

[156] M. F. Leite, J. A. Dranoff, L. Gao, and M. H. Nathanson. Expression and subcellular localization of the ryanodine receptor in rat pancreatic acinar cells. *Biochem J*, 337 (Pt 2):305–9, Jan 1999.

[157] P. K. Lepage, M. P. Lussier, H. Barajas-Martinez, S. M. Bousquet, A. P. Blanchard, N. Francoeur, R. Dumaine, and G. Boulay. Identification of two domains involved in the assembly of transient receptor potential canonical channels. *J Biol Chem*, 281(41):30356–64, Oct 2006.

[158] R. E. Lesh, G. F. Nixon, S. Fleischer, J. A. Airey, A. P. Somlyo, and A. V. Somlyo. Localization of ryanodine receptors in smooth muscle. *Circ Res*, 82(2):175–85, Feb 1998.

[159] A. M. Lewis, R. Masgrau, S. R. Vasudevan, M. Yamasaki, J. S. O'Neill, C. Garnham, K. James, A. Macdonald, M. Ziegler, A. Galione, and G. C. Churchill. Refinement of a radioreceptor binding assay for nicotinic acid adenine dinucleotide phosphate. *Analytical Biochemistry*, 371(1):26–36, Dec 2007.

[160] R. S. Lewis. The molecular choreography of a store-operated calcium channel. *Nature*, 446(7133):284–7, Mar 2007.

[161] R. A. Liddle. Cholecystokinin cells. *Annu Rev Physiol*, 59:221–42, Jan 1997.

[162] P. Lipp and E. Niggli. Fundamental calcium release events revealed by two-photon excitation photolysis of caged calcium in guinea-pig cardiac myocytes. *The Journal of Physiology*, 508 (Pt 3):801–9, May 1998.

[163] P. Lipp, D. Thomas, M. J. Berridge, and M. D. Bootman. Nuclear calcium signalling by individual cytoplasmic calcium puffs. *EMBO J*, 16(23):7166–73, Dec 1997.

[164] S. Liu. Increasing alternative promoter repertories is positively associated with differential expression and disease susceptibility. *PLoS ONE*, 5(3):e9482, Jan 2010.

[165] E. Lloyd-Evans, A. J. Morgan, X. He, D. A. Smith, E. Elliot-Smith, D. J. Sillence, G. C. Churchill, E. H. Schuchman, A. Galione, and F. M. Platt. Niemann-pick disease type c1 is a sphingosine storage disease that causes deregulation of lysosomal calcium. *Nat Med*, 14(11):1247–55, Nov 2008.

[166] E. Lloyd-Evans, H. Waller-Evans, K. Peterneva, and F. M. Platt. Endolysosomal calcium regulation and disease. *Biochem Soc Trans*, 38(6):1458, Dec 2010.

[167] J. Logan, K. Edwards, and N. Saunders. Real-time pcr: current technology and applications. *Caister Academic Press*, pages 137–147, Jan 2009.

[168] J. J. López, C. Camello-Almaraz, J. A. Pariente, G. M. Salido, and J. A. Rosado. Ca2+ accumulation into acidic organelles mediated by ca2+- and vacuolar h+-atpases in human platelets. *Biochem J*, 390(Pt 1):243–52, Aug 2005.

[169] J. J. López, P. C. Redondo, G. M. Salido, J. A. Pariente, and J. A. Rosado. Two distinct ca2+ compartments show differential sensitivity to thrombin, adp and vasopressin in human platelets. *Cell Signal*, 18(3):373–81, Mar 2006.

[170] J. T. Low, A. Shukla, N. Behrendorff, and P. Thorn. Exocytosis, dependent on ca2+ release from ca2+ stores, is regulated by ca2+ microdomains. *J Cell Sci*, 123(Pt 18):3201–8, Sep 2010.

[171] J. T. Low, A. Shukla, and P. Thorn. Pancreatic acinar cell: new insights into the control of secretion. *Int J Biochem Cell Biol*, 42(10):1586–9, Oct 2010.

[172] J. P. Luzio, N. A. Bright, and P. R. Pryor. The role of calcium and other ions in sorting and delivery in the late endocytic pathway. *Biochem Soc Trans*, 35(Pt 5):1088–91, Nov 2007.

[173] P. E. MacDonald and P. Rorsman. Oscillations, intercellular coupling, and insulin secretion in pancreatic beta cells. *Plos Biol*, 4(2):e49, Feb 2006.

[174] A. Macgregor, M. Yamasaki, S. Rakovic, L. Sanders, R. Parkesh, G. C. Churchill, A. Galione, and D. A. Terrar. Naadp controls cross-talk between distinct ca2+ stores in the heart. *The Journal of biological chemistry*, 282(20):15302–11, May 2007.

[175] D. H. Maclennan and E. Zvaritch. Mechanistic models for muscle diseases and disorders originating in the sarcoplasmic reticulum. *Biochim Biophys Acta*, 1813(5):948–64, May 2011.

[176] E. Málaga-Trillo and E. Sempou. Prps: Proteins with a purpose: Lessons from the zebrafish. *Prion*, 3(3):129–33, Jul 2009.

[177] M. Mándi, B. Tóth, G. Timár, and J. Bak. Ca2+ release triggered by naadp in hepatocyte microsomes. *Biochem J*, 395(2):233–8, Apr 2006.

[178] R. Masgrau, G. C. Churchill, A. J. Morgan, S. J. H. Ashcroft, and A. Galione. Naadp: a new second messenger for glucose-induced ca2+ responses in clonal pancreatic beta cells. *Curr Biol*, 13(3):247–51, Feb 2003.

[179] T. Matozaki, B. Göke, Y. Tsunoda, M. Rodriguez, J. Martinez, and J. A. Williams. Two functionally distinct cholecystokinin receptors show different modes of action on ca2+ mobilization and phospholipid hydrolysis in isolated rat pancreatic acini. studies using a new cholecystokinin analog, jmv-180. *The Journal of biological chemistry*, 265(11):6247–54, Apr 1990.

[180] M. Matsumoto and E. Nagata. Type 1 inositol 1,4,5-trisphosphate receptor knock-out mice: their phenotypes and their meaning in neuroscience and clinical practice. *J Mol Med*, 77(5):406–11, May 1999.

[181] M. Matsumoto, T. Nakagawa, T. Inoue, E. Nagata, K. Tanaka, H. Takano, O. Minowa, J. Kuno, S. Sakakibara, M. Yamada, H. Yoneshima, A. Miyawaki, Y. Fukuuchi, T. Furuichi, H. Okano, K. Mikoshiba, and T. Noda. Ataxia and epileptic seizures in mice lacking type 1 inositol 1,4,5-trisphosphate receptor. *Nature*, 379(6561):168–71, Jan 1996.

[182] N. Matsuo, K. Tanda, K. Nakanishi, N. Yamasaki, K. Toyama, K. Takao, H. Takeshima, and T. Miyakawa. Comprehensive behavioral phenotyping of ryanodine receptor type 3 (ryr3) knockout mice: decreased social contact duration in two social interaction tests. *Front. Behav. Neurosci.*, 3:3, Jan 2009.

[183] G. Meissner. Ryanodine receptor/ca2+ release channels and their regulation by endogenous effectors. *Annu Rev Physiol*, 56:485–508, Jan 1994.

[184] G. Meissner, E. Rios, A. Tripathy, and D. A. Pasek. Regulation of skeletal muscle ca2+ release channel (ryanodine receptor) by ca2+ and monovalent cations and anions. *The Journal of biological chemistry*, 272(3):1628–38, Jan 1997.

[185] A. Menteyne, A. Burdakov, G. Charpentier, O. H. Petersen, and J.-M. Cancela. Generation of specific ca(2+) signals from ca(2+) stores and endocytosis by differential coupling to messengers. *Curr Biol*, 16(19):1931–7, Oct 2006.

[186] J. L. Mershon, R. S. Baker, and K. E. Clark. Estrogen increases inos expression in the ovine coronary artery. *Am J Physiol Heart Circ Physiol*, 283(3):H1169–80, Sep 2002.

[187] G. Meur, A. K. T. Parker, F. V. Gergely, and C. W. Taylor. Targeting and retention of type 1 ryanodine receptors to the endoplasmic reticulum. *The Journal of biological chemistry*, 282(32):23096–103, Aug 2007.

[188] O. Mignen, J. L. Thompson, D. I. Yule, and T. J. Shuttleworth. Agonist activation of arachidonate-regulated ca2+-selective (arc) channels in murine parotid and pancreatic acinar cells. *The Journal of Physiology*, 564(Pt 3):791–801, May 2005.

[189] K. J. Mitchell, F. A. Lai, and G. A. Rutter. Ryanodine receptor type i and nicotinic acid adenine dinucleotide phosphate receptors mediate ca2+ release from insulin-containing vesicles in living pancreatic beta-cells (min6). *J Biol Chem*, 278(13):11057–64, Mar 2003.

[190] P. J. Mohler and X. H. T. Wehrens. Mechanisms of human arrhythmia syndromes: abnormal cardiac macromolecular interactions. *Physiology (Bethesda)*, 22:342–50, Oct 2007.

[191] I. Moreschi, S. Bruzzone, N. Bodrato, C. Usai, L. Guida, R. A. Nicholas, M. U. Kassack, E. Zocchi, and A. D. Flora. Naadp+ is an agonist of the human p2y11 purinergic receptor. *Cell Calcium*, 43(4):344–55, Apr 2008.

[192] A. J. Morgan and A. Galione. Fertilization and nicotinic acid adenine dinucleotide phosphate induce ph changes in acidic ca(2+) stores in sea urchin eggs. *The Journal of biological chemistry*, 282(52):37730–7, Dec 2007.

[193] A. J. Morgan and A. Galione. Naadp induces ph changes in the lumen of acidic ca2+ stores. *Biochem J*, 402(2):301–10, Mar 2007.

[194] A. J. Morgan and A. Galione. Investigating cadpr and naadp in intact and broken cell preparations. *Methods*, 46(3):194–203, Nov 2008.

[195] A. J. Morgan and R. Jacob. Differential modulation of the phases of a ca2+ spike by the store ca2+-atpase in human umbilical vein endothelial cells. *The Journal of Physiology*, 513 (Pt 1):83–101, Nov 1998.

[196] H. Motulsky.... Analyzing radioligand binding data. *Current Protocols in Protein Science*, Jan 2000.

[197] T.-W. Mu, D. M. Fowler, and J. W. Kelly. Partial restoration of mutant enzyme homeostasis in three distinct lysosomal storage disease cell lines by altering calcium homeostasis. *Plos Biol*, 6(2):e26, Feb 2008.

[198] T. Nagata, S. Iizumi, K. Satoh, H. Ooka, J. Kawai, P. Carninci, Y. Hayashizaki, Y. Otomo, K. Murakami, K. Matsubara, and S. Kikuchi. Comparative analysis of plant and animal calcium signal transduction element using plant full-length cdna data. *Molecular biology and evolution*, 21(10):1855–70, Oct 2004.

[199] L. Navazio, M. A. Bewell, A. Siddiqua, G. D. Dickinson, A. Galione, and D. Sanders. Calcium release from the endoplasmic reticulum of higher plants elicited by the nadp metabolite nicotinic acid adenine dinucleotide phosphate. *Proc Natl Acad Sci USA*, 97(15):8693–8, Jul 2000.

[200] E. Naylor, A. Arredouani, S. R. Vasudevan, A. M. Lewis, R. Parkesh, A. Mizote, D. Rosen, J. M. Thomas, M. Izumi, A. Ganesan, A. Galione, and G. C. Churchill. Identification of a chemical probe for naadp by virtual screening. *Nat Chem Biol*, 5(4):220–6, Apr 2009.

[201] C. L. Newton, G. A. Mignery, and T. C. Südhof. Co-expression in vertebrate tissues and cell lines of multiple inositol 1,4,5-trisphosphate (insp3) receptors with distinct affinities for insp3. *The Journal of biological chemistry*, 269(46):28613–9, Nov 1994.

[202] N. Noguchi, S. Takasawa, K. Nata, A. Tohgo, I. Kato, F. Ikehata, H. Yonekura, and H. Okamoto. Cyclic adp-ribose binds to fk506-binding protein 12.6 to release ca2+ from islet microsomes. *The Journal of biological chemistry*, 272(6):3133–6, Feb 1997.

[203] G. J. Obermair, P. Tuluc, and B. E. Flucher. Auxiliary ca(2+) channel subunits: lessons learned from muscle. *Curr Opin Pharmacol*, 8(3):311–8, Jun 2008.

[204] S. Obermüller, C. Kiecke, K. von Figura, and S. Höning. The tyrosine motifs of lamp 1 and lap determine their direct and indirect targetting to lysosomes. *J Cell Sci*, 115(Pt 1):185–94, Dec 2002.

[205] C. J. O'Kane and W. J. Gehring. Detection in situ of genomic regulatory elements in drosophila. *Proc Natl Acad Sci USA*, 84(24):9123–7, Dec 1987.

[206] P. Pacher, A. P. Thomas, and G. Hajnóczky. Ca2+ marks: miniature calcium signals in single mitochondria driven by ryanodine receptors. *Proc Natl Acad Sci USA*, 99(4):2380–5, Feb 2002.

[207] P. Palade. The hunt for an alternate way to generate naadp. focus on "naadp as a second messenger: neither cd38 nor base-exchange reaction are necessary for in vivo generation of naadp in myometrial cells". *Am J Physiol, Cell Physiol*, 292(1):C4–7, Jan 2007.

[208] R. Palty, W. F. Silverman, M. Hershfinkel, T. Caporale, S. L. Sensi, J. Parnis, C. Nolte, D. Fishman, V. Shoshan-Barmatz, S. Herrmann, D. Khananshvili, and I. Sekler. Nclx is an essential component of mitochondrial na+/ca2+ exchange. *Proc Natl Acad Sci USA*, 107(1):436–41, Jan 2010.

[209] E. Pantazaka and C. W. Taylor. Targeting of inositol 1,4,5-trisphosphate receptor to the endoplasmic reticulum by its first transmembrane domain. *Biochem J*, 425(1):61–9, Jan 2010.

[210] E. Parkinson-Lawrence, M. Fuller, J. J. Hopwood, P. J. Meikle, and D. A. Brooks. Immunochemistry of lysosomal storage disorders. *Clin Chem*, 52(9):1660–8, Sep 2006.

[211] L. E. Pascal, L. D. True, D. S. Campbell, E. W. Deutsch, M. Risk, I. M. Coleman, L. J. Eichner, P. S. Nelson, and A. Y. Liu. Correlation of mrna and protein levels: cell type-specific gene expression of cluster designation antigens in the prostate. *BMC Genomics*, 9:246, Dec 2008.

[212] A. Patapoutian, S. Tate, and C. J. Woolf. Transient receptor potential channels: targeting pain at the source. *Nat Rev Drug Discov*, 8(1):55–68, Jan 2009.

[213] S. Patel, G. C. Churchill, and A. Galione. Unique kinetics of nicotinic acid-adenine dinucleotide phosphate (naadp) binding enhance the sensitivity of naadp receptors for their ligand. *Biochem J*, 352 Pt 3:725–9, Dec 2000.

[214] S. Patel, G. C. Churchill, and A. Galione. Coordination of ca2+ signalling by naadp. *Trends Biochem Sci*, 26(8):482–9, Aug 2001.

[215] S. Patel, G. C. Churchill, T. Sharp, and A. Galione. Widespread distribution of binding sites for the novel ca2+-mobilizing messenger, nicotinic acid adenine dinucleotide phosphate, in the brain. *J Biol Chem*, 275(47):36495–7, Nov 2000.

[216] S. Patel and R. Docampo. Acidic calcium stores open for business: expanding the potential for intracellular ca2+ signaling. *Trends in Cell Biology*, 20(5):277–86, May 2010.

[217] S. Patel, J. S. Marchant, and E. Brailoiu. Two-pore channels: Regulation by naadp and customized roles in triggering calcium signals. *Cell Calcium*, 47(6):480–90, Jun 2010.

[218] S. Patel, L. Ramakrishnan, T. Rahman, A. Hamdoun, J. S. Marchant, C. W. Taylor, and E. Brailoiu. The endo-lysosomal system as an naadp-sensitive acidic ca(2+) store: Role for the two-pore channels. *Cell Calcium*, Apr 2011.

[219] E. Peiter, F. J. M. Maathuis, L. N. Mills, H. Knight, J. Pelloux, A. M. Hetherington, and D. Sanders. The vacuolar ca2+-activated channel tpc1 regulates germination and stomatal movement. *Nature*, 434(7031):404–8, Mar 2005.

[220] G. J. S. Pereira, H. Hirata, G. M. Fimia, L. G. do Carmo, C. Bincoletto, S. W. Han, R. S. Stilhano, R. P. Ureshino, D. Bloor-Young, G. Churchill, M. Piacentini, S. Patel, and S. S. Smaili. Nicotinic acid adenine dinucleotide phosphate (naadp) regulates autophagy in cultured astrocytes. *The Journal of biological chemistry*, May 2011.

[221] C. C. Petersen, O. H. Petersen, and M. J. Berridge. The role of endoplasmic reticulum calcium pumps during cytosolic calcium spiking in pancreatic acinar cells. *J Biol Chem*, 268(30):22262–4, Oct 1993.

[222] C. C. Petersen, E. C. Toescu, and O. H. Petersen. Different patterns of receptor-activated cytoplasmic ca2+ oscillations in single pancreatic acinar cells: dependence on receptor type, agonist concentration and intracellular ca2+ buffering. *EMBO J*, 10(3):527–33, Mar 1991.

[223] C. C. Petersen, E. C. Toescu, B. V. Potter, and O. H. Petersen. Inositol triphosphate produces different patterns of cytoplasmic ca2+ spiking depending on its concentration. *FEBS Letters*, 293(1-2):179–82, Nov 1991.

[224] O. H. Petersen. Ca2+ signaling in pancreatic acinar cells: physiology and pathophysiology. *Braz J Med Biol Res*, 42(1):9–16, Jan 2009.

[225] O. H. Petersen, D. Burdakov, and A. V. Tepikin. Polarity in intracellular calcium signaling. *Bioessays*, 21(10):851–60, Oct 1999.

[226] O. H. Petersen, O. V. Gerasimenko, A. V. Tepikin, and J. V. Gerasimenko. Aberrant ca(2+) signalling through acidic calcium stores in pancreatic acinar cells. *Cell Calcium*, Mar 2011.

[227] O. H. Petersen, R. Sutton, and D. N. Criddle. Failure of calcium microdomain generation and pathological consequences. *Cell Calcium*, 40(5-6):593–600, Jan 2006.

[228] O. H. Petersen and A. V. Tepikin. Polarized calcium signaling in exocrine gland cells. *Annu Rev Physiol*, 70:273–99, Jan 2008.

[229] M. R. Picciotto and K. Wickman. Using knockout and transgenic mice to study neurophysiology and behavior. *Physiol Rev*, 78(4):1131–63, Oct 1998.

[230] R. C. Piper and J. P. Luzio. Cuppling calcium to lysosomal biogenesis. *Trends Cell Biol*, 14(9):471–3, Sep 2004.

[231] S. J. Pitt, T. M. Funnell, M. Sitsapesan, E. Venturi, K. Rietdorf, M. Ruas, A. Ganesan, R. Gosain, G. C. Churchill, M. X. Zhu, J. Parrington, A. Galione, and R. Sitsapesan. Tpc2 is a novel naadp-sensitive ca2+ release channel, operating as a dual sensor of luminal ph and ca2+. *The Journal of biological chemistry*, 285(45):35039–46, Nov 2010.

[232] A. Pizard, C. Richer, N. Bouby, N. Picard, P. Meneton, M. Azizi, and F. Alhenc-Gelas. Genetic deficiency in tissue kallikrein activity in mouse and man: effect on arteries, heart and kidney. *Biological Chemistry*, 389(6):701–6, Jun 2008.

[233] T. Pozzan and R. Rizzuto. High tide of calcium in mitochondria. *Nat Cell Biol*, 2(2):E25–7, Feb 2000.

[234] M. Prakriya, S. Feske, Y. Gwack, S. Srikanth, A. Rao, and P. G. Hogan. Orai1 is an essential pore subunit of the crac channel. *Nature*, 443(7108):230–3, Sep 2006.

[235] P. R. Pryor, F. Reimann, F. M. Gribble, and J. P. Luzio. Mucolipin-1 is a lysosomal membrane protein required for intracellular lactosylceramide traffic. *Traffic*, 7(10):1388–98, Oct 2006.

[236] R. Puertollano and K. Kiselyov. Trpmls: in sickness and in health. *Am J Physiol Renal Physiol*, 296(6):F1245–54, Jun 2009.

[237] S.-Y. Rah, M. Mushtaq, T.-S. Nam, S. H. Kim, and U.-H. Kim. Generation of cyclic adp-ribose and nicotinic acid adenine dinucleotide phosphate by cd38 for ca2+ signaling in interleukin-8-treated lymphokine-activated killer cells. *The Journal of biological chemistry*, 285(28):21877–87, Jul 2010.

[238] J. Rengifo, C. J. Gibson, E. Winkler, T. Collin, and B. E. Ehrlich. Regulation of the inositol 1,4,5-trisphosphate receptor type i by o-glcnac glycosylation. *J Neurosci*, 27(50):13813–21, Dec 2007.

[239] R. Rizzuto, P. Pinton, W. Carrington, F. S. Fay, K. E. Fogarty, L. M. Lifshitz, R. A. Tuft, and T. Pozzan. Close contacts with the endoplasmic reticulum as determinants of mitochondrial ca2+ responses. *Science*, 280(5370):1763–6, Jun 1998.

[240] J. A. Rosado. Acidic ca(2+) stores in platelets. *Cell Calcium*, Dec 2010.

[241] D. Rosen, A. M. Lewis, A. Mizote, J. M. Thomas, P. K. Aley, S. R. Vasudevan, R. Parkesh, A. Galione, M. Izumi, A. Ganesan, and G. C. Churchill. Analogues of the nicotinic acid adenine dinucleotide phosphate (naadp) antagonist ned-19 indicate two binding sites on the naadp receptor. *The Journal of biological chemistry*, 284(50):34930–4, Dec 2009.

[242] A. Rottach, E. Kremmer, D. Nowak, H. Leonhardt, and M. C. Cardoso. Generation and characterization of a rat monoclonal antibody specific for multiple red fluorescent proteins. *Hybridoma (Larchmt)*, 27(5):337–43, Oct 2008.

[243] M. Ruas, K. Rietdorf, A. Arredouani, L. C. Davis, E. Lloyd-Evans, H. Koegel, T. M. Funnell, A. J. Morgan, J. A. Ward, K. Watanabe, X. Cheng, G. C. Churchill, M. X. Zhu, F. M. Platt, G. M. Wessel, J. Parrington, and A. Galione. Purified tpc isoforms form naadp receptors with distinct roles for ca(2+) signaling and endolysosomal trafficking. *Curr Biol*, 20(8):703–9, Apr 2010.

[244] H. Sakai, E. Lingueglia, G. Champigny, M. G. Mattei, and M. Lazdunski. Cloning and functional expression of a novel degenerin-like na+ channel gene in mammals. *The Journal of Physiology*, 519 Pt 2:323–33, Sep 1999.

[245] R. Salceda and G. Sánchez-Chávez. Calcium uptake, release and ryanodine binding in melanosomes from retinal pigment epithelium. *Cell Calcium*, 27(4):223–9, Apr 2000.

[246] C. Saldaña, M. Díaz-Muñoz, A. Antaramián, A. González-Gallardo, P. García-Solís, and V. Morales-Tlalpan. Mcf-7 breast carcinoma cells express ryanodine receptor type 1: functional characterization and subcellular localization. *Mol Cell Biochem*, 323(1-2):39–47, Mar 2009.

[247] L. Schaefer, H. Sakai, M. Mattei, M. Lazdunski, and E. Lingueglia. Molecular cloning, functional expression and chromosomal localization of an amiloride-sensitive na(+) channel from human small intestine. *FEBS Letters*, 471(2-3):205–10, Apr 2000.

[248] M. Schieder, K. Rötzer, A. Brüggemann, M. Biel, and C. A. Wahl-Schott. Characterization of two-pore channel 2 (tpcn2)-mediated ca2+ currents in isolated lysosomes. *The Journal of biological chemistry*, 285(28):21219–22, Jul 2010.

[249] I. Schulz, E. Krause, A. González, A. Göbel, L. Sternfeld, and A. Schmid. Agonist-stimulated pathways of calcium signaling in pancreatic acinar cells. *Biological Chemistry*, 380(7-8):903–8, Jan 1999.

[250] T. Shachar, C. L. Bianco, A. Recchia, C. Wiessner, A. Raas-Rothschild, and A. H. Futerman. Lysosomal storage disorders and parkinson's disease: Gaucher disease and beyond. *Movement disorders : official journal of the Movement Disorder Society*, May 2011.

[251] M. W. Sherwood, I. A. Prior, S. G. Voronina, S. L. Barrow, J. D. Woodsmith, O. V. Gerasimenko, O. H. Petersen, and A. V. Tepikin. Activation of trypsinogen in large endocytic vacuoles of pancreatic acinar cells. *Proc Natl Acad Sci USA*, 104(13):5674–9, Mar 2007.

[252] W. C. Skarnes, B. A. Auerbach, and A. L. Joyner. A gene trap approach in mouse embryonic stem cells: the lacz reported is activated by splicing, reflects endogenous gene expression, and is mutagenic in mice. *Genes Dev*, 6(6):903–18, Jun 1992.

[253] J. T. Smyth, S.-Y. Hwang, T. Tomita, W. I. DeHaven, J. C. Mercer, and J. W. Putney. Activation and regulation of store-operated calcium entry. *J Cell Mol Med*, 14(10):2337–49, Oct 2010.

[254] J. Sneyd, K. Tsaneva-Atanasova, V. Reznikov, Y. Bai, M. J. Sanderson, and D. I. Yule. A method for determining the dependence of calcium oscillations on inositol trisphosphate oscillations. *Proc Natl Acad Sci USA*, 103(6):1675–80, Feb 2006.

[255] S. Soares, M. Thompson, T. White, A. Isbell, M. Yamasaki, Y. Prakash, F. E. Lund, A. Galione, and E. N. Chini. Naadp as a second messenger: neither cd38 nor base-exchange reaction are necessary for in vivo generation of naadp in myometrial cells. *Am J Physiol, Cell Physiol*, 292(1):C227–39, Jan 2007.

[256] D. J. States, T. F. Walseth, and H. C. Lee. Similarities in amino acid sequences of aplysia adp-ribosyl cyclase and human lymphocyte antigen cd38. *Trends Biochem Sci*, 17(12):495, Dec 1992.

[257] M. Steen, T. Kirchberger, and A. H. Guse. Naadp mobilizes calcium from the endoplasmic reticular ca(2+) store in t-lymphocytes. *The Journal of biological chemistry*, 282(26):18864–71, Jun 2007.

[258] D. D. Stefani, A. Raffaello, E. Teardo, I. Szabò, and R. Rizzuto. A forty-kilodalton protein of the inner membrane is the mitochondrial calcium uniporter. *Nature*, Jun 2011.

[259] H. Streb, R. F. Irvine, M. J. Berridge, and I. Schulz. Release of ca2+ from a nonmitochondrial intracellular store in pancreatic acinar cells by inositol-1,4,5-trisphosphate. *Nature*, 306(5938):67–9, Jan 1983.

[260] P. Sulem, D. F. Gudbjartsson, S. N. Stacey, A. Helgason, T. Rafnar, M. Jakobsdottir, S. Steinberg, S. A. Gudjonsson, A. Palsson, G. Thorleifsson, S. Pálsson, B. Sigurgeirsson, K. Thorisdottir, R. Ragnarsson, K. R. Benediktsdottir, K. K. Aben, S. H. Vermeulen, A. M. Goldstein, M. A. Tucker, L. A. Kiemeney, J. H. Olafsson, J. Gulcher, A. Kong, U. Thorsteinsdottir, and K. Stefansson. Two newly identified genetic determinants of pigmentation in europeans. *Nature Genetics*, 40(7):835–7, Jul 2008.

[261] H. Takeshima, M. Iino, H. Takekura, M. Nishi, J. Kuno, O. Minowa, H. Takano, and T. Noda. Excitation-contraction uncoupling and muscular degeneration in mice lacking functional skeletal muscle ryanodine-receptor gene. *Nature*, 369(6481):556–9, Jun 1994.

[262] H. Takeshima, T. Ikemoto, M. Nishi, N. Nishiyama, M. Shimuta, Y. Sugitani, J. Kuno, I. Saito, H. Saito, M. Endo, M. Iino, and T. Noda. Generation and characterization of mutant mice lacking ryanodine receptor type 3. *J Biol Chem*, 271(33):19649–52, Aug 1996.

[263] H. Takeshima, S. Komazaki, K. Hirose, M. Nishi, T. Noda, and M. Iino. Embryonic lethality and abnormal cardiac myocytes in mice lacking ryanodine receptor type 2. *EMBO J*, 17(12):3309–16, Jun 1998.

[264] M. Tang, K. A. Pelkey, D. Ng, E. Ivakine, C. J. McBain, M. W. Salter, and R. R. McInnes. Neto1 is an auxiliary subunit of native synaptic kainate receptors. *Journal of Neuroscience*, 31(27):10009–10018, Jul 2011.

[265] C. W. Taylor, A. A. Genazzani, and S. A. Morris. Expression of inositol trisphosphate receptors. *Cell Calcium*, 26(6):237–51, Dec 1999.

[266] C. W. Taylor, Taufiq-Ur-Rahman, and E. Pantazaka. Targeting and clustering of ip3 receptors: key determinants of spatially organized ca2+ signals. *Chaos*, 19(3):037102, Sep 2009.

[267] C. W. Taylor and S. C. Tovey. Ip(3) receptors: toward understanding their activation. *Cold Spring Harb Perspect Biol*, 2(12):a004010, Dec 2010.

[268] T. L. Thai, G. C. Churchill, and W. J. Arendshorst. Naadp receptors mediate calcium signaling stimulated by endothelin-1 and norepinephrine in renal afferent arterioles. *Am J Physiol Renal Physiol*, 297(2):F510–6, Aug 2009.

[269] D. D. H. Thomas, N. Weng, and G. E. Groblewski. Secretagogue-induced translocation of crhsp-28 within an early apical endosomal compartment in acinar cells. *Am J Physiol Gastrointest Liver Physiol*, 287(1):G253–63, Jul 2004.

[270] P. Thorn, P. Brady, J. Llopis, D. V. Gallacher, and O. H. Petersen. Cytosolic ca2+ spikes evoked by the thiol reagent thimerosal in both intact and internally perfused single pancreatic acinar cells. *Pflugers Arch*, 422(2):173–8, Nov 1992.

[271] P. Thorn, O. Gerasimenko, and O. H. Petersen. Cyclic adp-ribose regulation of ryanodine receptors involved in agonist evoked cytosolic ca2+ oscillations in pancreatic acinar cells. *EMBO J*, 13(9):2038–43, May 1994.

[272] P. Thorn, A. M. Lawrie, P. M. Smith, D. V. Gallacher, and O. H. Petersen. Local and global cytosolic ca2+ oscillations in exocrine cells evoked by agonists and inositol trisphosphate. *Cell*, 74(4):661–8, Aug 1993.

[273] A. V. Titievsky, T. Takeo, A. V. Tepikin, and O. H. Petersen. Decrease of acidity inside zymogen granules inhibits acetylcholine- or inositol trisphosphate-evoked cytosolic ca2+ spiking in pancreatic acinar cells. *Pflugers Arch*, 432(5):938–40, Sep 1996.

[274] D. J. Tobin. The cell biology of human hair follicle pigmentation. *Pigment Cell Melanoma Res*, 24(1):75–88, Feb 2011.

[275] F. W. Tse, A. Tse, and B. Hille. Cyclic ca2+ changes in intracellular stores of gonadotropes during gonadotropin-releasing hormone-stimulated ca2+ oscillations. *Proc Natl Acad Sci USA*, 91(21):9750–4, Oct 1994.

[276] W. H. Turner and A. F. Brading. Smooth muscle of the bladder in the normal and the diseased state: pathophysiology, diagnosis and treatment. *Pharmacol Ther*, 75(2):77–110, Aug 1997.

[277] E. van Meel and J. Klumperman. Imaging and imagination: understanding the endo-lysosomal system. *Histochem Cell Biol*, 129(3):253–66, Mar 2008.

[278] S. van Weely, M. van den Berg, J. A. Barranger, M. C. S. Miranda, J. M. Tager, and J. M. Aerts. Role of ph in determining the cell-type-specific residual activity of glucocerebrosidase in type 1 gaucher disease. *J Clin Invest*, 91(3):1167–75, Mar 1993.

[279] V. Vanderheyden, B. Devogelaere, L. Missiaen, H. D. Smedt, G. Bultynck, and J. B. Parys. Regulation of inositol 1,4,5-trisphosphate-induced ca2+ release by reversible phosphorylation and dephosphorylation. *Biochimica et biophysica acta*, 1793(6):959–70, Jun 2009.

[280] J. Vandesompele, K. D. Preter, F. Pattyn, B. Poppe, N. V. Roy, A. D. Paepe, and F. Speleman. Accurate normalization of real-time quantitative rt-pcr data by geometric averaging of multiple internal control genes. *Genome Biol*, 3(7):RESEARCH0034, Jun 2002.

[281] P. Vanhoutte. B2 kinin receptors: a major player in the release of nitric oxide and edhf. *Dialogues in Cardiovascular Medicine*, 6(4):223–232, 2001.

[282] S. R. Vasudevan, A. Galione, and G. C. Churchill. Sperm express a ca2+-regulated naadp synthase. *Biochem J*, 411(1):63–70, Apr 2008.

[283] S. R. Vasudevan, A. M. Lewis, J. W. Chan, C. L. Machin, D. Sinha, A. Galione, and G. C. Churchill. The calcium-mobilizing messenger nicotinic acid adenine dinucleotide phosphate participates in sperm activation by mediating the acrosome reaction. *The Journal of biological chemistry*, 285(24):18262–9, Jun 2010.

[284] E. Venturi, S. Pitt, E. Galfré, and R. Sitsapesan. From eggs to hearts: What is the link between cyclic adp-ribose and ryanodine receptors? *Cardiovascular Therapeutics*, Dec 2010.

[285] S. Vergarajauregui and R. Puertollano. Two di-leucine motifs regulate trafficking of mucolipin-1 to lysosomes. *Traffic*, 7(3):337–353, Mar 2006.

[286] E. B. Vitner, F. M. Platt, and A. H. Futerman. Common and uncommon pathogenic cascades in lysosomal storage diseases. *Journal of Biological Chemistry*, 285(27):20423–20427, Jul 2010.

[287] M. Wakui, Y. V. Osipchuk, and O. H. Petersen. Receptor-activated cytoplasmic ca2+ spiking mediated by inositol trisphosphate is due to ca2(+)-induced ca2+ release. *Cell*, 63(5):1025–32, Nov 1990.

[288] D. Wiemuth and S. Gründer. A single amino acid tunes ca2+ inhibition of brain liver intestine na+ channel (blinac). *The Journal of biological chemistry*, 285(40):30404–10, Sep 2010.

[289] J. Williams and D. Yule. Stimulus-secretion coupling in pancreatic acinar cells. *Physiology of the Gastrointestinal Tract, 4th ed.*, pages 1337–1369, Jan 2006.

[290] D. Willoughby and D. M. F. Cooper. Organization and ca2+ regulation of adenylyl cyclases in camp microdomains. *Physiol Rev*, 87(3):965–1010, Jul 2007.

[291] H. L. Wilson and A. Galione. Differential regulation of nicotinic acid-adenine dinucleotide phosphate and cadp-ribose production by camp and cgmp. *Biochem J*, 331 (Pt 3):837–43, May 1998.

[292] S. Yamaguchi, A. Jha, Q. Li, A. A. Soyombo, G. D. Dickinson, D. Churamani, E. Brailoiu, S. Patel, and S. Muallem. Transient receptor potential mucolipin 1 (trpml1) and two-pore channels are functionally independent organellar ion channels. *The Journal of biological chemistry*, 286(26):22934–42, Jul 2011.

[293] M. Yamasaki, R. Masgrau, A. J. Morgan, G. C. Churchill, S. Patel, S. J. H. Ashcroft, and A. Galione. Organelle selection determines agonist-specific ca2+ signals in pancreatic acinar and beta cells. *J Biol Chem*, 279(8):7234–40, Feb 2004.

[294] M. Yamasaki, J. M. Thomas, G. C. Churchill, C. Garnham, A. M. Lewis, J.-M. Cancela, S. Patel, and A. Galione. Role of naadp and cadpr in the induction and maintenance of agonist-evoked ca2+ spiking in mouse pancreatic acinar cells. *Curr Biol*, 15(9):874–8, May 2005.

[295] M. Yamasaki-Mann, A. Demuro, and I. Parker. cadpr stimulates serca activity in xenopus oocytes. *Cell Calcium*, 45(3):293–9, Mar 2009.

[296] X. Yang, E. E. Schadt, S. Wang, H. Wang, A. P. Arnold, L. Ingram-Drake, T. A. Drake, and A. J. Lusis. Tissue-specific expression and regulation of sexually dimorphic genes in mice. *Genome Res*, 16(8):995–1004, Aug 2006.

[297] D. I. Yule, A. M. Lawrie, and D. V. Gallacher. Acetylcholine and cholecystokinin induce different patterns of oscillating calcium signals in pancreatic acinar cells. *Cell Calcium*, 12(2-3):145–51, Jan 1991.

[298] A. N. K. Yusufi, J. Cheng, M. A. Thompson, J. C. Burnett, and J. P. Grande. Differential mechanisms of ca(2+) release from vascular smooth muscle cell microsomes. *Exp Biol Med (Maywood)*, 227(1):36–44, Jan 2002.

[299] B. P. Zambrowicz, A. Abuin, R. Ramirez-Solis, L. J. Richter, J. Piggott, H. BeltrandelRio, E. C. Buxton, J. Edwards, R. A. Finch, C. J. Friddle, A. Gupta, G. Hansen, Y. Hu, W. Huang, C. Jaing, B. W. Key, P. Kipp, B. Kohlhauff, Z.-Q. Ma, D. Markesich, R. Payne, D. G. Potter, N. Qian, J. Shaw, J. Schrick, Z.-Z. Shi, M. J. Sparks, I. V. Sligtenhorst, P. Vogel, W. Walke, N. Xu, Q. Zhu, C. Person, and A. T. Sands. Wnk1 kinase deficiency lowers blood pressure in mice: a gene-trap screen to identify potential targets for therapeutic intervention. *Proc Natl Acad Sci USA*, 100(24):14109–14, Nov 2003.

[300] F. Zhang, S. Jin, F. Yi, and P.-L. Li. Trp-ml1 functions as a lysosomal naadp-sensitive ca2+ release channel in coronary arterial myocytes. *J Cell Mol Med*, 13(9B):3174–85, Sep 2009.

[301] F. Zhang and P.-L. Li. Reconstitution and characterization of a nicotinic acid adenine dinucleotide phosphate (naadp)-sensitive ca2+ release channel from liver lysosomes of rats. *Journal of Biological Chemistry*, 282(35):25259–25269, Jun 2007.

[302] F. Zhang, M. Xia, and P.-L. Li. Lysosome-dependent ca(2+) release response to fas activation in coronary arterial myocytes through naadp: evidence from cd38 gene knockouts. *Am J Physiol, Cell Physiol*, 298(5):C1209–16, May 2010.

[303] F. Zhang, G. Zhang, A. Y. Zhang, M. J. Koeberl, E. Wallander, and P.-L. Li. Production of naadp and its role in ca2+ mobilization associated with lysosomes in coronary arterial myocytes. *Am J Physiol Heart Circ Physiol*, 291(1):H274–82, Jul 2006.

[304] X. Zhang, Y. N. Tallini, Z. Chen, L. Gan, B. Wei, R. Doran, L. Miao, H.-B. Xin, M. I. Kotlikoff, and G. Ji. Dissociation of fkbp12.6 from ryanodine receptor type 2 is regulated by cyclic adp-ribose but not beta-adrenergic stimulation in mouse cardiomyocytes. *Cardiovasc Res*, 84(2):253–62, Nov 2009.

[305] M. X. Zhu, J. Ma, J. Parrington, P. J. Calcraft, A. Galione, and A. M. Evans. Calcium signaling via two-pore channels: local or global, that is the question. *Am J Physiol, Cell Physiol*, 298(3):C430–41, Mar 2010.

[306] M. X. Zhu, J. Ma, J. Parrington, A. Galione, and A. M. Evans. Tpcs: Endolysosomal channels for ca2+ mobilization from acidic organelles triggered by naadp. *FEBS Letters*, 584(10):1966–74, May 2010.

[307] X. Zong, M. Schieder, H. Cuny, S. Fenske, C. Gruner, K. Rötzer, O. Griesbeck, H. Harz, M. Biel, and C. Wahl-Schott. The two-pore channel tpcn2 mediates naadp-dependent ca(2+)-release from lysosomal stores. *Pflugers Arch*, 458(5):891–9, Sep 2009.